Influence Of Ion Energy On The Reactive Ion Etching Induced Optical Damage And Annealing Of Gallium Nitride

A thesis
submitted in partial fulfilment
of the requirements for the Degree
of
Doctor of Philosophy in Physics
in the
University of Canterbury

by

Suk Ing Liem

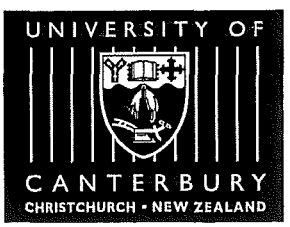

University of Canterbury
2003

Abstract

Photoluminescence (PL) has been successfully applied to study the optical properties of GaN. The PL results of the a-GaN samples made by the University of Victoria Wellington and poly-GaN samples made by the University of Canterbury have been able to give feedback to the preparation stage in order to modify the growth parameters.

Reactive Ion Etching (RIE) induces defects in semiconductor GaN, and its effects on the optical properties of c-GaN have been studied and investigated, using the PL technique. The results and analysis of Ar and SF_6 plasma etching with various etching voltages on the optical properties through the changes of the PL intensity, linewidth and peak position of c-GaN have been discussed and presented.

Effects of annealing in vacuum, hydrogen and nitrogen ambient on the optical properties of GaN has also been investigated. Detailed study of these annealing effects on the PL intensity, linewidth, peak position are presented to show the crystal relaxation and defects created due to the annealing processes.

Acknowledgements

This thesis is dedicated to my family for their love, encouragement and support.

The work described in this thesis was carried out in the Physics and Astronomy Department at the University of Canterbury. The assistance of the academic staff of this department is gratefully acknowledged.

I would specially like to thank my supervisor, Dr. Roger Reeves for his enthusiasm and interest at working in the laboratory, encouragement and his patient guidance throughout all stages of this work.

I wish also to thank:

- Dr. Steve Durbin for discussions, helpful comments, and his keen interest in the GaN project.
- Dr. Glynn Jones and Dr. Jenni Adams, as my mentor and adviser of study, who directed me to work with Dr. Roger Reeves on this project and maintained helpful advice throughout all stages of my study and finishing this work.
- My fellow students in Physics and Astronomy Department, who have made the students life enjoyable and given mutual encouragement.
- Mr. Bob Flygenring, Mr. Wayne Smith, Mr. Ross Ritchie, Mr. Owen Caughley, Mr. Paul Arnold, Mr. Ryurick Hristev, Ms. Helen Devereux for their excellent assistance at providing the technical support.
- My best friend Shifera Anggawijaya, her happiness and encouragement have brightened my days of hard working time.

Finally, I would like to thank Prof. Gregory A. MacRae and his parents, Mr. and Mrs. Anthony and Wendy MacRae, for their encouragement and love.

Financial assistance has been provided by The MacDiarmid Institute, The Ministry of Science and Technology through The Marsden Fund, and The University of Canterbury and is gratefully acknowledged.

Contents

Chapter 1

Introduction

1.1 Background and Overview

The research on the group III nitride semiconductors began effectively from about 1970 when a number of researchers started applying hetero-epitaxial growth to produce reasonably high quality GaN films on sapphire substrates.
However, excitement was generated recently [1, 19, 20, 24, 45, 46, 52, 53, 65, 70, 82], by the fact that the nitride semiconductors AlN, GaN, InN are all direct band gap materials. And their energy gaps ranging from the controversially small band gap of 0.8 eV or 1.9 eV (InN) through 3.4 eV (GaN) to 6.2 eV (AlN). They could form a complete series of ternary alloys which spans the whole of the visible spectrum and extends well into the UV region, i.e. continuously variable from 200 nm to 650 nm. This makes them ideal candidates for tailored optoelectronics devices operating anywhere within this wavelength range. And more specifically for visible light emitters in the blue and green parts of the spectrum. Some successful applications of GaN are in:

- Light Emitting Diode
  The need for blue LEDs has been acute for a long time for full colour displays. Red LEDs with efficiencies greater than 10% have been commercially available for some years [80]. But efficiencies of green and blue diodes are much lower than that, restricting the possibilities for LED full colour display panels. The attempt to achieve high efficiencies from blue LEDs using IV-VI compound semiconductors has been partially successful [29]. However, the problem of operating lifetime needs to be solved and this leaves the field open to III-V semiconductors. Blue InGaN LEDs with efficiencies around 5 to 10% developed by Nichia Chemical Company in Japan (1994/1995) [55, 56, 57] led to the development of large outdoor full colour displays [43] and opened up other display possibilities, such as traffic lights and white light sources. Solid state white light emitting devices are more durable with less power consumption than incandescent bulbs or fluorescent lamps. More exciting is that a recent report on a high brightness GaN based blue LED showed the quantum efficiency approaching 38% [http//www.compoundsemiconductor.net].

- Short Wavelength Laser Diode (LD)
  The long-sought blue LD now shows considerable promise. Several reports have appeared which describe room temperature pulsed operation of short wavelength LDs [2, 58, 59, 60, 61, 62]. Semiconductor LDs have a wide range use from optical communication systems to compact disk (CD) players. The shorter wavelength means that the light can be focused more sharply, which would increase the storage capacity of optical disks. Digital versatile disks (DVDs), which entered production in 1996, rely on red wavelength aluminium indium gallium phosphide (AlInGaP) semiconductor lasers and have a data capacity of about 4.7 gigabytes. In contrast, CDs which use infrared aluminium gallium arsenide (AlGaAs) laser diodes have a data capacity of about 0.65 gigabytes. By using the violet wavelength of InGaN-based compound semiconductors, the capacity can be increased to more than 15 gigabytes. The violet InGaN may also improve the performance of laser printers and undersea optical communication.

- GaN applications in electronics devices are suitable for high power and high temperature devices. For example heterostructure field effect transistors (FETs), heterojunction bipolar transistors (HBTs), metal oxide semiconductor field effect transistors (MOSFETs) and diode rectifiers have all been realised in the AlGaInN system with promising high temperature (greater than 300 °C) and high voltage performance [68].

- Furthermore, a recent report on GaN has demonstrated potential for micro-electronic-mechanical systems (MEMs), such as cantilevers [81]. This is because GaN and its based material have tough, high piezoelectric, optically transparent properties, and the possibilities of integration with optical and electronic devices.

1.2 Properties and Related Issues of GaN

1.2.1 Crystal Structure

GaN crystallises mainly under wurtzite structure in the ambient conditions, and thermodynamically stable structure for bulk GaN, has lattice parameters that:
$a_0 = 3.1892 \pm 0.0009$ Å
$c_0 = 5.1850 \pm 0.0005$ Å
$c_0/a_0 = 1.6258 \pm 0.0006$
(from the Data Review edited by Edgar, 1994 [24]).

Figure 1.1 shows the hexagonal wurtzite structure of GaN [53]. As a diamond structure, each atom has tetrahedral coordination of the nearest neighbours. The spread in values of the lattice parameters represents the sample-to-sample carrier densities, lattice mismatch, stoichiometry, strain, etc, as well as experimental uncertainties.

Wurtzite films tend to grow two-dimensionally from a large number of nucleation sites, resulting in columnar growth. GaN wurtzite structure has 2 formular units per unit cell (4 atoms per cell) and a molecular weight of 83.728 g/mol.

1.2.2 Electronic Band Structure

One of the most important properties of GaN is its direct band gap allowing efficient light emission and lasers. The band structure of GaN in figure 1.2 is similar to direct band gap zincblende semiconductors such as GaAs, but there are significant differences. One of the differences is that the valence band degeneracy is lifted in GaN by the crystal field interaction, and consequently there are three band gap excitons, usually labelled A, B, C excitons. The effective mass approximation has very limited use for the GaN valence bands, since valence bands in GaN are highly non-parabolic, while the effective mass approximation is very useful in GaAs and other III-V semiconductors. Strain has less dramatic effect on the valence band dispersion in GaN than in for example GaAs. This is due to the fact that the hexagonal crystal with crystal field splitting $\triangle_{cr}$ in the wurtzite structure can be interpreted as an internally strained cubic structure. In this sense, the wurtzite structure acts like a pre-strained cubic crystal. Therefore, the effects of quantum well confinement and strain on the GaN valence band structure is much less dramatic than in GaAs and related III-V structures. The band gap of wurtzite (hexagonal) α-GaN is higher than that of zincblende (cubic) β-GaN.

Most important for light emitting diodes and lasers based on GaN is direct fundamental optical transition at or near the Γ_{point} (k=0). This transition is between the uppermost valence band states and the lowest conduction band minimum. The conduction band at Γ_7 has s-character. The valence band is characterised by strongly coupled Γ_9, upper Γ_7, and lower Γ_7 levels, which are related to the Γ_8 and Γ_7 levels of zincblende crystals, split by the wurtzite crystal field. The holes (and associated excitons) in these three valence bands are conventionally called A, B, C type holes or excitons, as shown in figure 1.2.

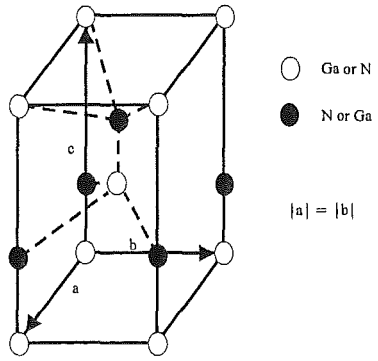

Figure 1.1: GaN Crystal Structure

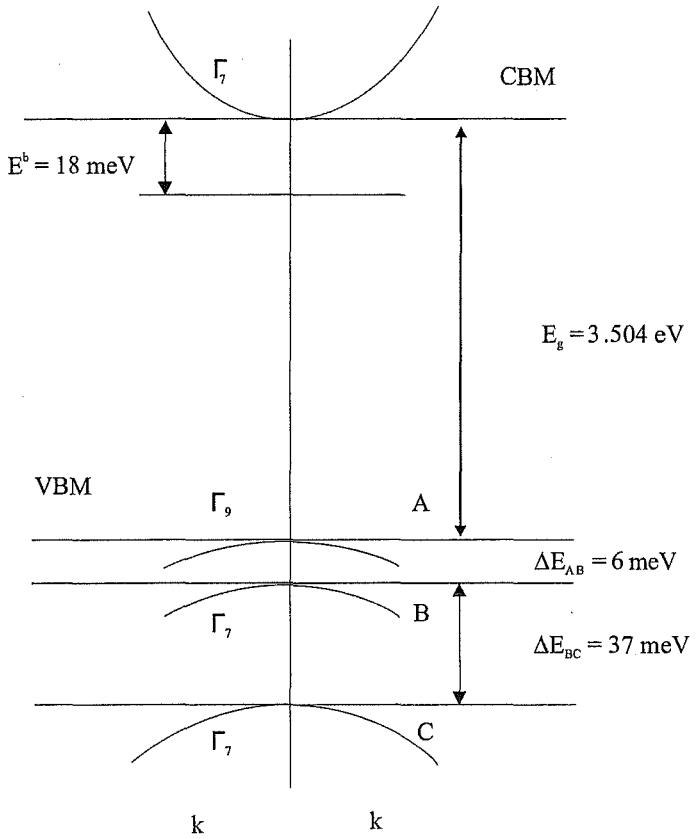

Figure 1.2: GaN Band Structure [14, 23, 27, 48].

There are still substantial variations between band gap energies and splitting energies determined or predicted by different experimental or theoretical methods. It means there is a necessity for a lot more electronic band structure work to obtain a more complete and more reliable set of band parameters for device design.

1.2.3 Crystal Growth

Common epitaxial techniques used for growing nitride semiconductors are Halide Vapour Phase Epitaxy (HVPE), Metal Organic Vapour Phase Epitaxy (MOVPE), Molecular Beam Epitaxy (MBE).

- Hallide Vapour Phase Epitaxy (HVPE)
  III-V semiconductor devices have always depended on the epitaxial growth of high-quality thin films on modest substrate material. Growing bulk crystals of III-V semiconductor suffered from problems with stoichiometry. In the 1960s GaAs technology was established largely based on the growth of epitaxial films on bulk GaAs substrates, the process employed being chloride vapour phase epitaxy. HCl gas was passed over a heated boat containing liquid Ga forming GaCl vapour which was transported in a stream of hydrogen, together with a separately injected flow of $AsCl_3$, over a heated GaAs substrate. The chloride interacted at the substrate surface to form a deposited film of solid GaAs, leaving waste products in the form of Cl_2 and HCl gases. Typical growth temperature was 800 °C and growth rates of order $10\mu m\,h^{-1}$. Stoichiometry could be controlled by adjusting the Ga boat temperature and the $AsCl_3$ flow rate. In the early 1970s attempts were made to obtain crystalline films of GaN, and ammonia was used as the source of nitrogen. NH_3 is a more stable molecule than $AsCl_3$, and therefore required higher growth temperature, typically 1000-1100 °C, but other features of the method were similar, apart from the use of He as the carrier gas [33]. The process took place in a quartz furnace tube, Ga was contained in an Al_2O_3 boat and the sapphire substrates mounted downstream. Growth rates varied from about 1 to about 50 $\mu m\,h^{-1}$ according to the position of the substrate along the tube axis. Background doping levels were typically $n = 10^{18}$ to 10^{19} cm^{-3}.

- Metal Organic Vapour Phase Epitaxy (MOVPE)
  MOVPE is a development of chloride VPE, but employing metal-organic compounds to transport the group III elements, and hydrides to transport group V elements. The growth of GaN by MOVPE was first reported by Manasevit *et al* [41], but in this early work films suffered from poor morphology and frequently cracked after growth. Background carrier densities were also high, usually being greater than 10^{18} cm^{-3}. It was not until the mid 1980s when Amano *et al* [3, 5] demonstrated the use of a thin AlN buffer layer that smooth, crack-free films could be produced. After heating

the substrate to high temperatures in a hydrogen ambient, the AlN layer was deposited at about 600 °C, then the temperature was raised to 1040 °C in order to grow the GaN film. Film quality was much improved by a reduction in the fluctuation in crystal orientation of the subgrain boundaries in the GaN film. The authors suggested that the buffer layer provided a high density of nucleation sites, with a smaller range of misorientations with respect to the substrate, and that it promoted the subsequent lateral growth of GaN due to a reduction in interfacial energy between the substrate and the epitaxial film.

- Molecular Beam Epitaxy (MBE)
  MBE was developed during the 1970s for the growth of III-V compound semiconductors, initially GaAs and AlGaAs, though gradually applied to many other material system such as GaInAsP, AlGaInAs, AlGaInP, CdHgTe, CdZnMgSSe, Si and Si/Ge. Its success depends on the fact that growth takes place in an all stainless steel ultrahigh vacuum vessel with background pressure in the range 10^{-10} to 10^{-11} Torr. To ensure high purity conditions and the precise control of composition inherent in the use of molecular beams of atoms, switches that are on and off almost instantaneously by mechanical shutters are used. The ability to change composition within the space of a single monolayer of material and the availability of an ideal in-situ monitoring technique in the form of reflection high-energy electron diffraction (RHEED) gives MBE a unique capability in this field.

  No other growth method allows the accurate monitoring of the surface structure of the growing film, nor the ability, literally, to count monolayers as they are deposited. MBE growth is characterised by growth temperatures typically in the range 400-800 °C, (Ga tends to re-evaporate at higher temperatures) and this, because molecular nitrogen is almost totally inert at these temperatures, implies the need for a source of active nitrogen. Three approaches have been employed based on RF plasma activation of N_2, microwave cyclotron resonance excitation of N_2 (the so-called ECR source) or thermal cracking of ammonia directly on the substrate. The growth rate up to 1 $\mu m\,h^{-1}$ has been developed [90], although causing difficulties with ammonia attack on the UHV pumping system. Another difficulty suffered by most MBE growers when growing nitrides is the inability to observe RHEED oscillations, which implies failure to achieve two-dimensional growth (the key to high-quality film growth in other materials).

  The pioneering work in MBE growth of nitrides was carried out by Yoshida *et al* [91, 92, 93, 94], who demonstrated the growth of AlGaN over the whole composition range and used cathodoluminescence to map the band gap composition relationship. They demonstrated the value of an AlN buffer layer in improving the quality of GaN films grown on (0001) sapphire and produced the first AlN/GaN heterostructures.

A key limiting issue for the growth of GaN has been the lack of an ideal substrate, since GaN substrates are not readily available, and other semiconductors have larger lattice mismatches. In most work, the GaN thin film has been grown on a sapphire or SiC substrate. For sapphire $a_0 = 4.758$Å, $c_0 = 12.991$Å and for 6H-SiC $a_0 = 3.08$Å, $c_0 = 15.12$Å.

1.3 The Aims of the Project

The University of Canterbury programme on GaN project is to use Photoluminescence (PL), Photoconductivity (PC), electrical measurements and microscopy to characterise the changes induced by Reactive Ion Etching (RIE). The goal is to understand and minimise the mechanisms of RIE induced damage. RIE induces defects in semiconductor materials. These defects can serve as local non-radiant recombination centres for electron-hole pairs, affecting the radiant lifetimes and luminescence efficiencies of optical properties of the semiconductors. A study of RIE damage effect on optical properties of GaN is important as this semiconductor is the leading material for blue light emitting devices and high temperature electronics. In particular this study will investigate:

1. The changes in GaN optical properties as a function of etching DC bias voltage. Our preliminary results show two regimes where increasing voltage can either increase or stabilise optical damage. This needs additional study to find out why some material belongs to one regime and not the other.

2. The changes in GaN optical properties as a function of etching gas used. Previous work showed that etching with different gases of GaN grown on sapphire substrate resulted in increased band edge emission intensity and a shift to higher energy of the peak position. On the other hand, GaN grown on SiC gave opposite results.

3. The influences of annealing in vacuum, hydrogen and nitrogen ambient on the optical properties of etched GaN by Ar and SF_6 gases.

1.4 Chapter Summary

- **Chapter I Introduction**
  briefly introduces GaN and related issues:crystal and electronic band structure, the growth of GaN, and device applications. Also mentions about motives and aims of this project.

- **Chapter II Background Theory**
  gives an overview on background theory of optical processes in GaN and plasma etching in general.

- **Chapter III Experimental Technique**
  describes experimental techniques of Photoluminescence, Reactive Ion Etching, Atomic Force Microscopy, and Annealing. Also instrument calibration is described here.

- **Chapter IV Photoluminescence of Amorphous GaN**
  shows and briefly discusses photoluminescence results of amorphous GaN.

- **Chapter V Photoluminescence of Polycrystalline GaN**
  shows and briefly discusses photoluminescence results of polycrystalline GaN.

- **Chapter VI Etching DC Bias Voltage Dependence Using Ar and SF_6 Gas**
  shows and discusses the changes on GaN optical properties and surface morphology as a function of etching voltage, using Ar and SF_6 as the etching gas.

- **Chapter VII Effects of Annealing on Optical Properties of GaN**
  shows and discusses the influences of annealing in vacuum, H_2 and N_2 ambient on the optical properties of Ar- and SF_6-etched GaN.

- **Chapter VIII Conclusions and Recommended Further Work**
  gives the conclusions and recommends further work of this project.

Chapter 2

Theory Overview

2.1 Optical Processes in Nitride Semiconductors

The general reference for this section is chapter 10 of Nitride Semiconductors and Devices of Hadis Morkoc [51].

2.1.1 Absorption and Emission

The important optical processes in semiconductors which directly influence device operation are absorption and emission of photons. Absorption and emission spectroscopy can be employed to extract useful information about the semiconductor, particularly a direct-bandgap semiconductor such as GaN. Simply saying, the semiconductor is transparent to below the gap radiation while absorbing above the gap radiation.

Light emission which is termed **photoluminescence** is a result of incident photon absorption, electron-hole pair generation and a photon of different wavelength emission. The incident photons, when absorbed, excite electrons from the valence band into the conduction band through momentum-conserving processes since the photon momentum is negligible. The electrons and holes thermalize to the bottom of their respective bands via phonon emission before recombining across the bandgap and emitting photons of the bandgap energy. The recombination resulting in photon emission is **radiative recombination**. It can be **spontaneous emission** or **stimulated emission** when an electromagnetic field of appropriate frequency is involved, such as that found in a semiconductor laser. That which does not produce photons is **non-radiative recombination** in which the energy is exchanged with the lattice as heat through phonons. In a direct-bandgap semiconductor, non-radiative recombination is enhanced due to defects.

The spatial rate of change of the intensity at the same point is given by:

$$dI/dx = -\alpha I \tag{2.1}$$

with I represents the optical intensity at point x in a semiconductor, and α is the absorption coefficient with a unit of inverse cm.

The spontaneous emission spectrum can be calculated from:

$$I(h\nu) = \frac{8\pi n^2 h\nu^3}{c^2}\alpha(h\nu)e^{\frac{F_n - F_p}{kT}}e^{\frac{-h\nu}{kT}} \tag{2.2}$$

using:

- dielectric function of absorptive medium
- the power of an electromagnetic field propagating along the x direction
- Einstein's A and B coefficients for a two-level system and a system at thermal equilibrium at the temperature T [25, 36, 88, 95],
- semiconductor with parabolic bands
- assumption that the recombination and generation rates are equal at thermal equilibrium, and simplification of the probabilities to a non-degenerate semiconductor (the assumption can be used provided that the exciting light intensity is very low for PL experiment).

F_n and F_p are the quasi Fermi levels for electrons and holes, respectively.

The spectral emission response is proportional to the product of the absorption coefficient and $e^{\frac{-h\nu}{kT}}$. On the lower-energy side, the emission spectrum has the spectral dependence of the absorption coefficient and above the bandgap, it roughly declines exponentially.

2.1.2 Band to Band Transition

The average lifetime of carriers before radiative recombination is called the **radiative lifetime** τ_r.In addition to the radiative processes, there are non-radiative processes in semiconductors because of imperfections which act as non-radiative centres. For a semiconductor containing non-radiative traps, in an experiment such as time-dependent PL, the decay rate can be expressed as:

$$\frac{1}{\tau_{\text{tot}}} = \frac{1}{\tau_{\text{rad}}} + \frac{1}{\tau_{\text{nonrad}}} \tag{2.3}$$

In a PL experiment, the emission lineshape is determined by the joint density of states, and the probability of participating states being available for recombination. The former has the form $(h\nu - E_g)^{1/2}$ and the latter $e^{\frac{-E}{kT}} = e^{\frac{-h\nu}{kT}}$. When the semiconductor is excited by the above bandgap photon radiation, the two lineshapes put together lead to a lineshape of the form:

$$(h\nu - E_g)^{1/2}e^{\frac{-h\nu}{kt}} \tag{2.4}$$

Lower-energy photons do not excite electrons into the conduction band.

2.1.3 Optical Transitions in GaN

Optical transitions in GaN can be grouped into two categories:

- Intrinsic transitions are those that are associated with semiconductors void of impurities and defects. Free excitons and their phonon replicas, and free to free transitions represent intrinsic transitions.
- Extrinsic transitions have their genesis in impurities and defects. The impurity bound excitons transitions involving impurities such as free-to-bound and bound-to-bound, and defects constitute extrinsic transitions.

Excitonic Transitions in GaN

When the charged centre concentration in semiconductors is sufficiently low, a free electron and a free hole can be attracted to one another through Coulombic attraction. An electron can orbit the hole, similar to the case of a hydrogen atom, called an **exciton**. At low temperatures and in high-quality samples with low donor and acceptor concentration as well as a low density of defect centres, the photo-excited carriers with opposite charge not only are attracted to one another, but also to neutral centres via a Van der Waals interaction. Since this additional attraction reduces the exciton binding energy, the neutral impurities are efficient in trapping excitons to form bound excitons as denoted by $\mathbf{D^0X}$ and $\mathbf{A^0X}$ for neutral donor and acceptor bound excitons. Excitons can also be bound to ionised donors and acceptors and are termed $\mathbf{D^+X}$ and $\mathbf{A^+X}$.
Using the hydrogenic model, the binding energy, or the ionisation energy of such a system is given by:

$$E_{\mathrm{x}} = \frac{m_r^* q^4}{2h^2\epsilon^2 n^2} \tag{2.5}$$

where the quantities have their usual meanings, m_r^* is the relative mass and n is an integer with $n = 1$ corresponding to the ground state of the exciton.

- **Free Excitons**
  Excitons in GaN take on a special meaning in that the valence band is not degenerate due to the crystal field and spin-orbit interactions at the Γ_{point}. The three emerging states are termed Γ_9^v, upper Γ_7^v, and lower Γ_7^v. The related free-exciton transitions from the conduction band to those three valence bands are termed **A**,**B**, and **C** excitons. They are:

  A $\equiv \Gamma_7^c \rightarrow \Gamma_9^v$ **(heavy hole state)**

  B $\equiv \Gamma_7^c \rightarrow \Gamma_7^v$ the upper one **(light hole state)**

C $\equiv \Gamma_7^c \rightarrow \Gamma_7^v$ the lower one **(crystal-field split band)**
In an ideal wurzite crystal, i.e strain free, they have the following symmetries: excitons associated with all three bands are allowed in the α **polarisation** ($\overline{E} \perp$ c and $k \parallel$ c). In the σ **polarisation** ($\overline{E} \perp$ c and $k \perp$ c), A and B excitons are observable with the C exciton being very weak. In the π **polarisation** ($\overline{E} \parallel$ c and $k \perp$ c), A and C excitons are observable with the B exciton being weak. Here $\overline{E}$ and k are the electric field and momentum vectors, and c denotes the c-axis of the crystal. GaN samples on SiC, which are under symmetry-reducing compressive strain, exhibit a strong C exciton in σ polarisation. Each of these three excitonic states are expected to have fine structure due to an exciton polariton longitudinal transverse splitting which is on the order of 1-2 meV.

An observation of only the intrinsic transitions and the excited states of the A and B band excitons in GaN was reported by Reynold *et al* [74] and Smith *et al* [80]. This paves the way for the determination of exciton binding energies, exciton Bohr radii, the dielectric constant, and with the aid of the quasi-cubic model, the spin-orbit and crystal field parameters, Δ_{so} and Δ_{cf}. The absolute energy values of these transitions depend on the local strain and thus do not represent a fully relaxed GaN. Assuming hydrogen-like excitons, the A and B exciton binding energies can be deduced to be about 20 meV and 22 meV. By noting several of the excited states and using Elliot's theory [26] relating the excited state of the excitonic transitions as:

$$E_n - E_m = -E_b\left(\frac{1}{n^2} - \frac{1}{m^2}\right) \tag{2.6}$$

where n and m are integers, and E_b denotes the binding energy of the exciton in question, one can get the exciton binding energy, and was deduced to be 23 meV.

Assuming that $E_{1,2}$ and $E_{2,3}$ can be represented by the difference in energy between the A and B bandgaps, and B and C exciton bandgaps, further assuming that the binding energy of B and C excitons are equal, then the spin orbit parameter $\Delta_{so} = 17.3$ meV and crystal field parameter $\Delta_{cf} = 24.7$ meV.

Using an electron mass of $m_n^* = 0.22m_o$ and a hole mass of $m_p^* = 0.8m_o$ combined with the A exciton binding energy, a dielectric constant of $\epsilon = 10.7$ was obtained.

Using the expression:

$$a_r = \frac{4\pi\epsilon\hbar^2}{m_r^* q^2} \tag{2.7}$$

the Bohr radii a_r of the A and B excitons were determined to be about 31 and 28 Å, respectively.

Since GaN with a low background carriers concentration is not yet available, fundamental optical studies have been done in epitaxial layers which unfortunately were strained to varying degrees due the mismatch of the thermal expansion coefficients between the layer and the substrate on which it is deposited. To circumvent this complication, thick and presumably unstrained GaN layers on sapphire have been used to determine the energies of intrinsic and extrinsic transitions in GaN. However, even the thick films, tens of micrometers, on sapphire may not be completely strain free. Evidence for the residual strain is provided by curling of these samples when the sapphire substrates are thinned. Monemar *et al* [50], who have examined numerous thin and thick layers on various substrates including homoepitaxial layers on GaN substrates, reported in [37], concluded that the A, B and C exciton lines in GaN relaxed to an accuracy of ± 2 meV are 3.478, 3.484, and 3.502 eV, respectively, at 2 K.

The improved linewidths in GaN grown by MOCVD lead to the resolution of three transitions near the donor bound exciton region. A typical MBE-grown sample on a GaN substrate shows two sharp neutral donor bound exciton (D^0X) lines [6], most likely associated with two different donors at 3.4709 and 3.4718 eV. These two levels could also be attributed to spin splitting of the same donor. The sample also exhibits an acceptor bound exciton (A^0X) at 3.4663 eV and the A and B free exciton transitions at 3.4785 and 3.483 eV, respectively.

The transition energies are dependent on the substrate employed due to the expansion coefficient mismatch. And these energies vary from one sample to the next, even on the same type of substrate and growth temperature, presumably due to variations in the local structure, such as inhomogeneities. Due to the relatively larger thermal expansion coefficient of sapphire, GaN films on that substrate undergo an in-plane compressive strain, and the reverse occurs for the out of plane strain. In contrast, the GaN films on SiC are under an in-plane tensile strain [49, 50, 77].

The temperature dependence of the excitonic resonances is also dependent on the particular sample and the local strain [77, 87]. The reduced deviation with increasing temperature has been attributed to partial relaxation. The bound exciton transitions decrease in intensity rapidly as the temperature increases, while the free exciton transitions are observable even at room temperature. This is indicative of small localisation energies associated with the bound exciton. Meyer [44] followed the thermally activated dissociation of bound excitons and described the dependence on temperature with two activation energies. The above band gap excitation creates free excitons which can localise at impurity sites. As the temperature is elevated, impurities such as donors ionise with an interplay with localisation, which causes the bound excitons to decay as the temperature is increased and eventually completely dissociate leaving the free exciton A as the dominant transition.

- **Bound Exciton**
  Excitons could be bound to neutral and ionised donors and acceptors. The common donors and acceptors used to dope GaN are Mg and Si respectively. In GaN, the neutral donor bound exciton D^0X is often dominant , because of the presence of donors, either due to impurities and/or nitrogen vacancies, and its efficient radiation characteristics. In samples containing acceptors, the acceptor bound exciton A^0X is observed. The ionised donor-bound exciton has also been seen [76].The identification was confirmed by the energy ordering of this particular transition with respect to the neutral donor bound exciton. Additional confirmation was obtained by observing the increased intensity of the peak as the donor concentration was increased, a task accomplished by irradiating the sample with high energy electrons which create donor like nitrogen vacancies. Excitons bound to neutral acceptor A^0X can be found in samples doped with p-type impurities, it means acceptor sites are present.

  The localisation energy of bound excitons can be utilised to extract binding-energy information through Hayne's rule [31] which has been successfully applied to Si. Doing so for GaN led to the localisation energy being about 10% of the binding energy for acceptor-bound excitons and 20% for the donor-bound excitons [44]. The localisation energy for donor bound excitons is about 6-7 meV, whereas that for the acceptor Mg is about 19 meV. Note that getting the impurity binding energies from the exciton localisation energy is at best an indirect measurement. Doing so, for acceptors lead to binding energies of about 120 meV. In fact, there is no other supporting evidence for acceptors with such low binding energies. Other methods such as the Donor Acceptor (DA) transitions and the thermal ionisation methods with proper screening should be utilised collectively to get at the binding energies of donors and acceptors [42, 44].

2.1.4 Free to Bound Transitions

At low temperatures the carriers are frozen on the impurities because the thermal energy required for their ionisation is no longer available. In a PL experiment, electrons excited into the conduction band can recombine radiatively with holes frozen on the acceptors at the acceptor energy levels. Thus, the resultant emitted photon energy is the difference between the conduction band and acceptor level or the bandgap minus the acceptor binding energy, $E_g - E_A$. These transitions involving free carriers and bound charges constitute **free to bound transitions**. If the impurity concentration is increased, acceptors become closer to one another and their wave functions begin to overlap with an associated broadening of the level which is called the **impurity band**. With continued increase in impurity concentration, the impurity band may widen so much so that it would overlap with the nearest band, the conduction band in the case of donors and the valence band in the case of acceptors. As a result, the carriers are freed and this delocalisation is called the **Mott transition** which begins to be observed even before

such overlap because the impurity band is half filled owing to spin degeneracy. The higher portion of the PL spectrum deviates from the simple exponential by spreading out to higher and lower energies, and also changing because of bandgap renormalisation (**red shift**). Deep impurities and defects causing radiative decay of electrons to their ground states can be probed with PL.

2.1.5 Donor Acceptor Transitions

Though some semiconductors represent the purest material available, all contain both donors and acceptors, and are known by the term compensated. The nomenclature results from acceptors capturing electrons from the donor states. Consequently, a **compensated semiconductor** contains both ionised donors and acceptors. Carriers generated by optical excitation can be trapped at the donor and acceptor sites causing them to be neutral. In returning towards equilibrium, some electrons on the neutral donor sites will recombine with holes on the neutral acceptors, a process termed **Donor Acceptor Pair (DAP) transition.** The DAP transition energy is given by

$$h\nu = E_g - E_D - E_A + \frac{q^2}{\epsilon R} \tag{2.8}$$

where E_D and E_A are the donor and acceptor binding energies, and the last term on the right hand side is the Coulomb interaction contribution resulting from the interaction of ionised donors and acceptors. R is the distance between such donors and acceptors, and is assumed much larger than the lattice constant. This is easily satisfied in semiconductors that are not highly doped. In high quality samples, many DAP transitions can be observed for many values of R. The Coulomb interaction causes the energy of the final state to be lowered.

In GaN, free and donor bound excitons are prevalent as the samples are naturally n-type. As the p doping, i.e. with Mg, increases, the PL spectrum reveals the acceptor bound exciton (A^0X). With increasing Mg concentration, the neutral Donor Acceptor (D^0 - A^0)transition begins to appear whose strength shows a nearly monotonic increase at around 3.25-3.26 eV with its LO phonon replicas relative to the exciton emission at 1.7 K [35].

In additon to the peak position, further confirmation for this identification is provided by a blue shift at a rate of about 2-3 meV per decade of intensity as the excitation intensity is increased [35]. The (D^0 - A^0) peak position can not be used unequivocally to determine the acceptor binding energy, as it depends on the average strength of the Coulomb interaction between recombining pairs which, in turn, is a function of the doping level, and the non radiative recombination rate.

2.1.6 Defect Related Transition

A number of theoretical calculations have been performed on the native defects in GaN [8, 22, 34, 47, 63, 84]. While none of these theories agree with one another fully, many of them suggest that a nitrogen vacancy V_N produces a single donor and is responsible for the n-type behavior in undoped GaN. Furthermore, if it is a simple donor with its s-like deep level in the gap just below the conduction band edge, the nitrogen vacancy would provide a natural explanation of the 0.2 eV feature in the Tansley-Foley optical absorption data [85]. The predominance of donor bound excitons discussed above and the n-type background in GaN films are consistent with the N vacancy premise [73]. Many defects caused by vacancies, antisites and interstitials are possible in GaN [8, 85]. Some of these defects appear in luminescence experiments where there are two prominent transitions which are discussed below. One transition appears at about 2.2 eV, proverbially referred to as the **yellow luminescence**, and the other at about 2.9 eV, the **blue emission**.

- **Yellow Luminescence**
  Many wide bandgap semiconductors, including GaN, suffer from emission near the midgap, which is yellow-green in the case of GaN. There are two arguments for the origin of this transition. One suggests transitions from shallow donors to deep acceptors, while the other evokes transitions from deep donor states to shallow acceptor states.

  Hoffmann *et al* [32] suggested that the yellow band in GaN results from the recombination between a shallow donor and a deep level. They proposed that the deep level may be a double donor, although an acceptor cannot be ruled out.

  Reynolds *et al* [75] reported on the similarities between the green luminescence band in ZnO and the yellow luminescence band in GaN, and drew a conclusion that the origin of these bands may be the same. That is from the recombination between a shallow donor level and a deep level.

  The excitation source for PL measurements creates hot electrons in the conduction band. Peaks in the PL emission band occur whenever the energy of the PL peak coincides with the sum of the energies of the donor level plus an integral multiple of a principal optical phonon energy. At adjacent energy values, an equilibrium number of electrons will arrive at the donor level and thus take part in the recombination with the deep level. The deep level will also have accompanying excited states due to an interaction with local vibrational modes as well as lattice modes. It would be expected that the dominant transition would occur between the shallow donor and the ground state of the deep level. Transitions will also occur between the shallow donor and the excited states of the deep level, with reduced oscillator strengths. This model agrees with that proposed by Hoffmann *et al* [32] for GaN and has the added advantage that it can explain the broad nature of the emission band. The modulated energy structure does not occur on the low energy side of the green band. This would be expected

since the phonons that are involved in cascading hot electrons from the conduction band to the donor level are not involved with the low energy emission. This emission is accounted for by the recombination of donor electrons with excited states of the deep level. The deep level may be a complex center whose excited states consist of both local vibrational modes and lattice modes. These excited states are so distributed that they do not produce a resovable modulated structure on the low energy side of the green band.

2.2 Dry Etching

2.2.1 Introduction

Dry etching is a method by which a solid state surface is etched in the gas phase, physically by ion bombardment, chemically by a chemical reaction with a reactive species at the surface, or combined physical and chemical mechanisms.
The most common dry etching methods are:
CAIBE = Chemically Assisted Ion Beam Etching
RIBE = Reactive Ion Beam Etching
MERIE = Magnetically Enhanced Reactive Ion Etching
MIE = Magnetically enhanced Ion Etching
PE = Plasma Etching
RIE = Reactive Ion Etching
PE and RIE are the most widely used techniques in IC manufacture and micromachining. RIE method was used in this project. RIE has a good selectivity,could work on chemical or physical etch mechanism, isotropic or anisotropic profile, and the pressure range of 10^{-3} to 10^{-1} Torr [78, 79].

The general reference for this section is Fundamentals of Microfabrication [40], chapter 2.

2.2.2 Physics of DC Plasma

The simplest plasma reactor consists of opposed parallel plate electrodes in a chamber maintainable at low pressure, typically ranging from 0.001 to 1 Torr. The electrical potentials established in the reaction chamber filled with an inert gas such as argon at a reduced pressure determine the energy of ions and electrons striking the surfaces immersed in the discharge. Electrical breakdown of the argon gas in this reactor will occur when electrons, accelerated in the existing field, transfer an amount of kinetic energy greater than the argon ionisation potential (i.e. 15.7 eV) to the argon neutrals. Such energetic collisions generate a second free electron and a positive ion for each successful strike. Both free electrons reenergize, creating an avalanche of ions and electrons that results in a gas breakdown emitting a characteristic glow. Avalanching requires the ionisation of 10 to 20 gas molecules by one secondary electron. At the start of a sustained gas

breakdown, a current begins flowing and the voltage between the two electrodes drops. The discharge current builds up to the point where the voltage drop across a current limiting resistor is equal to the difference between the supply voltage and the electrode potential different. To sustain a plasma, a mechanism to generate additional free electrons must exist after the plasma-generating electrons have been captured at the positively charged anode. Plasma-sustaining electrons are generated at the cathode which emits secondary electrons (Auger electrons) when struck by ions. The continuous generation of those 'new' electrons prompts a sustained current and a stable plasma glow. It is easy to understand why plate (electrode) separation and gas pressure are critical. Plates positioned too closely prevent ionising collisions, but plates separated too far cause too many inelastic collisions of ions which lose energy. Once equilibrium is reached, the glow region of the plasma, being a good electrical conductor, hardly sustains a field and its potential is almost constant.

The permanent positive charge of a plasma with respect to the electrodes is a striking characteristic and is a result of the random motion of the electrons and ions. The positive charge of a plasma can be understood from kinetic theory which predicts that for a random velocity distribution the flux of ions, j_i, and electrons, j_e, upon a surface is given by:

$$j_{i,e} = \frac{n_{i,e} < \nu_{i,e} >}{4} \tag{2.9}$$

where n and $< \nu >$ are the densities and average velocities, respectively. Because ions are heavier than electrons (typically 4,000 to 100,000 times as heavy), the average velocity of electrons is larger. Consequently, the electron flux is larger than ion flux, and the plasma loses electrons to the walls, thereby acquiring a positive charge. The bombarding energy of ions is proportional to the potential difference between the plasma potential and the surface being struck by ions.

The degree of ionisation in a plasma depends on a balance between the rate of ionisation and the rate at which particles are lost by volume recombination and by losses to the walls of the apparatus. Wall losses generally dominate over volume recombination. Accordingly, the occurrence of a breakdown in a given apparatus depends on the gas pressure (particle density), the type of gas, electric field strength (electron velocity), and on surface-to-volume ratio of the plasma.

All glow discharge are non-equilibrium as the average electron energy ($< v_e >= kT_e$) is considerably higher than the average ion energy ($< v_i >= kT_i$), so a discharge or plasma can not be described adequately by one single temperature ($T_{\text{electron}}/T_{\text{gas}} = 10$ to 100). High temperature electrons in a low temperature gas occur due to the small mass of electrons (m_e) compared to ions and neutrals. In collisions between electrons and argon atoms (M_A), the ratio m_e/M_A is only 1.3×10^{-5}. Thus, in collisions, electrons have a poor energy transfer and stay warmer longer than the heavier ions and neutrals. Electrons can attain a high average energy, often many electron volts (equivalent to tens of thousands of de-

grees above the gas temperature), permitting electron-molecule collisions to excite high temperature type reactions which form free radicals in a low temperature neutral gas. Generating the same reactive species without a plasma would require temperatures in the $\sim 10^3$ to 10^4 K range, destroying resists and damaging most inorganic films.

A plasma typically is weakly ionised: the number of ions is very small compared to the number of reactive neutrals such as radicals. The ratio between ionised and neutral gas species in a glow discharge plasma is of the order of 10^{-6} to 10^{-4}. This fact is crucial in understanding which entities are responsible for the actual etching of a substrate placed in a glow discharge.

Of the different dry etching techniques, the choice of technique depends on the efficiency or 'strength' of a particular plasma evaluated by parameters such as:

- the average electron energy, $< v_e >$, also called electron temperature, i.e. $< v_e >= kT_e$(e.g.1 $\rightarrow$ 10eV)
- the average ion energy, i.e. $< v_i >= kT_i$(e.g. 0.04 eV)
- the electron density (e.g. between 10^9 and 10^{12} cm^{-3})
- plasma ion density (e.g. 10^8 to 10^{12} cm^{-3})
- neutral species density (e.g. 10^{15} to 10^{16} cm^{-3})
- the ion current density (e.g. 1 to 10 mA/cm^2)

A quantity of particular use in characterising a plasma's average electron or ion energy is the ratio of the electrical field to the pressure:

$$kT_{i,e} \sim \frac{E}{P} \tag{2.10}$$

With increasing field strength, the velocity of free electrons or ions increases because of acceleration by the field ($\sim E$) but velocity is lost by inelastic collisions. Since an increases in pressure decreases the electron or ion mean free path, there being more collisions, the electrons or ion energy decreases with increasing pressure ($\sim \frac{1}{P}$).

Using such a described DC plasma for dry etching, in one of the arrangements the substrate to be etched is placed on the cathode (target) in an argon plasma, while sufficiently energetic ions (between 200 to 1000 eV) induce physical etching, ie, ion etching or sputtering in which atoms are billiard ball-wise ejected from the bombarded substrate. Externally applied voltages concentrate across the cathode plasma sheath and ions are accelerated in that field before hitting the cathode. Each ion will collide numerous times with other gas species before transversing the plasma sheath as the sheath thickness is larger than the mean free path. As

a result of these collisions, the ions lose a lot of their energy and move across the sheath with a drift velocity that is less than the free fall velocity. But these vertical velocities are still very large compared to the random thermal velocities discussed above. The resulting bombarding ion flux, j_i, is given by:

$$j_i = qn_i\mu_i E \tag{2.11}$$

With E, the electric field, n_i , the ion density, μ_i, the ion mobility, and q the charge. Reducing the pressure in the reactor increases the mean free path. Consequently, ions accelerated towards the cathode at lower pressure can gain more energy before a collision takes place. In an alternate mode, reactive species generated by the DC plasma may combine with the substrate to form volatile products that evaporate, chemically etching the substrate.

2.2.3 Physics of RF Plasmas

In an RF-generated plasma, a radio frequency voltage applied between the two electrodes causes the free electrons to oscillate and to collide with gas molecules leading to a sustainable plasma. RF-excited discharge can be sustained without relying on the emission of secondary electrons from the target. Electrons pick up enough energy during oscillation in an RF field to cause ionisation, thus sustaining the plasma at lower pressures than in a DC plasma. Another asset RF has over DC sputtering is that RF allows etching of dielectrics as well as metals.

In the simplest case of RF ion sputtering, the substrates to be etched are laid on the cathode (target) of a discharge reactor. The reactor consists of a grounded anode and powered cathode or target, enclosed in a low-pressure gas atmosphere. An RF plasma, formed at low gas pressure, again consists of positive cations, negative anions, radicals, vibrationally excited polyatomic species, and photons (the UV photons create the familiar plasma glow). As with a DC plasma, the neutral species greatly outnumber the electrons and ions; the degree of ionisation only being on the order of 10^{-4} to 10^{-6} for parallel plate gas discharges. The RF frequency typically employed is 13.56 MHz (a frequency chosen because of its non-interference with radio-transmitted signals). The RF power supply rates between 1 and 2 kW. With one of the two electrodes capacitively coupled to the RF generator, the capacitively coupled electrode automatically develops a negative DC bias and becomes the cathode with respect to the other electrode. This DC bias (also called **self-bias** V_{DC}) is induced by the plasma itself and is established as follows. When initiating as AC plasma arc, electrons, being more mobile than ions, charge up the capacitively coupled electrode; since no charge can be transferred over the capacitor, the electrode surface retains a negative DC bias.

The energy of charged particles bombarding the surface in a glow discharge is determined by three different potentials established in the reaction chamber: the plasma potential, V_p, ie the potential of the glow region; the self bias, V_{DC}; and

the bias on the capacitively coupled electrode, $(V_{RF})_{pp}$. The following analysis clarifies how these potentials relate to one another and how they contribute to dry etching. The voltage build-up, V_{DC}, on an insulating electrode by the electron flux (2.9) is given by:

$$V_{\mathrm{DC}} = \frac{kT_e}{2e} \ln\left(\frac{T_e m_i}{T_i m_e}\right) \tag{2.12}$$

where T_e and T_i are the electron and ion temperature defined by average energy of electrons and ions, and m_e and m_i are the electron and ion masses, respectively [10]. The electron loss creates and electric sheath field in front of any surface immersed in the plasma, counteracting further electron losses. This sheath or dark space also forms a narrow region between the conductive glow region and the cathode where most of the voltage is dropped as in the DC plasma case (the cathode being capacitively coupled acts effectively as an insulator for DC currents). The other electrode is grounded and conductive (no charge build-up and no voltage build-up) and automatically becomes the anode with respect to the capacitively coupled electrode. The time average of the plasma potential, V_p, the DC cathode potential (self-bias potential), V_{DC}, and the peak-to-peak RF voltage $(V_{RF})_{pp}$, applied to the cathode are approximately related as:

$$2V_p = \frac{(V_{RF})_{pp}}{2} - \mid V_{\mathrm{DC}} \mid \tag{2.13}$$

Clearly the magnitude of the self-bias depends on the amplitude of the RF signal applied to the electrodes. In the RF discharge the time-averaged RF potential of the glow region, referred to as the plasma potential, V_p, is more significantly positive with respect to the grounded electrode than in the case of a DC plasma.

Positive argon ions from the plasma are extracted by the large field at the cathode and are sputtering that electrode at near normal incidence with energies ranging from a few to several electronvolts, depending on the plasma conditions and the chamber construction. One of the most important parameters determining the plasma condition is the total reactor pressure. As pressure is lowered below 0.05 to 0.1 Torr, the total ion energy, E_{max}, rises as both the self-bias voltage and the mean free path of the bombarding ions increases. Subsequently, ion-substrate bombardment energy rises sharply with decreasing pressure. The maximum energy of positive ions striking a substrate placed on the cathode is proportional to:

$$E_{\mathrm{max}} = e(\mid V_{\mathrm{DC}} \mid + V_p) = eV_{\mathrm{T}} \tag{2.14}$$

with $V_{\mathrm{T}} = \mid V_{\mathrm{DC}} \mid + V_p$, whereas the maximum energy for a substrate on the grounded electrode (ie the anode) is proportional to $E_{\mathrm{max}} = eV_p$.

The situation where the wafers are put on the cathode is referred to as 'reactive ion etching' or 'reactive sputter etching'.

The chamber construction, especially the ratio of anode to cathode area, influences the rates of V_T/V_p and, consequently, as calculated from equation (2.14),the energy of the sputtering ions on these respective electrodes. To deduce the influence of the geometry of the anode and cathode on dry etching, we compare the sheath voltages in front of the anode and cathode, using the Child-Langmuir equation. The equation expresses the relationship between the ion-current flux, j_i, the voltage drop, V, over the sheath thickness of the dark-space, d; and the mass of the current carrying ions, m_i. The relation can be deduced from equation (2.11) assuming the presence of a space-charge limited current:

$$j_i = \frac{KV^{3/2}}{\sqrt{m_i d^2}} \tag{2.15}$$

in which K is a constant [89]. The current density of the positive ions must be equal on both the anode and cathode, resulting in the following relation for the sheath-voltages:

$$\frac{V_T^{3/2}}{d_T^2} = \frac{V_p^{3/2}}{d_p^2} \tag{2.16}$$

The plasma behaves electrically as a diode (large blocking voltage drop towards the capacitively coupled cathode and small voltage drop on the anode/plasma interface) in parallel with the sheath capacitance. As soon as any electrode tends to become positive relative to the plasma, the current rises dramatically, causing the plasma to behave as if a diode were present in the equivalent electrical circuit of the plasma. Hence, a planar, parallel set-up also is called a diode set-up.

The dark spaces in a plasma are areas of limited conductivity and can be modeled as capacitors, ie:

$$C \approx \frac{A}{d} \tag{2.17}$$

The plasma potential is determined by the relative magnitudes of the sheath capacitance which in turn depend on the relative areas of anode and cathode. An RF voltage will split between two capacitances in series according to:

$$\frac{V_T}{V_p} = \frac{C_p}{C_T} \tag{2.18}$$

Using equations (2.17) and (2.18), we can write:

$$\frac{V_T}{V_p} = (\frac{A_p}{d_p})(\frac{d_T}{A_T}) \tag{2.19}$$

and substituting into equation (2.16), we obtain:

$$\frac{V_T}{V_p} = (\frac{A_p}{A_T})^4 = R^4 \tag{2.20}$$

where A_p is the anode area and A_T the cathode area. If there were two symmetric electrodes, both blocked capacitively, the plasma potential would be very large and sputtering would occur on both surfaces. If the area of the cathode were significantly smaller than the other areas in contact with the discharge, the plasma potential would be small and little sputtering would occur on the anode, whereas the cathode would sputter very effectively. In actual sputtering systems, the larger electrode consists of the entire sputtering chamber, creating a small dark space, whereas no sputtering takes place from these dark spaces.

Higher ion energies (V_T large), translate into lower etch selectivity and can be a cause of **device damage**. Consequently, a key feature for good **etch performance** is effective ionisation to turn out very high quantities of low energy ions and radicals at low pressures. In answer to this need, equipment builders have to come up with low-energy, high-density plasmas, for example, Magnetron's ICPs (inductively coupled plasmas) [18] and ECRs (electron cyclotron resonance) [78].

2.2.4 Device Damage and Etch Performance

Device damage comes in many 'flavours' including:

- alkali (sodium) and heavy metal contamination
- catastrophic dielectric breakdown
- current-induced oxide aging
- particulate contamination
- UV damage
- Temperature excursion which can activate metallurgical reactions
- 'Rogue' stripping processes which simply do not remove all the residue
- plasma-induced charges, surface damage, ion implantation

Etch performance is being judged in terms of etch rate, selectivity, uniformity (evenness across one wafer and from wafer to wafer), surface quality, reproducibility, residue, microloading effects, device damage, particle control, post-etch corrosion, and profile control. Selectivity as high as 40:1 might be required

in the future for ICs and even more for micromachines. It is generally believed that radiation damage of a plasma can be annealed out. In reality, very little is understood of the damage a plasma can do. The higher the etch rate, the better the wafer throughput. Good selectivity, uniformity, and profile control are more easily achieved at lower etch rates. Trenches of various depths are made in Si in the manufacture of MOS devices. Shallow trenches (0.5 to 1.5 μm) are used to aid in reducing the effects of lateral diffusion during processing and to make flat structures (planarisation). Deeper trenches (1.5 to 10 μm) are used to create structures that become capacitors and isolation regions in integrated circuits. For the shallowest trenches, photoresist is adequate as a mask. For deeper etching, a silicon dioxide mask may be needed. In micromachining one would like to obtain aspect ratios of 100 and beyond, so the degree of difficulty in masking keeps mounting. With aspect ratios above 2:1 or 2.5:1, the etching action at the bottom of a trench tends to slow down or stop altogether.

Chapter 3

Experimental Techniques

3.1 Photoluminescence

3.1.1 Photoluminescence Experiment

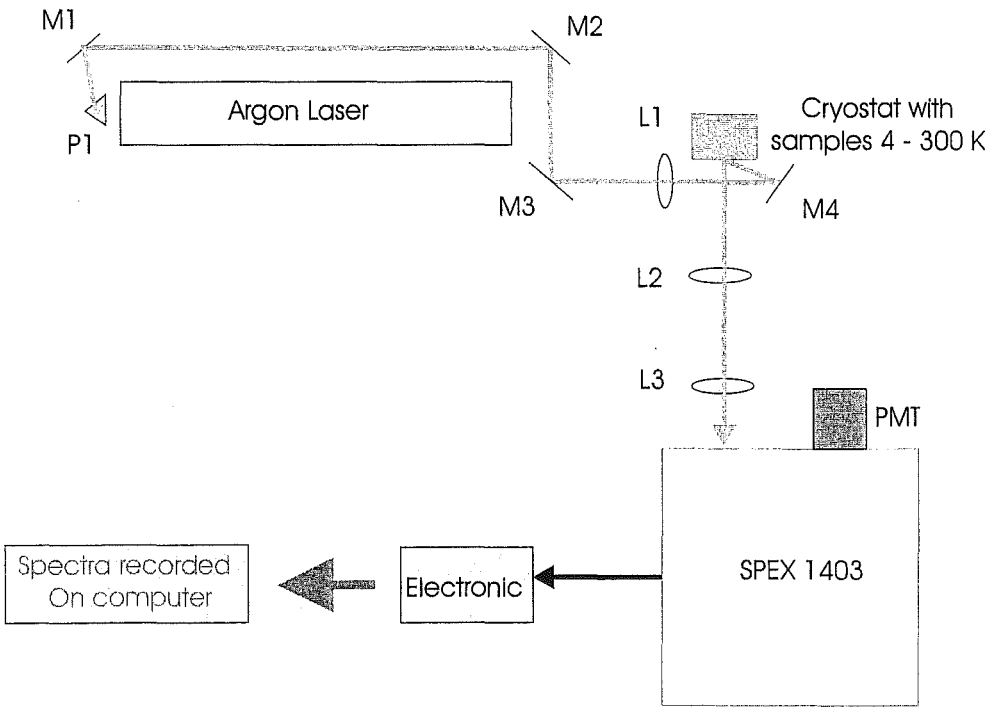

Figure 3.1: Schematic of PL experiment.

A schematic PL experiment is shown in figure 3.1.

1. Argon Laser
   A continuous wave (CW) Argon gas laser was used as the excitation source. Near UV 333 nm laser wavelength was chosen as the excitation wavelength for these experiments, and 20 mW laser power was maintained by adjusting

the laser current to about 49 A. For all the experiments the laser spot diameter on the sample of about 100 μm was used by adjusting the focusing lens, resulting in the power density of about 2.5 mW/mm^2.

2. Optics
   With the laser strongest output beam using G3873-019 (output coupler) and G3802-035 (high reflector) pair of mirrors, the output consists of three different wavelengths of 333 nm, 357 nm, and 364 nm. A prism (P1) was needed to disperse the beam and the 333 nm wavelength was spatially filtered by an iris for these experiments. Four mirrors (M1, M2, M3, M4) are needed to guide and reflect the beam from the laser onto the samples. L1 is a focusing lens to adjust the laser spot size on the sample. L2 collects the scattered emission light from the sample, and L3 is a focusing lens with f# 7.5 that best suits the SPEX 1403, to focus the collected light to the entrance slit of the spectrometer. All of the lens are made from quartz to transmit UV light.

3. Cryostat
   The lab is equipped with a helium gas closed cycle cryostat which can maintain temperature from 25 K to 300 K, and a continuous flow liquid helium cryostat - the Oxford Microstat system, which can maintain a temperature from 4 K to 300 K. Both cryostats need to be evacuated with a pump before use to provide thermal insulation from the outside.

4. The Vacuum Pump
   For low temperature experiments, a mechanical and a hot oil diffusion pump were used to maintain the vacuum inside the cryostat down to about 10^{-4} Torr.
   One thing that we need to care about when pumping and cooling the samples is cryopumping. To prevent this from happening, the pump is usually turned off before the temperature goes down to below 140-120 K.

5. Sample Mounting
   GaN samples usually are thin film samples. Mounting the GaN samples to the sample holder is best done by sticking them with the silver paste. It needs to be carefully done, because silver paste can flouresce well in the visible light region.

6. SPEX 1403
   SPEX 1403 spectrometer is an 0.85-m double monochromator that selectively passes radiation on the basis of its frequency. Slit width is one of the factor that influences the spectrometer resolution. Slit width can be thought in terms of spectral band pass rather than mechanical slit width. Bandpass is a function of the reciprocal linear dispersion which, inturn, depends on the wavelength, the grating constant, the focal length of the instrument and the spectral order. At 19435 cm^{-1} (514.5 nm) the reciprocal linear dispersion for a SPEX 1403 with 1,800 gr/mm grating is 10 cm^{-1}/mm. Thus, for the experiments in this project when the scan step sizes were taken mostly at

4 cm^{-1} and 20 cm^{-1}, the slit width of maximum 400 μm and 2,000 μm were used, depending on the strength of the PL intensity observed. If the intensity was strong enough, a smaller than maximum slit width could be used, and if the intensity was weak, the maximum slit width would be used. There are 4 slits on the SPEX 1403, the entrance slit, two middle slits and an exit slit. Usually the middle slits were set twice as wide as the entrance and exit slits. Thus, the combination of slit widths commonly used were: 100/200/200/100 μm or 200/400/400/200 μm for 4 cm^{-1} scan step size, and 400/800/800/400 μm for 20 cm^{-1} scan step size.

7. Photomultiplier Tube (PMT)
   In this project, a RCA C31034 PMT with an S1 spectral response was used for photoelectric detection. The PMT was mounted in a thermoelectrical cooled housing and cooled to approximately -25°C.

8. Electronics
   The output signal from PMT is sent to a discriminator. Basically, the discriminator differentiates the stronger PL current from the weaker noise or dark current. For GaN the best lowest limit is 9 counts per second. Then the signal is amplified, sent to a photon counter and recorded on a computer. The commonly used amplification is 100 times.

9. Computer and Igor Software Package
   A program called **Lab Routines** made by Geoff Graham in Pascal was installed and used for all PL measurements. The commercial Igor software package, which is an integrated program for visualizing, analysing, transforming and presenting data, was used to analyse and visualize all PL measurement results in this project.

3.2 Reactive Ion Etching (RIE)

3.2.1 Introduction

The key etch issues [86] which define the quality of an etching process are:

- Etch Rate
  Etch rate is simply the rate of removal for a given material in a specific process environment. It is desirable to have high etch rate in order to keep throughput high. However, a high etch rate often results in less selectivity and more damage to the wafer surface compare to a low etch rate.

- Selectivity
  Selectivity is the ratio of etch rates of the materials being intentionally etched to that of the mask or overlaying material, see figure 3.2. Good selectivity is required by most processes in order to ensure critical dimension and profile control. Small geometries require thin layers of resist, meaning the selectivity must be high.

- Critical Dimension
  Critical dimension is the dimension of a specific geometry feature, either line-width or spacing between lines, that must be within specific design tolerances.

- Uniformity
  Maintaining uniformity across the wafer surface is key to ensuring consistent device quality. A nonuniform etch has a direct impact on the devices and any future layers to be deposited. Uniformity can be measured wafer-to-wafer, batch-to-batch or even from device-to-device within a wafer.

- Etch Profiles: Isotropic and Anisotropic
  Isotropic simply means etching equally well in all directions, see figure 3.2. Isotropic etching is usually the result of a chemical etch or process (such as wet processes) and limits the use of these processes to devices which do not require submicron features. This is due to the fact that isotropic etching results in loss of linewidth.

  Anisotropic means that the rate of etching perpendicular to the wafer surface is much greater than that lateral to the surface, see figure 3.3. Anisotropic allows for much smaller linewidth and features.

- Aspect Ratio
  The aspect ratio of an etch profiles is defined as the ratio of the vertical dimension (z) to the lateral dimension (a) such that: AR=z/a. Typical aspect ratio for dry etching can be as high as 10/1, while wet etching are in the 1/2 to 1/3 range.

There are various types of plasma etch reactors and they are grouped into three broad categories:

- Sputter etching, which is a physical process, uses a non-reacting gas such as

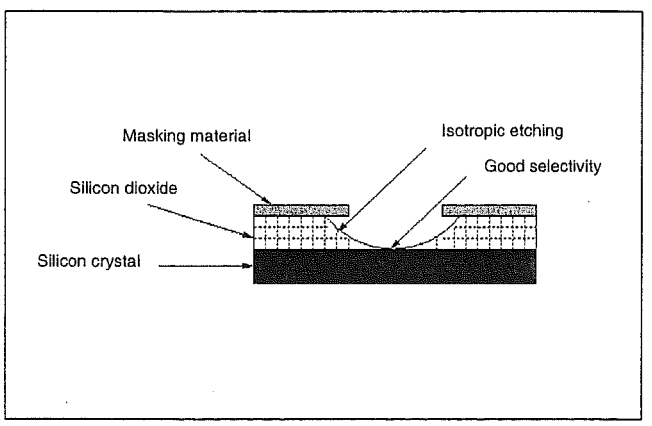

Figure 3.2: Chemical etch, isotropic and selective.

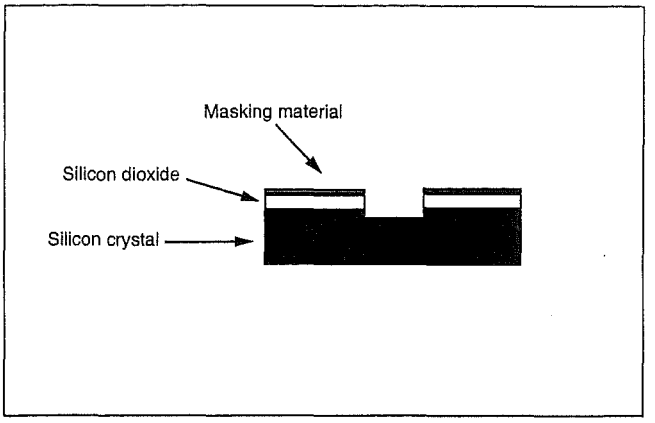

Figure 3.3: Plasma etch, anisotropic and nonselective.

argon (Ar), and etches by ion bombardment only. The etching is anisotropic and non-selective. Critical dimension control is fair to good.

- Chemical etching, where ion bombardment does not significantly contribute to the etching process. The process gases are selected to react chemically with the surface to be etched. The etching is selective and isotropic, but with poor critical dimension control.
- Combined chemical and physical processes in which ion bombarment enhances the chemical etching. Both reacting and non-reacting process gases are used. The etching profile can be varied from isotropic to anisotropic by adjusting the sheath potential and good critical dimension control.

In this project Reactive Ion Etching (RIE) was done using an Oxford Instruments Plasma Technology type Plasmalab 80 Plus system. This RIE technique, can combine chemical and physical processes and provide etching profiles that range from isotropic to anisotropic.

The typical plasma etch system consists of one or more process chambers and a numbers of auxiliary subsystems such as: RF power generator, matching network, wafer temperature control system, wafer handling system, gas delivery system, vacuum system, endpoint detection, system controller, process chamber. Figure 3.4 shows a simple schematic of a RIE system.

3.2.2 Etching Parameters

Etching process parameters and its effects:

1. Power
   RF power creates and maintains the plasma by adding energy to the system.

The level of RF power applied to the plasma has three major effects on the plasma process. Increasing the RF power:

- Increases the ionisation and dissociation of the gas molecules providing a higher concentration of active species. This typically increases etching rate.
- Increases the magnitude of the sheath potentials thereby increasing the degree of etching anisotropy, but at the same time reducing selectivity and increasing surface damage.
- Increases the amount of heat dissipated in the plasma and the wafer. A higher wafer temperature results in a higher etching rate. On the downside, a temperature too high can damage the photoresist and cause loss of linewidth. At the extreme, burning the resist not only destroys the wafer, it severely contaminates the chamber.

In particular, this project investigates the influences of various etching DC bias voltage on the optical properties of GaN. Various etching DC bias voltage were attainable by adjusting and maintaining the RF power.

2. Frequency
Although the frequency of operation is fixed in most plasma processing equipment, a brief overview of the effects of frequency will aid in the

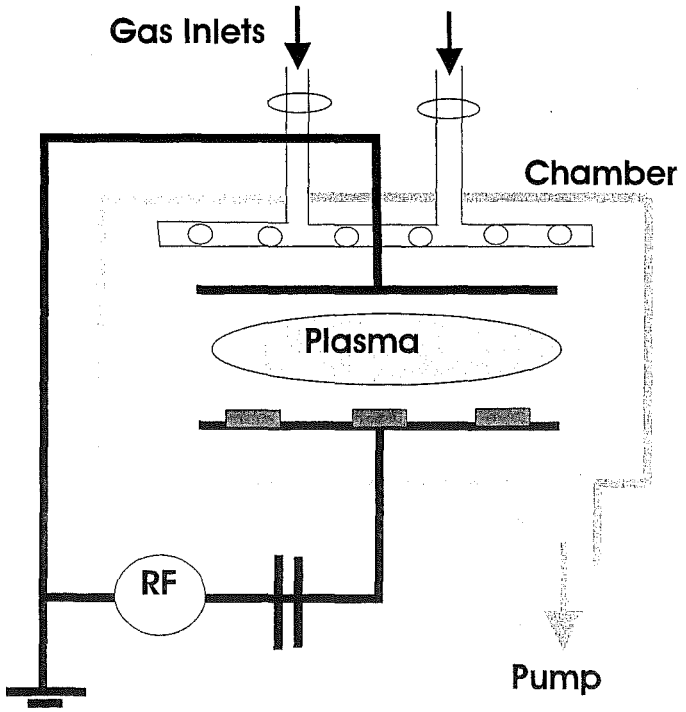

Figure 3.4: Schematic of RIE.

comparison of various types of equipment that use different frequencies. At frequencies below 10kHz, the plasma behaves like a DC plasma that extinguishes and reignites every half cycle with a polarity reversal. At higher frequencies, 50-500 kHz for example, the plasma still resembles a DC plasma in that the polarity reverses every half cycle but the plasma always remains ignited. At still higher frequencies, say 10-50 MHz, the inertia of the ions prevents them from being extracted from the gap between the electrodes. In this range of frequencies and higher, each electrode then behaves like a cathode with a dark space or ion sheath around it. The result is a slower etch rate.
The available RIE machine in the lab has a frequency of operation at 13.56 MHz.

3. Pressure
System pressure is an important process parameter because pressure affects the nature of the plasma in several ways. Increasing pressure:

   - Increases the ionisation and excitation rate by increasing the rate of collision between electrons and gas molecules. The etching rate increases if it depends primarily on the concentration of ions and free radicals.
   - Reduces the bias voltage.
   - Reduces ion energy by increasing the collision rate between ions and other particles. This may reduce the etching rate if the process depends on ion energy to initiate a chemical or physical reaction. The increased collisions cause the etching to be less directional and more isotropic. A continued increase in pressure can reduce ion density or even extinguish the plasma because the ions lose so much energy as a result of inelastic collisions that they have insufficient energy to produce secondary electrons when they strike the cathode.

   The etching pressure for the GaN samples in this project was maintained at 0.1 Torr.

4. Temperature
Both wafer temperature and process temperature have an effect on the quality of etching. Increased process temperature facilitates an increase in the rate of chemical reactions in the chamber. This, in turn, results in a higher etching rate. However, just as in the case of pressure, once the temperature increases above a certain threshold the etching rate can be suppressed. An increased wafer temperature generally results in a higher etching rate as well, due to more chemical reactions at the surface.
The temperature between 290 K to 300 K was always maintained for etching of the GaN samples in this project. There was no photoresist mask used in the etching processes, so it was not necessary to maintain these etching processes at low temperature.

5. Gas flow
   The concept of residence time is important to the understanding of the effects of variations in gas flow rate. Residence time is defined as the average time a gas molecule spends in the reaction chamber. The active species in a plasma are not stable and may have a short lifetime. If the average lifetime is shorter than the residence time, the effects of the gas flow rate is small. If on the other hand, the lifetime is long compared to the residence time, changes in flow rate can have a large effect on the etching rate.
   Ar and SF_6 gas were used for the etching processes in this project and 60 sccm gas flow rate was used for all the processes.

6. Electrode spacing
   For a given set of conditions for gas composition, applied voltage, frequency and pressure, there is an optimum electrode spacing. Reducing the spacing beyond this point reduces plasma density due to a lower ionisation rate because of reduced collisions with electrons having sufficient energy to cause ionisation. Increasing the distance between the electrodes does increase the number of collisions between the ions causing them to lose energy.

7. Chamber contamination
   Contamination does not, for the most part, have a direct effect on the plasma. It can, however, have a noticeable effect on the etching rate and process yield. A particle one-tenth the size of a critical dimension can destroy a device.
   The RIE machine provided was used for many etching processes with difference gases, e.g: Ar, SF_6, N_2, etc. It is possible that the gas from a previous etching process contaminates the following etching process if a different etching gas was used.

8. Loading
   Loading is the term given to the change in the rate of etching due to a change in the area being etched. This effect is most severe when the etch reaction is limited by the availability of active species. Increasing the area being etched reduces the rate of etching because the available etchant species must be shared by a larger area.
   The area of GaN samples in this experiment were typically 0.25 cm^2.

3.3 Atomic Force Microscopy

3.3.1 Introduction

In this project Atomic Force Microscopy (AFM) made by Digital Instruments, model NanoScope IIIA was used to look at the sample's surfaces. AFM is also called Scanning Force Microscopy (SFM) and has three primary modes:

- Contact Mode AFM

- Non-contact Mode AFM
- Tapping Mode AFM

Tapping Mode AFM was used in this project.
Figure (3.5) shows the basic components of AFM.

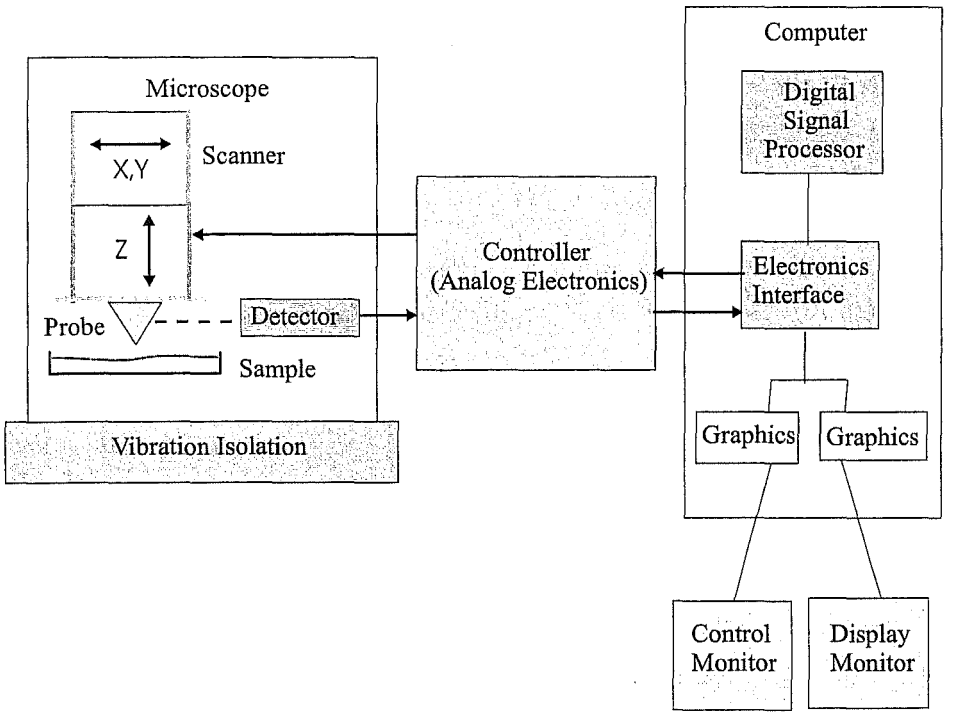

Figure 3.5: Basic components of AFM.

3.3.2 Tapping Mode AFM

- Tapping Mode AFM operates by scanning a tip attached to the end of an oscillating cantilever across the sample surface.
- The cantilever is oscillated at or near its resonance frequency with an amplitude ranging typically from 20 nm to 100 nm. The frequency of oscillation can be at or on either side of the resonant frequency.
- The tip lightly 'taps' on the sample surface during scanning, contacting the surface at the bottom of its swing.
- The feedback loop maintains a constant oscillation amplitude by maintaining a constant RMS of the oscillation signal acquired by the split photodiode detector.

- The vertical position of the scanner at each (x,y) data point in order to maintain a constant 'setpoint' amplitude is stored by the computer to form the topographic image of the sample surface.
- By maintaining a constant oscillation amplitude, a constant tip-sample interaction is maintained during imaging.

The advantages of Tapping Mode AFM are:

- Higher lateral resolution on most samples (1 to 5 nm).
- Lower forces and less damage to soft samples imaged in air.
- Lateral forces are virtually eliminated, so there is no scraping.

The disadvantage of this mode is a slightly slower scan speed than Contact Mode AFM.

3.4 Annealing

A schematic of annealing apparatus is shown in figure 3.6.

- **Furnace**
  A ceramic furnace was used.
- **Temperature control and gauge**
  Temperature control and gauge (T gauge) maintains the temperature of annealing process. GaN sample is usually annealed in temperature between 500 °C to 900 °C [39, 54, 69]. In this project, the samples were annealed at temperature 700 °C for 8 hours.
- **Sample**
  Usually three or four samples were put in a 5 cm × 1.5 cm × 0.5 cm ceramic boat and annealed simultaneously.
- **Pump**
  A mechanical and an oil pumps were used to vacuum the annealing tube down to about 10^{-4} Torr.
- **Gas source**
  Gas source supplies the ambient gas needed in the annealing process. In this project, thermal vacuum annealing, annealing in hydrogen and nitrogen ambient have been done to the samples.
- **Pressure gauge**
  Two pressure gauges were used to measure and control the pressure inside the sample's tube, and the tube before the oil pump.

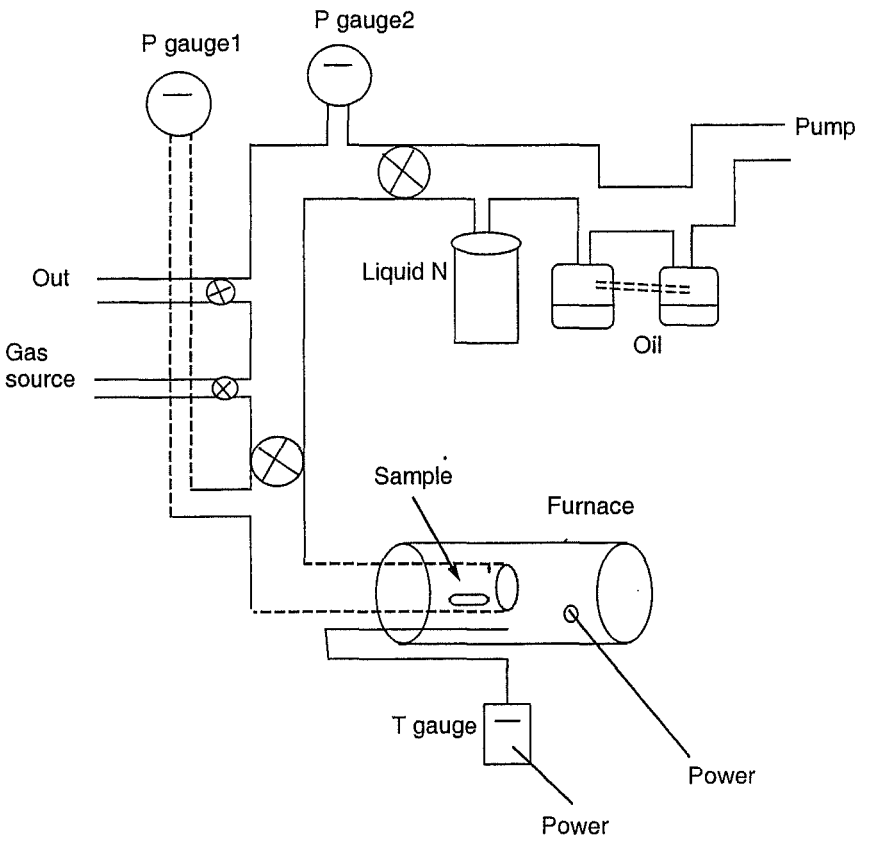

Figure 3.6: Schematic of annealing apparatus.

3.5 Samples

Samples that were investigated in this project are:

- Amorphous gallium nitride (a-GaN)
  All the a-GaN samples were prepared in a collaboration between The Victoria University Wellington and The Industrial Research Limited, Lower Hutt. The a-GaN samples are listed in the Table 3.1.

No	Sample	Substrate
1	GaN 129016 E300 (6)	Glass
2	GaN 123027	Glass
3	GaN 1240813	Glass
4	InN 111057	Glass
5	GN 10106	Glass
6	GN 205033	Stainless Steel
7	GN 120118	Quartz
8	GN 212067	Qartz
9	GN 113126	Quartz
10	GN 117122	Quartz
11	GN 101063	Quartz
12	GN 101063	Silicon
13	GN 101061	Silicon
14	GN 113022	Silicon
15	GN 113026	Quartz
16	GN 120119	Quartz

Table 3.1: The list of a-GaN samples.

- Poly-crystalline gallium nitride (poly-GaN)
  The poly-GaN samples were grown by the Electrical and Electronic Engineering Department of the University of Canterbury.
  The list of these samples is shown in the Table 3.2.

- Crystalline gallium nitride (c-GaN)
  The c-GaN that was used is a commercial sample, from the GaN wafer run number 101030803 supplied by SVT Associates. The structure is 0.3 μm GaN, Si-doped at 5×10^{17} cm^{-3} on sapphire (0001) substrate with a thin AlN nucleation layer, and grown by Molecular Beam Epitaxy (MBE). This sample was cut to three series of samples for Ar etching experiments. Those are: c-GaN/sap/30803/Ar/AL25-30 (6 samples), c-GaN/sap/30803/Ar/AL31-38 (8 samples), c-GaN/sap/30803/Ar/AL39-47 (9 samples) and 2 series of samples for SF_6 etching experiments, those are: c-GaN/sap/30803/SF_6/1-8 (8 samples), c-GaN/sap/30803/SF_6/9-18 (10 samples).

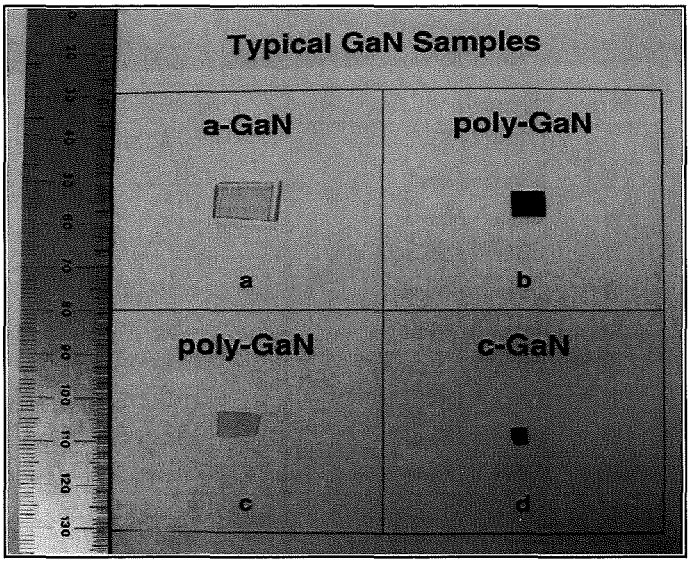

Figure 3.7: Typical pictures of (a) a-GaN on quartz substrate, (b) poly-GaN on silicon substrate, (c) poly-GaN on quartz substrate and (d) c-GaN on sapphire substrate.

Typical figures of (a) a-GaN sample on quartz substrate, (b) poly-GaN sample on silicon substrate, (c) poly-GaN sample on quartz substrate and (d) c-GaN sample on sapphire substrate are shown in figure 3.7.

No	Sample	Substrate
1	01GN/Si-1	Silicon
2	01GN/Si-1	Silicon
3	02GN/Si-2	Silicon
4	03GN/Si-3	Silicon
5	04GN/Si-4	Silicon
6	05GN/Si-5	Silicon
7	05GN/Si-5	Silicon
8	05GN/Si-5	Silicon
9	06GN/Si-6	Silicon
10	06GN/Si-6	Silicon
11	09-02GN/Si-1	Silicon
12	10-02GN/Si-2	Silicon
13	13-02GN/Si-3	Silicon
14	10-02GN/Si-2	Silicon
15(a)	08-GN/Q-1 (clear)	Quartz
15(b)	11-GN/Q-2 (dark)	Quartz
16	22-02GN/GaAs-1	Gallium Arsenide
17	21-02GN/Q-7	Quartz
18	23-02GN/Q-8	Quartz
19	23-02GN/Q-8	Quartz
20	24-02GN/Q-9	Quartz
21	25-02GN/GaAs-2	Gallium Arsenide
22	26-02GN/Q-10	Quartz
23	27-02GN/Q-11	Quartz
24	28-02GN/Q-12	Quartz
25	29-02GN/Sa-2	Sapphire
26	30-02GN/Q-13	Quartz
27	31-02GN/Q-14	Quartz
28	32-02GN/Q-15	Quartz
29	33-02GN/Q-16	Quartz
30	20-02GN/Q-6	Quartz
31	34-02GN/Sa:Ca-1	Sapphire
32	37-GaN/Sa-03	Sapphire
33	41-GaN/Sa-04	Sapphire
34	70-GaN/Sa-12	Sapphire

Table 3.2: The list of poly-GaN samples.

Chapter 4

Photoluminescence of Amorphous GaN

4.1 Introduction

Most of the work on semiconductors has concentrated on crystalline material, but amorphous semiconductors have a number of advantages; for example their cheapness of manufacture and suitability for deposition on arbitrary substrates. However, there are general limitations which have prevented large-scale adoption of amorphous semiconductors in applications:

- localised states in the band gap, arising from imperfect bonding configuration and
- limited electron mobility.

Amorphous GaN (a-GaN) was grown during the early stage of GaN research in the 1970s [30], but only a few things are known. The interest on a-GaN has been excited by the publication of preliminary experimental [66] and theoretical [83] work, showing that a-GaN has remarkable promise as an opto electronic material.

In New Zealand, the group of the University of Victoria Wellington, Industrial Research Ltd, Institute of Geological and Nuclear Science have been working on a-GaN. In their prior work, the a-GaN was prepared by ion assisted deposition (IAD). Raman Scattering and optical conductivity measurements have been done to the samples, showing an amorphous nature of the materials and a low density of homopolar bonds [7].

In this chapter a brief survey of the a-GaN PL is presented. It is included for the completion of this project.

4.2 PL Results and Discussion

4.2.1 PL Results of GaN 129016 E300 (6)

Sample GaN 129016 E300 (6) was deposited with 300 eV nitrogen ion energy and the GaN film thickness is 153 nm. The PL results of this sample and its PL

temperature dependence measurements are shown in figure 4.1. For this sample, even though the UV region is not shown on the graphs, it was measured and looked for. However, no near band edge PL in the UV region could be detected at our level of sensitivity. A broad PL line was observed in the region from 1.8 eV to 2.8 eV, peaking around 2.25 eV and 2.53 eV. This PL line is similar to the yellow luminescence (YL) line in a crystalline GaN (c-GaN) but is much wider here, see appendix B on page 193 for a typical PL result of c-GaN. The extra width could be the result of larger disorder in the structure of a-GaN.

The temperature dependence measurement of this sample shows that for the first peak (the lower energy peak) increasing temperature from 4 K to 60 K results in an increase in the peak intensity, then as the temperature increases from 60 K to 240 K, the peak intensity decreases sharply, and increasing temperature from 240 K to 280 K results in an increases of the peak intensity again.
The second peak (the higher energy peak) has a lower intensity than the first peak. As the temperature increases from 4 K to 60 K, the intensity of second peak does not greatly change, increasing temperature from 60 K to 240 K results in a decrease of the peak intensity, then as the temperature increases from 240 K to 280 K, the peak intensity increases sharply.

Figure 4.2 shows the PL peak position of GaN 129016 E300 (6) as a function of temperature. The lower energy PL peak position does not greatly change as the temperature increases, the peak position is almost constant at about 2.25 in average. Except for the data at temperature 4 K, the peak position is at 2.21 eV. And the higher energy PL peak position slightly decreases or redshifted as the temperature increases.

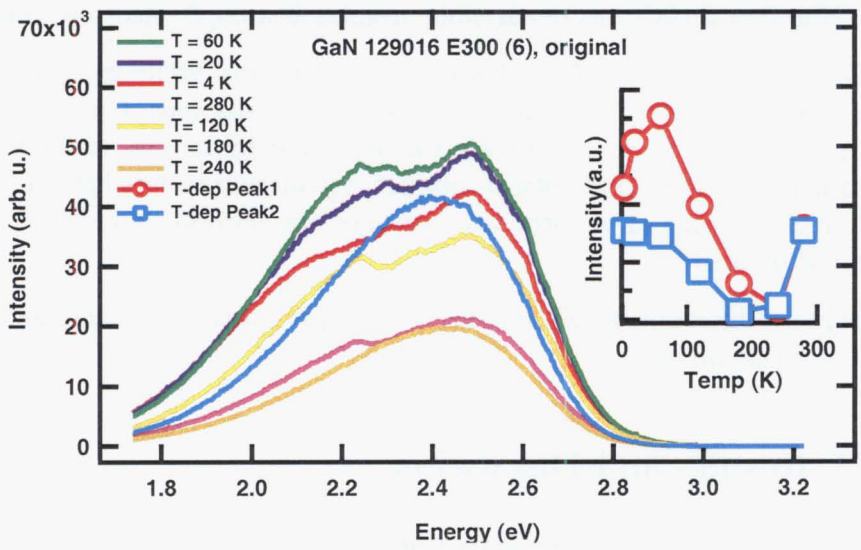

Figure 4.1: PL results of GaN 129016 E300 (6) and the temperature dependence.

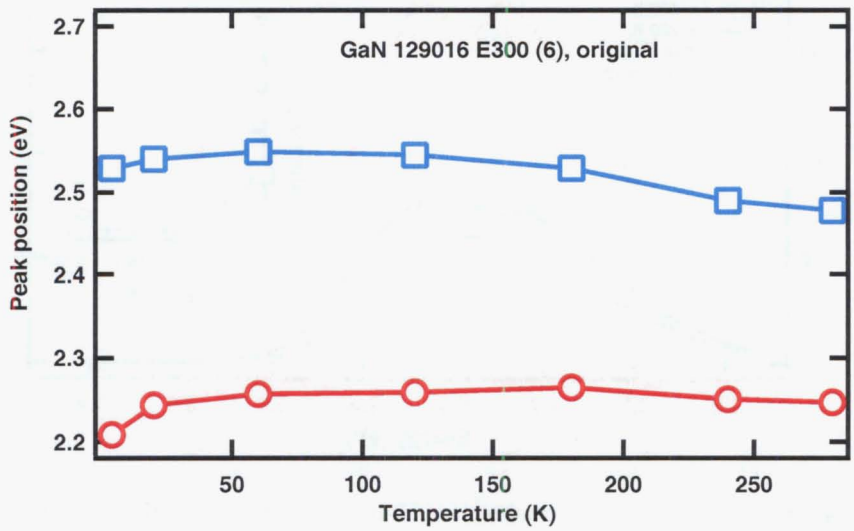

Figure 4.2: PL peak position of GaN 129016 E300 (6) as a function of temperature.

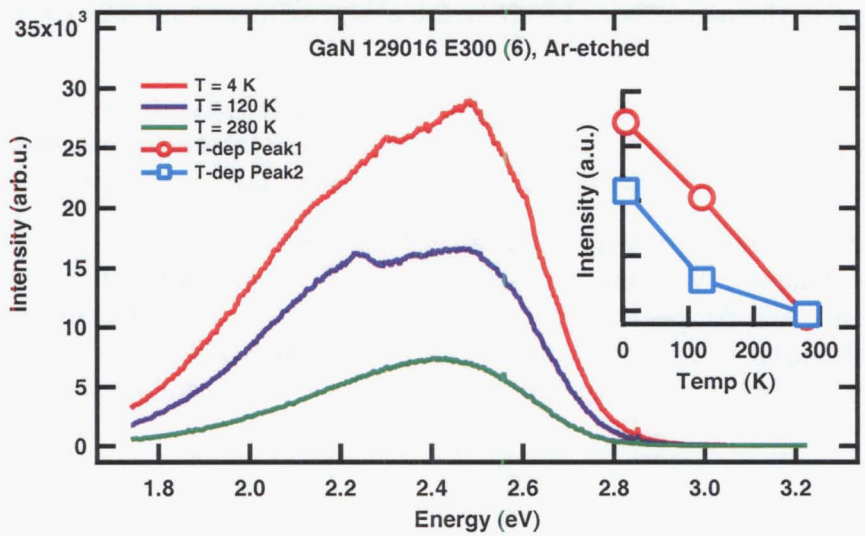

Figure 4.3: PL results of Ar-etched GaN 129016 E300 (6) and the temperature dependence.

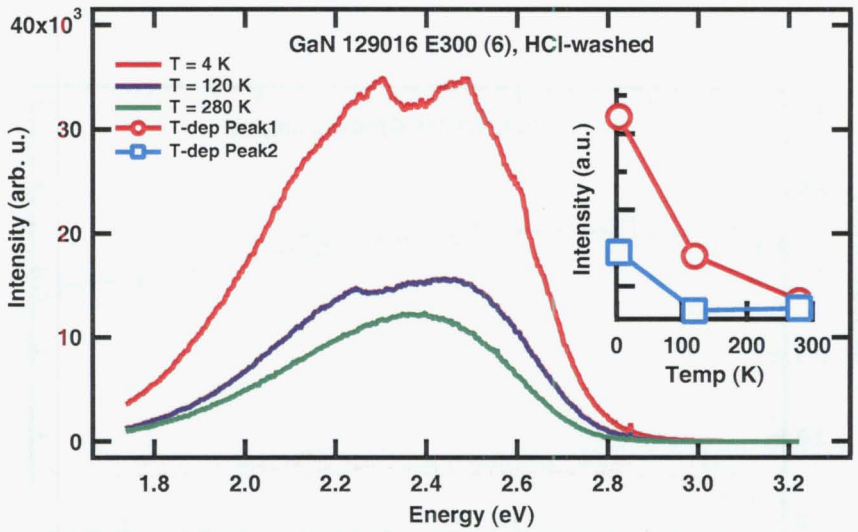

Figure 4.4: PL results of HCl-washed at 50-60 ^{0}C GaN 129016 E300 (6) and the temperature dependence.

Figures 4.3 shows the PL results of Ar-etched GaN 129016 E300 (6) and the temperature dependence. And figure 4.4 shows PL results of 80% HCl-washed GaN 129016 E300 (6) at 50-60 °C for 1 minute and its temperature dependence. There was also no near band edge emission in the UV region observed at our level of sensitivity from these etched and washed samples. Similarly, they show two broad lines in the region from 1.8 eV to 2.8 eV, peaking around 2.25 eV and 2.53 eV.

Ar-etched and HCl-washed samples have a relatively lower intensity than the as-grown sample. And the temperature dependence measurement shows that increasing temperature results in a sharp decrease of both peaks intensities.

The relatively lower intensity of Ar-etched and HCl-washed samples are interpreted as follows. Washing process in 50-60 °C of 80% HCl thins down the a-GaN film. And Ar gas etching is a physical process, where ions only bombard the sample surface. The PL result of the Ar-etched and HCl-washed a-GaN show that these processes damaged the surface of the sample, leading to a lower PL intensity.

4.2.2 PL Results of GaN 123027

Figure 4.5 shows the PL results of sample GaN 123027 on glass substrate and its temperature dependence measurement. From this sample, there was no near band edge emission in the UV region detected in our level of sensitivity.There was a broad PL line observed from 3.5 eV to 1.8 eV, peaking at about 2.6 eV.

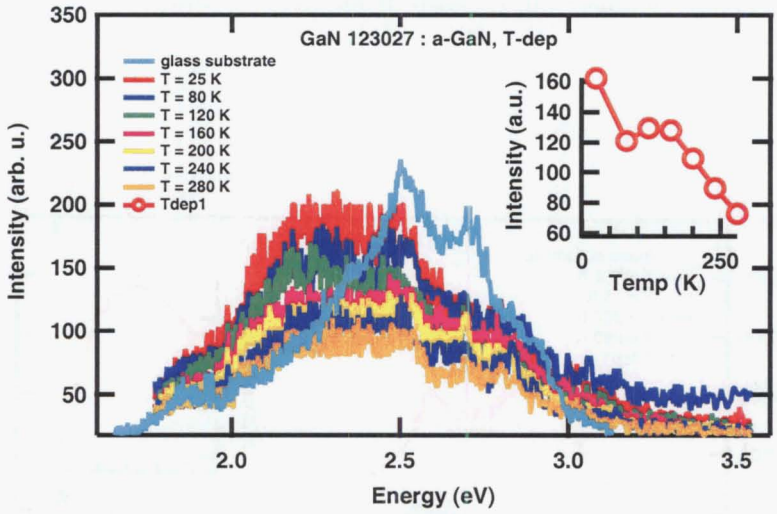

Figure 4.5: PL results of GaN 123027 and the temperature dependence.

The PL lines of the GaN film and the glass substrate of this sample have only a slight difference. Thus, it is interpreted that the measured PL signal is originally from the glass substrate. Also the signal is weak compared to the noise.

The temperature changes gives only a slight change in the PL spectrum. Generally, the PL peak intensity of this sample decreases as the temperature increases, except at the temperature from 80 K to 160 K there is a slight increase of the PL peak intensity as the temperature increases.

4.2.3 PL Results of InN 111057

This sample is the only amorphous indium nitride (a-InN) film on glass substrate sample measured in this project. Figure 4.6 shows the PL measurement results of this sample and its temperature dependence measurement. The PL line of the glass substrate is almost two times higher and wider than the PL line of the InN film of this sample, but has a similar shape. Thus it is interpreted that the PL line of the sample is not originally from the InN film, but mainly a contribution from the glass substrate. Also the only PL emission line observed from this sample is in the region of 3.1 eV to 1.8 eV, peaking around 2.3 eV, making it difficult to relate it to InN emission. Even though the exact position of InN emission is still controversial, with one side stating it is around 0.7 eV, Davydov *et al* [21], and another side stating it is around 1.8 eV, Tansley *et al* [85].

The PL peak intensity is insignificantly changed as the temperature changes, with a slight increase of peak intensity with increasing temperature from 26 K to 120 K, then a slight decrease of peak intensity with increasing temperature from 120

K to 200 K, and keeps decreasing until 280 K. Again, it adds doubt on the origin of the PL spectrum of this sample being from the InN film.

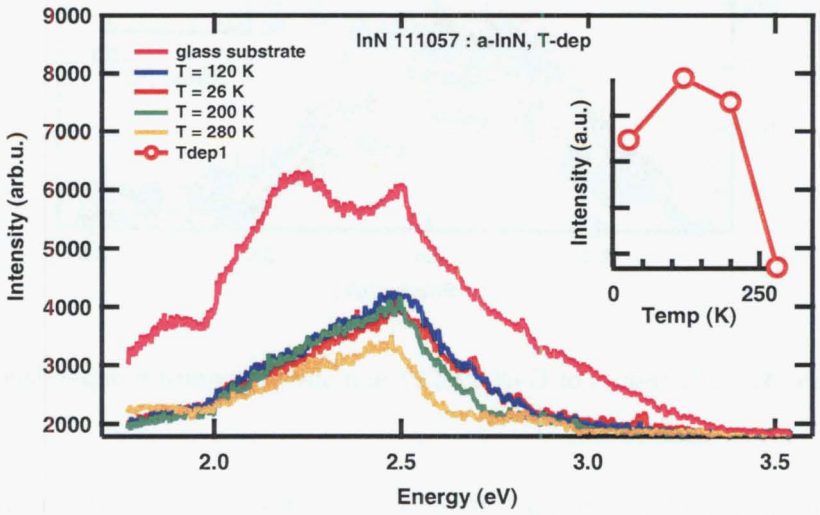

Figure 4.6: PL results of InN 111057 and the temperature dependence.

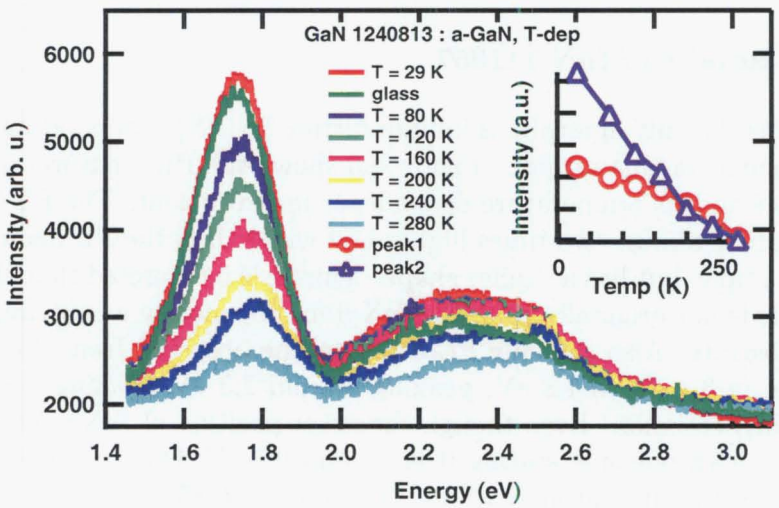

Figure 4.7: PL results of GaN 1240813 and the temperature dependence.

4.2.4 PL Results of GaN 1240813

PL results of sample GaN 1240813 are shown in figure 4.7. At our level of sensitivity, there were two broad PL lines detected from this sample, those are 3.1 eV to 2.0 eV emission line, peaking at about 2.3 eV, and 2.0 eV to 1.5 eV emission line, peaking at about 1.7 eV. But none of these lines is the near band edge emission line in the UV region. The same lines were also observed from the PL results of the glass substrate of this sample. It is apparent these lines are probably PL lines of the glass substrate, not of the GaN film.

The temperature dependence measurement of this sample shows that as the temperature increases, both of the peak intensities of the PL lines of this sample decrease. It is different from the YL peak of c-GaN which increases as the temperature is increased, see appendix B on page 193.

4.2.5 PL Results of GN 10106/Glass, GN 101063/Q and Si, GN 212067/Q, GN 113126/Q, GN 120118/Q, GN 117122/Q, GN 205033/Steel

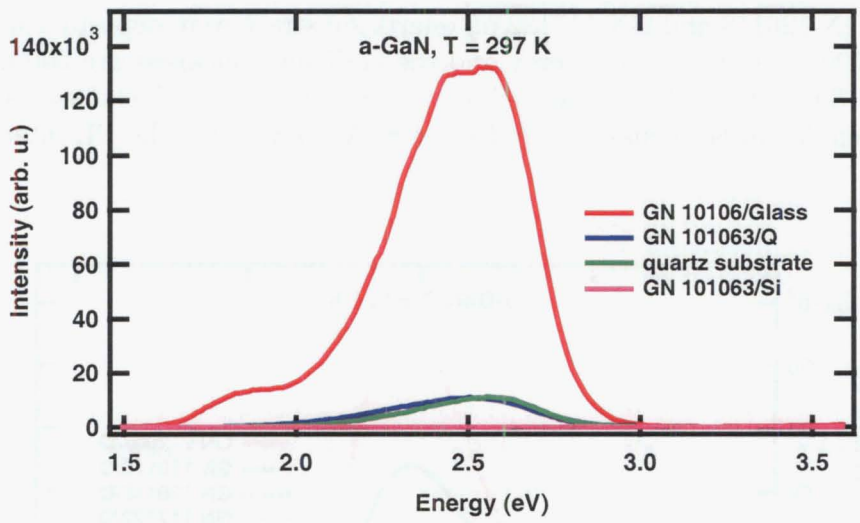

Figure 4.8: PL results of GN 10106 on glass substrate; GN 101063 on quartz and Silicon substrate, at T = 297 K.

Figure 4.8 shows PL results of samples: GN 10106 on glass substrate; GN 101063 on quartz and Silicon substrate. The PL was measured in room temperature. These three samples were deposited with the same deposition conditions, with 500 eV nitrogen ion energy and the GaN film thickness was 140 nm.

At our level of sensitivity, there was no near band edge PL in the UV region detected from these samples. Sample GN 10106 on glass substrate shows a broad

PL line from 1.6 eV to 3 eV, and a relatively strong PL intensity, peaking at about 2.5 eV. Sample GN 101063 on quartz substrate shows a broad PL line from 1.9 eV to 2.9 eV and the peak position at 2.5 eV, this line is similar to the PL line of the quartz substrate. And sample GN 101063 on silicon substrate does not show PL line in the observed region, from 1.5 ev to 3.6 eV.

Figure 4.9 shows PL results of samples: GN 212067, GN 113126, GN 120118 and GN 117122 on quartz substrate; GN 205033 on stainless steel substrate. The PL measurements were taken at T = 297 K. There was also no near band edge PL in the UV region detected from these samples, at our level of sensitivity.

Sample GN 212067 on quartz substrate was deposited with 500 eV nitrogen ion energy and hydrogenated. The GaN film thickness is 100 nm. The PL result shows a broad PL line from 1.8 ev to 3.0 eV, and the peak position at about 2.5 eV. The PL intensity of this hydrogenated sample was the strongest compare to other samples grown on quartz substrate.

Sample GN 113126 on quartz substrate was deposited with 500 eV nitrogen ion energy and the GaN film thickness is 150 nm. A broad PL line from 1.8 eV to 3.0 eV, peaking at about 2.5 eV is shown from the PL result of this sample. The PL intensity of this sample is relatively stronger than of other samples grown on quartz substrate.

Sample GN 120118 and GN 117122 on quartz substrate were deposited with 500 eV and 700 eV nitrogen ion energy and the GaN film thickness are 200 nm and 150 nm. The PL results of these different depositions and thicknesses samples show a similar broad emission line from 1.8 eV to 3.0 eV. The PL intensity of

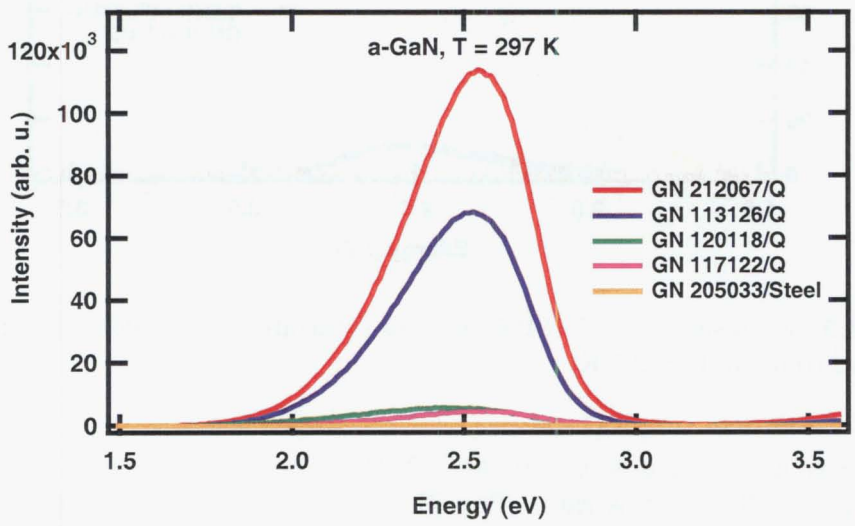

Figure 4.9: PL results of GN 212067, GN 113126, GN 120118 and GN 117122 on quartz substrate; GN 205033 on stainless steel substrate, at T = 297 K.

these samples is relatively weak. And the PL line of these samples is similar to the PL line of the quartz substrate, see figure 4.8 for the comparison to quartz PL line. It is interpreted that the PL line of these samples is mainly a contribution from the quartz substrate.

Sample GN 205033 on steel substrate which was deposited with 500 eV nitrogen ion energy and the thickness is 500 nm does not show PL line in the observed region from 1.5 eV to 3.6 eV.

4.2.6 PL Results of GN 101061 and GN 113022

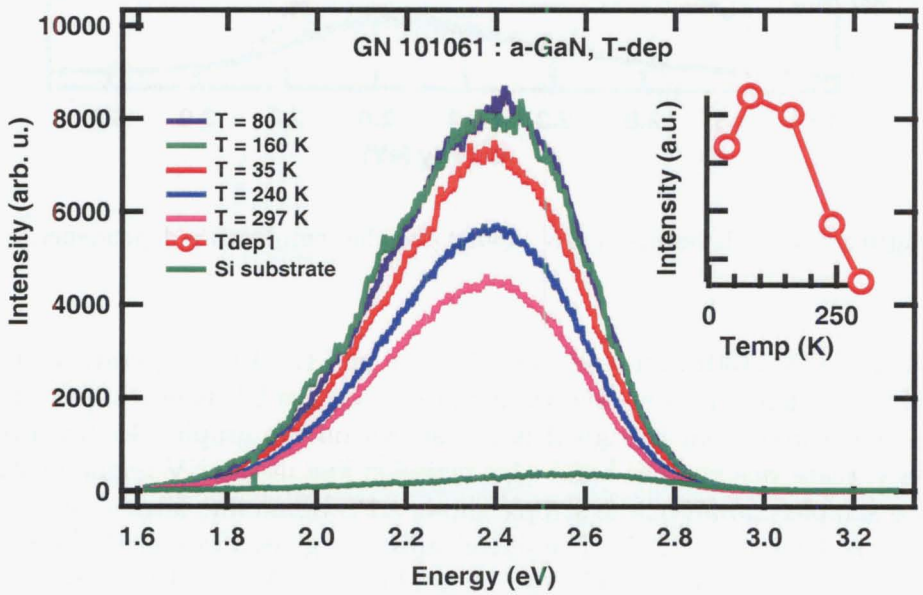

Figure 4.10: PL results of GN 101061 and the temperature dependence.

Figure 4.10 shows PL results of GN 101061 on silicon substrate, and the PL temperature dependence of the peak intensity. The UV region of GN 101061 was measured, even though it is not shown on the graph. However, there was no near band edge emission line detected from this sample at our level of sensitivity. A broad PL line was observed from 1.8 eV to 3.1 eV. At the temperature 4 K, the peak position of the sample is at 2.4 eV and the peak position of the silicon substrate is at about 2.6 eV. The peak intensity ratio of sample to silicon substrate is 67:1. There are obvious differences of the PL peak positions and intensities of the sample and substrate, making it apparent that the PL is originally from the a-GaN film and not the substrate.

The PL temperature dependence result shows that generally the higher the temperature the lower the PL intensity, except from T = 35 K to T = 80 K in this case, the intensity peak is increasing when the temperature increases.

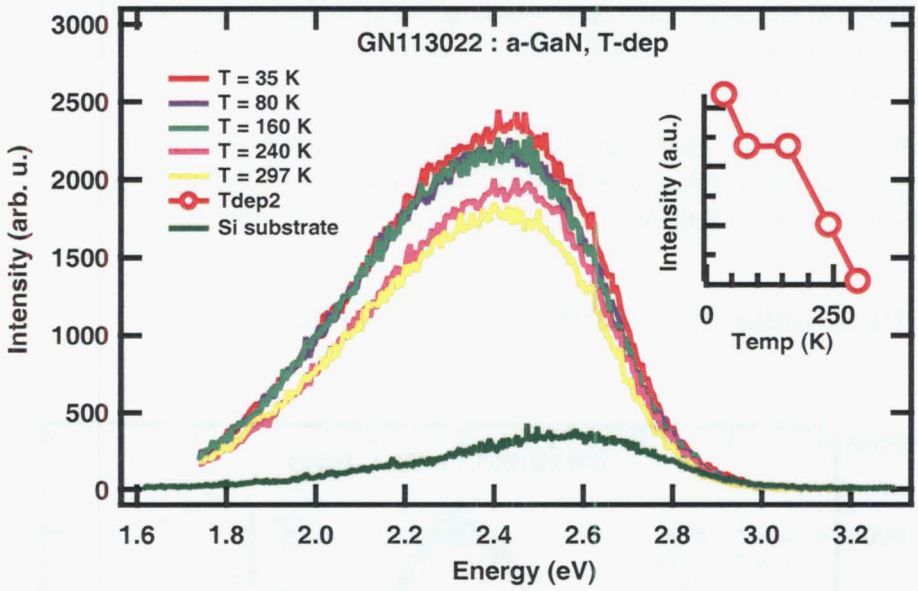

Figure 4.11: PL results of GN 113022 and the temperature dependence.

PL results of GN 113022 on a silicon substrate and the PL temperature dependence of the peak intensity are shown in figure 4.11. The UV region of GN 113022 was also measured, even though it is not shown on the graph. At our level of sensitivity, there was no near band edge emission line in the UV region observed from this sample. However, the sample shows a PL broad line from about 1.8 eV to 3.1 eV, peaking at or 2.5 eV. The silicon substrate gives a weaker PL broad line at the same region, with the peak position at about 2.6 eV. The PL intensity ratio of the sample to silicon substrate is 13:1. There are obvious differences between PL peak position and intensity of the a-GaN film and of the Si substrate. Thus the measured PL signal is originally from the GaN film.

The temperature dependence measurement shows that generally the higher the temperature the lower the PL peak intensity, except from T = 80 K to T = 160 K, the PL peak intensity is almost constant as the temperature increases.

4.2.7 PL Results of GN 113026 and GN 120119

Figure 4.12 shows PL measurement results of GN 113026 and GN 120119 on quartz substrate. At our level of sensitivity there was no near band edge emission in the UV region observed from these samples. The PL lines of the quartz substrate and of the samples are similar. The PL line peak position of the quartz substrate and the GN 113026 sample are at 2.7 eV, and the GN 120119 is at 2.6 eV. The peak intensity of the quartz substrate is the strongest, 5601 (a.u.), the GN 113026 sample is 4801 (a.u.), and the GN 120119 is 4298 (a.u.). It is

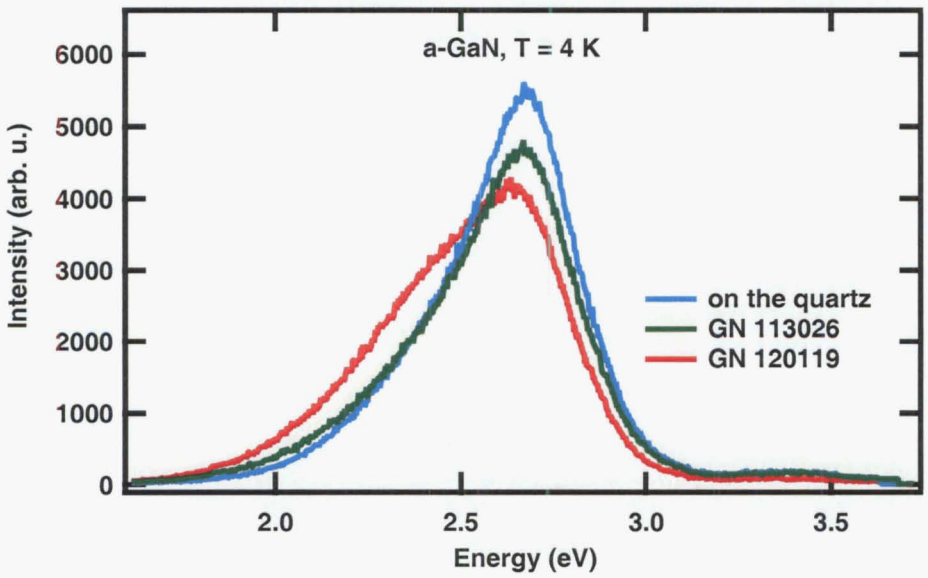

Figure 4.12: PL results of GN 113026 and GN 120119, at T = 4 K.

apparent that the PL emission line is originally from the quartz substrate.

4.3 Conclusion

PL and the temperature dependence measurements of fifteen a-GaN and one a-InN samples were taken. Six samples: GaN 129016 E300 (6) and GN 10106 on glass substrate, GN 212067 and GN 113126 on quartz substrate, GN 101061 and GN 113022 on silicon substrate are considered as promising samples, however they need further investigations.

None of these samples show a near band edge emission, at our level of sensitivity. They show a broad YL line mainly from about 1.8 eV to 3.0 eV, and peak intensity at about 2.5 eV. The YL line of these samples are wider and have stronger PL intensity than the YL line of c-GaN, see appendix B on page 193 for comparison to a typical PL result of c-GaN.

Defects cause the YL in c-GaN. These defects can be due to native defects and/or impurities. Considering that defects also cause the YL in these a-GaN samples, and a-GaN has a more disordered structure than c-GaN, the YL line of these samples is probably caused by native defects instead of impurities.

PL measurement only is insufficient to fully understand and describe the quality of these a- GaN samples. Therefore, further investigation on these samples is suggested.

Chapter 5

Photoluminescence of Polycrystalline GaN

5.1 Introduction

The so-called polycrystalline GaN (poly-GaN) samples are the samples that were grown by the Electrical and Electronic Engineering of the University of Canterbury. The GaN films were grown by Plasma-Assisted Molecular Beam Epitaxy (PAMBE) using a 60-cc effusion cell for gallium and an inductively coupled RF plasma source for active nitrogen. Growth rates as measured by Rutherford Backscattering Spectroscopy (RBS) are approximately 100 nm/hr for films grown with the gallium cell at 895 °C. The (0001) sapphire substrate was typically outgassed at 650 °C in another chamber. It was subsequently nitrided by exposure to the nitrogen plasma prior to the start of growth. These samples are listed in Table 3.2. For ease, these samples can be put into four groups:

- GaN films grown on silicon substrate (01GN/Si-1 to 13-02GN/Si-13).
- GaN films grown on quartz substrate (08-GN/Q-1, 11-GN/Q-2, 21-02GN/Q-7 to 33-GN/Q-16).
- GaN films grown on gallium arsenide substrate (22-02GN/GaAs-1, 25-02GN/GaAs-2)
- GaN films grown on sapphire substrate (29-02GN/Sa-2, 34-02GN/Sa:Ca-1, 37-GaN/Sa-03, 41-GaN/Sa-04, 70-GaN/Sa-12)

5.2 GaN Films Grown on Silicon Substrate

The Electrical and Electronic Engineering Department began to grow GaN films on silicon substrate about 2 years ago. They started the growth on silicon substrate because it is cheap and easy to get.

At our level of sensitivity, the PL results of samples grown on silicon substrate do not show the near band edge (NBE) emission line in the UV region. A broad line

was observed in the region from 1.8 eV to 3.0 eV. This line is not of the GaN film nor silicon substrate. The origin of this line is probably from noise and scattered light from the silver paste or else, also the detector sensitivity is best in that region. More over, the spectrometer slits were wide open, 500/1000/1000/500 μm.

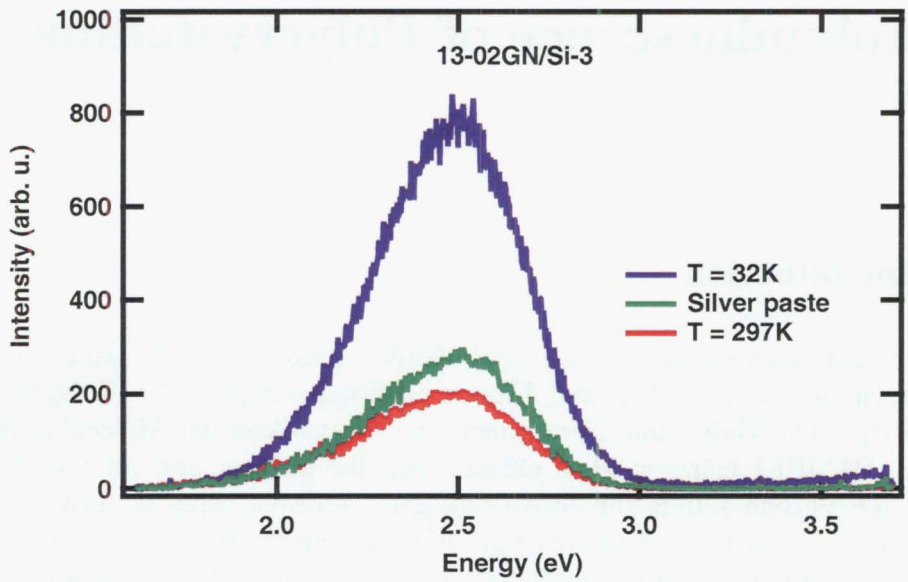

Figure 5.1: PL result of sample 13-02GN/Si-3 on silicon substrate.

Figures 5.1 and 5.2 show PL results of sample 13-02GN/Si-3 and 04GN/Si-4. Other samples which were grown on the silicon substrate show a similar or even weaker PL signal than the one shown in figures 5.1 and 5.2.
In conclusion, the GaN samples grown on silicon substrate do not have the preferable PL properties.

5.3 GaN Films Grown on Quartz Substrate

There are three main groups of GaN films grown on quartz substrate made by the Electrical and Electronic Engineering Department of Canterbury:

- The first group of samples were grown at a low temperature, they are 08-GN/Q-1 and 11-GN/Q-2 which were grown at 57 °C and 100 °C. These samples do not show a PL emission, and the captured signals are weak and merely noise.
- The second group of GaN films on quartz substrate are 21-02GN/ Q-7 and 23-02GN/ Q-8 which were grown at 500 °C, 24-02GN/ Q-9 which was

grown at 150 °C. The in situ RHEED measurement of these samples show a polycrystalline structure property.

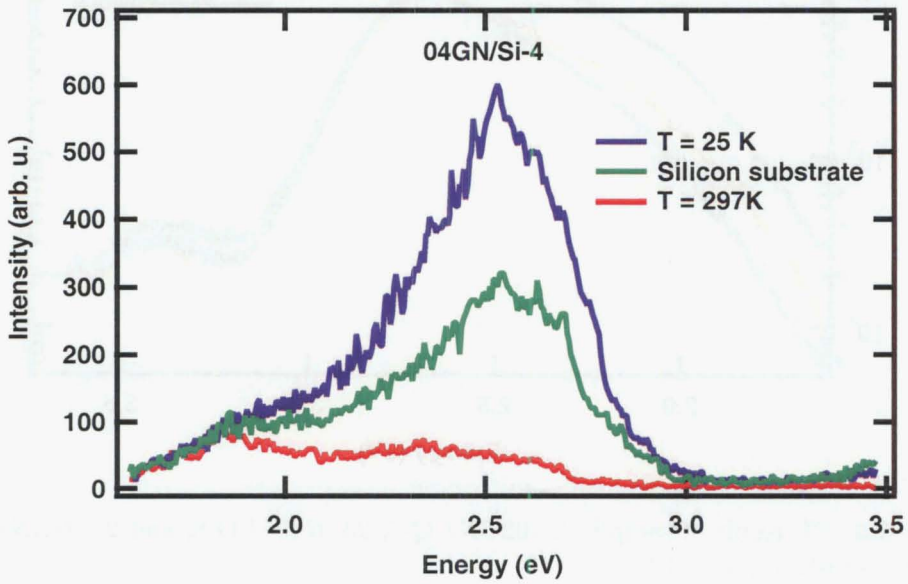

Figure 5.2: PL result of sample 04GN/Si-4 on silicon substrate.

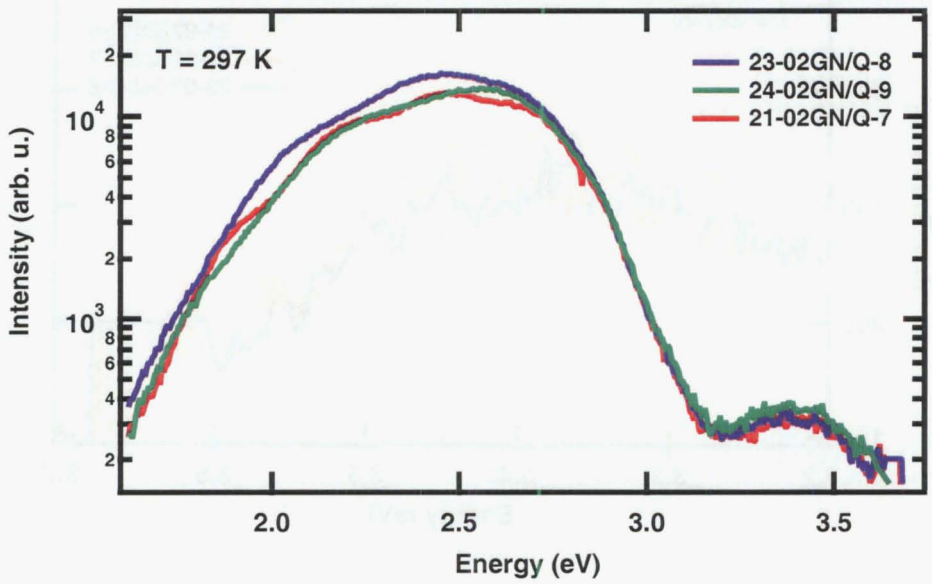

Figure 5.3: PL result of samples 21-02GN/ Q-7, 23-02GN/ Q-8, and 24-02GN/ Q-9 on quartz substrate, T = 297 K.

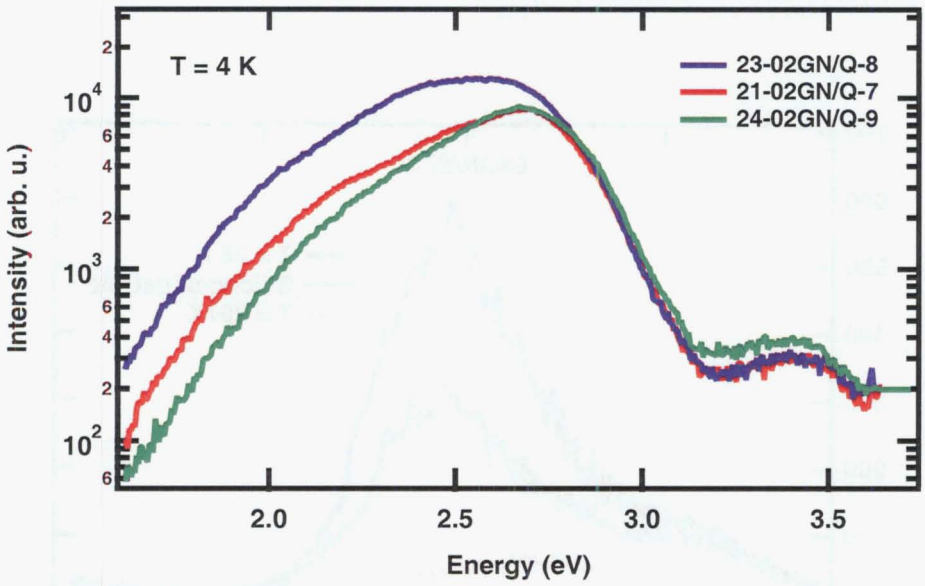

Figure 5.4: PL result of samples 21-02GN/ Q-7, 23-02GN/ Q-8, and 24-02GN/ Q-9 on quartz substrate, T = 4 K.

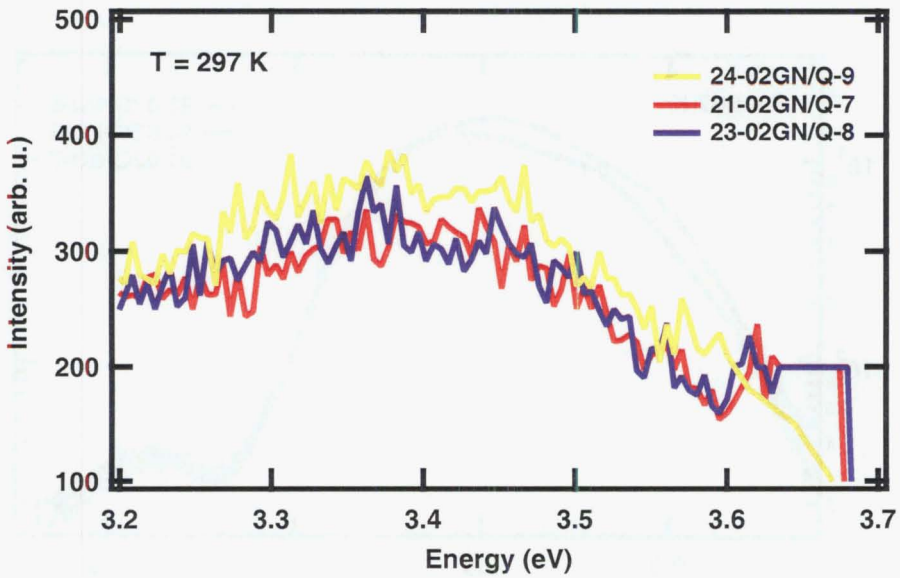

Figure 5.5: PL of the near band edge emission of samples 21-02GN/ Q-7, 23-02GN/ Q-8, and 24-02GN/ Q-9 on quartz substrate, T = 297 K.

PL results of the second group of GaN films grown on quartz substrate are shown in figures 5.3 to 5.6.

Figures 5.3 and 5.4 show the PL results of 21-02GN/Q-7, 23-02GN/Q-8, 24-02GN/Q-9 at 297 K and 4 K. There are two broad lines observed at about 3.5 eV (NBE) and 2.5 eV (YL). The YL line has much higher intensity than the NBE line, note the intensity axes is in logarithmic scale. The lines position is similar to c-GaN lines, however they are too broad and the NBE emission at about 3.5 eV is weak. For a comparison to a typical PL result of c-GaN, see appendix B, 193. The intensity of the lines only weakly depend on the temperature, they do not change much as the temperature changes from 297 K to 4 K. Figures 5.5 and 5.6 show in contrast with the c-GaN, the intensity of the NBE emission lines of these samples is lower at 4 K than 297 K.

- The third group of GaN films grown on quartz substrate are 26-02GN/ Q-10 to Q-16, almost all of them were grown at 500 °C, except 30-02GN/ Q-13 which was grown at 150 °C and 31-02GN/ Q-14 which was grown at 650 °C.
  The in situ RHEED measurement shows that these samples also have a polycrystalline structure property.

  PL results of the third group of GaN films grown on quartz substrate are shown in figures 5.7 to 5.10.
  Figures 5.7 and 5.8 show the PL results of 21-02GN/Q-10 to 33-02GN/Q-16

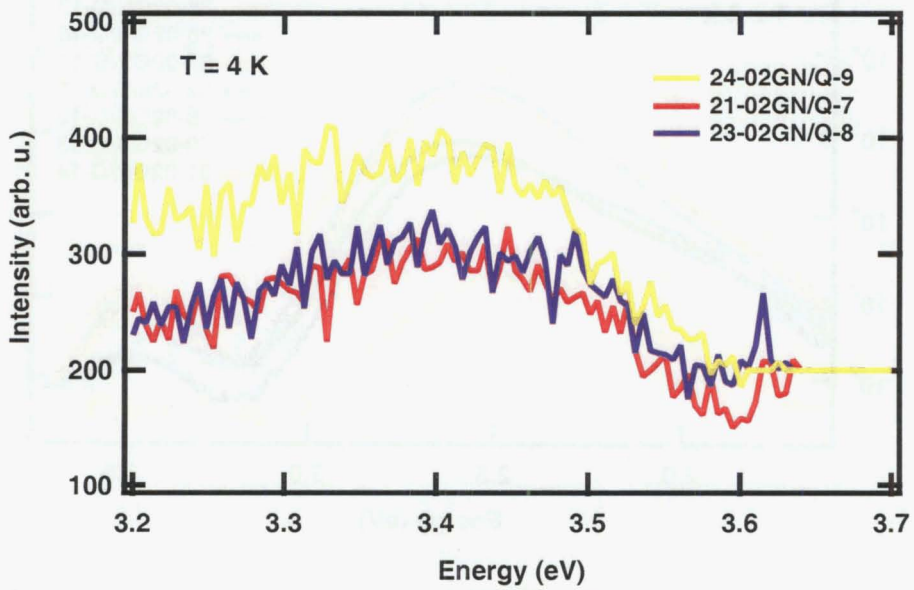

Figure 5.6: PL of the near band edge emission of samples 21-02GN/ Q-7, 23-02GN/ Q-8, and 24-02GN/ Q-9 on quartz substrate, T = 4 K.

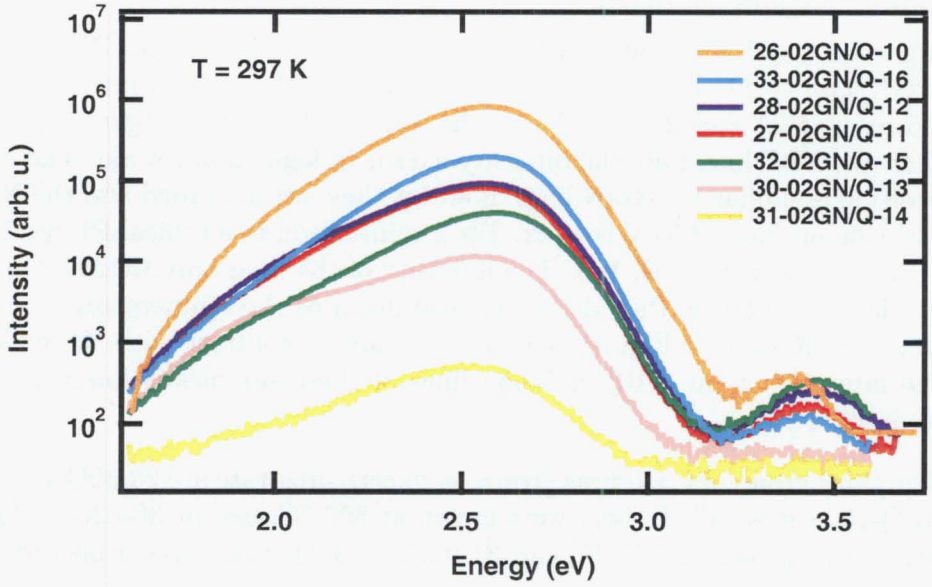

Figure 5.7: PL result of samples 26-02GN/ Q-10, 27-02GN/ Q-11, 28-02GN/ Q-12, 30-02GN/ Q-13, 31-02GN/ Q-14, 32-02GN/ Q-15, and 33-02GN/ Q-16 on quartz substrate, T = 297 K.

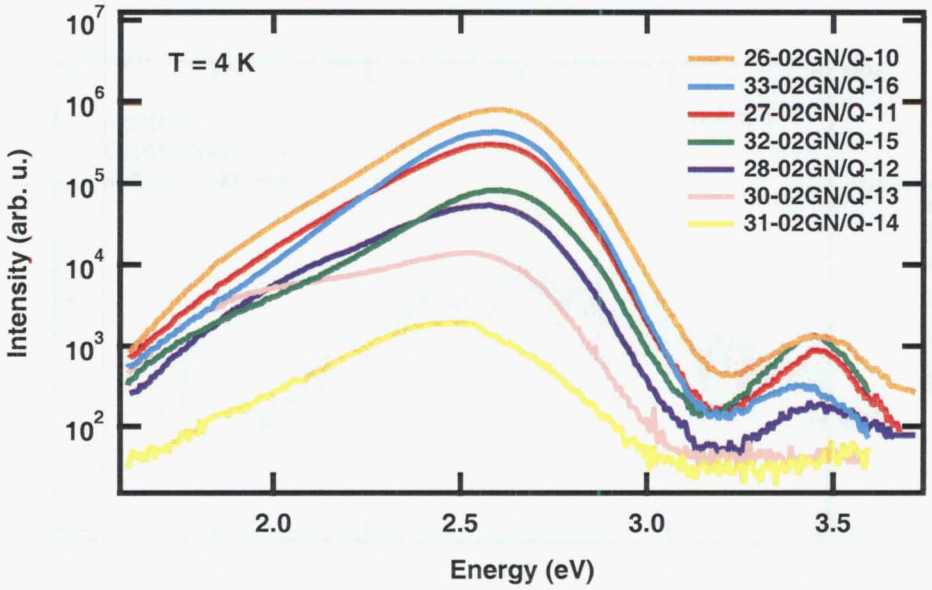

Figure 5.8: PL result of samples 26-02GN/ Q-10, 27-02GN/ Q-11, 28-02GN/ Q-12, 30-02GN/ Q-13, 31-02GN/ Q-14, 32-02GN/ Q-15, and 33-02GN/ Q-16 on quartz substrate, T = 4 K.

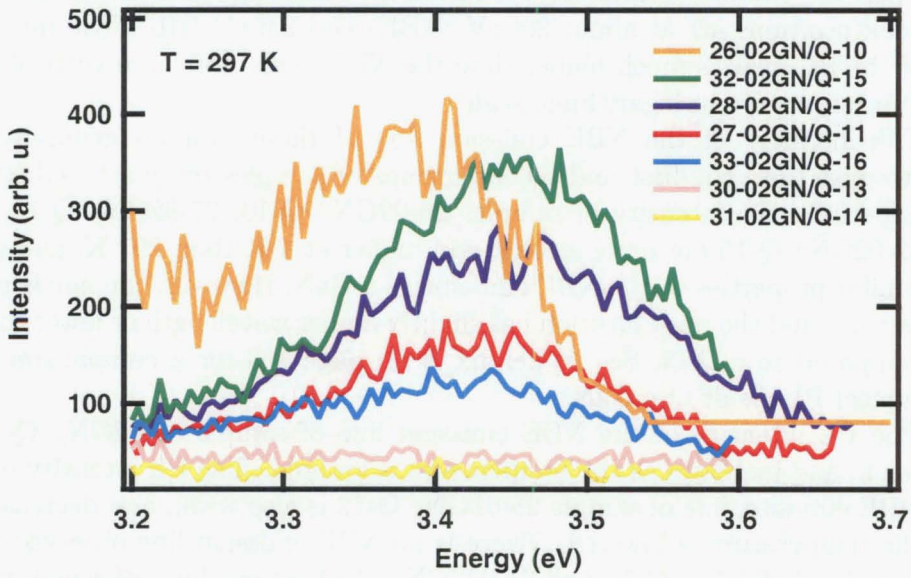

Figure 5.9: PL result of near band edge emission of samples 26-02GN/ Q-10, 27-02GN/ Q-11, 28-02GN/ Q-12, 30-02GN/ Q-13, 31-02GN/ Q-14, 32-02GN/ Q-15, and 33-02GN/ Q-16 on quartz substrate, T = 297 K.

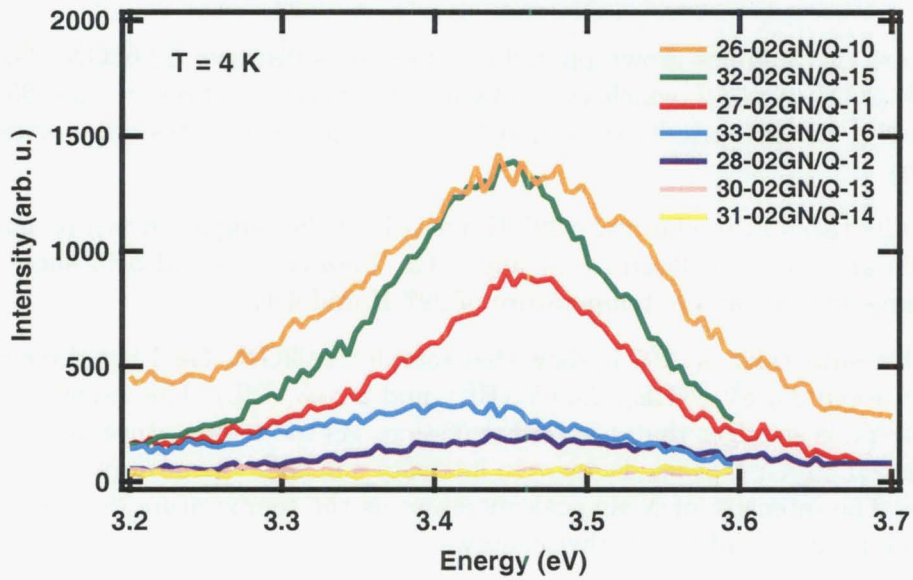

Figure 5.10: PL result of near band edge emission of samples 26-02GN/ Q-10, 27-02GN/ Q-11, 28-02GN/ Q-12, 30-02GN/ Q-13, 31-02GN/ Q-14, 32-02GN/ Q-15, and 33-02GN/ Q-16 on quartz substrate, T = 4 K.

at 297 K and 4 K. And figures 5.9, 5.10 show their NBE emission line.

There are two broad lines observed from the PL results of these samples, the peak positions are at about 3.4 eV (NBE) and 2.6 eV (BL). The intensity of the BL peak is much higher than the NBE peak, note: the vertical axes of intensity are in logarithmic scale.
The intensity of the NBE emission line of these samples generally are stronger than the first and second groups of samples on quartz substrate. Especially the intensity of samples 26-02GN/ Q-10, 27-02GN/ Q-12, and 32-02GN/ Q-15 are quite strong, and higher at 4 K than 297 K, and show similar properties to the NBE emission of c-GaN. However, the line is much broader and the peak position has slightly higher wavelength or lower energy compared to c-GaN. See Appendix B on page 193 for a comparison to a typical PL result of c-GaN.
The PL intensity of the NBE emission line of sample 33-02GN/ Q-16 is weak, and increases as the temperature is lowered. The PL intensity of the NBE emission line of sample 28-02GN/ Q-12 is also weak, and decreases as the temperature is lowered. There is no NBE emission line observed from samples 30-02GN/ Q-13 and 31-02/GN/ Q-14, at our level of sensitivity.

Overall, the PL results show that GaN films grown on quartz substrate give promising results, especially samples 26-02GN/ Q-10, 27-02GN/ Q-12, and 32-02GN/ Q-15.

5.4 GaN Films Grown on Gallium Arsenide Substrate

There are two samples grown on gallium arsenide substrate: 22-02GN/ GaAs-1 and 25-02GN/ GaAs-2, which were grown at temperature of 500 °C and 650 °C. The in-situ RHEED results show that these samples have a crystalline structure property.

PL results taken at temperature 297 K and 4 K of the samples grown on gallium arsenide are shown in figures 5.11 and 5.12. Figures 5.13 and 5.14 show their NBE emission line at the temperature of 297 K and 4 K.

The PL results taken at 297 K show that sample 22-02GN/ Ga-1 has three broad lines at about 3.4 eV (NBE), 2.5 eV (BL), and 2.2 eV (YL). The intensity of the BL and YL is stronger than the NBE emission. As the temperature decreases to 4 K, the BL and YL peaks decrease in intensity and shift the position to a higher energy. The intensity of NBE peak increases as the temperature decreases, and the peak position shifts to higher energy.

Sample 25-02GN/ Ga-2 has two broad lines at about 3.4 eV (NBE) and 2.6 eV (BL). The intensity of the PL peaks from this sample are relatively weaker than from the other sample on a gallium arsenide substrate. The intensity of the NBE and BL peaks of this sample decrease as the temperature decrease, and both peaks are weak at the temperature of 4 K.

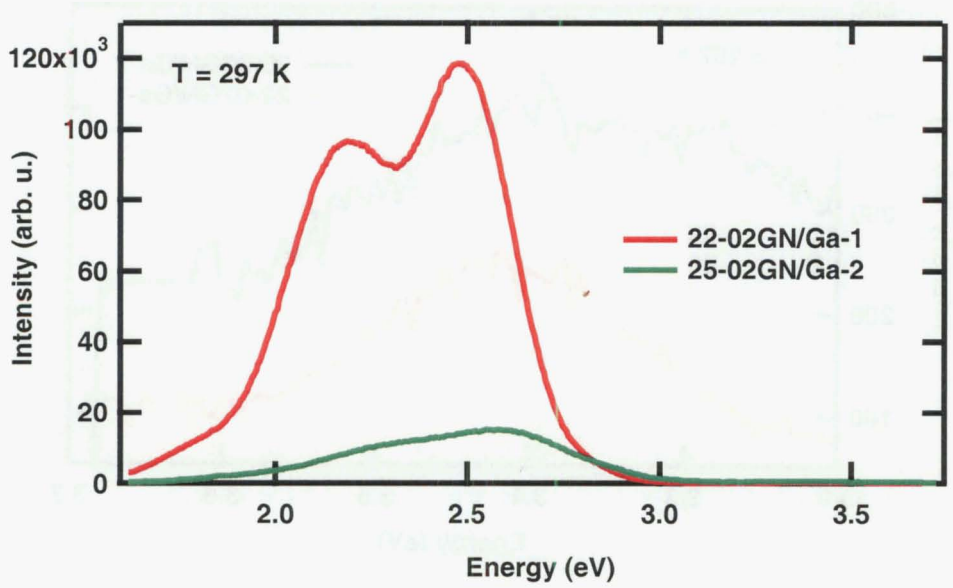

Figure 5.11: PL result of samples 22-02GN/ Ga-1, 25-02GN/ Ga-2 on gallium arsenide substrate, T = 297 K.

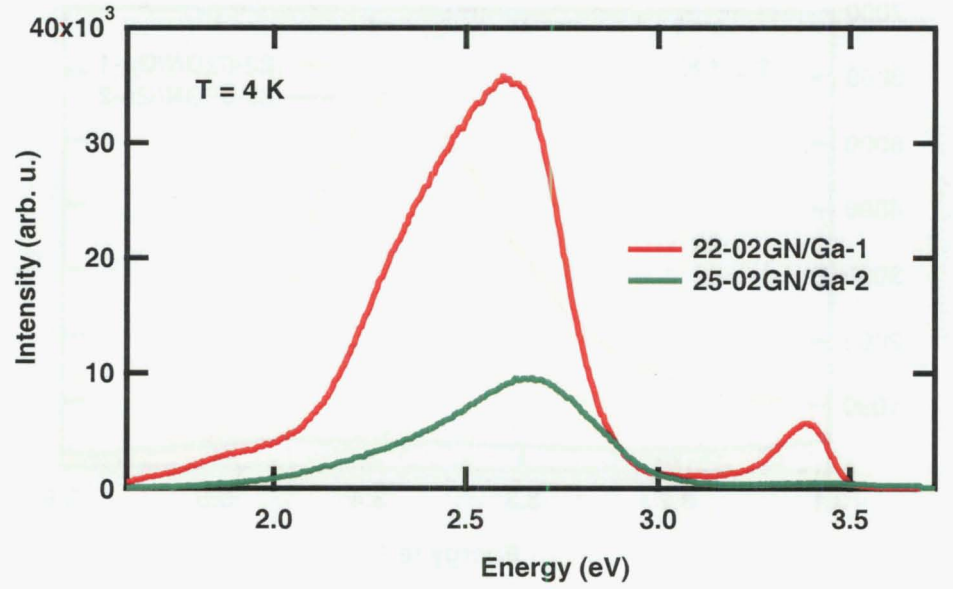

Figure 5.12: PL result of samples 22-02GN/ Ga-1, 25-02GN/ Ga-2 on gallium arsenide substrate, T = 4 K.

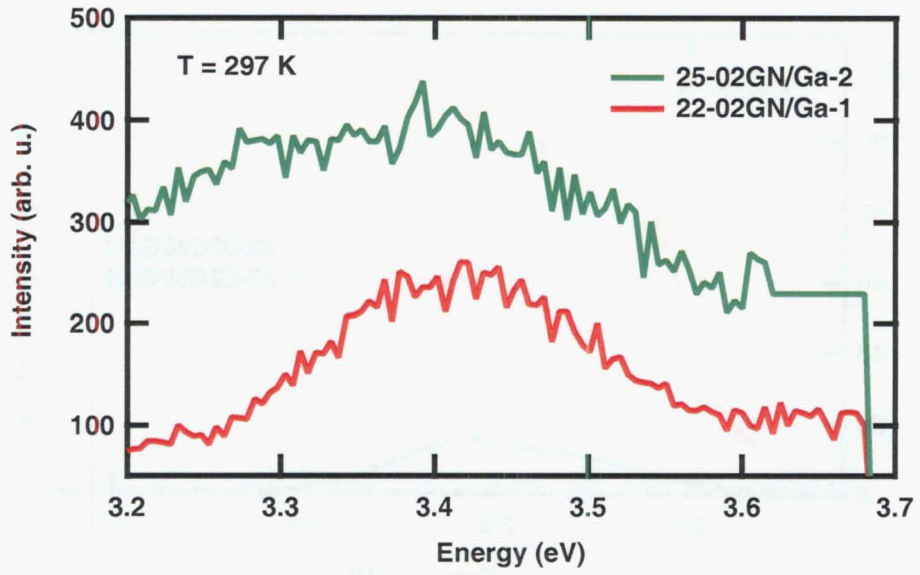

Figure 5.13: PL of the near band edge emission of samples 22-02GN/ Ga-1, 25-02GN/ Ga-2 on gallium arsenide substrate, T = 297 K.

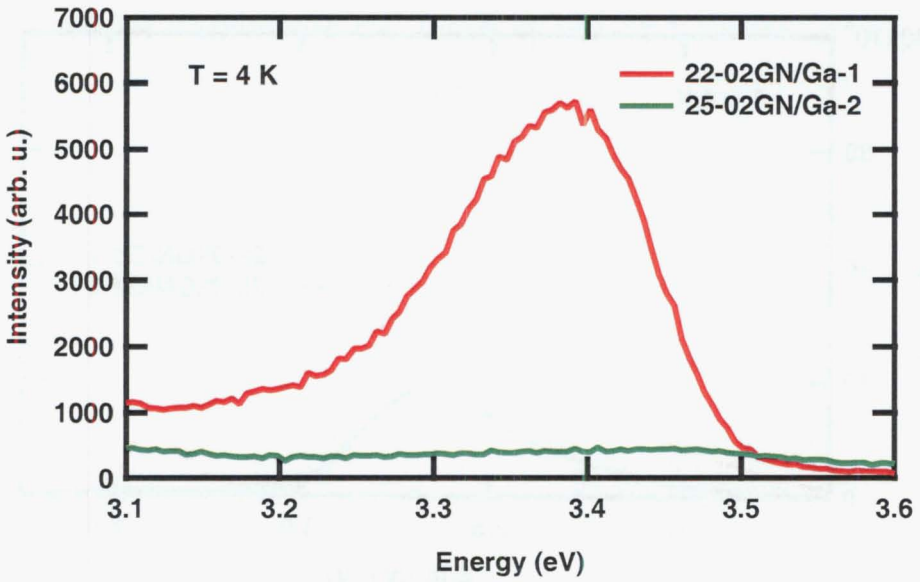

Figure 5.14: PL of the near band edge emission of samples 22-02GN/ Ga-1, 25-02GN/ Ga-2 on gallium arsenide substrate, T = 4 K.

In summary, the PL results of the samples 22-02GN/ GaAs-1 and 25-02GN/ GaAs-2 show a NBE emission line at 3.4 eV. However, the NBE emission line is weak and broad. The BL at 2.6 eV and YL 2.2 eV lines are more dominant and have much stronger intensity than the NBE line.

5.5 GaN Films Grown on Sapphire Substrate

There are five samples grown on sapphire substrate: 29-02GN/ Sa-2, 34-02GN/ Sa:Ca-1, 37-GaN/ Sa-03, 41-GaN/ Sa-04, and 70-GaN/ Sa-12. All the samples were grown at temperature of 500 °C or higher, up to about 800 °C. The in-situ RHEED results show that these samples have a crystalline structure property.

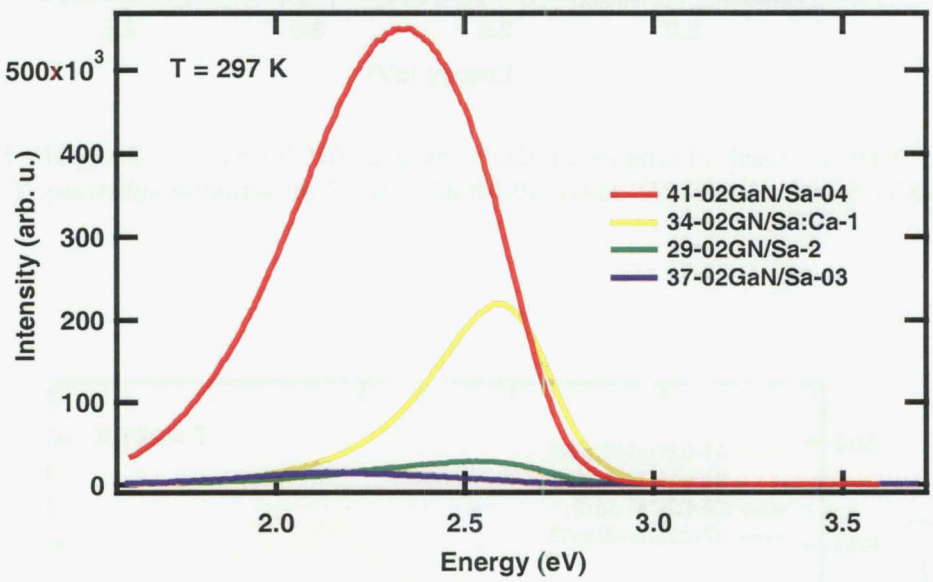

Figure 5.15: PL result of samples 29-02GN/ Sa-2, 34-02GN/ Sa:Ca-1, 29-02GN/ Sa-2, 37-02GaN/ Sa-03, 41-02GaN/ Sa-04 on sapphire substrate, T = 297 K.

PL results taken at temperature 297 K and 4 K of the samples grown on sapphire substrate are shown in figures 5.15 and 5.16, except for sample 70-02GaN/ Sa-12 which was only measured at low temperature.
Figures 5.17 and 5.18 show their NBE emission line at the temperature of 297 K and 4 K.

The PL result at 297 K of sample 29-02GN/ Sa-2 shows two broad lines at about 3.51 eV (NBE) and 2.58 eV (BL). The intensity of both peaks BE and BL increase sharply as temperature decreases from 297 K to 4 K, and the peaks position shift to 3.52 eV (NBE) and 2.53 (BL). The linewidth (FWHM) of the NBE line is broad, about 250 meV.

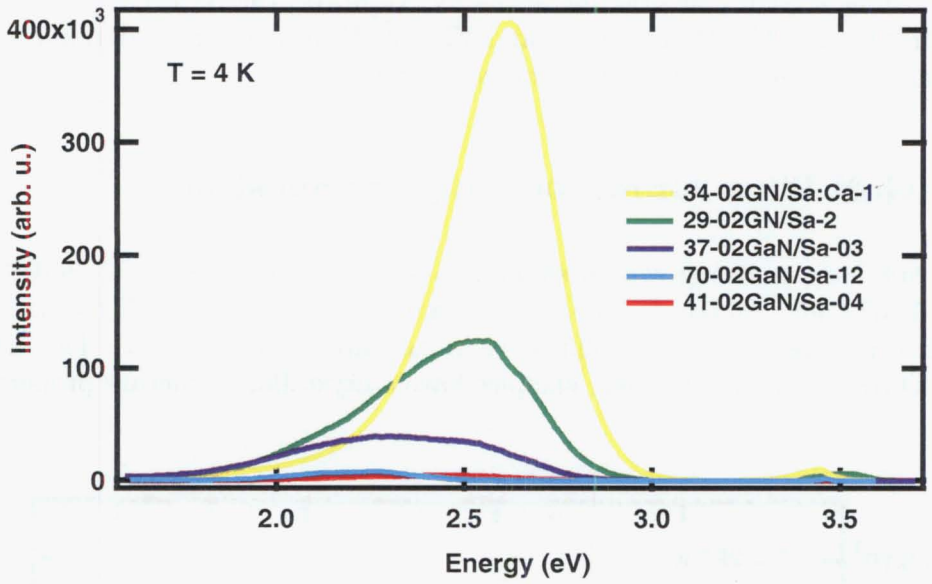

Figure 5.16: PL result of samples 29-02GN/ Sa-2, 34-02GN/ Sa:Ca-1, 29-02GN/ Sa-2, 37-02GaN/ Sa-03, 41-02GaN/ Sa-04, 70-02GaN/ Sa-12 on sapphire substrate, T = 4 K.

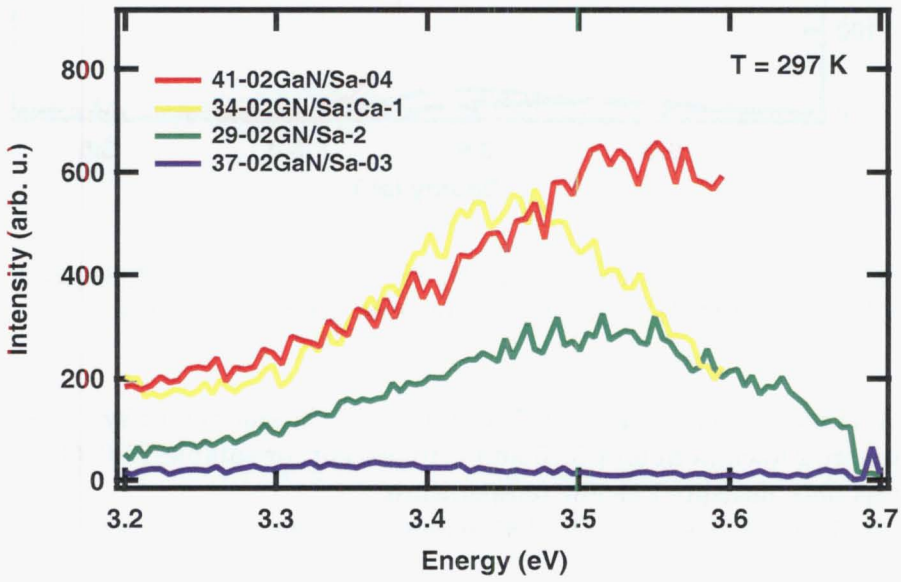

Figure 5.17: PL of the near band edge emission of samples 29-02GN/ Sa-2, 34-02GN/ Sa:Ca-1, 29-02GN/ Sa-2, 37-02GaN/ Sa-03, 41-02GaN/ Sa-04 on sapphire substrate, T = 297 K.

At our level of sensitivity, sample 37-02GaN/Sa-03 does not show NBE emission in the UV region at 297 K nor 4 K. It has a weak but broad line from about 2.76 eV to 1.65 eV, peaking at about 2.10 eV (YL). The intensity of this YL peak increases as the temperature decreases.

The PL results of sample 41-02GaN/ Sa-04 show an unreliable and weak NBE emission at the temperature of 297 K which disappears at the temperature of 4 K. A broad and strong line from 2.95 eV to about 1.55 eV (YL) was also observed. The intensity of this YL line at the temperature of 297 K is much stronger than other samples and decreases sharply as the temperature decreases to 4 K.

Sample 70-02GaN/ Sa-12 shows the most preferable properties among others. The PL was taken at temperature 4 K and much smaller slits (200/ 400/ 400/ 200 μm) of the spectrometer, and the results show that there are two peaks observed at 3.47 eV (NBE) and 2.27 eV (YL). This sample has a relatively sharper linewidth (about 49 meV) of the NBE line than of other samples (about 200 to 300 meV). And the intensity of YL is comparable to intensity of the NBE emission line, that is about 4.6 times of the NBE line.

Sample 34-02GN/ Sa:Ca-1 is a c-GaN doped by calcium, and was expected to be a p-type of GaN film. The PL results show there are two peaks at 3.46 eV (NBE) and 2.58 eV (BL) observed from this sample. At the temperature of 4 K, the intensity of YL is almost twice higher than the intensity at the temperature

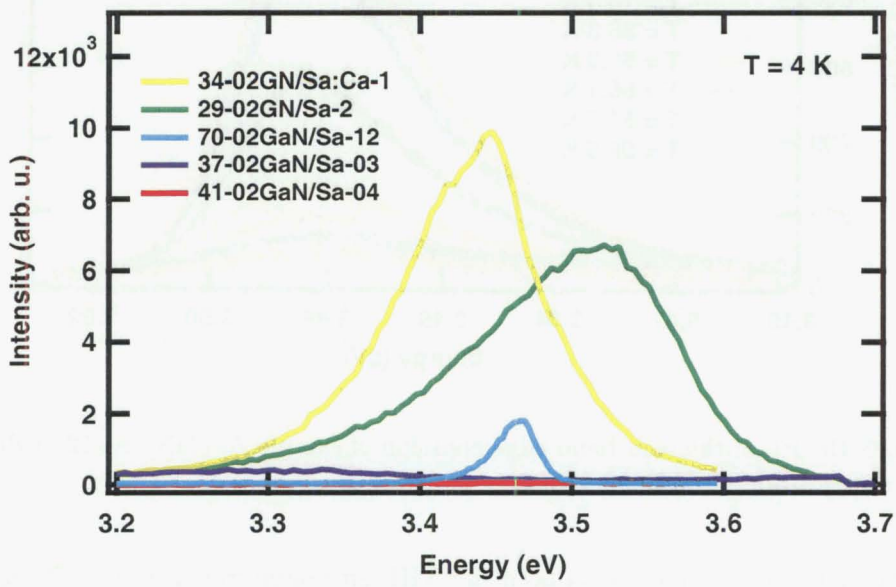

Figure 5.18: PL of the near band edge emission of samples 29-02GN/ Sa-2, 34-02GN/ Sa:Ca-1, 29-02GN/ Sa-2, 37-02GaN/ Sa-03, 41-02GaN/ Sa-04, 70-02GaN/ Sa-12 on sapphire substrate, T = 4 K.

of 297 K. The intensity of NBE increases sharply as the temperature decreases, and the peak position shifts from 3.46 eV at the temperature of 297 K to 3.44 eV at the temperature of 4 K.

In summary, the PL results of the GaN films grown on sapphire substrate show the NBE emission line in the UV region, except sample 37-02GaN/ Sa-03. However, most of the NBE emission line are weak and broad. The BL and/or YL line is more dominant and has much stronger intensity than the NBE emission line. In particular, sample 70-02GaN/ Sa-12 shows a strong, narrow (about 49 meV) NBE emission line, and the intensity of the NBE line is comparable to the intensity of the YL line.

5.6 PL Temperature Dependence of 70-02GaN/ Sa-12

Sample 70-02GaN/Sa-12 has similar properties to a good quality c-GaN (see Appendix B on page 193), therefore it is interesting to observe its NBE emission peak position and intensity temperature dependence.

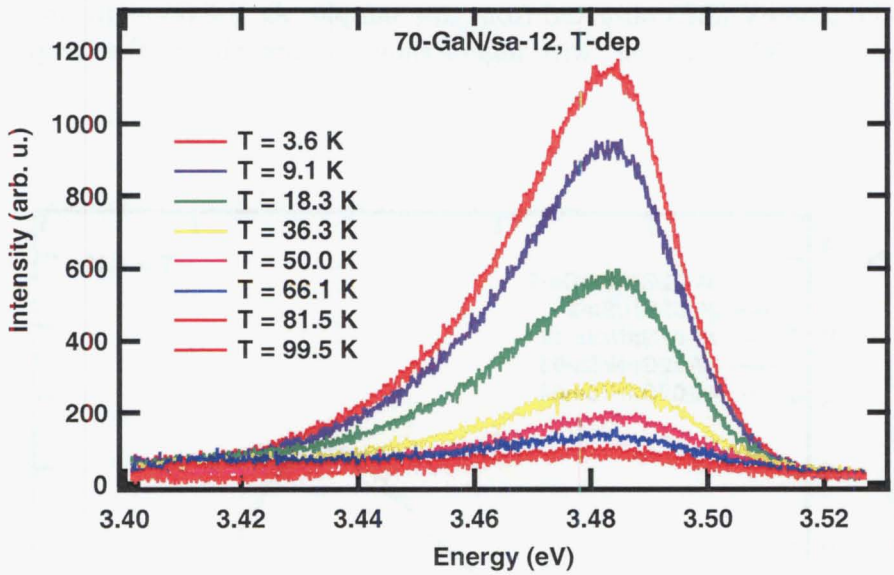

Figure 5.19: PL of the near band edge emission of sample 70-GaN/ Sa-12 at different temperatures from 3.6 K to 99.5 K.

Figure (5.19) shows the PL results of the NBE emission line of sample 70-02GaN/ Sa-12 at different temperature from 3.6 K to 99.5 K. At temperature higher than 100 K, the signal becomes weak.

Figure 5.20 shows the NBE peak position as a function of temperature of sample 70-02GaN/ Sa-12. The peak position is almost constant at about 3.48 eV from

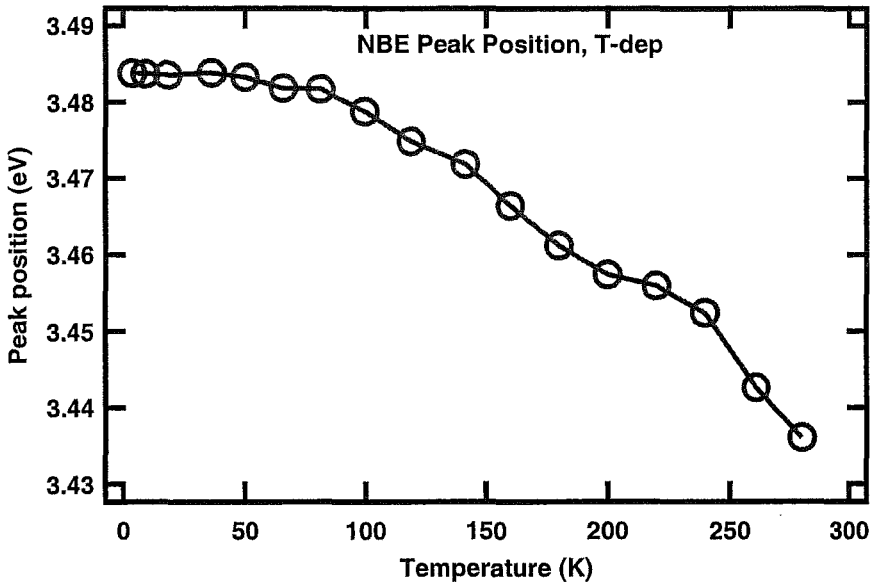

Figure 5.20: The peak position of the near band edge emission of sample 70-02GaN/ Sa-12 as a function of temperauture.

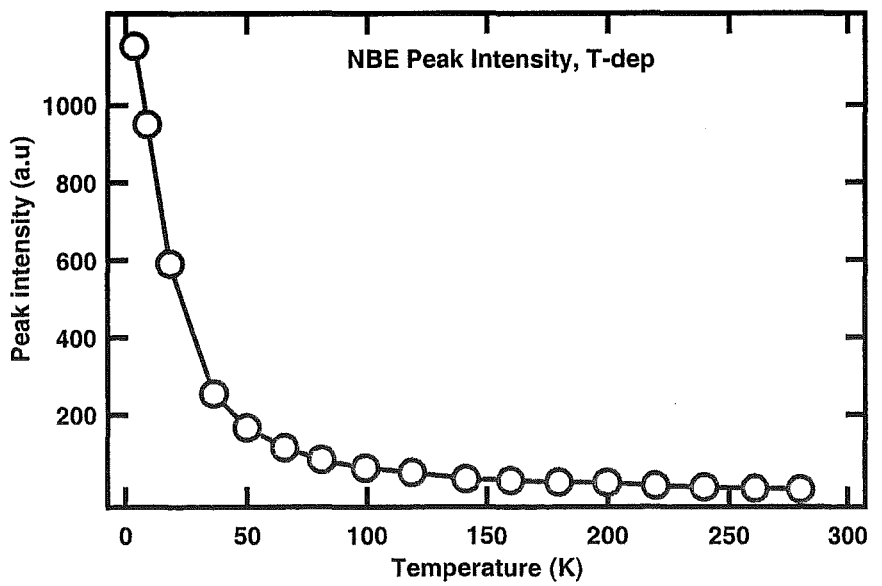

Figure 5.21: The peak intensity of the near band edge emission of sample 70-02GaN/ Sa-12 as a function of temperature.

the temperature of 3.6 K to about 80 K, then it shifted to a lower energy as the temperature became higher than 80 K. The peak position at 280 K is about 50 meV higher energy than the peak position at 3.6 K.

Figure 5.21 show the NBE peak intensity as a function of temperature of sample 70-02GaN/ Sa-12. The NBE peak intensity decreases sharply as the temperature increases from 3.6 K to 50 K, then decreases relatively slower at temperature higher than 50 K.

5.7 Conclusion and Further Work

- GaN films grown on silicon substrate
  There are thirteen GaN samples grown on silicon substrate at temperature about 250 °C or lower, and none of their PL results show an emission line. It gives a feedback that growing GaN film needs temperature higher than 250 °C.

- GaN films grown on quartz substrate
  There are ten GaN samples grown on quartz substrate at temperature mostly 500 °C. The RHEED in situ measurement of these samples shows a poly crystalline structure properties.

  The PL results show that GaN films grown on quartz substrate give promising results, especially samples 26-02GN/ Q-10, 27-02GN/ Q-12, and 32-02GN/ Q-15. The PL results of these particular samples show a relatively stronger NBE line intensity than others and the intensity increases as the temperature decreases, also show a closer properties to the good quality of GaN sample. However, the NBE linewidth is much broader than the NBE linewidth of a good quality GaN sample. The YL line is too dominant, the intensity of the YL line is much stronger than the intensity of NBE line.

- GaN films grown on gallium arsenide and sapphire substrate
  There are two samples grown on gallium arsenide substrate and five samples grown on sapphire substrate. The growth temperature of these samples is about 500 °C to 800 °C. The RHEED in situ measurement of these samples shows a crystalline structure properties.

  The PL results shows that almost all of the GaN films grown on gallium arsenide or sapphire substrate have near band edge emission line (NBE) and blue or yellow emission line (BL or YL). And the NBE line of these samples is relatively stronger than of the samples grown on quartz substrate. Except sample 37-02GaN/ Sa-03 has only a weak and broad YL line. However, most of the NBE line of these samples are weak and broad compare to a good quality of GaN sample, and the YL line is too dominant, with much stronger intensity than the NBE line.

  The most promising sample grown on sapphire substrate is sample 70-02GaN/ Sa-12. It shows a strong and narrow (about 5 nm) NBE line,

and its intensity is comparable to the intensity of the YL line. The NBE line peak position of this sample is shifted to the higher wavelength or lower energy as temperature increases, this behaviour is similar to a good quality of crystalline GaN sample.

The NBE line peak intensity of sample 70-02GaN/ Sa-12 decreases sharply as the temperature increases from 3.6 K to 80 K, then decreases slower at temperature higher than 80 K, this behaviour is closer to the bahaviour of donor or acceptor bound exciton line than free exciton line.

Chapter 6

Influence of Ion Energy on the RIE Induced Optical Damage of GaN

6.1 Introduction

Reactive Ion Etching (RIE) induces defects in semiconductor materials that can serve as local non-radiative recombination centres for electron-hole pairs, affecting the radiative lifetimes and luminescence efficiencies of the semiconductors. The study of etch-induced changes to the optical properties is needed to fully understand GaN device performance.

In this project, Ar and SF_6 gas were used, and the ion energy was varied for the RIE processes. Ar gas is relatively inert causes physical etching, eroding material at about 4 nm/min and SF_6 gas causes mainly chemical etching, eroding material about 29 nm/min [15].

6.2 Results of Previous Work

These are conclusions from previous work that has been done in the University of Canterbury and related to this work:

- In bulk MOVPE grown GaN, Ar plasma etching can increase the near band edge (NBE) and below band gap emission dramatically [13].
- The PL temperature dependence measurements of the NBE emission shows that donor bound excitons (D^0X) are dominant in Ar-etched samples, while the free exciton is dominant in unetched samples [13].
- UV illumination at low temperature on GaN sample shows that metastable behaviour of GaN is from the defect related blue (BL) and yellow (YL) luminescence bands. UV illumination at room temperature enhances the YL by a factor of 20 after a period of time, this effect can be applied for room temperature optical data storage and retrieval [13, 71].

- There is a relation between YL and BL emission which indicate that any microscopic model of the defects associated with the YL can also explain the BL [13, 71].

- Ar plasma etching of bulk GaN results in the introduction of neutral donors and the creation of metastable defects [13], showing an increase on the YL intensity by a factor of 20 compared to unetched sample [16].

- The NBE luminescence analysis of Ar-etched and SF_6-etched GaN show that more donor related defects were introduced on the top 100 nm GaN after Ar as compare to SF_6 etching [15].

- Ar plasma etching at lower voltage introduces less defects. These defects are metastable states that cause the BL to YL transitions to change with time, and an enhanced YL at room temperature. These properties on Ar-etched GaN have been used to enhance optical memory effect in the yellow band at low and room temperature [16].

- It is shown that metastable states or defects consist of identifiable nitrogen deficient surfaces on the top few monolayers and unidentifiable defects that propagate down to the etched surface for at least 100 nm in depth [16].

- Reactive Ion Etching (RIE) using SF_6 plasma gives an etch rate of 29 nm/min, and between 10^0C to 50^0C of substrate temperature, the etching rate does not change [17].

- PL results show that defect related states cause free excitons to be bound after SF_6 reactive ion etching. And these defect bound excitons have significant different behaviour from free excitons [17].

- RIE introduces metastable defects into GaN. These defects contribute to the BL and YL. The data provide a strong information for theories of YL, showing that further theoretical developments must include a detailed model of compensating centres and lattice relaxation [11].

- A study on the enhanced optical memory effect in etched-GaN samples and the time-dependent behaviour of below band gap defect related luminescence shows that characteristic decay times depends strongly on the optical memory effect and the appearance of defect bound excitonic states near band edge. As a result, an improved optical memory devices might be fabricated using reactive ion etched GaN [12].

However, the previous work did not put consideration on a significant problem that the variation of optical properties of different samples taken from different parts of the same wafer can hide any etch-induced changes. In this study, complete characterisation of each individual sample before etching was done to accurately determine the effect of etching on a particular sample.

In each series, one sample was always kept unetched or untreated and used as a reference for the original series. The samples before and after treatment had to be measured at different days, perhaps a few weeks apart. The untreated sample was to use its intensity, linewidth and peak position to standarize all the PL results in one series. The assumption was that the untreated sample should give the same PL result at any time of PL measurement if the same condition and system arrangement was applied.

6.3 Results and Analysis of Ar Gas Etching

Three series of experiments have been done to investigate RIE using Ar gas. All the Ar gas etching processes were done to the samples in 2.5 minutes with 0.1 Torr etching pressure and 60 sccm gas flow rate at room temperature. Etching DC bias voltage was obtained by adjusting the rf power from 100 W to 300 W, causing different etching DC bias voltages from about 260 V to 530 V.

The analysis of the optical changes due to RIE have been determined from the PL peak relative intensity and linewidth (FWHM) changes of the NBE emission line and the YL lines.

6.3.1 First Series of Ar Gas Etching

Sample	rf power (W)	rf reflected (W)	voltage (V)	pressure (mbar)	rf forward (W)
AL25	100	1	-280	7×10^{-5}	98
AL26	150	2	-365	7×10^{-5}	149
AL27	200	3	-415	7×10^{-5}	199
AL28			standard unetched		
AL29	250	4	-485	7×10^{-5}	251
AL30	300	4	-532	7×10^{-5}	298

Table 6.1: The first series of Ar gas etching conditions.

The samples for the first series of Ar gas etching experiment are c-GaN/sap/30803/ Ar-etched /AL25, AL26, AL27, AL28, AL29, AL30 (6 samples). The etching conditions for each of these samples are shown in Table 6.1. For this series, sample AL28 was kept as a reference sample, remains unetched, and the PL measurements were taken at a temperature of 25 K.

Figures 6.1 and 6.2 show NBE PL of unetched and etched c-GaN/sap/ 30803 / AL25-27 and AL29-30. For each sample the spectrum labelled 'original' is the spectrum of that individual sample before the etching process. Apparent in the spectra is NBE emission at 3.493 eV.

Unfortunately, in sample AL29 there was artefact measured at 2.2 eV and was

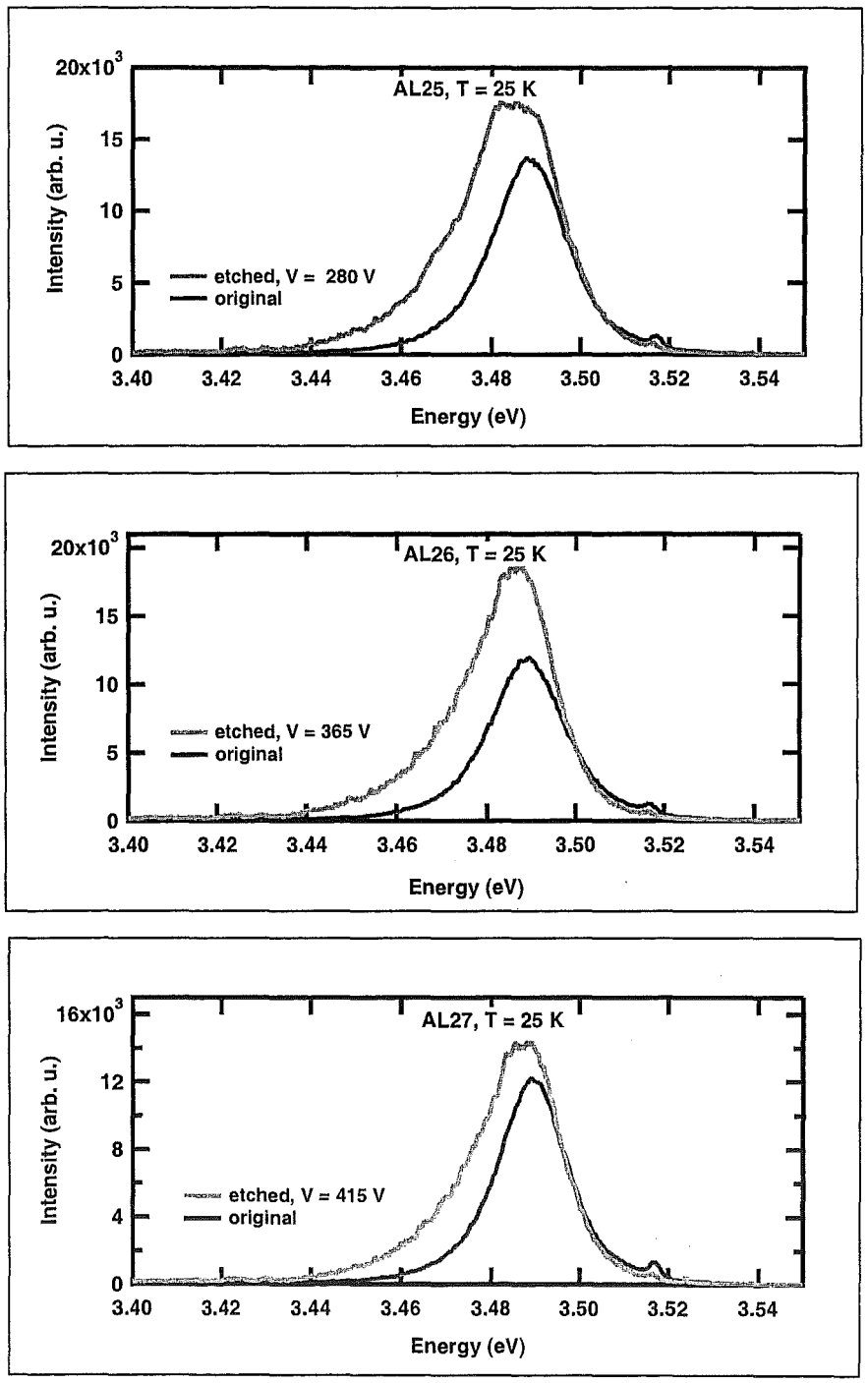

Figure 6.1: Near band edge PL of unetched and etched c-GaN/sap/30803/AL25-27 by Ar gas, at T = 25 K.

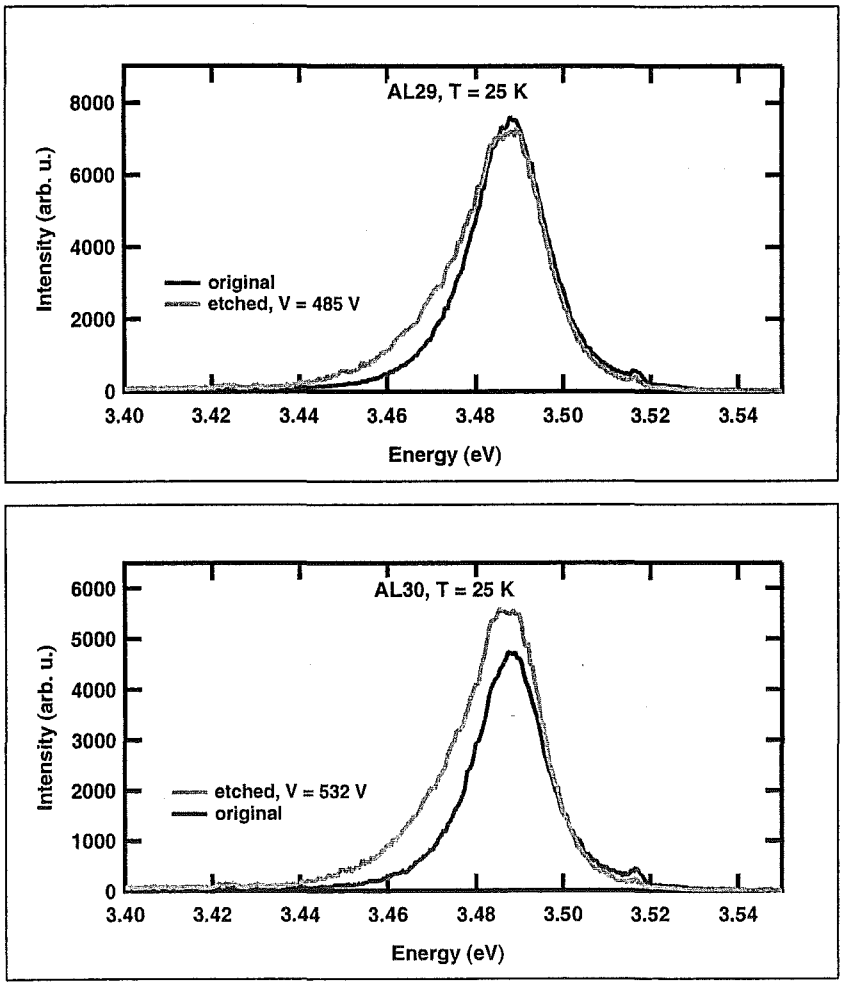

Figure 6.2: Near band edge PL of unetched and etched c-GaN/sap/ 30803 / AL29-30 by Ar gas, at T = 25 K.

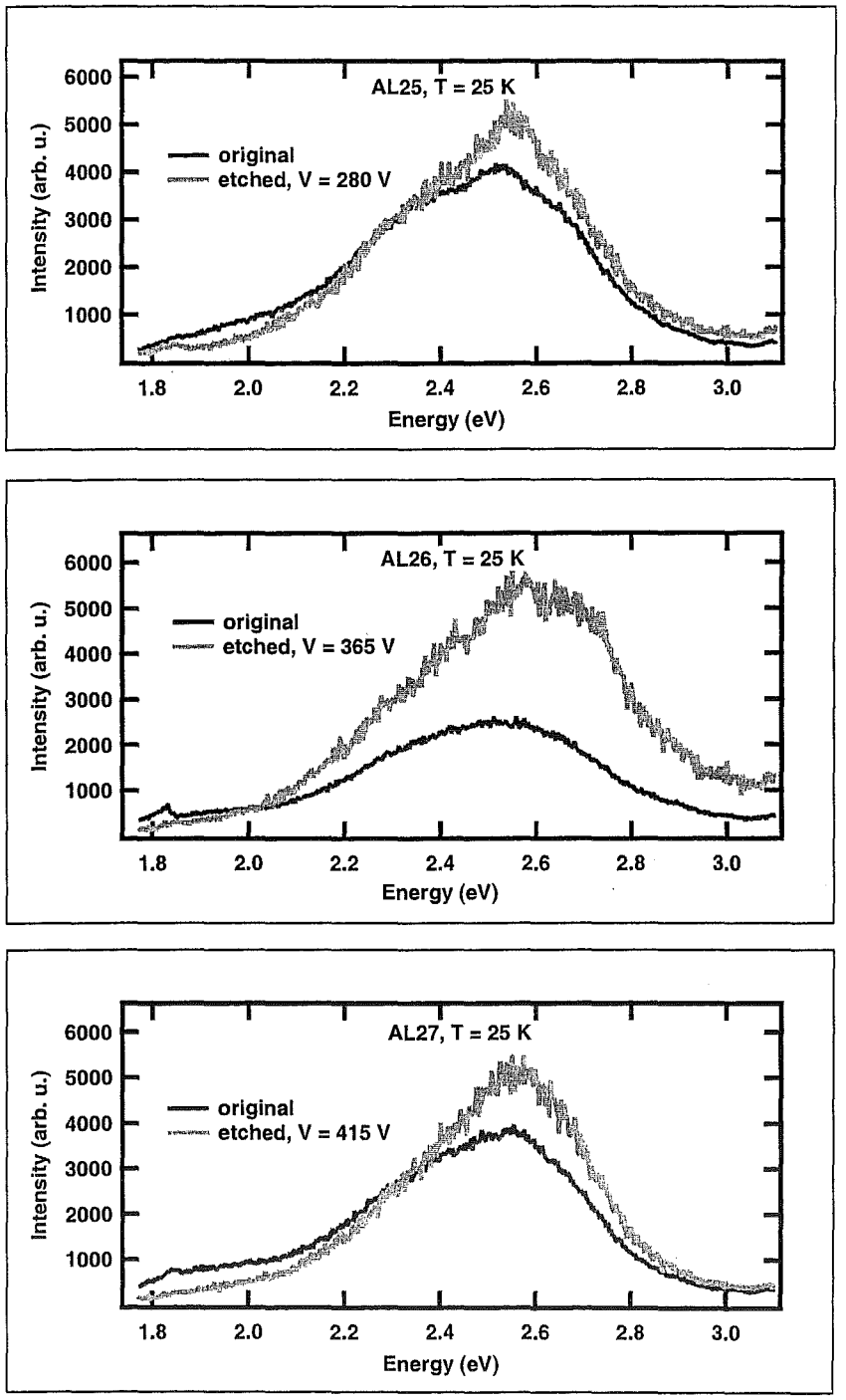

Figure 6.3: Yellow luminescence of unetched and etched c-GaN/sap/ 30803 / AL25-27 by Ar gas, at T = 25 K.

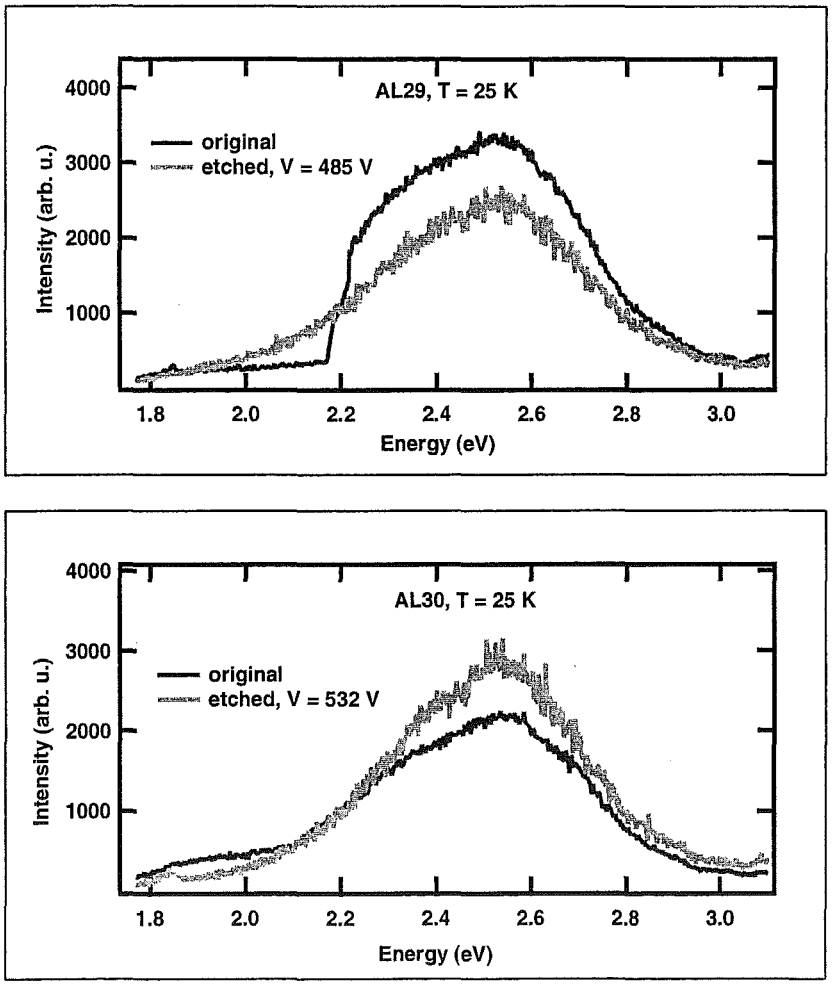

Figure 6.4: Yellow luminescence of unetched and etched c-GaN/sap/ 30803 / AL29-30 by Ar gas, at T = 25 K.

noticed only after the sample has been etched and thus the 'original' spectrum could not be re-recorded.

Figures 6.3 and 6.4 show PL of yellow luminescence (YL) of unetched and etched c-GaN/sap/30803/AL25-27 and AL29-30.

In this series, the YL spectrum consists of three peaks, the first peak is around 2.6 eV (YL1 peak), the second peak is around 2.4 eV (YL2 peak), and the third peak is around 2.0 eV (YL3 peak). The third peak of the YL does not always appear.

Analysis of the PL Results

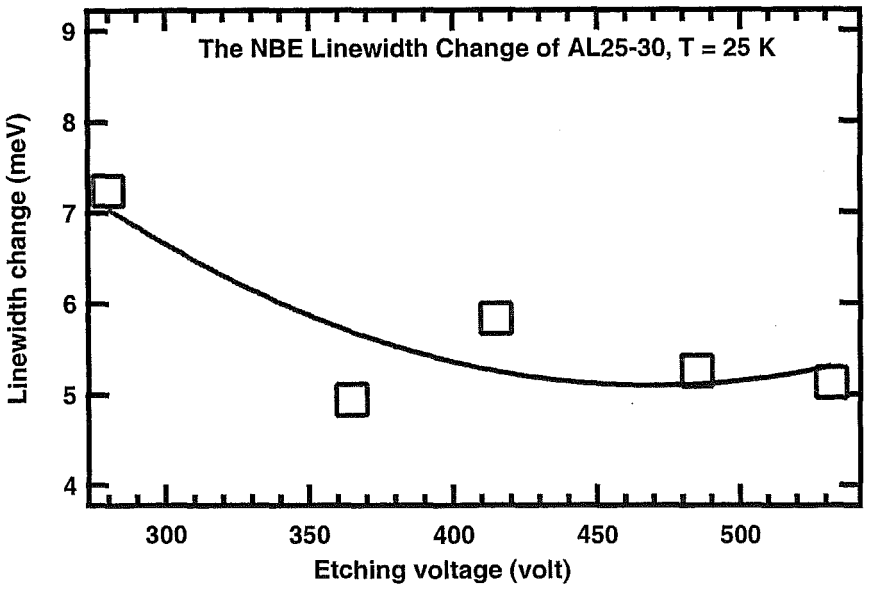

Figure 6.5: Near band edge PL relative linewidth change after etching of c-GaN/sap/ 30803 / AL25-30 by Ar gas, at T = 25 K, as a function of etching voltage.

Figure 6.5 shows the linewidth change to the NBE emission line as a function of etching DC bias voltage. The results show that the NBE linewidth after etching is wider than before etching, by the amount of 5 meV to 7.4 meV. A typical PL linewidth of NBE emission is about 14 meV. At the etching voltage of 280 V, the linewidth change is 7.4 meV, and then decreases to about 5.2 meV as the etching voltage increases to 532 V.

Figure 6.6 shows the relative intensity of the NBE emission after etching as a function of etching voltage. The NBE PL intensity after etching is relatively higher than before etching. At etching voltage of 280 V, the relative intensity

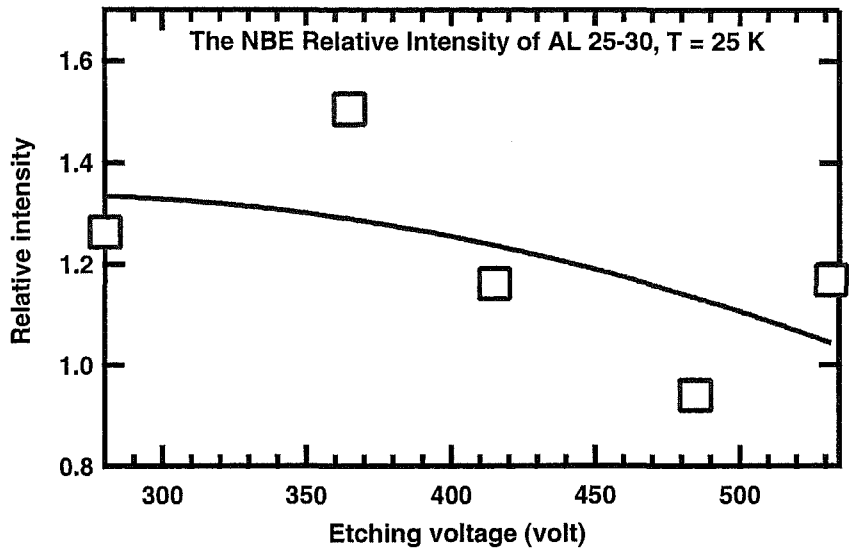

Figure 6.6: Near band edge PL intensity ratio etched/unetched of c-GaN/sap/ 30803 / AL25-30 by Ar gas, at T = 25 K, as a function of etching voltage.

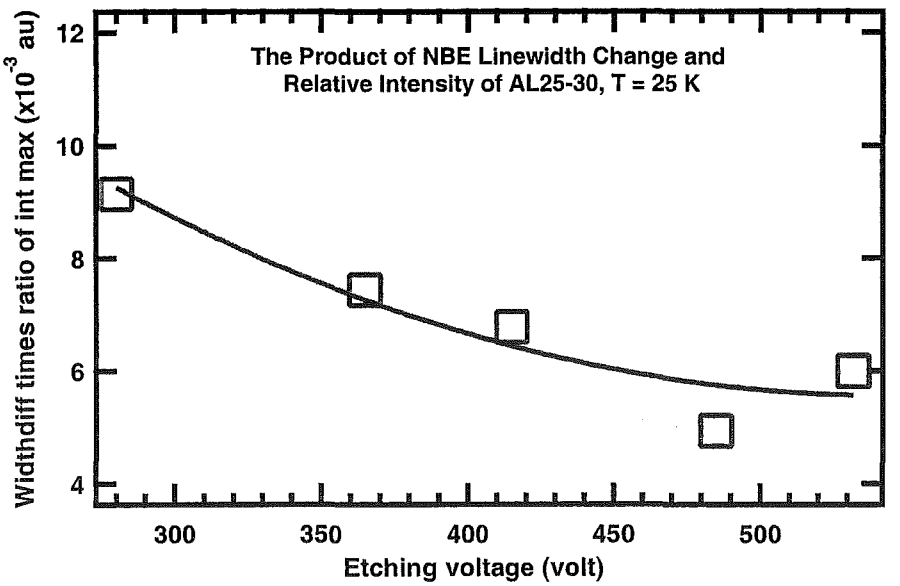

Figure 6.7: Product of near band edge PL peak intensity ratio and the linewidth change of etched c-GaN/sap/ 30803 / AL25-30 by Ar gas, at T = 25 K, as a function of etching voltage.

after etching is about 32% higher than before etching, and then it decreases slowly to only 5% higher than before etching at etching voltage of 532 V.

The data from figures 6.5 and 6.6 can be combined as the product of relative intensity peak and linewidth change. This product is plotted in figure 6.7 as a function of etching voltage. There is a rough correlation between the PL relative intensity and linewidth change, the decreasing PL relative intensity is compensated by increasing PL linewidth change and vice versa. However, overall the product show a slight decrease from about 9×10^{-3} to 5×10^{-3} as the etching voltage increases from 280 V to 532 V.

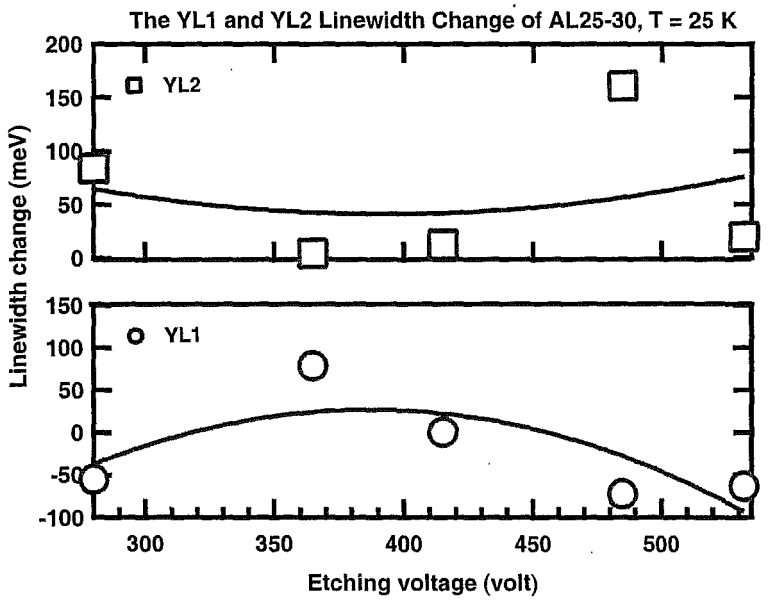

Figure 6.8: YL relative linewidth change after etching of c-GaN/sap/ 30803 / AL25-30 by Ar gas, at T = 25 K, as a function of etching voltage.

Figure 6.8 shows YL1 and YL2 linewidth change after etching as a function of etching voltage. In most of the samples YL1 is narrower, and YL2 is broader after etching, indicated by negative linewidth change for YL1 and positive linewidth change for YL2.

There is a rough correlation between the linewidth change of YL1 and YL2. At etching voltage of 280 V, the linewidth of YL1 is relatively narrower, then slowly becomes wider until it reaches the widest linewidth change at etching voltage about 400 V,and gradually narrowed again as the etching voltage increases. In contrast, YL2 is relatively wider at etching voltage of 280 V, and slowly narrowed up to etching voltage about 400 V, then becomes wider again as etching voltage increases.

Figure 6.9 shows the relative intensity of YL1 and YL2 after etching as a function

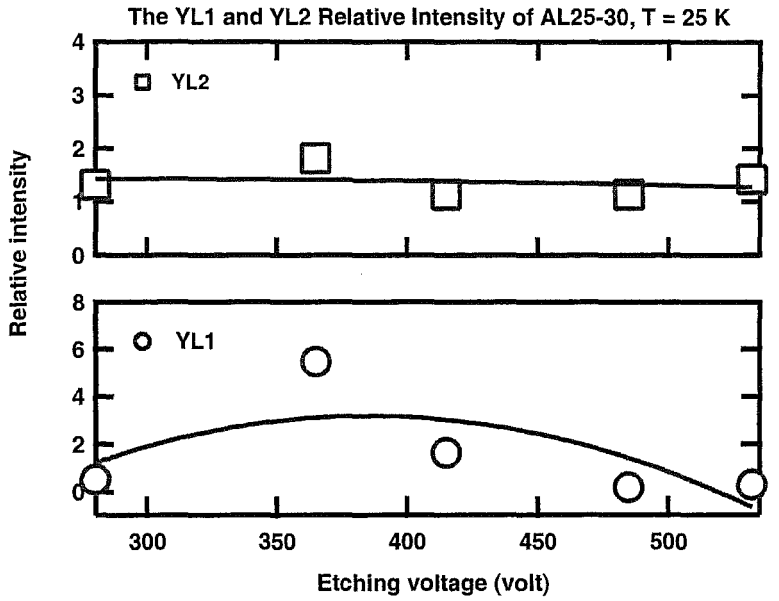

Figure 6.9: YL intensity ratio etched/unetched of c-GaN/sap/ 30803 / AL25-30 by Ar gas, at T = 25 K, as a function of etching voltage.

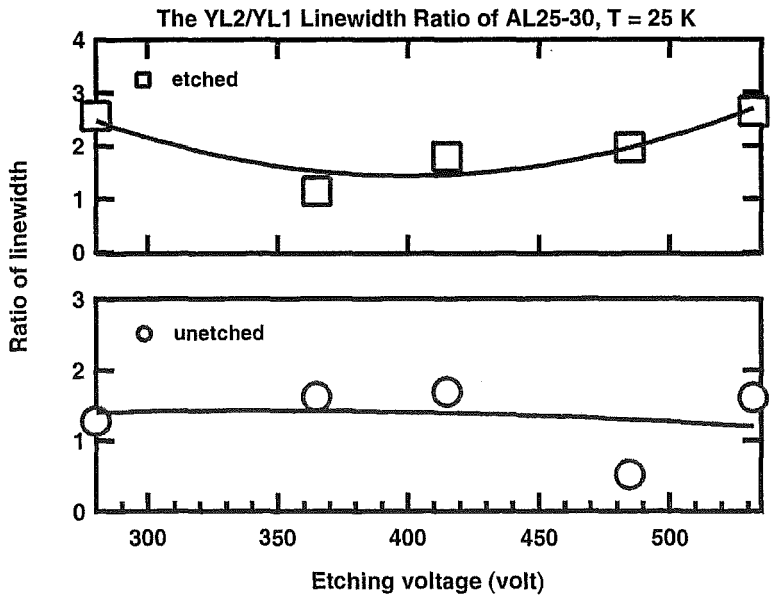

Figure 6.10: Relative linewidth change of YL2 to YL1 of unetched and etched c-GaN/sap/ 30803 / AL25-30 by Ar gas, at T = 25 K, as a function of etching voltage.

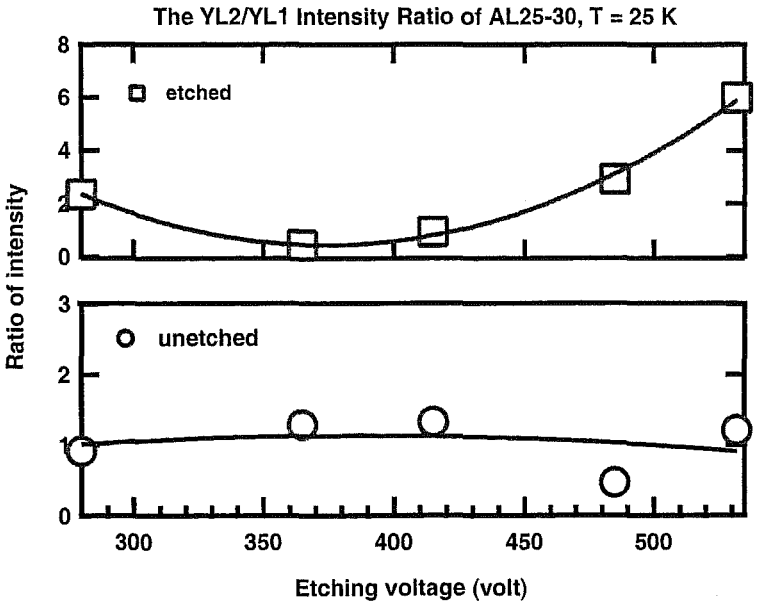

Figure 6.11: Relative intensity of YL2 to YL1 of unetched and etched c-GaN/sap/ 30803 / AL25-30 by Ar gas, at T = 25 K, as a function of etching voltage.

of etching voltage. The relative intensity of YL1 peak after etching is higher than before etching in the range of 280 V to 480 V etching voltage. The highest relative YL1 peak intensity after etching is more than three times of the YL1 peak before etching, it is reached at etching voltage about 360 V. The relative intensity of YL2 peak after etching is almost constant, about 30% higher than before etching, and independent on the etching voltage.

Figure 6.10 shows the relative linewidth of YL2 to YL1 before and after etching as a function of etching voltage. Before etching, YL2 is almost constantly about 40% wider than YL1. After etching, at the 280 V etching voltage YL2 is about 2.5 times wider than YL1, then decreases to about 1.5 times of YL1 at about 380 V and increases sharply back to more than 2.5 times wider than YL1 at 532 V etching voltage.

Figure 6.11 shows the relative peak intensity of YL2 to YL1 before and after etching as a function of etching voltage. Before etching, the peak intensity of YL1 and YL2 is almost the same, the ratio is close to 1. After etching, the intensity of YL2 is 2.3 times higher than YL1 at 280 V etching voltage, then gradually decreases to 0.5 times lower than the intensity of YL1 at 370 V. At etching voltage higher than 370 V, the intensity of YL2 sharply increase to about 6 times higher than the intensity of YL1 at 532 V etching voltage.

There is an obvious change of the YL spectrum after the etching processes where in most cases YL has higher intensity and wider linewidth after etching. Results

and analysis of YL1 and YL2 shows that YL changes mainly due to the changes of YL1, and YL2 does not greatly change after etching.

AFM Images and Analysis

Figure 6.12 shows AFM images of c-GaN/sap/ 30803 / AL25-30. The RMS roughness was measured for all etched samples and this data is plotted in figure 6.13.

At the etching voltage of 280 V, the RMS roughness of the sample's surface is about 7 nm, then gradually increases or samples surface is rougher as the etching voltage increases. The RMS roughness is about 17 nm at etching voltage around 400 V. At the etching voltages higher than 400 V, the RMS roughness of sample's surface decreases as the etching voltage increases, the RMS roughness is about 10 nm at etching voltage of 532 V. The RMS roughness for the untreated sample AL28 is about 11 nm.

6.3.2 Second Series of Ar Gas Etching

Sample	rf power (W)	rf reflected (W)	voltage (V)	pressure (mbar)	rf forward (W)
AL31	100	1	-260	1×10^{-8}	98
AL32	130	2	-328	1×10^{-8}	128
AL33			standard unetched		
AL34	150	2	-360	1×10^{-8}	149
AL35	180	3	-380	1×10^{-8}	179
AL36	200	3	-415	1×10^{-8}	199
AL37	250	4	-480	1×10^{-8}	250
AL38	300	4	-526	1×10^{-8}	295

Table 6.2: The second series of Ar gas etching conditions.

The second series of Ar gas etching experiment was done to improve the work that has been done in the first series, for example the second series consists of more samples.

The samples for the second series of Ar gas etching experiment are c-GaN/sap/ 30803 / Ar etched /AL31, AL32, AL33, AL34, AL35, AL36, AL37, AL38 (8 samples). The etching conditions for each of these samples are shown in Table 6.2. Sample AL33 was kept as an original reference sample in this series. The PL measurements were taken at a temperature of 25 K.

Figures 6.14 and 6.15 show the PL results of NBE emission of unetched and etched c-GaN/sap/ 30803/ AL31-35 and AL36-38. Apparent is NBE emission at 3.493 eV.

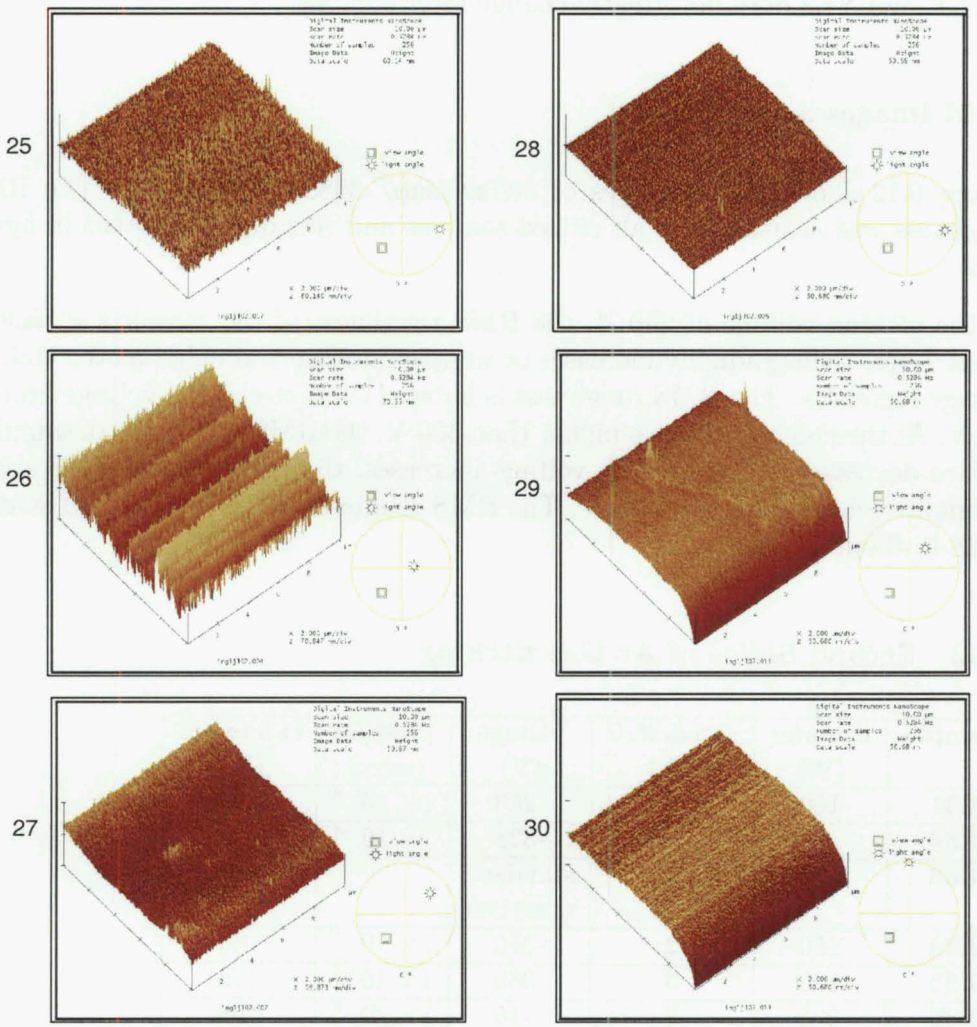

Figure 6.12: AFM images of the surface of etched c-GaN/sap/30803/ AL25-30 by Ar gas.

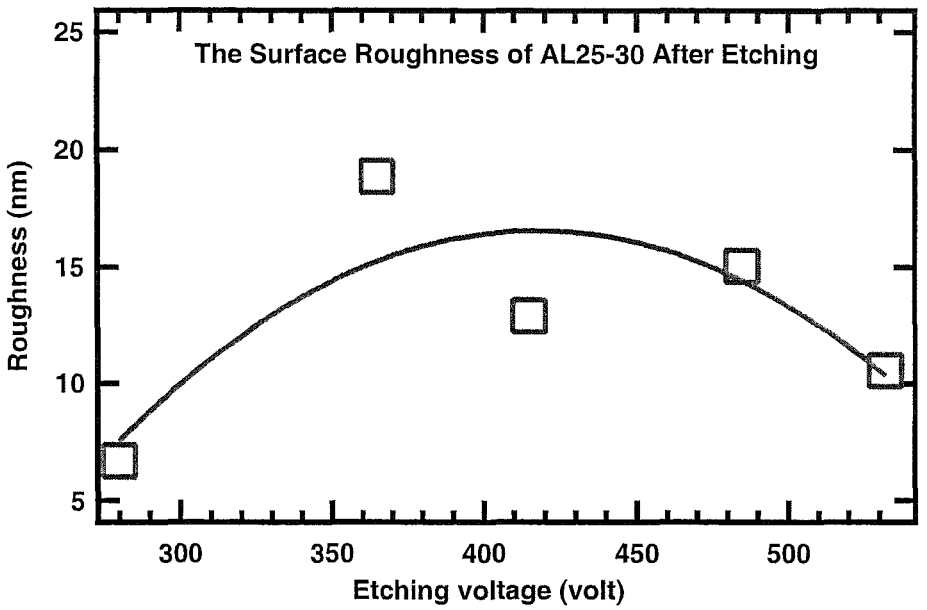

Figure 6.13: The surface roughness of etched c-GaN/sap/ 30803 / AL25-30 by Ar gas as a function of etching voltage.

Figures 6.16 and 6.17 show PL of YL of unetched and etched c-GaN/sap/ 30803/ AL31-35 and AL36-38.

In this series, the PL of YL spectrum consists of two peaks, the first peak is about 2.562 eV (YL1 peak), and the second peak is about 2.344 eV (YL2 peak).

Analysis of the PL Results

The analysis results of the sample AL31 which was etched at 260 V etching voltage is greatly different from other results and can give a wrong conclusion. The PL results from figures 6.14 and 6.16 for AL31 show that the PL peak position is clearly shifted to a completely different energy, this effect was not observed for the other data. The PL linewidth of sample AL31 after etching is much wider than the PL linewidth of other samples. The clear differences of sample AL31 PL spectrum than others, is probably caused by measuring PL sample AL31 at the roughest surface or burnt by laser area of the sample. Therefore, this data point will be ignored in the following analysis, even though it is shown on the graphs.

Figure 6.18 shows the linewidth change to NBE emission line as a function of etching voltage. The results show that the linewidth after etching is wider than before etching by the amount of 4 meV to 13 meV, and a typical PL linewidth of NBE emission is about 14 meV.

The linewidth change after etching at the etching voltage 328 V is about 5 meV,

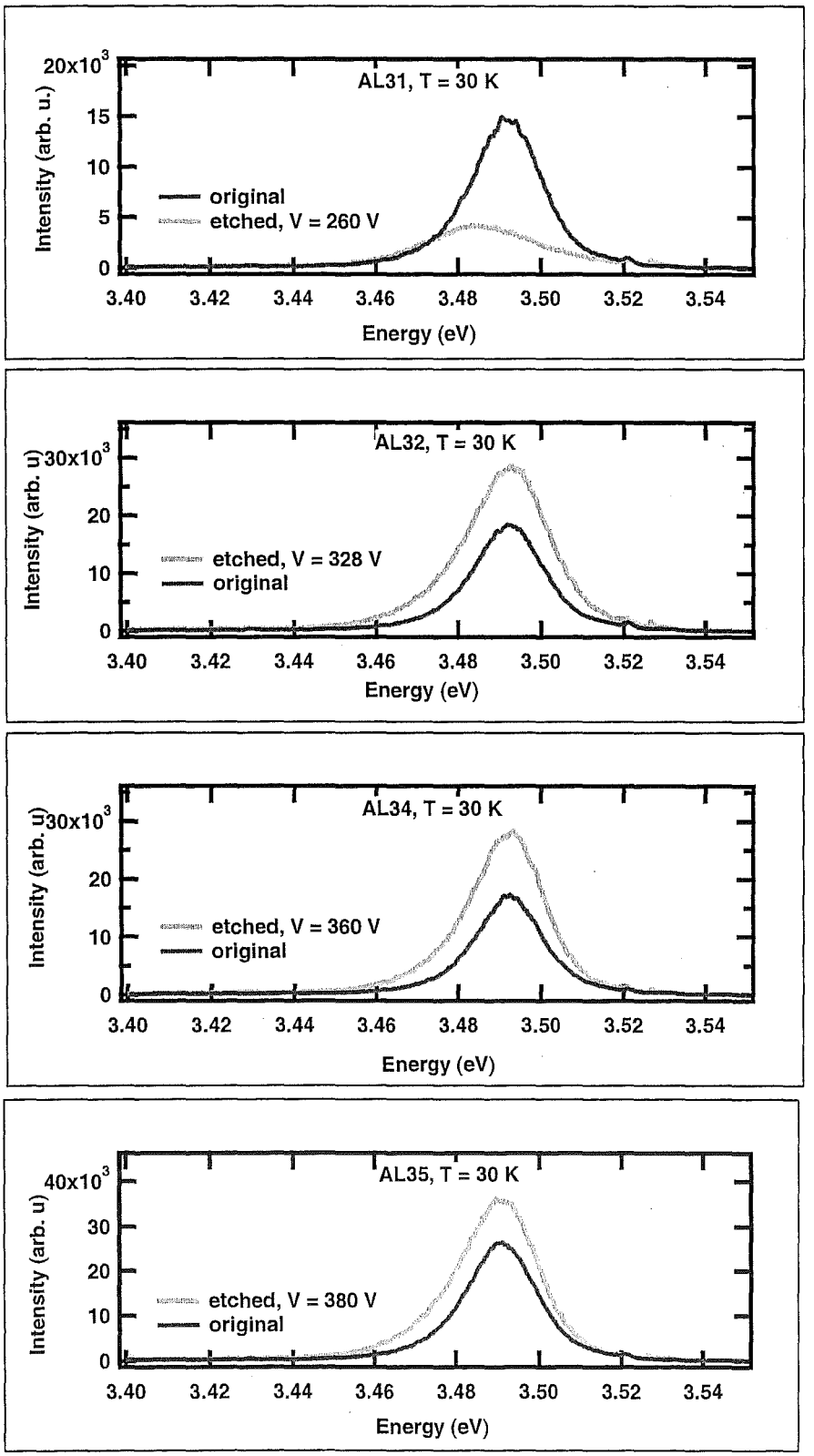

Figure 6.14: Near band edge PL of unetched and etched c-GaN/sap/30803/ AL31-35 by Ar gas, at T = 25 K.

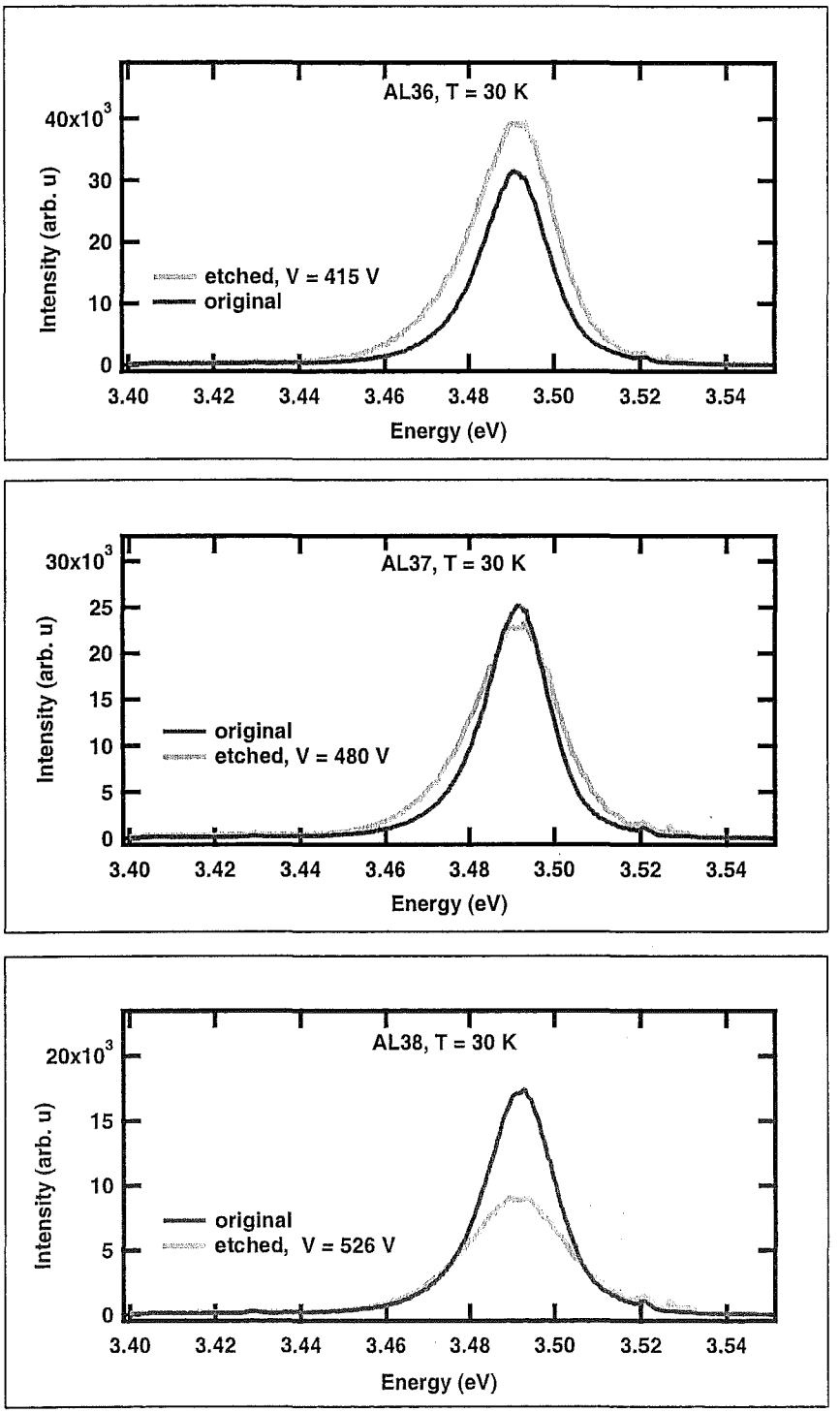

Figure 6.15: Near band edge PL of unetched and etched c-GaN/sap/30803/ AL36-38 by Ar gas, at T = 25 K.

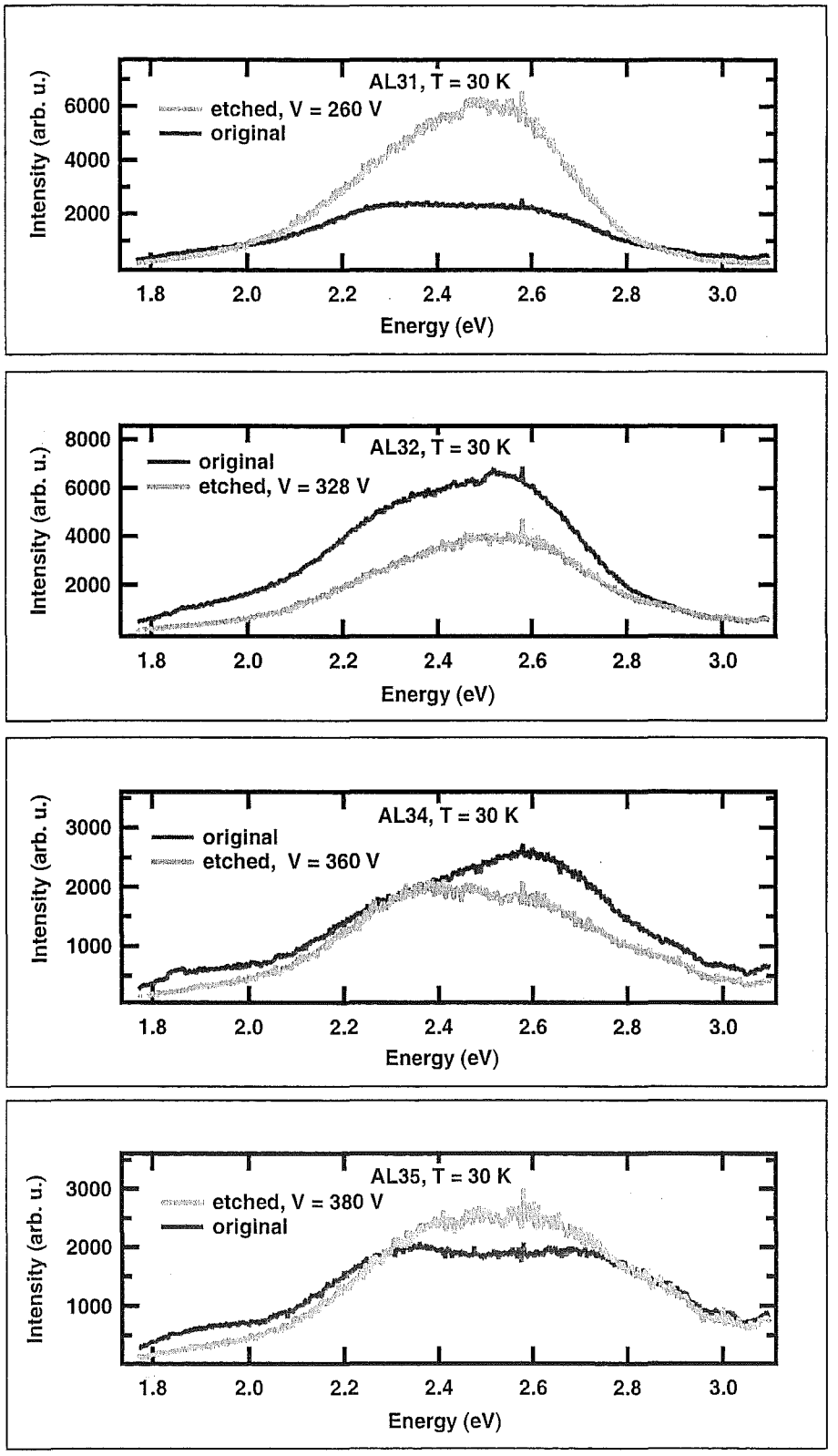

Figure 6.16: Yellow luminescence of unetched and etched c-GaN/sap/30803/ AL31-35 by Ar gas, at T = 25 K.

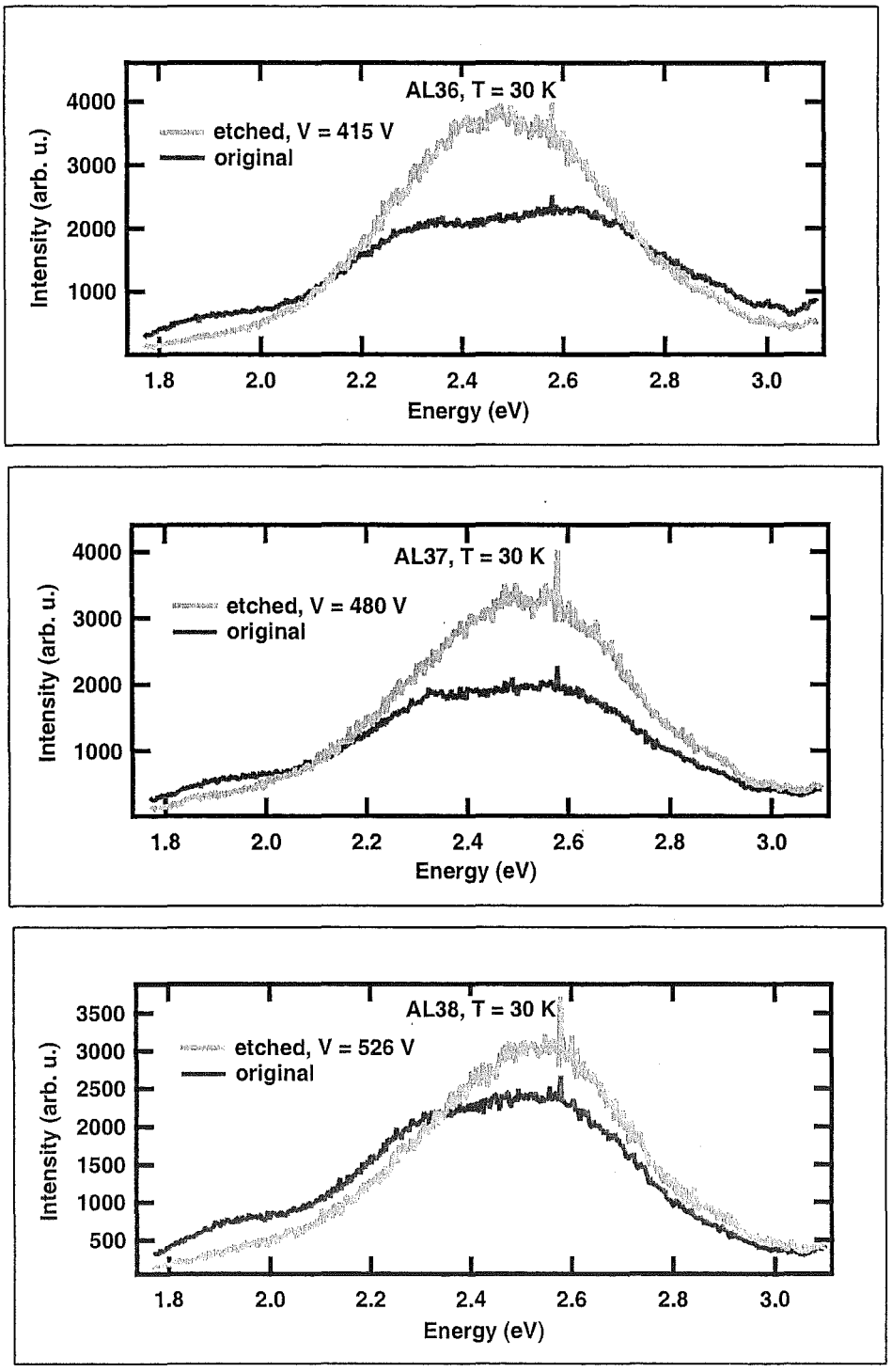

Figure 6.17: Yellow luminescence of unetched and etched c-GaN/sap/30803/ AL36-38 by Ar gas, at T = 25 K.

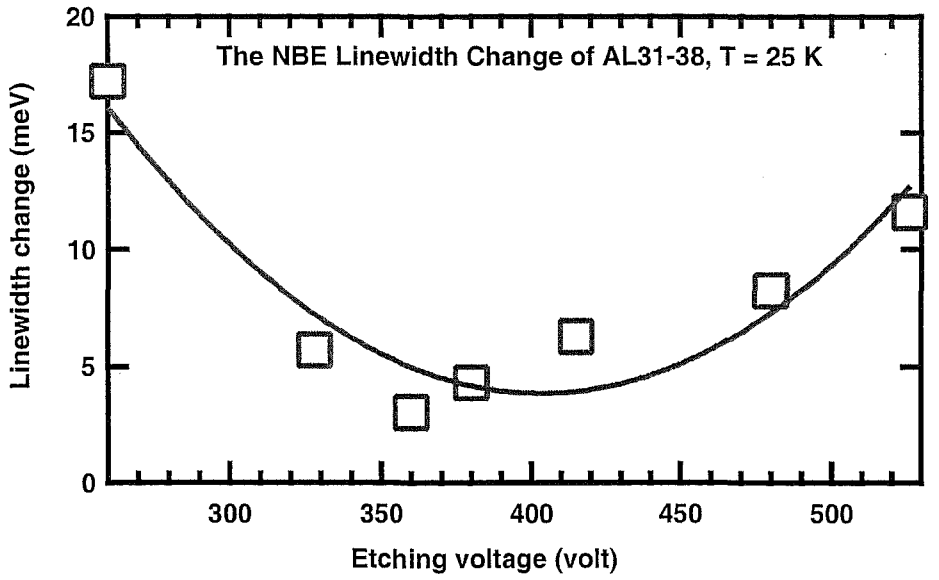

Figure 6.18: Near band edge PL relative linewidth change after etching of c-GaN/sap/30803/ AL31-38 by Ar gas, at T = 25 K, as a function of etching voltage.

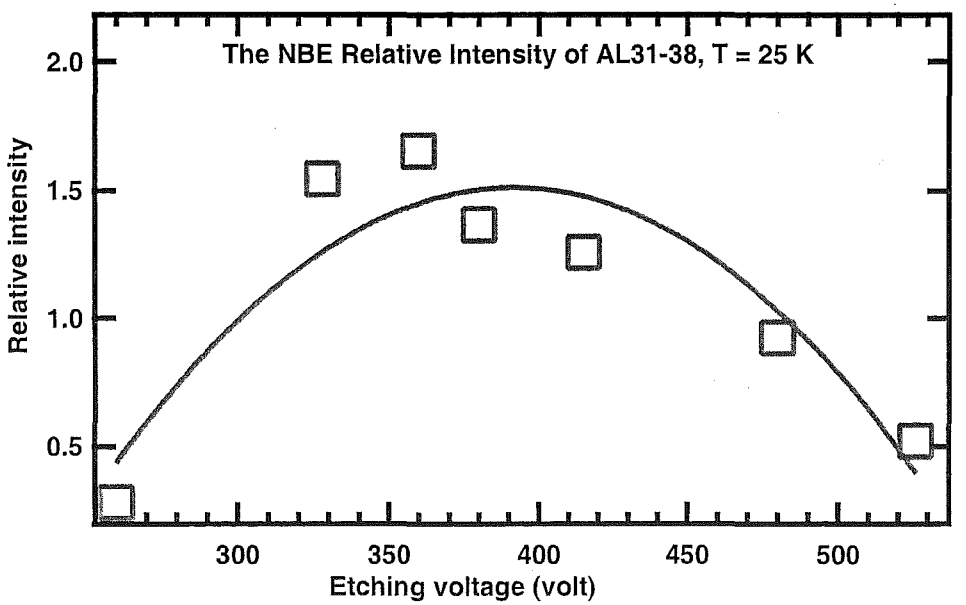

Figure 6.19: Near band edge PL intensity ratio etched/unetched of c-GaN/sap/30803/ AL31-38 by Ar gas, at T = 25 K, as a function of etching voltage.

then gradually increases to about 13 meV at the etching voltage of 526 V.

Figure 6.19 shows the relative NBE PL intensity after etching as a function of etching voltage. At the etching voltage lower than 450 V, the PL intensity after etching is higher than the intensity before etching. At etching voltage 328 V, the PL intensity after etching is about 1.5 times the PL intensity before etching, then gradually decreases to about 0.5 times the PL intensity before etching, at the etching voltage 526 V.

The data from figures 6.18 and 6.19 can be combined as product of linewidth change and relative PL peak intensity. This product is plotted in figure 6.20 as a function of etching voltage.

In this series, the PL relative intensity also correlates to the linewidth change in the way that the decreasing PL relative intensity is compensated by increasing PL linewidth change and vice versa, thus the total PL does not greatly change. The product result only weakly dependent on etching voltage.

Figure 6.21 shows the relative linewidth changes of YL1 and YL2 lines after etching as a function of etching voltage. The YL1 and YL2 linewidth in this series are generally wider after etching. The line fitting result shows that YL1 linewidth does not greatly change after etching, only between -30 meV to 80 meV wider than before etching. In contrast, the YL2 linewidth increases from -55 meV (narrower linewidth before etching) to 40 meV (wider linewidth after etching) as

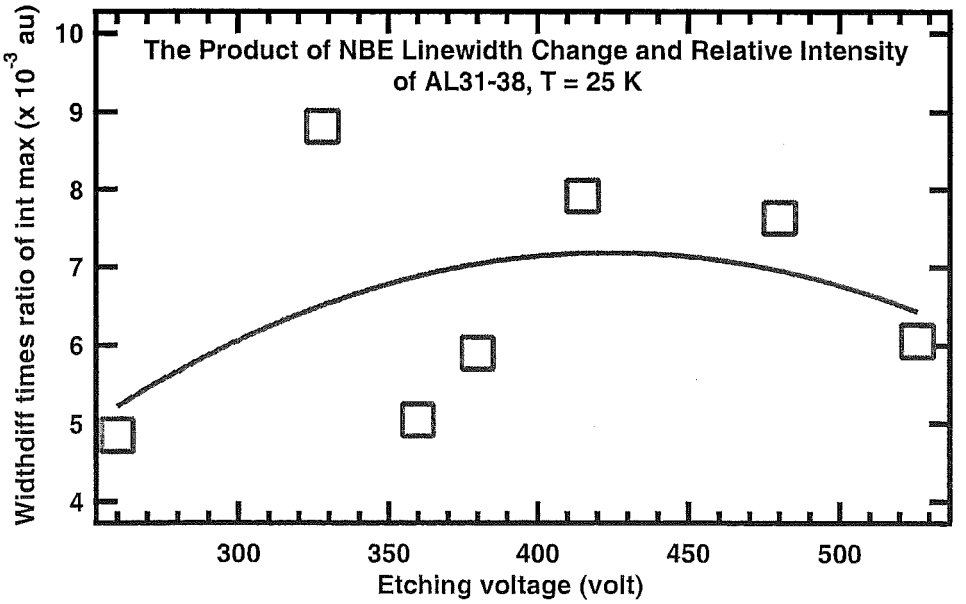

Figure 6.20: Product of the near band edge PL peak intensity ratio and the linewidth change of etched c-GaN/sap/30803/ AL31-38 by Ar gas, at T = 25 K, as a function of etching voltage.

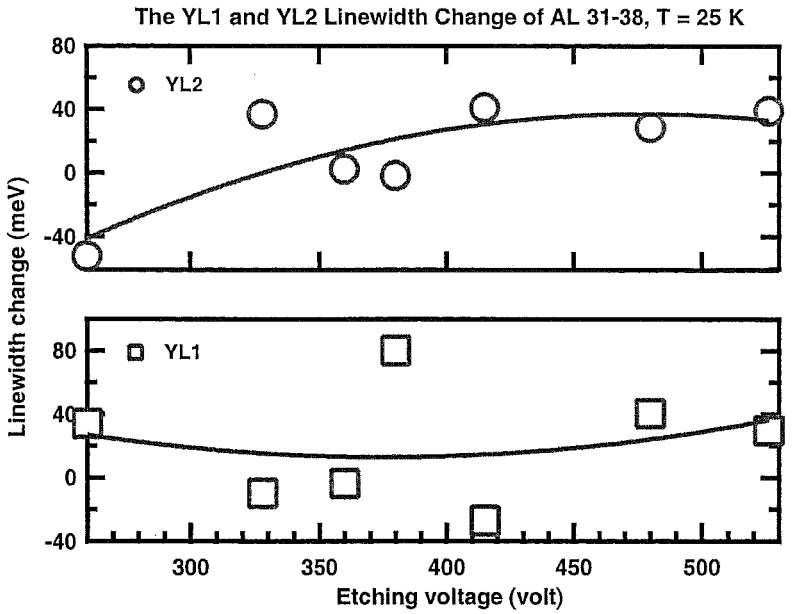

Figure 6.21: YL relative linewidth change after etching of c-GaN/sap/30803/ AL31-38 by Ar gas, at T = 25 K, as a function of etching voltage.

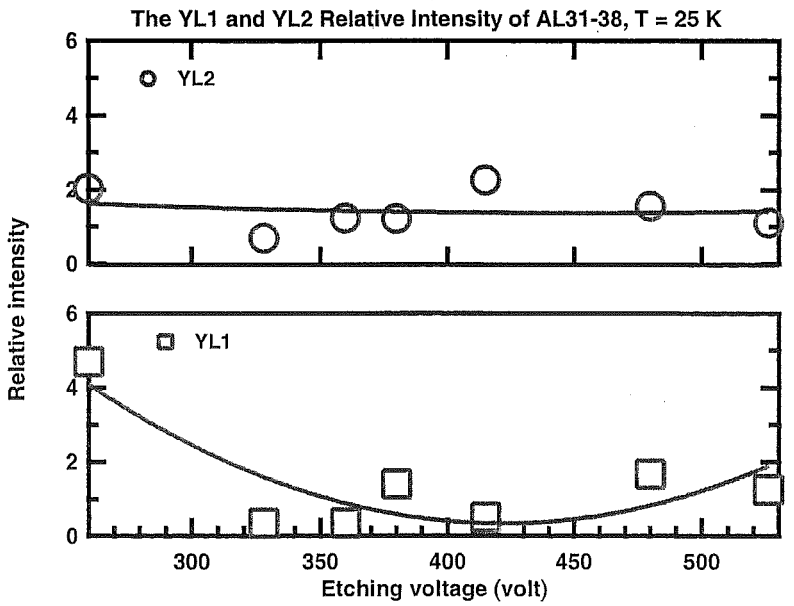

Figure 6.22: YL intensity ratio etched/unetched of c-GaN/sap/30803/ AL31-38 by Ar gas, at T = 25 K, as a function of etching voltage.

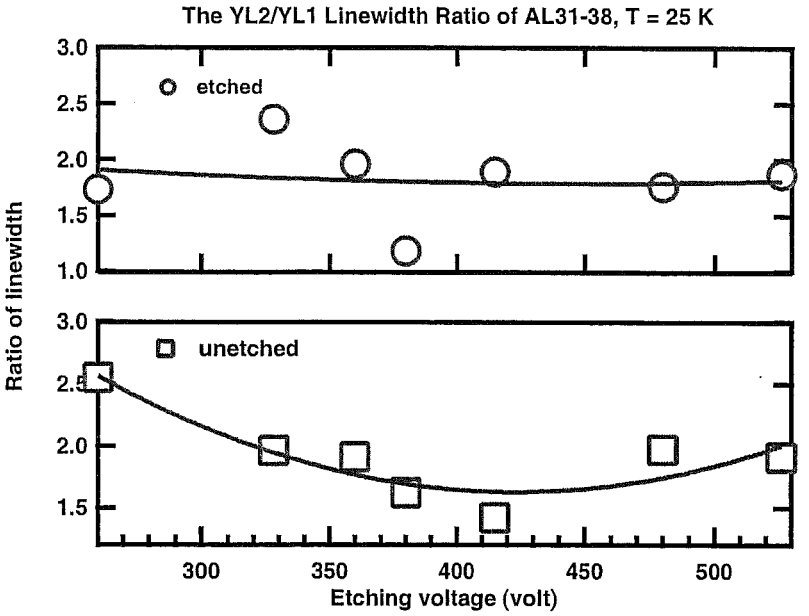

Figure 6.23: Relative linewidth change of YL2 to YL1 of unetched and etched c-GaN/sap/30803/ AL31-38 by Ar gas, at T = 25 K, as a function of etching voltage.

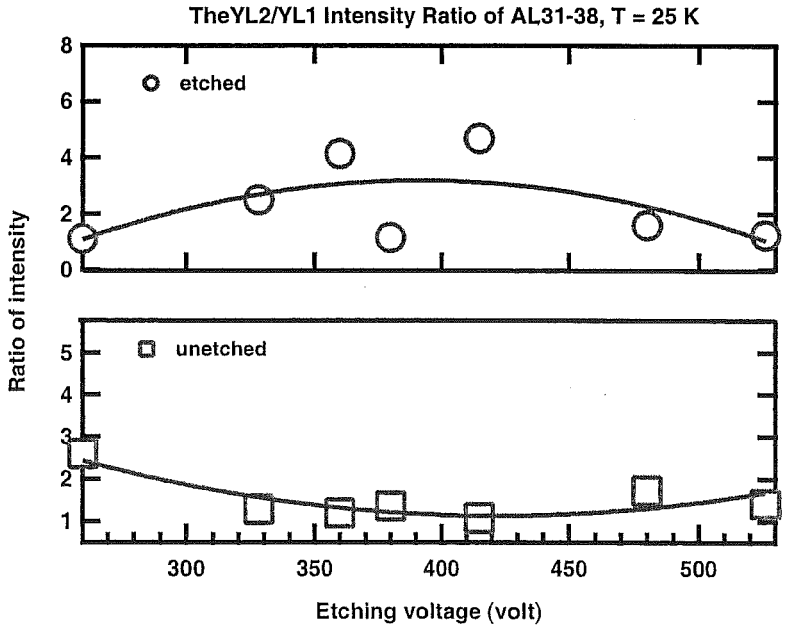

Figure 6.24: Relative intensity of YL2 to YL1 of unetched and etched c-GaN/sap/30803/ AL31-38 by Ar gas, at T = 25 K, as a function of etching voltage.

the etching voltage increases from 260 V to 480 V, at etching voltage higher than 480 V, the YL2 linewidth is almost constant.

There is a rough correlation between the linewidth change of YL1 and YL2, when the YL1 linewidth is relatively narrower, the YL2 linewidth are relatively wider to compensate the narrower linewidth of YL1, and vice versa. As a result, the total linewidth of YL1 and YL2 is almost constant.

Figure 6.22 shows the relative PL intensity of YL1 and YL2 after etching as a function of etching voltage.

The intensity of YL1 after etching is lower at the etching voltage lower than 400 V, then increases slightly as the etching voltage increases.

The intensity of YL2 after etching is always higher than before etching. The fitting result of intensity ratio of YL2 after and before etching is almost constant, after etching the intensity is about 50% higher than before etching, and only weakly dependent on the etching voltage, showing a slight decrease as the etching voltage increases.

Figures 6.23 shows the relative linewidth of YL2 to YL1 before and after etching as a function of etching voltage. YL1 linewidth is relatively narrower than YL2 for both etched and unetched samples. The relative linewidth of YL2 to YL1 in unetched samples roughly follows a parabolic function, with minimum value at about 415 V etching voltage. Unfortunately the relative linewith of YL2 to YL1 data for etched samples in this series is scattered and less conclusive.

Figure 6.24 shows the relative peak intensity of YL2 to YL1 before and after etching as a function of etching voltage. YL2 has higher peak intensity than YL1 for both unetched and etched samples. Before etching, the intensity ratios of YL2 to YL1 follows a parabolic function and the minimum value is reached at about 415 V etching voltage. After etching, the relative intensity of YL2 is greatly changed and most of the data indicate that the YL2 intensity increases more rapidly than YL1.

There is an obvious changes of YL spectrum after etching processes, in most cases YL has higher intensity and wider linewidth after etching. Results and analysis of YL1 and YL2 shows that YL changes mainly due to the changes of YL2 in this series, and YL1 does not greatly change after etching.

AFM Pictures and Analysis

Figure 6.25 shows AFM images of c-GaN/sap/ 30803 / AL31-38. The RMS roughness was measured for all etched samples and this data is plotted in figure 6.26 as a function of etching voltage. In this series, the surface roughness is smoother as the etching voltage increases, at the etching voltage of 260 V the RMS roughness is about 12.5 nm then decreases to about 4 nm at the etching voltage of 526 V. The RMS roughness for the untreated sample AL33 is about 8

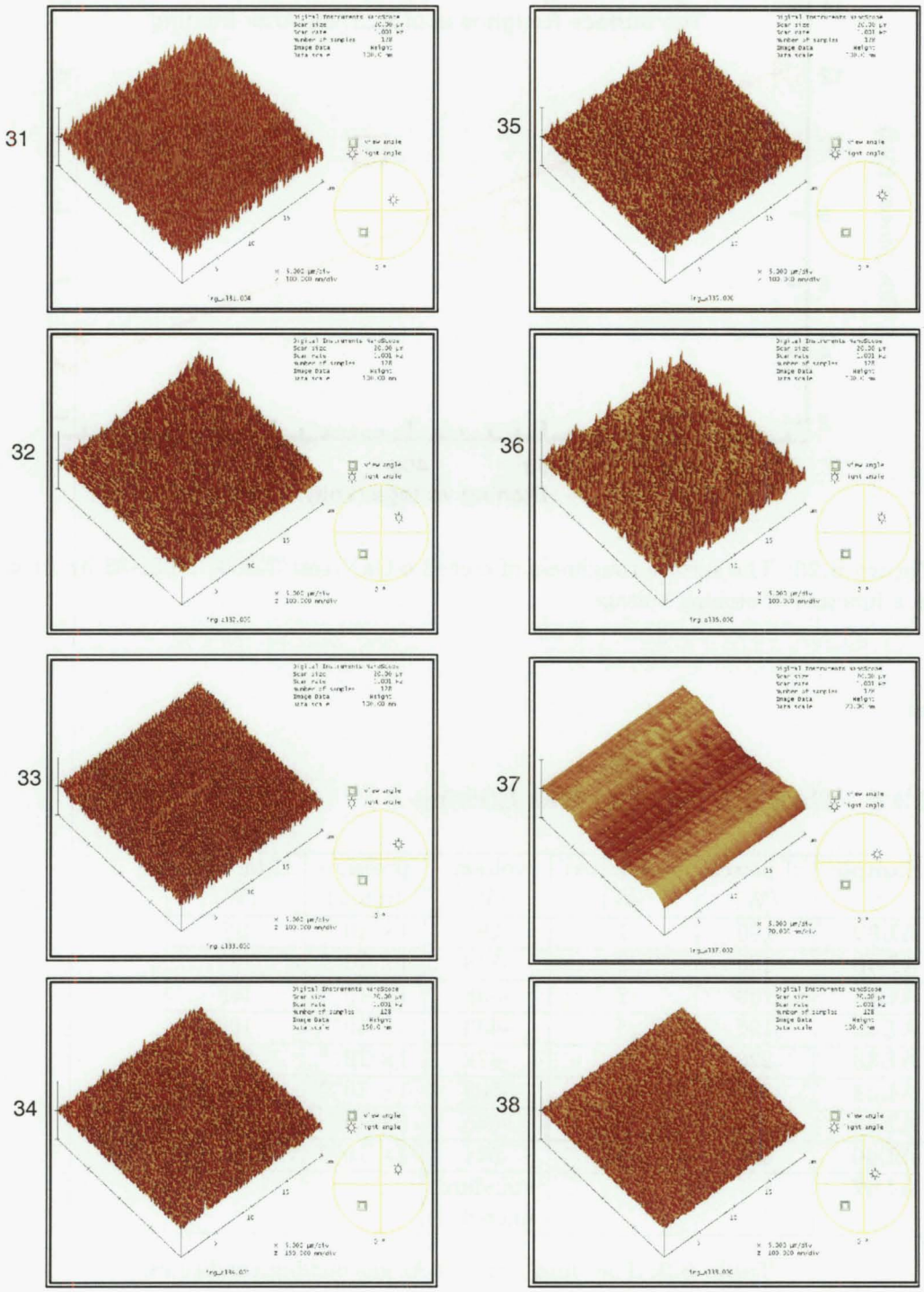

Figure 6.25: AFM images of the surface of etched c-GaN/sap/30803/ AL31-38 by Ar gas.

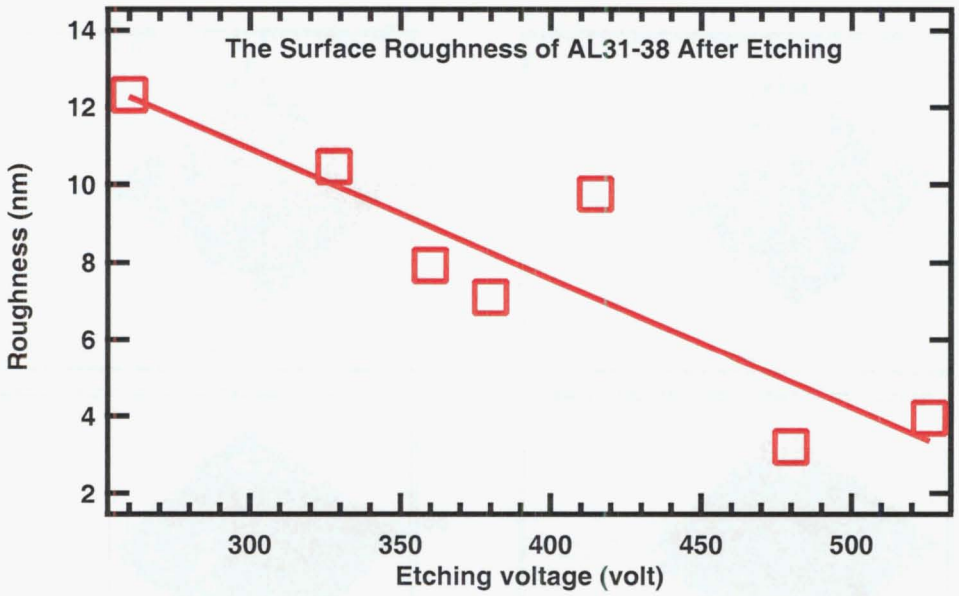

Figure 6.26: The surface roughness of etched c-GaN/sap/30803/ AL31-38 by Ar gas as a function of etching voltage.

nm.

6.3.3 Third Series of Ar Gas Etching

Sample	rf power (W)	rf reflected (W)	voltage (V)	pressure (mbar)	rf forward (W)
AL39	100	1	-295	1×10^{-8}	98
AL40	130	2	-348	1×10^{-8}	129
AL41	160	2	-398	1×10^{-8}	160
AL42	190	3	-433	1×10^{-8}	190
AL43	220	3	-472	1×10^{-8}	221
AL44	250	4	-509	1×10^{-8}	251
AL45	280	4	-535	1×10^{-8}	278
AL46	300	5	-551	1×10^{-8}	290
AL47			standard unetched		

Table 6.3: The third series of Ar gas etching conditions.

Some of the results from the first and second series of Ar etching gas experiments are inconsistent. The third series was done to clear the inconsistent results and confirm the conclusive results.

The samples for the third series of Ar gas etching experiment are c-GaN/sap/30803/

Ar etched /AL39, AL40, AL41, AL42, AL43, AL44, AL45, AL46, AL47 (9 samples). The etching conditions for each of these samples are shown in Table 6.3.

The original reference sample in this series was sample AL47. The PL measurements were taken at temperature 4 K.

Figures 6.27 and 6.28 show the NBE PL of unetched and etched c-GaN/sap/30803/AL39-42 and AL43-46. Apparent is the NBE emission at 3.493 eV.

Figures 6.29 and 6.30 show the PL results of YL of unetched and etched c-GaN/sap/30803/ AL39-42 and AL43-46.

In this series, the PL of YL spectrum consists of two peaks, the first peak is at 2.755 eV (YL1 peak), and the second peak is at 2.375 eV (YL2 peak).

Analysis of the PL Results

Figure 6.31 shows the linewidth change to NBE emission line as a function of etching voltage. The results show that the linewidth is wider after etching by the amount of 1.3 meV to 4.4 meV in this series, and a typical PL linewidth of the NBE emission line is about 14 meV.

The linewidth change is 1.3 meV at the etching voltage of 295 V, then increases and reaches the maximum linewidth change of 4.4 meV at etching voltage about 433 V. At higher etching voltage than 433 V, the linewidth change decreases to about 2.5 meV at the etching voltage of 551 V.

Figure 6.32 shows the relative NBE PL intensity after etching as a function of etching voltage. In this series, the PL intensity after etching is relatively lower than before etching, except for the PL intensity at 295 V etching voltage. At the etching voltage of 295 V, the PL intensity after etching is about 15% higher than before etching, then it decreases as the etching voltage increases, it reaches the minimum value about 0.4 of the intensity before etching at the etching voltage of 509 V.

The data from figures6.31 and 6.32 can be combined as product of linewidth change and relative PL peak intensity. This product is plotted in figure 6.33 as a function of etching voltage.

In this series, the PL relative intensity also correlates to the linewidth change in the way that the decreasing PL relative intensity is compensated by increasing PL linewidth change and vice versa, thus the total PL does not greatly change.

This analysis shows the product is weakly dependent on the etching voltage. It starts at about 0.15 at 295 V etching voltage, then increases to a maximum value about 0.2 at 398 V, and decreases to 0.1 at 551 V.

Figures 6.34 shows YL1 and YL2 linewidth changes after etching as a function of etching voltage.

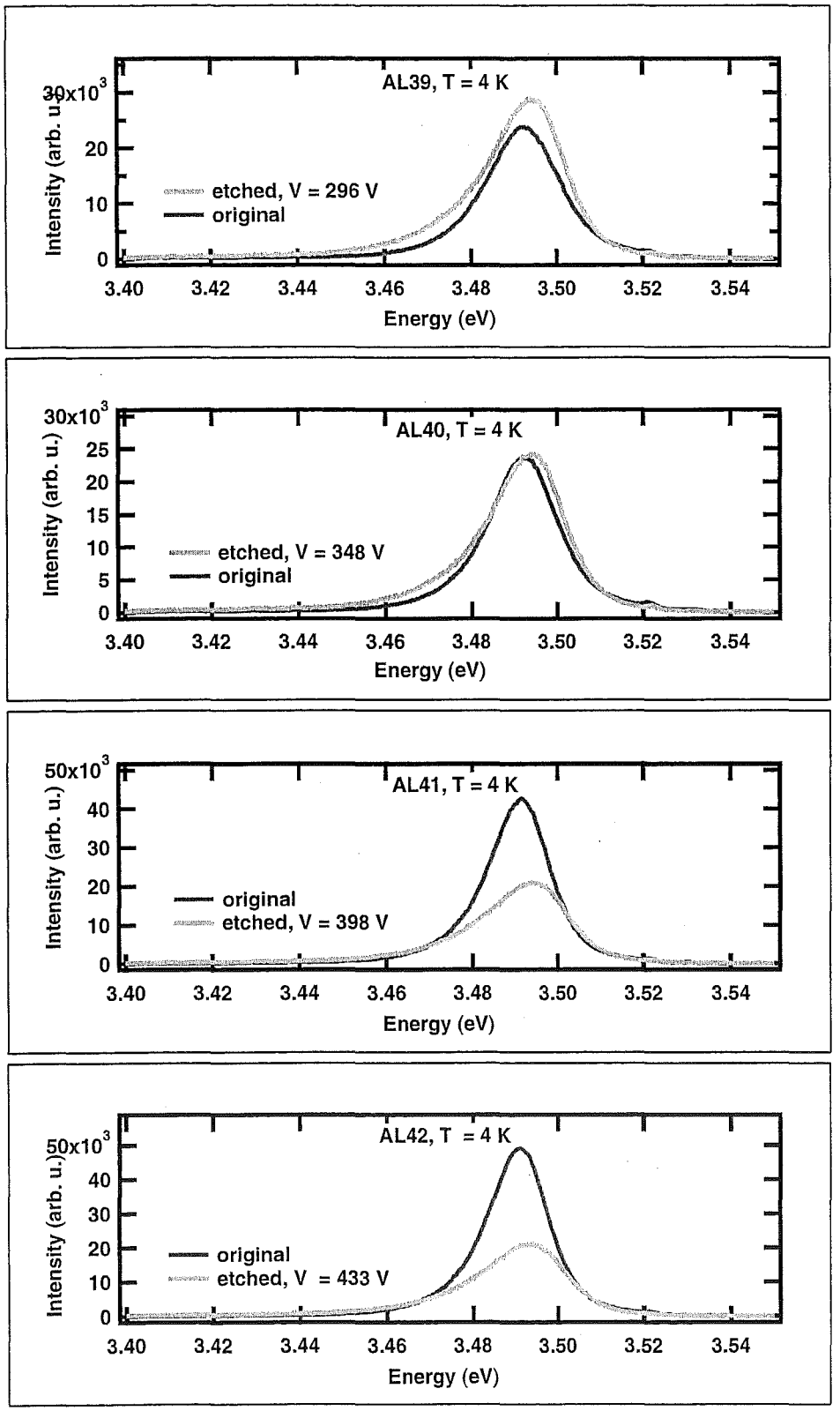

Figure 6.27: Near band edge PL of unetched and etched c-GaN/sap/30803/ AL39-42 by Ar gas, at T = 4 K.

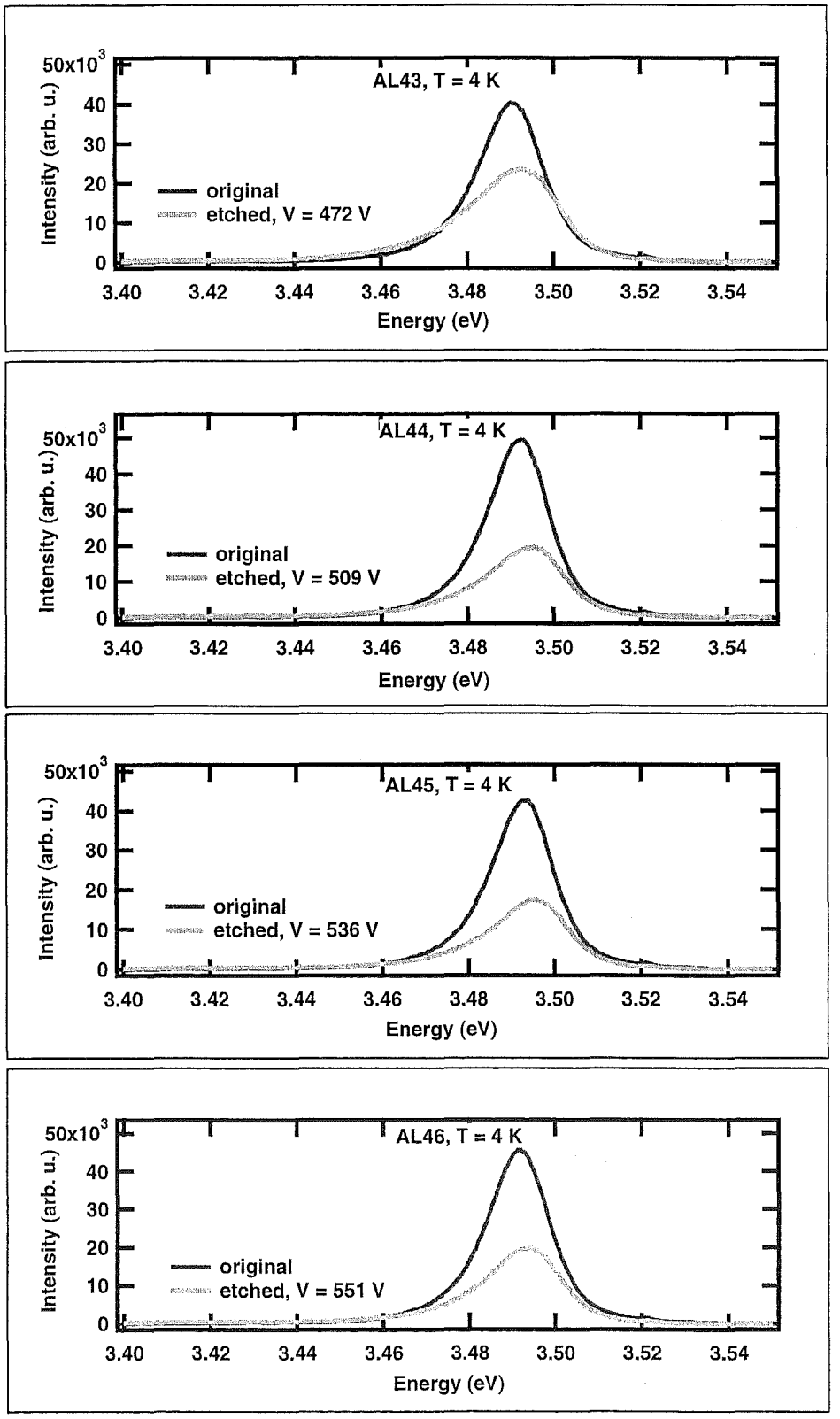

Figure 6.28: Near band edge PL of unetched and etched c-GaN/sap/30803/ AL43-46 by Ar gas, at T = 4 K.

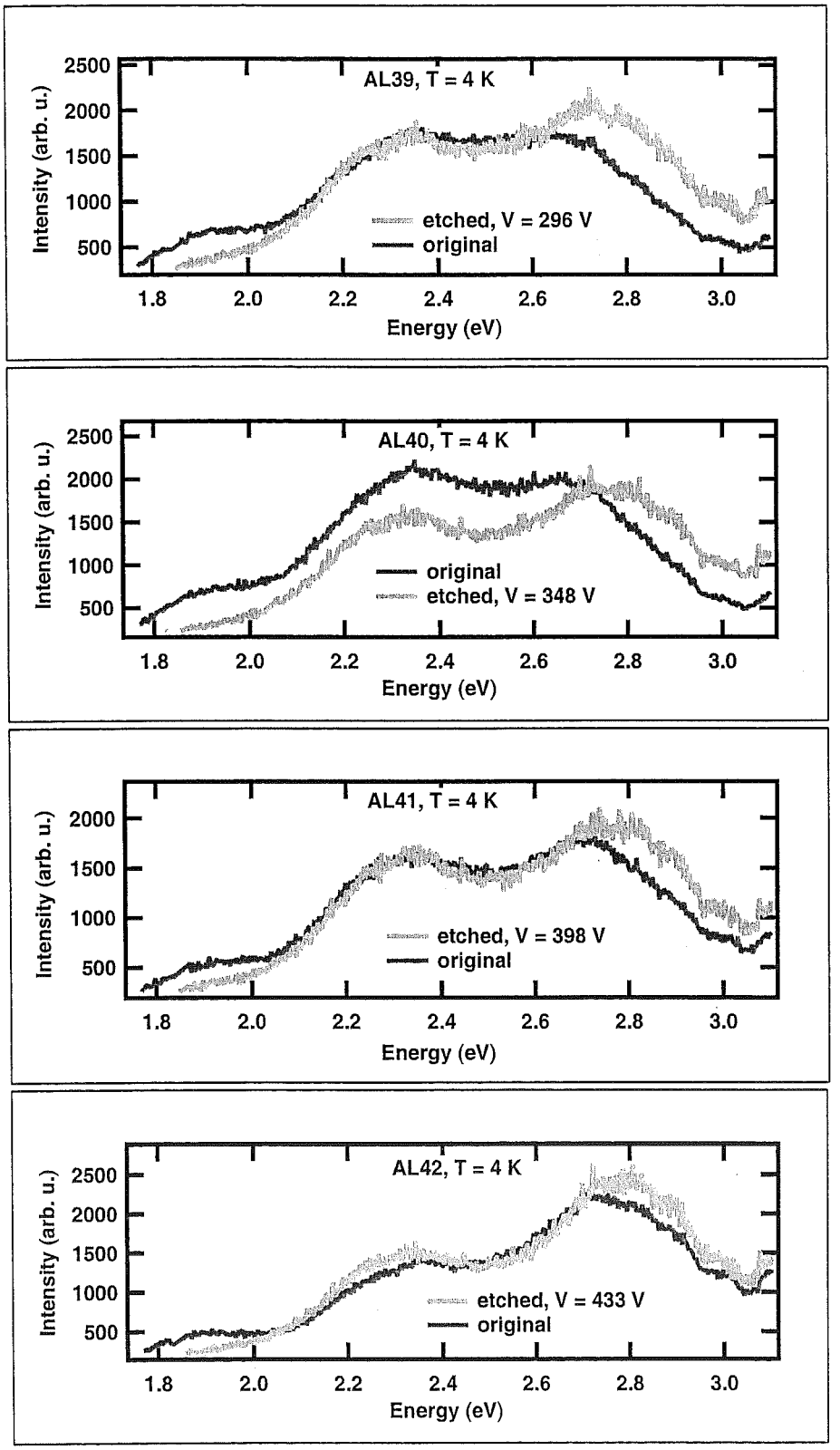

Figure 6.29: Yellow luminescence of unetched and etched c-GaN/sap/30803/ AL39-42 by Ar gas, at T = 4 K.

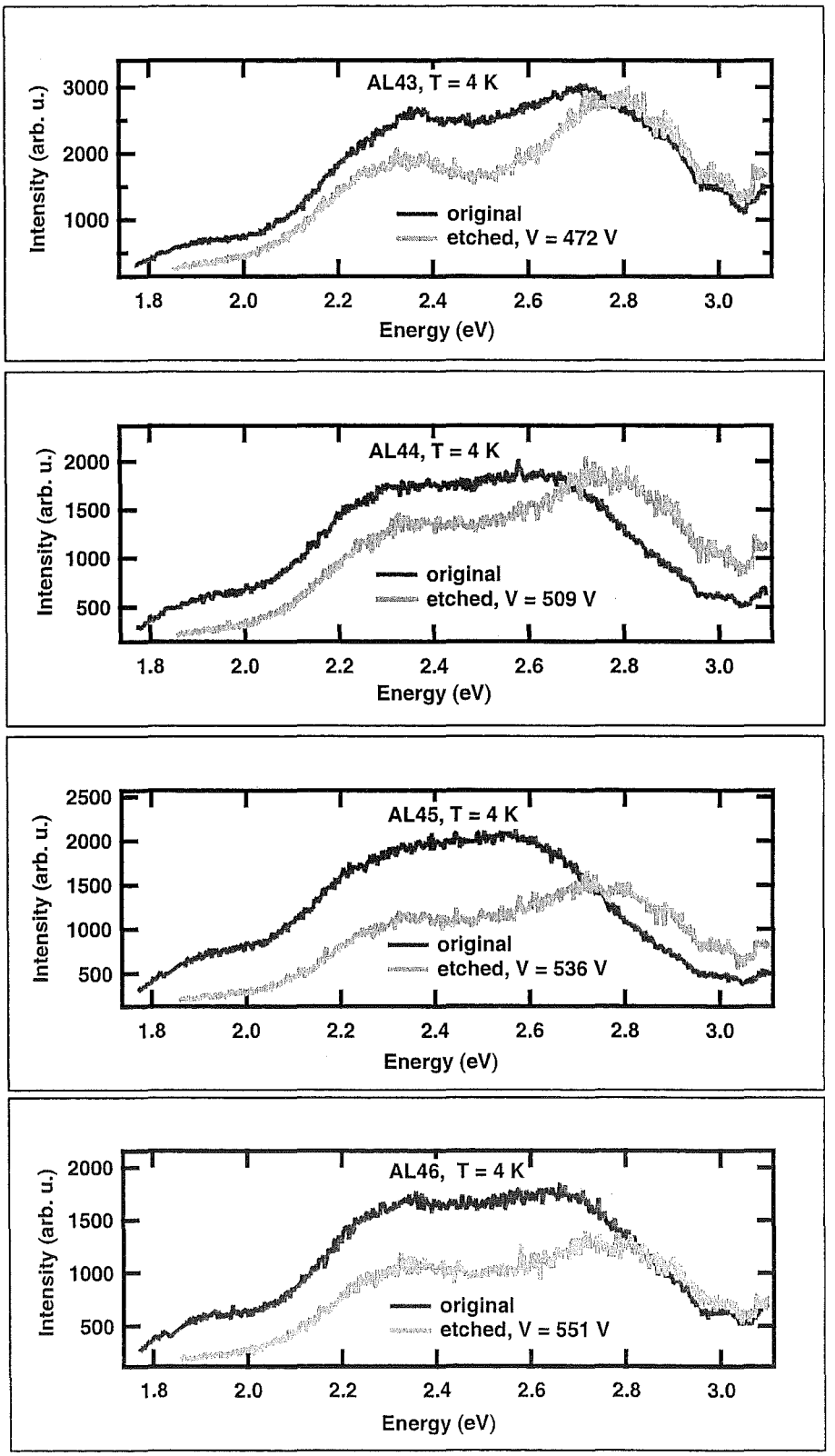

Figure 6.30: Yellow luminescence of unetched and etched c-GaN/sap/30803/ AL42-46 by Ar gas, at T = 4 K.

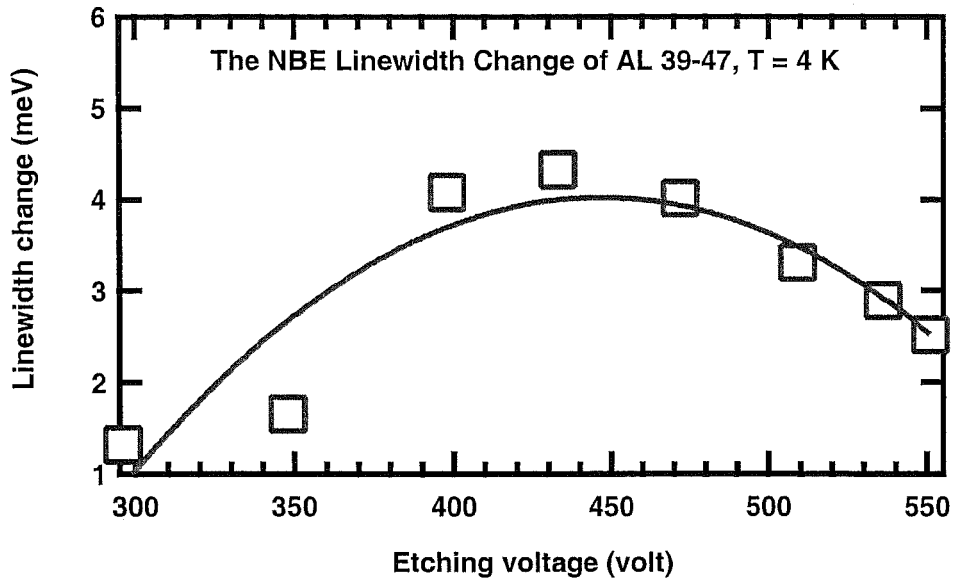

Figure 6.31: Near band edge PL relative linewidth change after etching of c-GaN/sap/30803/ AL39-47 by Ar gas, at T = 4 K, as a function of etching voltage.

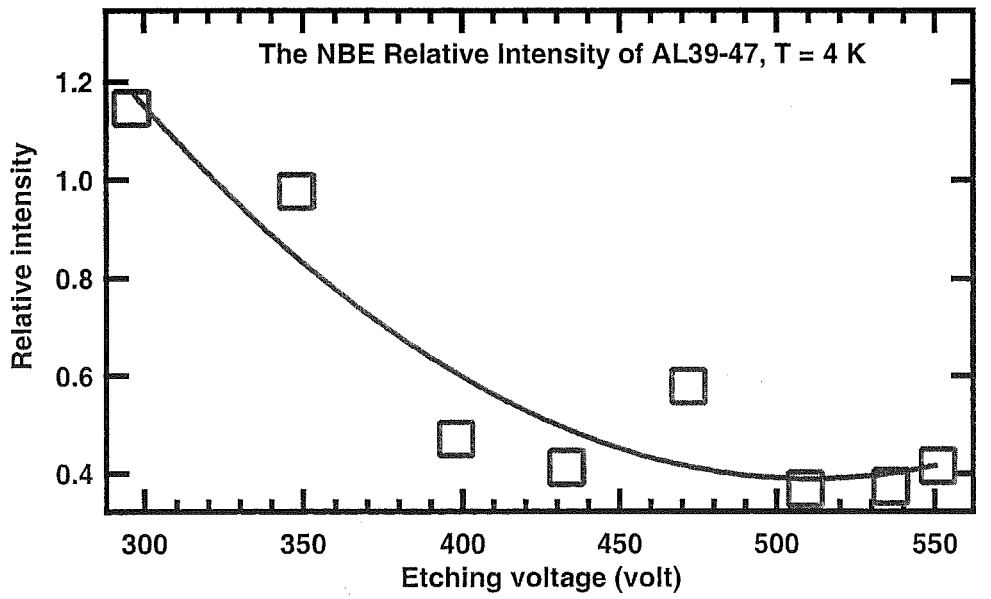

Figure 6.32: Near band edge PL intensity ratio etched/unetched of c-GaN/sap/30803/ AL39-47 by Ar gas, at T = 4 K, as a function of etching voltage.

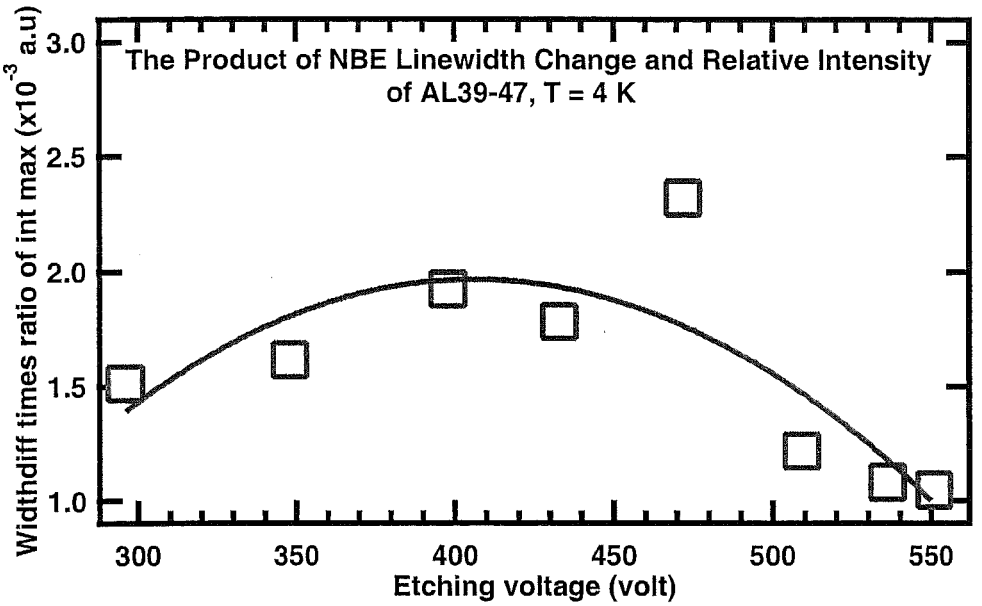

Figure 6.33: Product of the near band edge PL peak intensity ratio and the linewidth change of etched c-GaN/sap/30803/ AL39-47 by Ar gas, at T = 4 K, as a function of etching voltage.

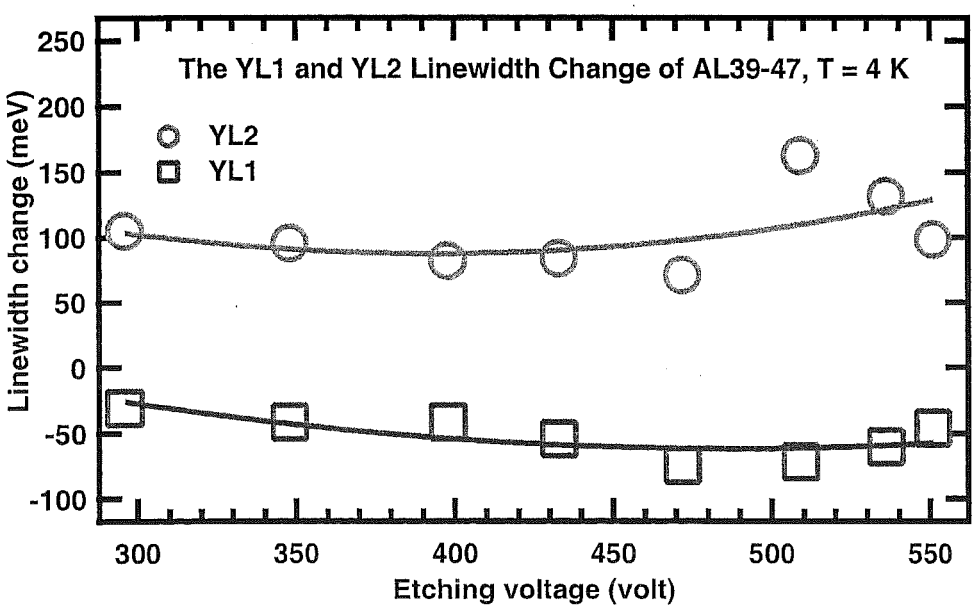

Figure 6.34: YL relative linewidth change after etching of c-GaN/sap/ 30803 / AL39-47 by Ar gas, at T = 4 K, as a function of etching voltage.

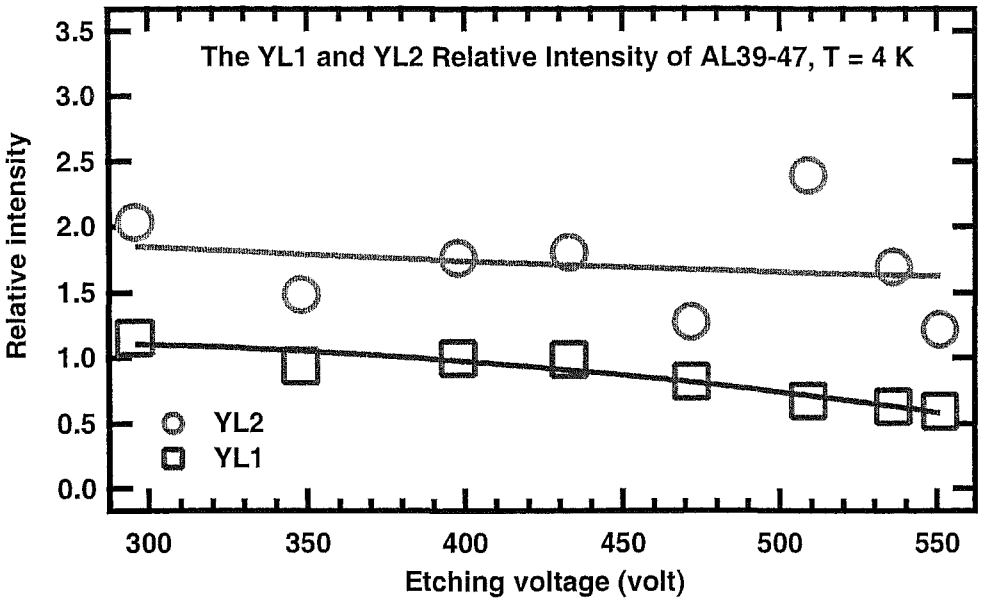

Figure 6.35: YL intensity ratio etched/unetched of c-GaN/sap/ 30803 / AL39-47 by Ar gas, at T = 4 K, as a function of etching voltage.

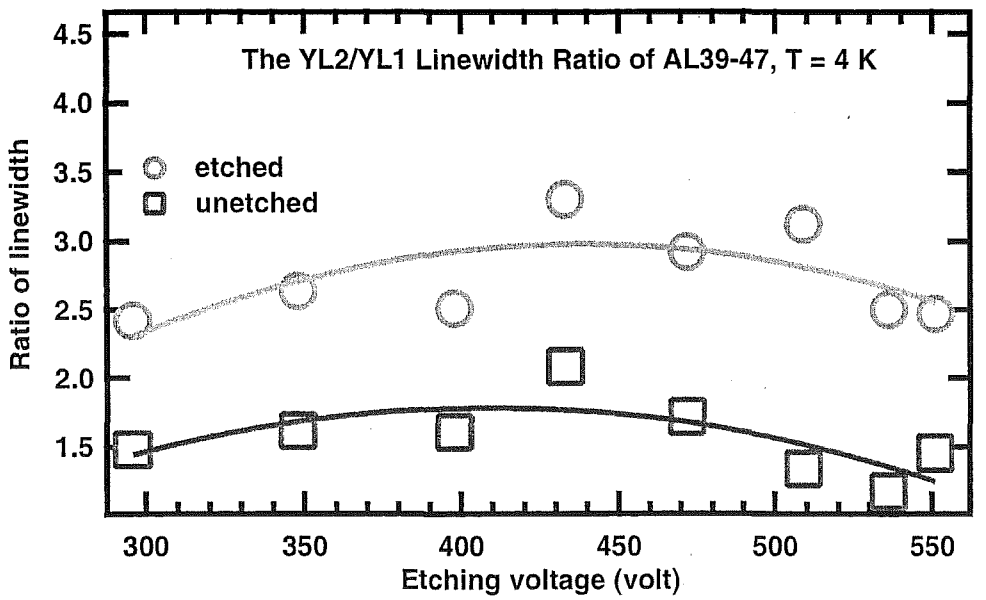

Figure 6.36: Relative linewidth change of YL2 to YL1 of unetched and etched c-GaN/sap/ 30803 / AL39-47 by Ar gas, at T = 4 K, as a function of etching voltage.

The YL1 linewidth after etching is narrower than before etching, it is shown by negative values of linewidth changes. And the YL2 linewidth after etching is wider then before etching, it is shown by positive values of linewidth changes. The changes of YL1 linewidth are from -30 meV to -75 meV and the changes of YL2 linewidth are from 70 meV to 160 meV.

The YL1 linewidth after etching is slightly narrowed as the etching voltage increases. In contrast, the YL2 linewidth after etching is slightly widened as the etching voltage increases.

There is a rough correlation between the linewidth change of YL1 and YL2, when the YL1 linewidth is relatively narrower, the YL2 linewidth are relatively wider to compensate the narrower linewidth of YL1, and vice versa. Overall, the total linewidth of YL does not greatly change.

Figure 6.35 shows the relative PL intensity of YL1 and YL2 after etching as a function of etching voltage. The intensity of YL1 after etching is similar to the intensity before etching at the etching voltage from 295 V to 433 V, then slowly decreases as etching voltage increases, at the etching voltage of 551 V, the intensity of YL1 after etching is about 60% of the intensity before etching. The relative intensity of YL2 in this series increase after etching, they are about 1.3 to 2.4 times of the intensity before etching. The fitting result shows that the overall relative intensity of YL2 slightly decreases as the etching voltage increases.

Figures 6.36 shows the relative linewidth of YL2 to YL1 before and after etching

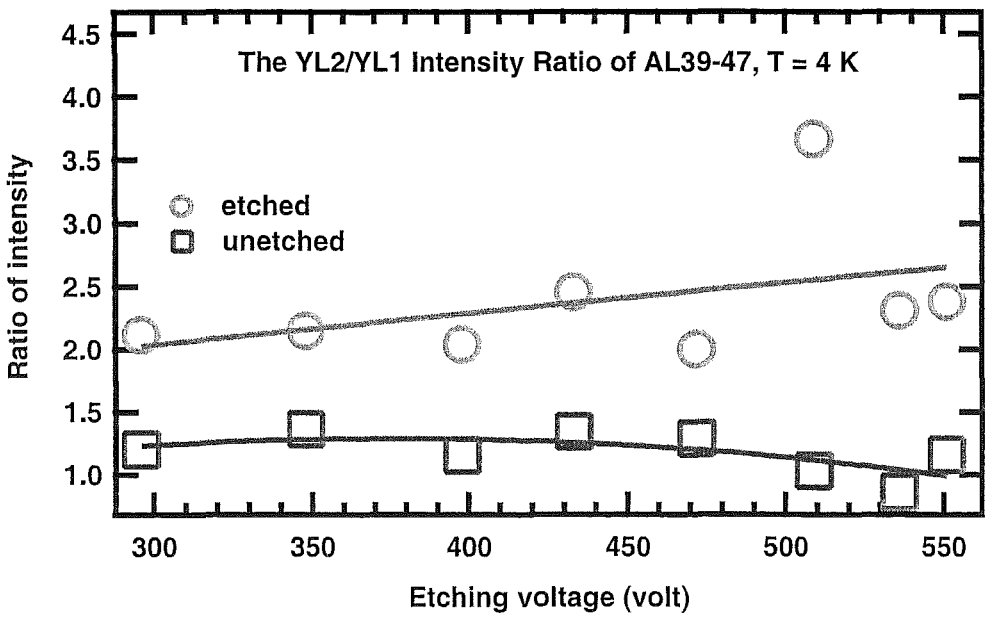

Figure 6.37: Relative intensity of YL2 to YL1 of unetched and etched c-GaN/sap/ 30803 / AL39-47 by Ar gas, at T = 4 K, as a function of etching voltage.

as a function of etching voltage. The YL1 linewidth is relatively narrower than the YL2 for both etched and unetched samples. After etching the relative linewidth of the YL2 to the YL1 is higher than before etching. Before etching the relative linewidth of the YL2 is about 1.2 to 2 times of the YL1, and after etching the relative linewidth of the YL2 is about 2.4 to 3.3 times of the YL1.

Figure 6.37 shows the relative peak intensity of YL2 to YL1 before and after etching as a function of etching voltage.

Before etching the relative peak intensity of the YL2 is only about 20% higher than of the YL1, and decreases slowly as etching voltage increases, and become similar to the intensity of the YL1.

After etching the relative peak intensity of the YL2 is about 2.1 times higher than of the YL1 at the etching voltage of 295 V, then increases slowly as the etching voltage increases. At the etching voltage of 551 V, the relative intensity of the YL2 is about 2.4 times higher than of the YL1. The data at the etching voltage of 509 V was discounted, because it is greatly different from other data and highly deviates from the fit result.

There are intensity and linewidth changes of the total of YL spectrum after etching processes, in this series the total YL has higher intensity and wider linewidth after etching. Results and analysis of YL1 and YL2 shows that the changes in YL intensity and linewidth are mainly due to the changes of YL2 intensity and linewidth in this series, and YL1 intensity and linewidth do not greatly change after etching.

AFM Pictures and Analysis

Unfortunately, sample 39 in this series was accidentally lost, so there is no AFM image for sample 39.

Figure 6.38 shows AFM images of c-GaN/sap/ 30803 / AL40-47 after etching. The RMS roughness was measured for all etched samples and this data is plotted in figure 6.39.

The surface RMS roughness decreases as the etching voltage increases. It means, at the higher etching voltage the sample's surface is smoother than at the lower etching voltage. At the etching voltage of 295 V the RMS roughness is about 7 nm then decreases to about 2 nm at the etching voltage of 551 V. The RMS roughness for the untreated sample AL47 is about 4 nm. By comparing the AFM images, it is also obvious that the sample's surface is smoother at higher etching voltage.

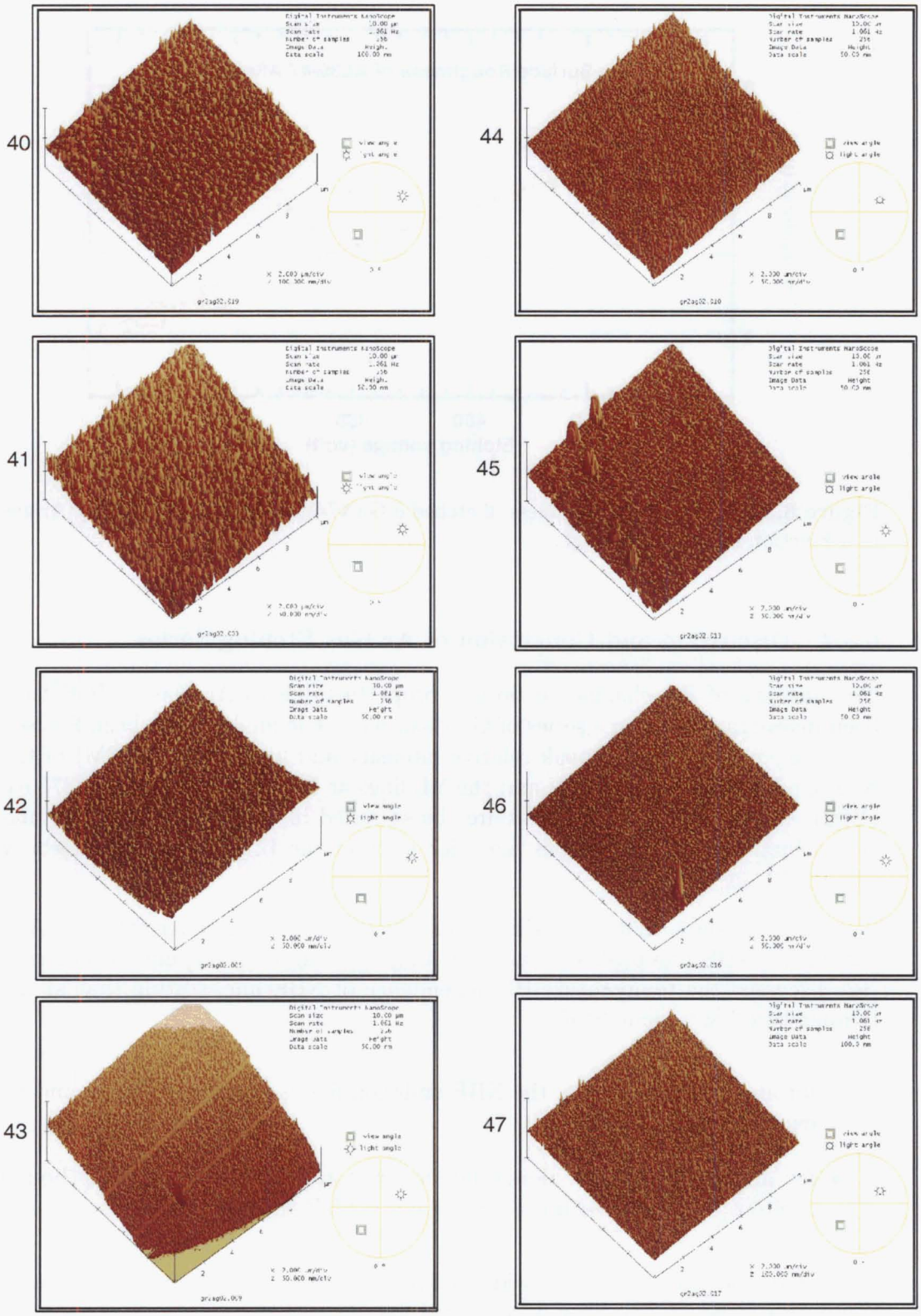

Figure 6.38: AFM images of the surface of etched c-GaN/sap/ 30803 / AL40-47 by Ar gas.

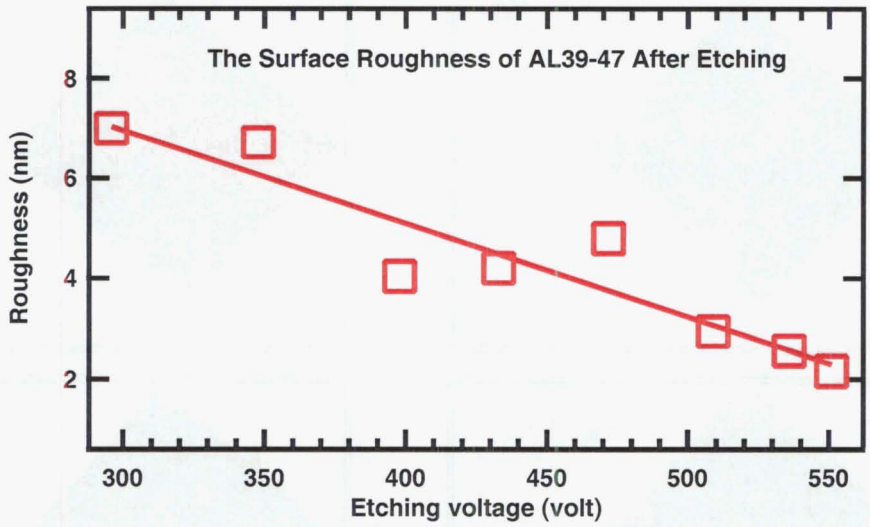

Figure 6.39: The surface roughness of etched c-GaN/sap/ 30803 / AL39-47 by Ar gas as a function of etching voltage.

6.3.4 Discussion and Conclusion of Ar Gas Etching Series

The analysis of the changes in optical properties due to Ar plasma RIE have been investigated on three series of GaN samples. The analysis has been focused on the changes of the PL peak relative intensity and linewidth (FWHM) of the NBE emission line at 3.493 eV and the YL lines at 2.755 eV (YL1) and 2.375 eV (YL2). These YL1 and YL2 lines are the so called blue luminescence (BL) and yellow luminescence (YL) from the prior work of the University of Canterbury [16, 12, 13, 11, 71].

All of results show that the NBE PL linewidth is wider after Ar etching. And there is no NBE line peak shift after etching. Cheung *et al* [17] and Brown *et al* [12] discussed the temperature PL dependence of NBE line, stating that at the temperature lower than 40 K:

- for an unetched sample, the NBE emission line is dominated by A_1 and B_1 excitonic peaks.
- for an etched sample, donor bound exciton (D^0X) and acceptor bound exciton (A^0X) related lines dominate the NBE emission line.

Therefore, the wider NBE linewidth after Ar etching can be interpreted as a result of a wider D^0X and/or A^0X related lines.

The prior work of The University of Canterbury concluded that Ar plasma etching increases the near band edge and below band gap emission dramatically [13].

However, the prior work did not consider a significant problem that the variation of optical properties of different samples taken from different parts of the same wafer can hide any etch-induced changes. In this project, a complete characterisation of each individual sample before etching was done to accurately determine the effect of etching on a particular sample. The results of this project show that only 50% of Ar-etched GaN samples increase the NBE emission after etching and another 50% actually decrease its NBE emission after etching. It implies that the conclusions of Ar plasma etching increasing the D^0X line dramatically, introducing a large number of donors originated from native defects that capture excitons efficiently and allow radiative recombinations of those excitons [13], need to be reviewed and reconsidered.

There is a correlation between NBE PL relative intensity after etching and linewidth change, in the way that the decreasing PL relative intensity is compensated by increasing PL linewidth change and vice versa. However, the total PL is slightly changed, showing a maximum change happens in the region of the etching voltage about 350 V to 450 V and a slight decrease at the etching voltage higher than 450 V. It means that Ar etching processes do not significantly increase the density of non radiative centres.

Ar etching increases the total YL linewidth and intensity. In most cases, the increased in linewidth and intensity of the total YL after etching is caused by the increased in linewidth and intensity of the YL2 line at 2.375 eV. The linewidth changes and relative intensity of YL1 and YL2 roughly correlate with each other. When YL1 has a narrow linewidth, the YL2 has a wide linewidth to compensate it, and vice versa. Also when the YL1 has a high intensity, the YL2 has a low intensity to compensate it, and vice versa. The increase in linewidth and intensity of YL after etching, also the correlation between YL1 and YL2 were reported from the prior work of the University of Canterbury [12, 13, 11, 16, 71].

YL is originated from defects and these defects are metastable states [16], [11]. It implies that Ar etching enhances or creates metastable states. However, merely PL technique is insufficient to fully explain YL.

For a surprise, Ar etching results in smoother surface as etching voltage increases, it is showed by the AFM images.

6.4 Results and Analysis of SF_6 Gas Etching

Two series of experiments have been done to investigate RIE using SF_6 gas induced damage on optical properties of GaN samples.

All the SF_6 gas etching processes were also done in 2.5 minutes with 0.1 Torr etching pressure and 60 sccm gas flow rate. Etching DC bias voltage was obtained by adjusting the rf power from 100 W to 300 W, giving the DC bias voltages from 74 V to 230 V. One sample was also kept as an original reference sample in each series of SF_6 gas etching experiments.

In this analysis, the optical changes due to RIE have also been determined from the PL peak relative intensity and linewidth (FWHM) changes of the NBE emission line and the YL lines.

6.4.1 First Series of SF_6 Gas Etching

Sample	rf power (W)	rf reflected (W)	voltage (V)	pressure (mbar)	rf forward (W)
1	100	1	-65	2×10^{-5}	99
2	130	2	-85	2×10^{-5}	129
3	160	2	-110	3×10^{-6}	160
4			standard unetched		
5	190	2	-140	3×10^{-6}	191
6	220	3	-158	3×10^{-6}	221
7	250	4	-187	3×10^{-6}	252
8	280	5	-209	3×10^{-6}	283

Table 6.4: The first series of SF_6 gas etching conditions.

The samples for the first series of SF_6 gas etching experiment are c-GaN/sap/ 30803/ SF_6 etched /1-8 (8 samples). The etching conditions for each of these samples are shown in Table 6.4. Sample 4 was kept as the original reference sample in this series. For this series, the PL measurements were taken at temperature 4 K.

Figures 6.40 and 6.41 show the PL results of unetched and etched c-GaN/sap/30803/ SF_6 / 1-3,5 and 6-8. Apparent is the NBE emission line, peaking at 3.493 eV.

Figures 6.42 and 6.43 show PL of YL of unetched and etched c-GaN/sap/30803/ SF_6 / 1-3,5 and 6-8. In this series, the PL of YL spectrum consists of three peaks, the first peak is at 2.666 eV (YL1 peak), the second peak is at 2.344 eV (YL2 peak), and the third peak is at 1.893 eV (YL3 peak).

Analysis of the PL Results

Figure 6.44 shows the linewidth change of the NBE emission line as a function of etching voltage. The linewidth after etching generally becomes wider than before etching, so as this series, the linewidth after etching is about 0.7 meV to 4.9 meV wider than before etching. Except for the etching voltage at 187 V, the linewidth is 2 meV narrower after etching. A typical PL linewidth of NBE emission line is about 14 meV

The linewidth change after etching slightly decreases as etching voltage increases. The change of the linewidth starts with 4.9 meV at 65 V etching voltage, then decreases to 2.2 meV at 209 V etching voltage.

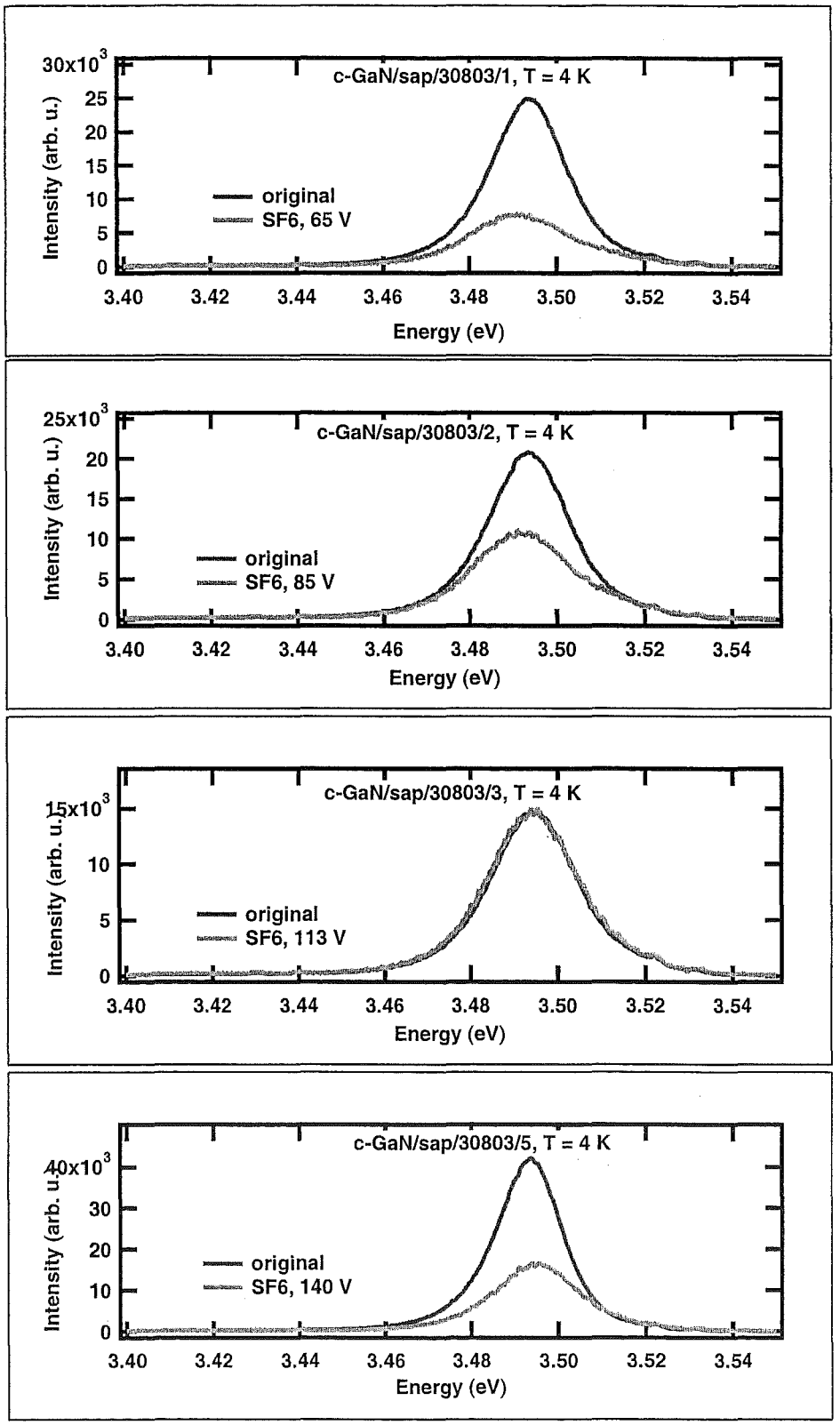

Figure 6.40: Near band edge PL of unetched and etched c-GaN/sap/30803/ 1-3,5 by SF_6 gas, at T = 4 K.

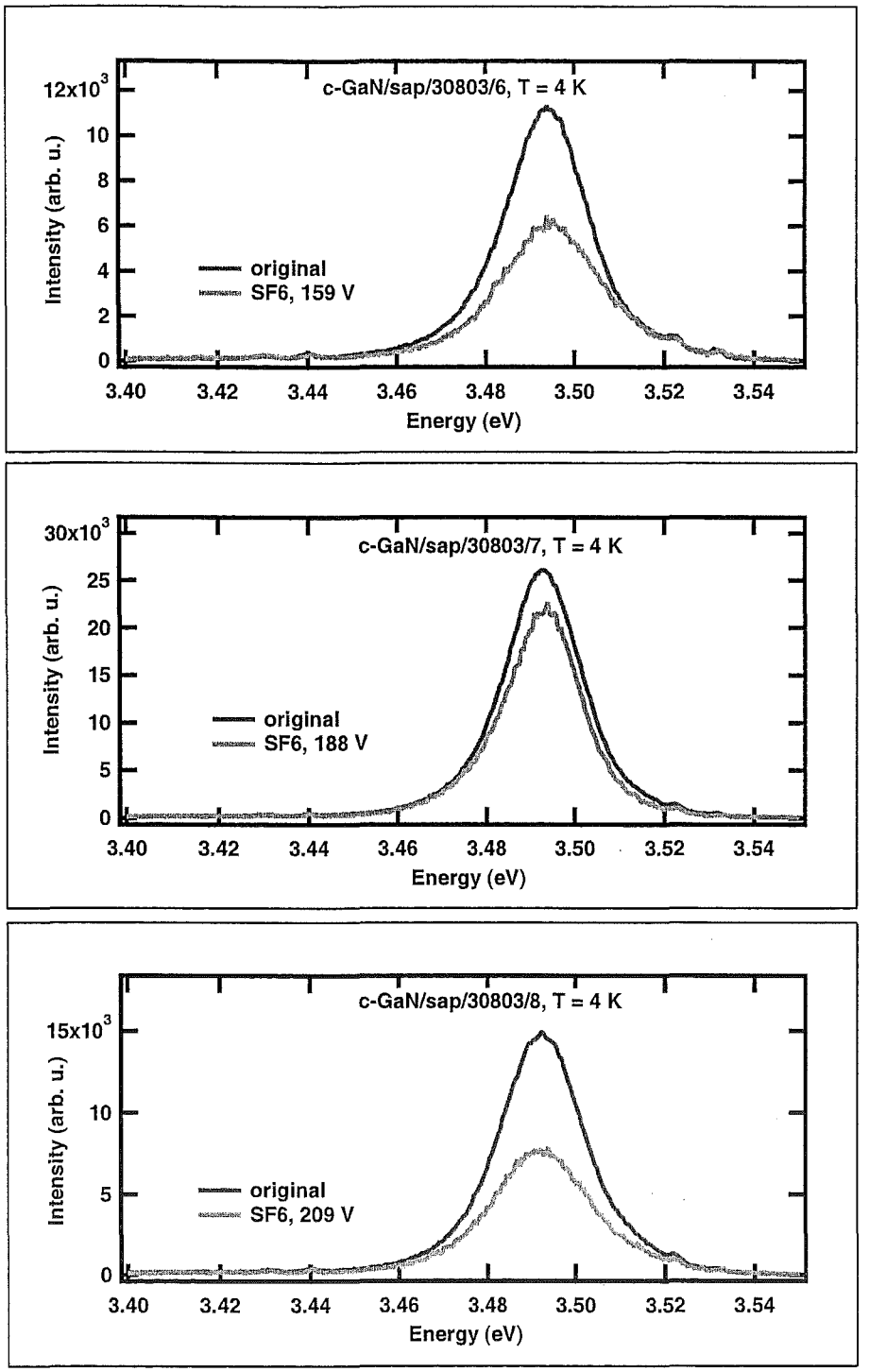

Figure 6.41: Near band edge PL of unetched and etched c-GaN/sap/30803/ 6-8 by SF_6 gas, at T = 4 K.

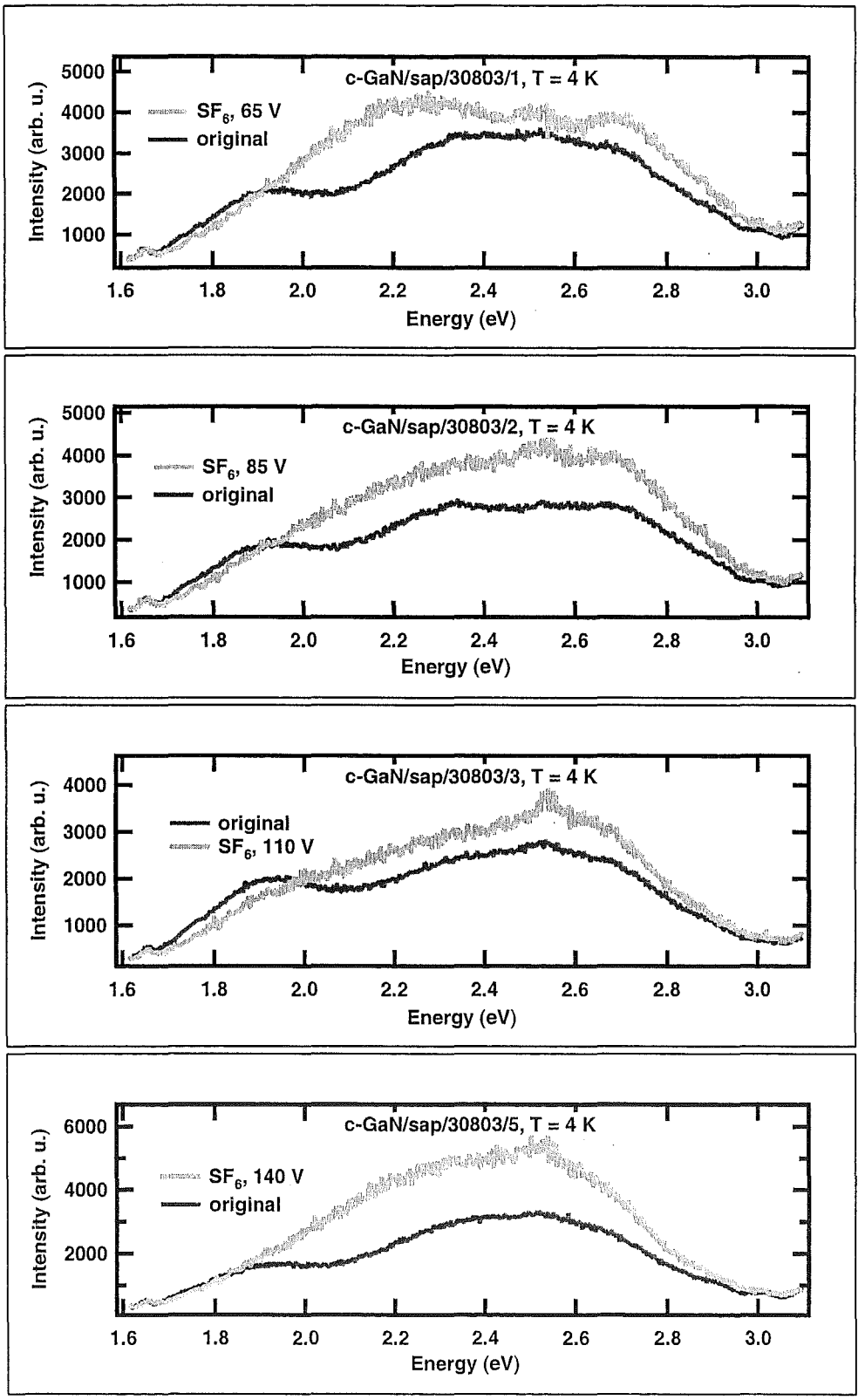

Figure 6.42: Yellow luminescence of unetched and etched c-GaN/sap/30803/ 1-3,5 by SF_6 gas, at T = 4 K.

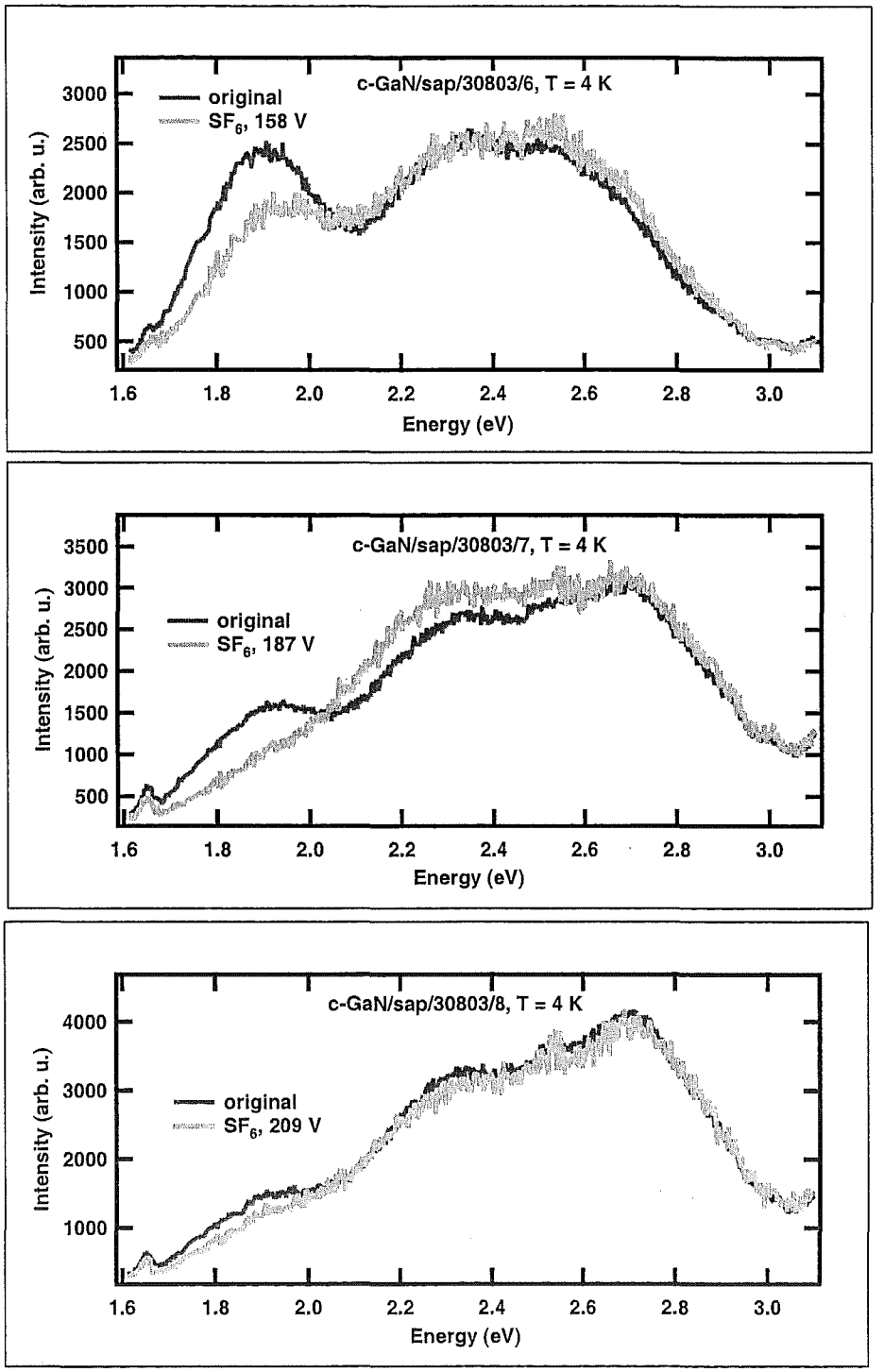

Figure 6.43: Yellow luminescence of unetched and etched c-GaN/sap/30803/ 6-8 by SF_6 gas, at T = 4 K.

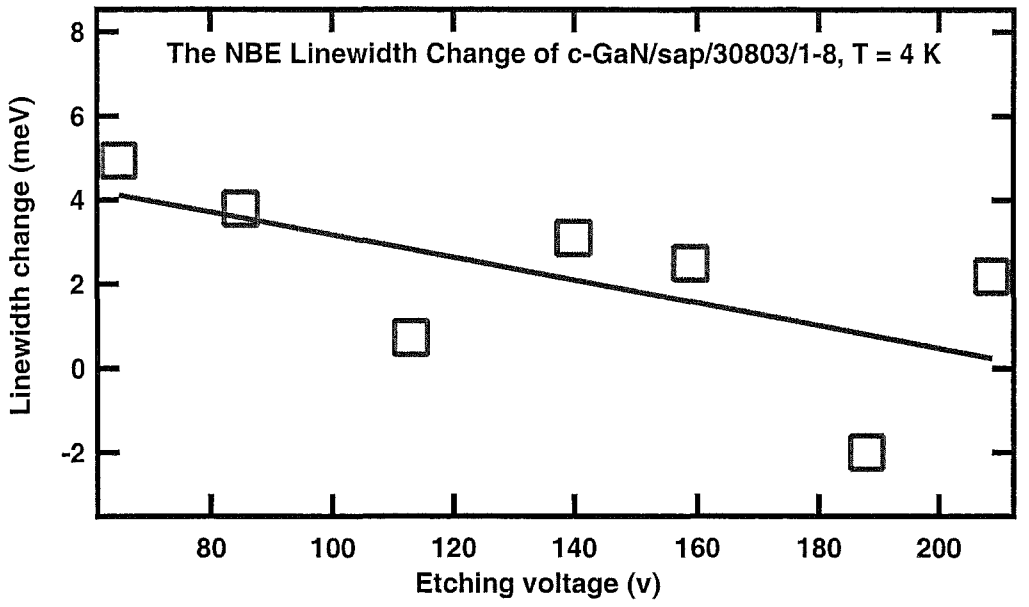

Figure 6.44: Near band edge PL relative linewidth change after etching of c-GaN/sap/30803/ 1-8 by SF_6 gas, at T = 4 K, as a function of etching voltage.

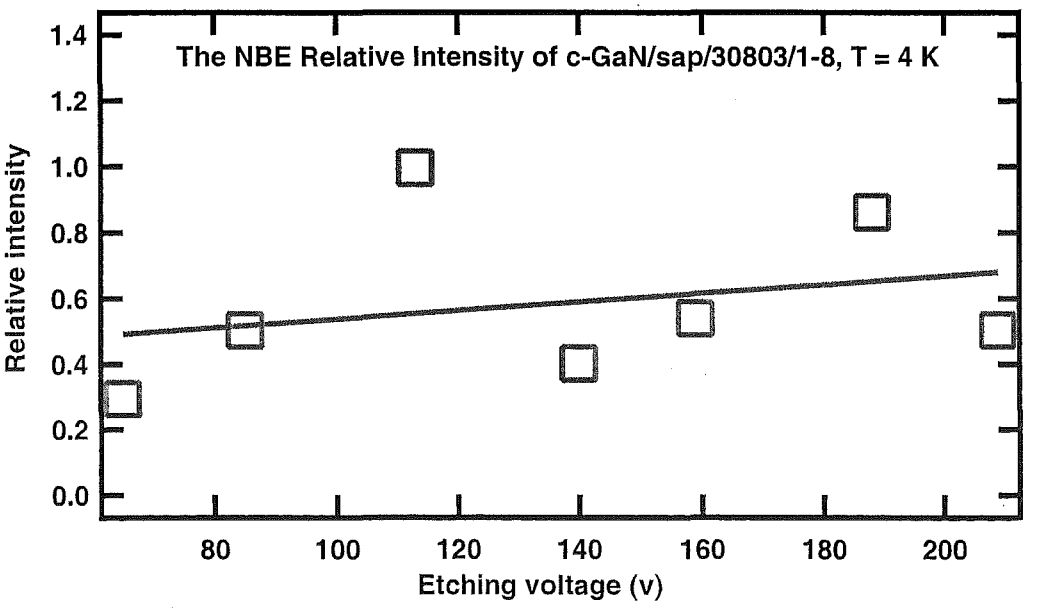

Figure 6.45: Near band edge PL intensity ratio etched/unetched of c-GaN/sap/30803/ 1-8 by SF_6 gas, at T = 4 K, as a function of etching voltage.

Figure 6.45 shows the relative NBE PL intensity after etching as a function of etching voltage. In this SF_6 gas etching series, the PL intensity after etching is relatively lower than before etching.

The relative intensity after etching increases as the etching voltage increases. At the etching voltage of 65 V, the intensity after etching is about 0.3 times of the intensity before etching, then the relative intensity slowly increases, at the etching voltage of 209 V the intensity after etching is about 0.5 times the intensity before etching.

The data from figures 6.44 and 6.45 can be combined as product of linewidth change and relative PL peak intensity. This product is plotted in figure 6.46 as a function of etching voltage.

In the SF_6 gas etching series, the NBE peak relative intensity correlates to its linewidth change in the way that the decreasing peak relative intensity is compensated by increasing its linewidth change and vice versa, thus the total PL does not greatly change. The product result is almost constant at about 1.5 (a.u) and weakly dependent on etching voltage. Except for the product result at the etching voltage of 187 V, its result is about -1.7 (a.u).

Figure 6.47 shows YL1, YL2 and YL3 linewidth changes after etching as a function of etching voltage.The YL1 and YL3 linewidth after etching are generally narrower after etching, as indicated by negative values of linewidth changes. The

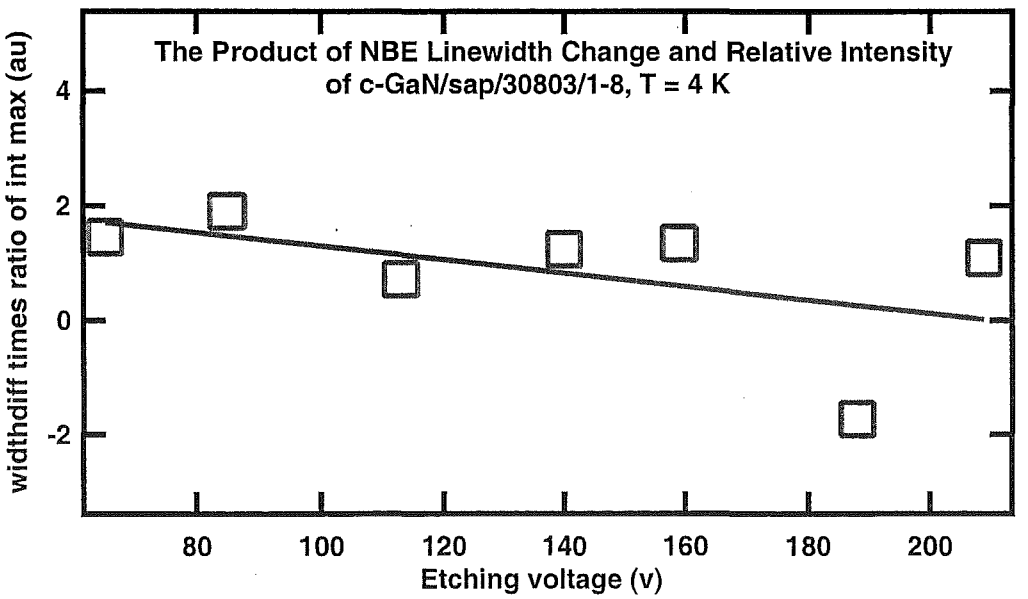

Figure 6.46: Product of near band edge PL peak intensity ratio and the linewidth change of etched c-GaN/sap/30803/ 1-8 by SF_6 gas, at T = 4 K, as a function of etching voltage.

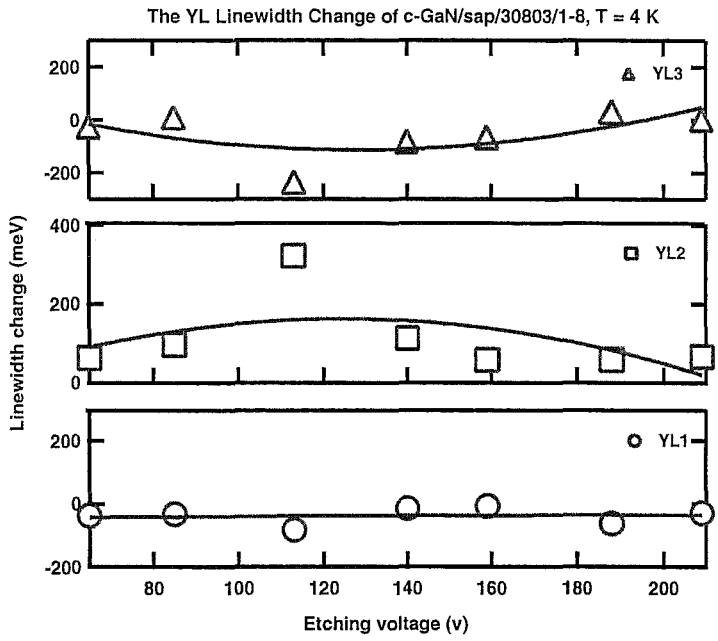

Figure 6.47: YL relative linewidth change after etching of c-GaN/sap/ 30803 / 1-8 by SF_6 gas, at T = 4 K, as a function of etching voltage.

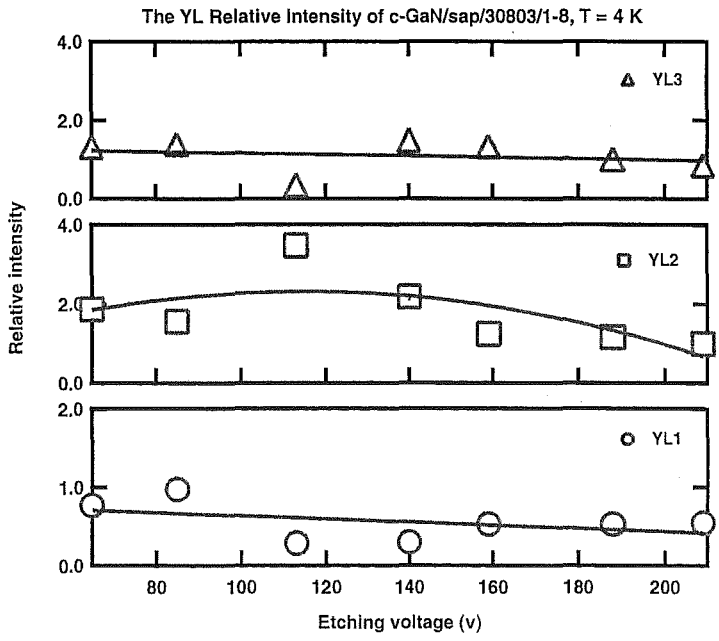

Figure 6.48: YL intensity ratio etched/unetched of c-GaN/sap/ 30803 / 1-8 by SF_6 gas, at T = 4 K, as a function of etching voltage.

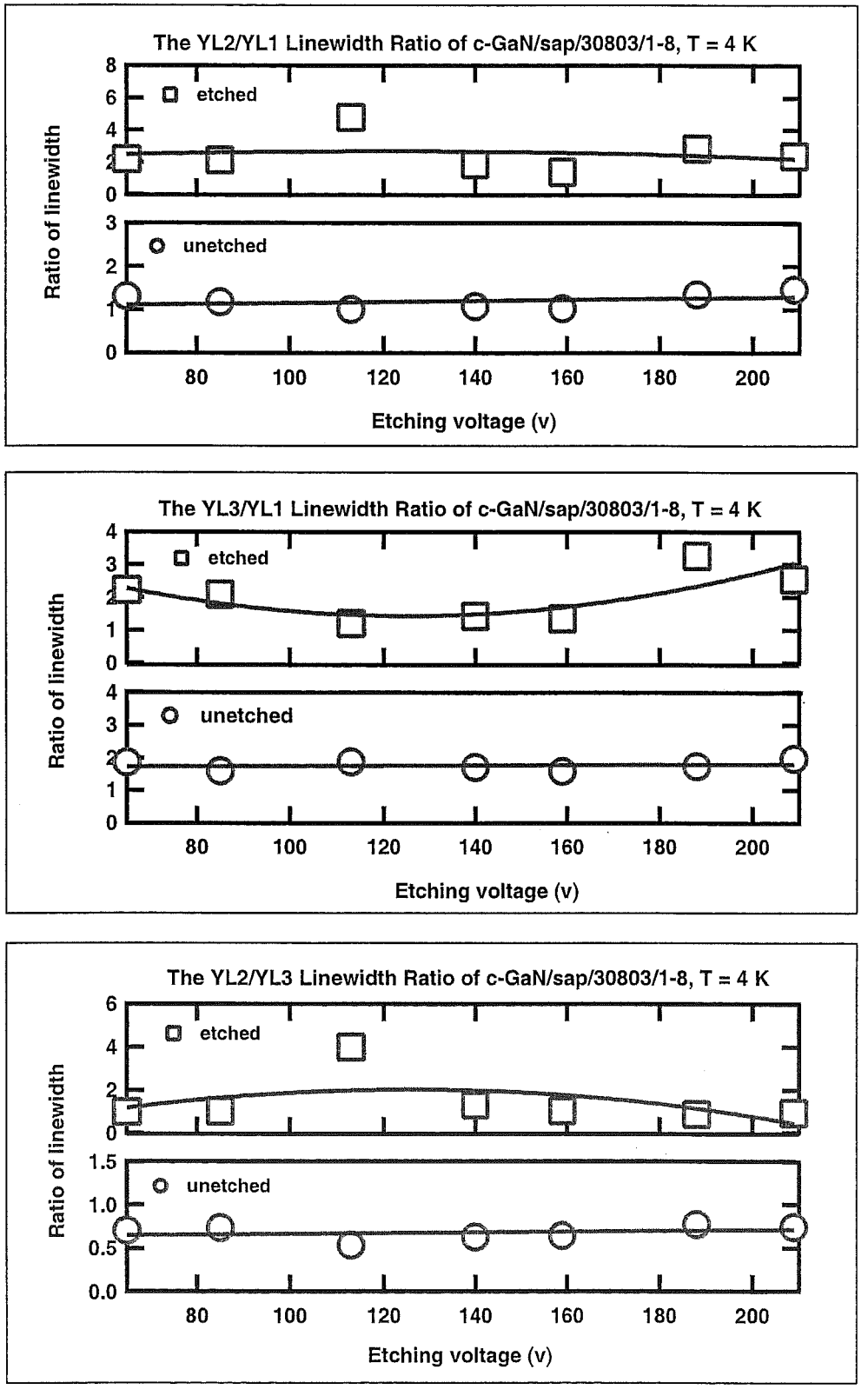

Figure 6.49: Relative linewidth change of YL2/YL1, YL3/YL1, and YL2/YL3 of unetched and etched c-GaN/sap/ 30803 / 1-8 by SF_6 gas, at T = 4 K, as a function of etching voltage.

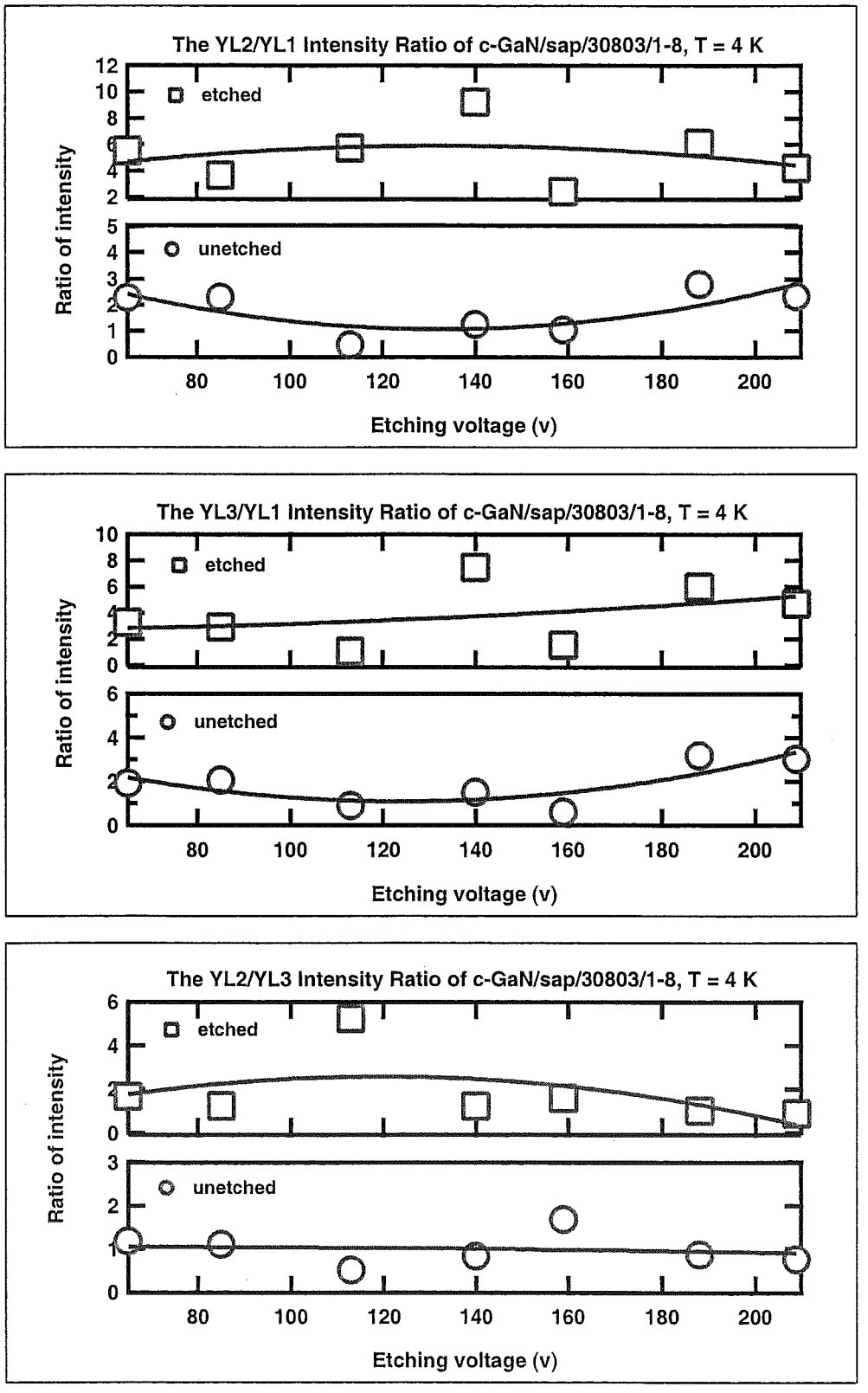

Figure 6.50: Relative peak intensities of YL2/YL1, YL3/YL1, and YL2/YL3 of unetched and etched c-GaN/sap/ 30803 / 1-8 by SF_6 gas, at T = 4 K, as a function of etching voltage.

YL1 and YL3 linewidth changes is in the range of -83 meV to -7 meV, and -236meV to 31 meV, respectively. The YL2 linewidth after etching is wider than before etching, it is shown by positive values of linewidth changes from 58 to 323 meV. In this series, the YL1, Yl2, YL3 linewidth do not change greatly after etching, and only weakly dependent on the etching voltage.

Figure 6.48 shows the relative PL intensity of YL1, YL2, and YL3 after etching as a function of etching voltage. The intensity of YL1 after etching is about 0.29 to 0.97 times of the intensity before etching. The intensity of YL2 after etching is relatively higher, about 1 to 2 times of the intensity before etching. And the intensity of YL3 after etching is also relatively higher, about 1 to 1.5 times of the intensity before etching.

The relative intensity of YL1, YL2 and YL3 after etching slightly decreases as the etching voltage increases. The relative intensity of YL1 after etching at 65 V is about 0.77 times the intensity before etching, then decreases to about 0.55 times the intensity before etching as the etching voltage increases to 209 V. The relative intensity of YL2 after etching at 65 V is about 1.86 times the intensity before etching, then decreases to 0.99 times the intensity before etching as the etching voltage increases to 209 V. And the maximum relative intensity is about 2.18 times the intensity before etching at 140 V etching voltage. The relative intensity of YL3 at etching voltage 65 V is about 1.3 times the intensity before etching, then decreases to 0.9 times the intensity before etching as the etching voltage increases to 209 V.

The data at 110 V etching voltage of the YL2 and YL3 were discounted, because they are questionable and could deviate the result.

Figure 6.49 shows the relative linewidth of YL2 to YL1, YL3 to YL1 and YL2 to YL3 before and after etching as a function of etching voltage.

The relative linewidth of YL2/YL1, YL3/YL1 and YL2/YL3 before etching are almost constant at 1.1, 1.8, and 0.7, respectively. YL1 has the narrowest linewidth and YL3 has the widest linewidth. After etching the relative linewidth between those three YL lines are more various, and only weakly dependent on the etching voltage. The relative linewidth of YL2/YL1 is varied from 1.1 at the etching voltage of 158 V to 2.9 at the etching voltage of 187 V, if we discount the questionable data at the etching voltage of 110 V. And the fitting result shows an almost constant line at about 2.3 ratio of YL2/YL1. At the etching voltage of 65 V, the ratio of YL3/YL1 is about 2.2, then decreases to the minimum value about 1.4 at the etching voltage of 130 V, and increases back to value about 3 at 209 V. The relative linewidth of YL2/YL3 after etching is almost constant at averagely 1.1, if we ignore the questionable data at the etching voltage of 110 V.

Figure 6.50 shows the relative peak intensity of YL2 to YL1, YL3 to YL1 and YL2 to YL3 before and after etching as a function of etching voltage. Before etching the peak intensity of YL2 and YL3 is similar and about 1.5 to 2 times higher than the intensity of YL1, dependent on each sample.

After etching the peak intensity of YL2 is slightly higher than of the YL3, the ratio of the intensities is about 1.3, and does not greatly change as the etching voltage increases.

The data of relative peak intensities of YL2/YL1 and YL3/YL1 are quite scattered and inconclusive. However, it is seen that after etching the YL2 and YL3 intensities are relatively increased higher than the intensity of YL1.

AFM Pictures and Analysis

Figure 6.51 shows AFM images of c-GaN/sap/ 30803 / 1-8 after etching. The RMS roughness was measured for all samples before and after etching from AFM results and this data is plotted in figure 6.52 as a function of etching voltage.

It is obvious that the RMS roughness of sample's surface after etching is rougher than before etching. Before etching the RMS roughness is between 3 nm to 6 nm, and after etching the RMS roughness is between 12 nm to 18 nm.

The fitting result shows that the sample's surface is rougher as the etching voltage increases. At the etching voltage of 65 V, the RMS roughness is about 12 nm then increases to about 17 nm at the etching voltage of 209 V.

6.4.2 Second Series of SF_6 Gas Etching

Sample	rf power (W)	rf reflected (W)	voltage (V)	pressure (mbar)	rf forward (W)
9	100	1	-74	5×10^{-5}	99
10	130	1	-105	5×10^{-5}	129
11	150	1	-124	5×10^{-5}	150
12	180	2	-150	5×10^{-5}	181
13			standard unetched		
14	200	2	-160	5×10^{-5}	200
15	220	3	-170	5×10^{-5}	221
16	250	4	-195	5×10^{-5}	252
17	280	4	-221	5×10^{-5}	283
18	300	5	-230	5×10^{-5}	290

Table 6.5: The second series of SF_6 gas etching conditions.

The second series of SF_6 gas etching experiment was done to confirm the results of the first series.

The samples for the second series of SF_6 gas etching experiment are c-GaN/sap/ 30803/ SF_6 etched / 9-18 (10 samples). The etching conditions for each of these samples are shown in Table 6.5. Sample 13 was kept as an original reference sample in this series. The PL measurements were taken at temperature 4 K.

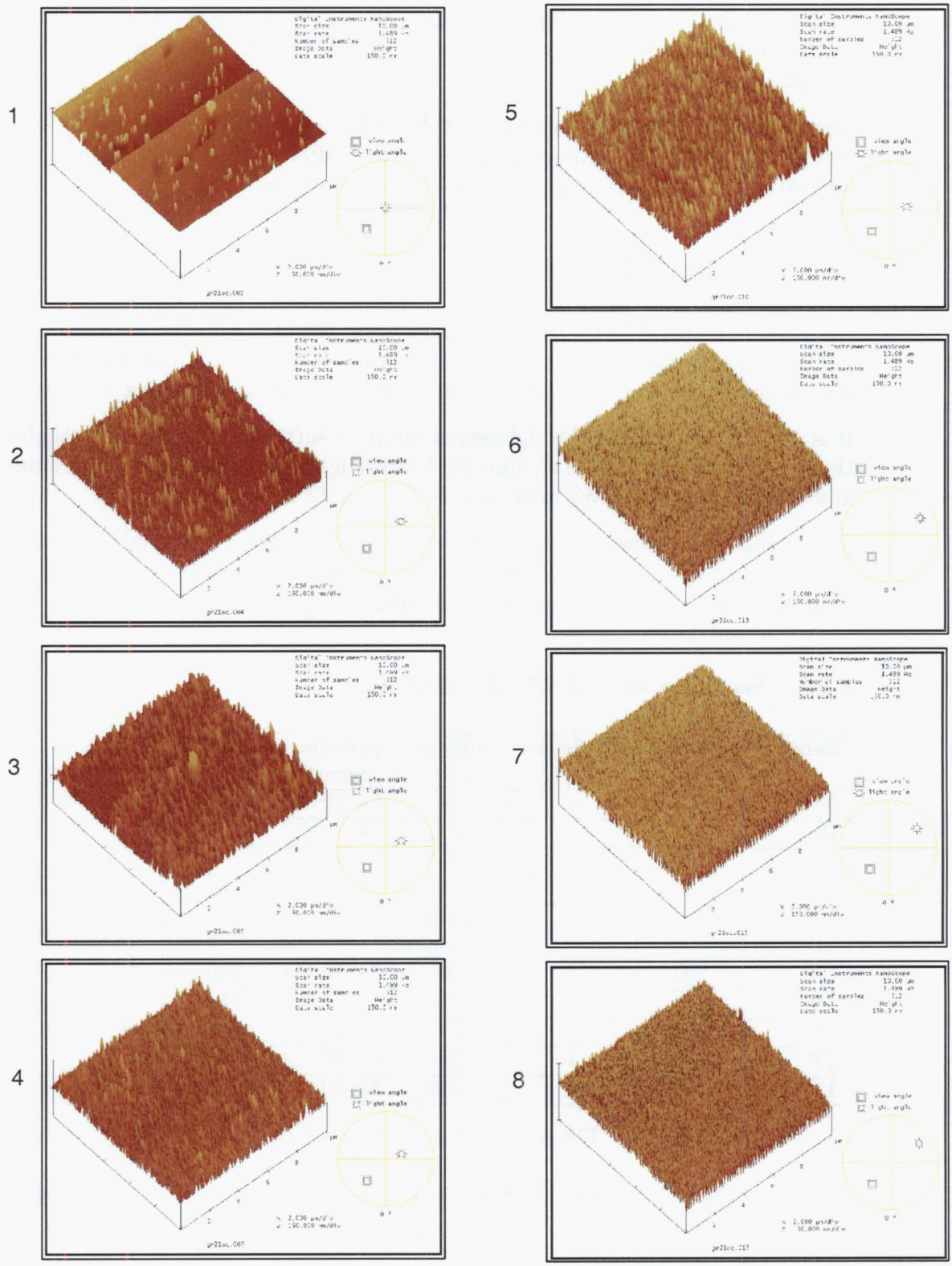

Figure 6.51: AFM images of the surface of etched c-GaN/sap/ 30803 / 1-8 by SF_6 gas.

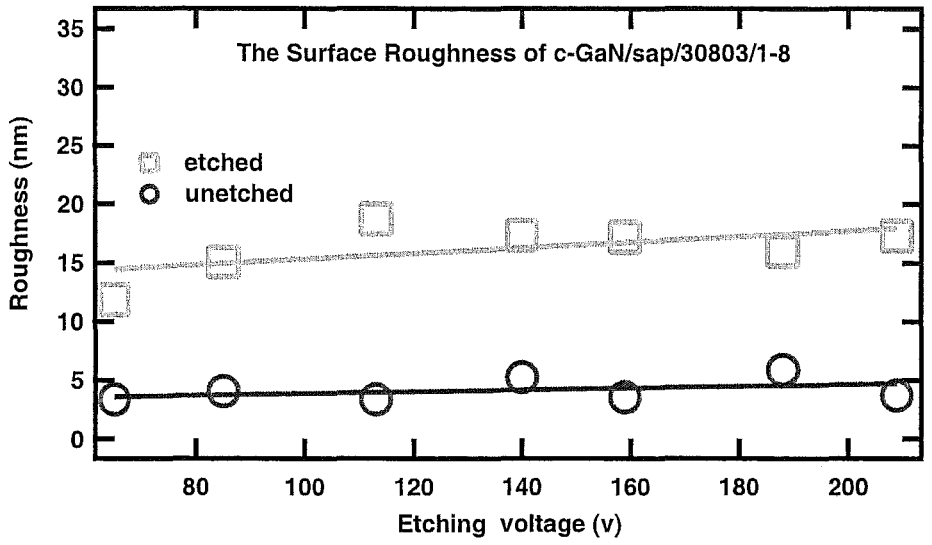

Figure 6.52: The surface roughness of etched c-GaN/sap/ 30803 / 1- by SF_6 gas as a function of etching voltage.

Figures 6.53, 6.54 and 6.55 show the PL results of the NBE emission line of unetched and etched c-GaN/sap/30803/ SF_6 / 9-11; 12, 14, 15; 16-18. Apparent from the spectra is the NBE emission line at 3.493 eV.

Figures 6.56, 6.57 and 6.58 show the YL of unetched and etched c-GaN/sap/30803/ SF_6 / 9-11; 12, 14, 15; 16-18. In this series, the YL spectrum consists of three lines, those are YL1, peaking at 2.666 eV; YL2, peaking at 2.317 eV; and YL3, peaking at 1.881 eV.

Analysis of the PL Results

Figure 6.59 shows the linewidth change to NBE line as a function of etching voltage. The linewidth after etching is only slightly wider than before etching. It is shown by a small positive value from 0 to 5.7 meV of the relative linewidth after etching. At the etching voltage of 74 V, the linewidth change is 2.1 meV then decreases and reaches the minimum value of 0.1 meV at the etching voltage about 135 V and increases back to 5.7 meV at the etching voltage of 221 V.

Figure 6.60 shows the relative NBE PL intensity after etching as a function of the etching voltage. In this SF_6 gas etching series, the PL intensity after etching is also relatively lower than before etching, except for the PL intensity at 150 V etching voltage, the intensity after etching is about 1.1 times higher than before etching. At the etching voltage of 74 V the relative intensity after etching is about 0.73 times of the intensity before etching, then increases to a maximum of 1 at the etching voltage of 124 V and decreases to 0.2 at the etching voltage of

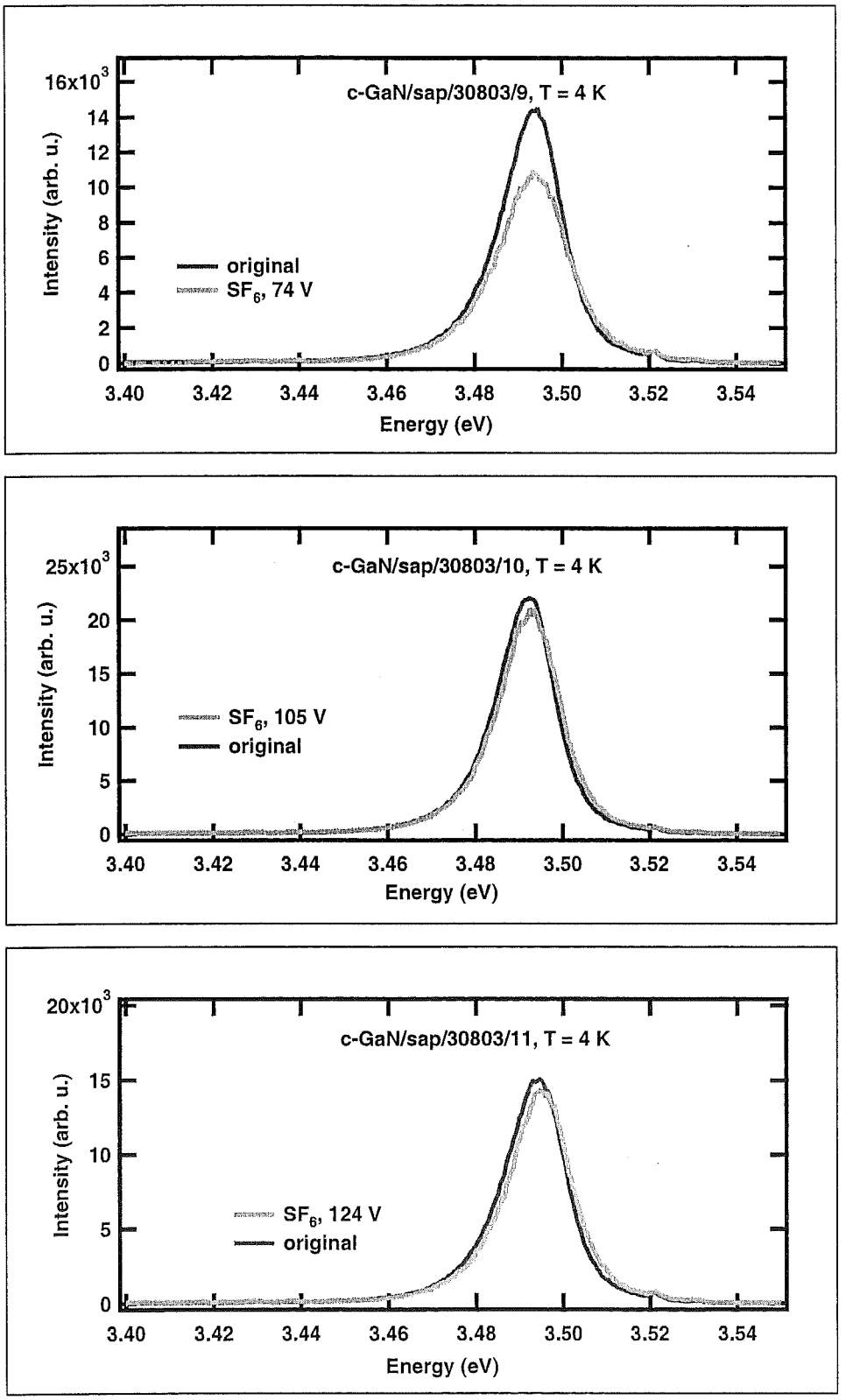

Figure 6.53: Near band edge PL of unetched and etched c-GaN/sap/30803/ 9-11 by SF_6 gas, at T = 4 K.

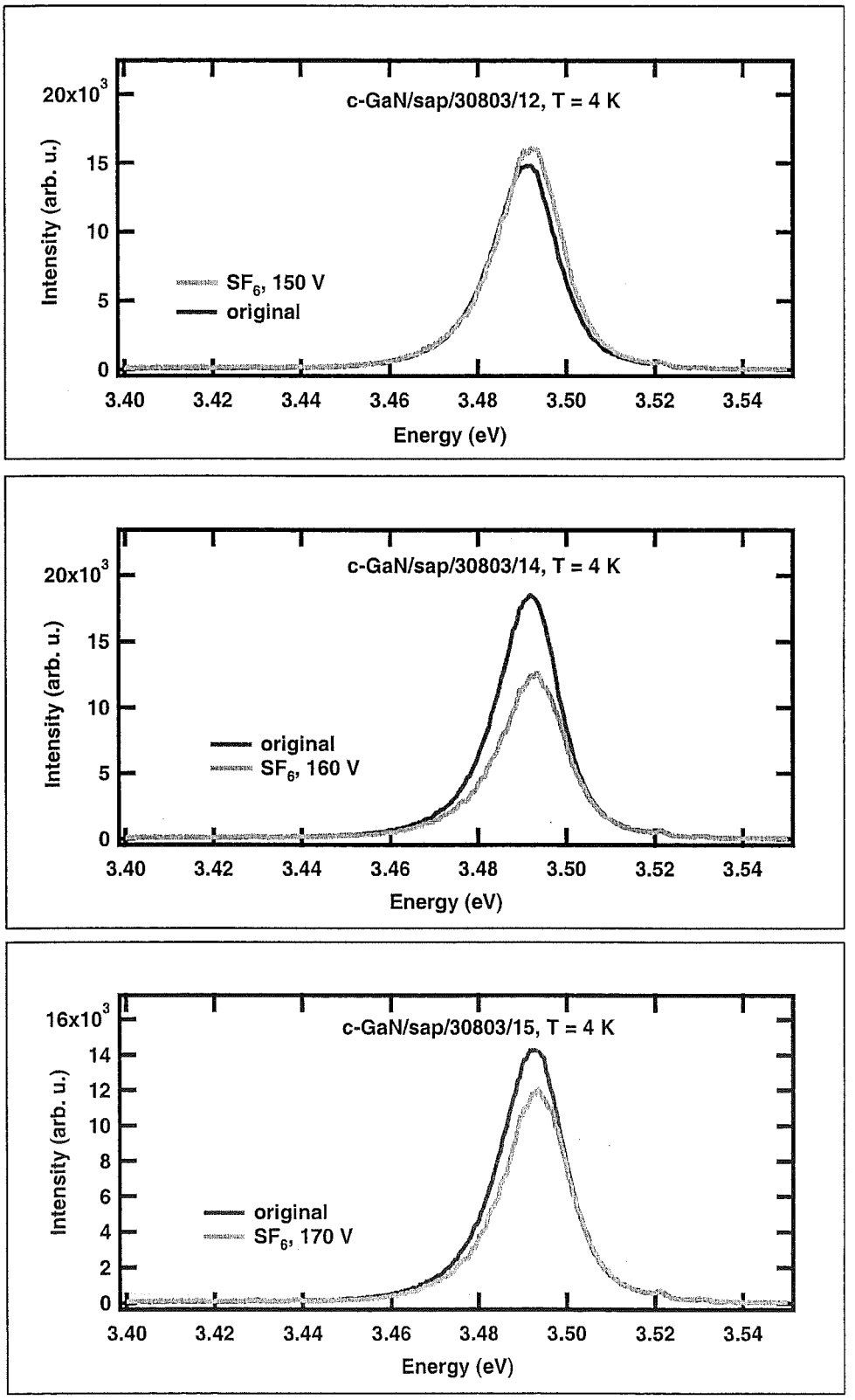

Figure 6.54: Near band edge PL of unetched and etched c-GaN/sap/30803/ 12, 14, 15 by SF_6 gas, at T = 4 K.

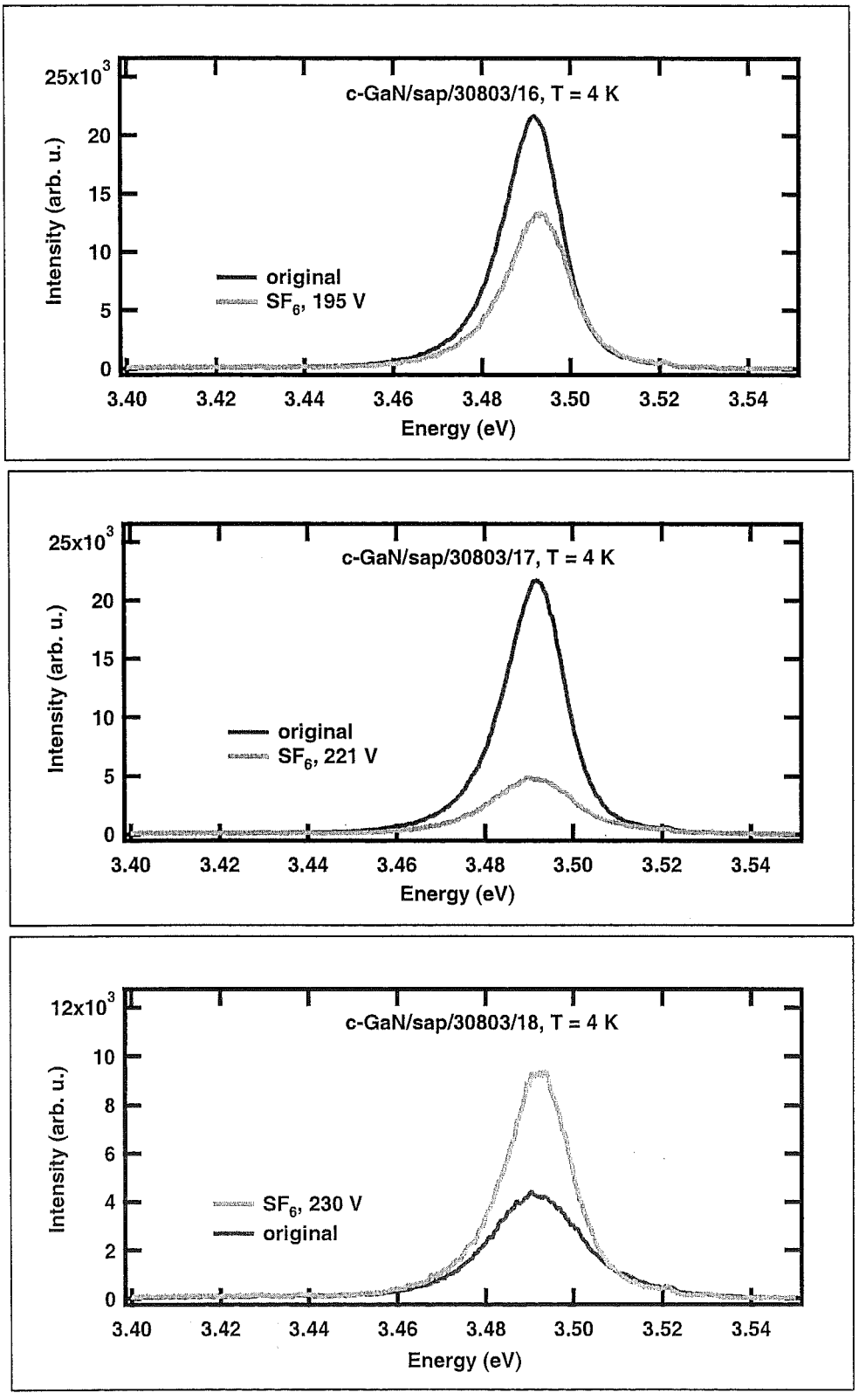

Figure 6.55: Near band edge PL of unetched and etched c-GaN/sap/30803/ 16-18 by SF_6 gas, at T = 4 K.

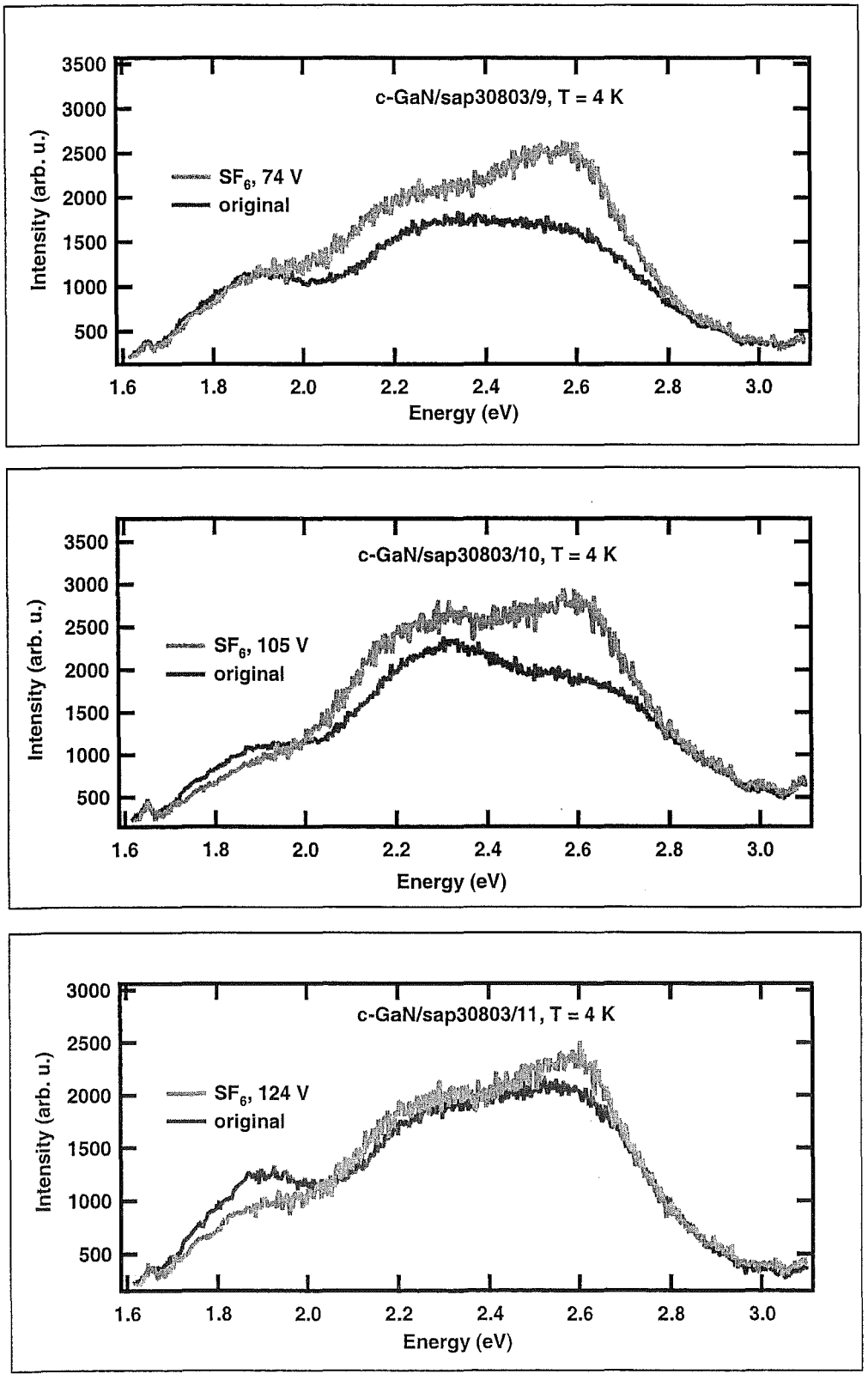

Figure 6.56: Yellow luminescence of unetched and etched c-GaN/sap/30803/ 9-11 by SF_6 gas, at T = 4 K.

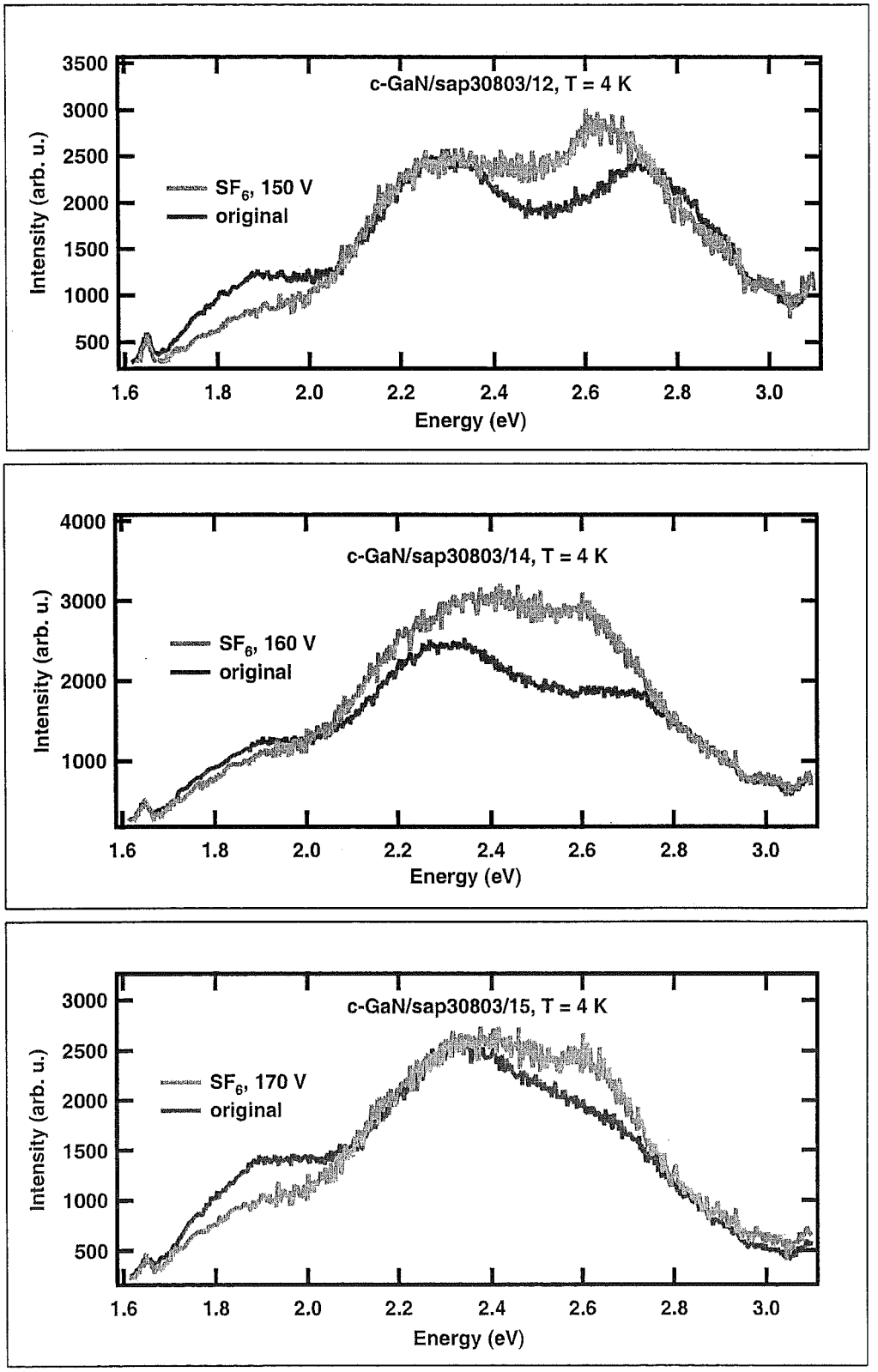

Figure 6.57: Yellow luminescence of unetched and etched c-GaN/sap/30803/ 12, 14, 15 by SF_6 gas, at T = 4 K.

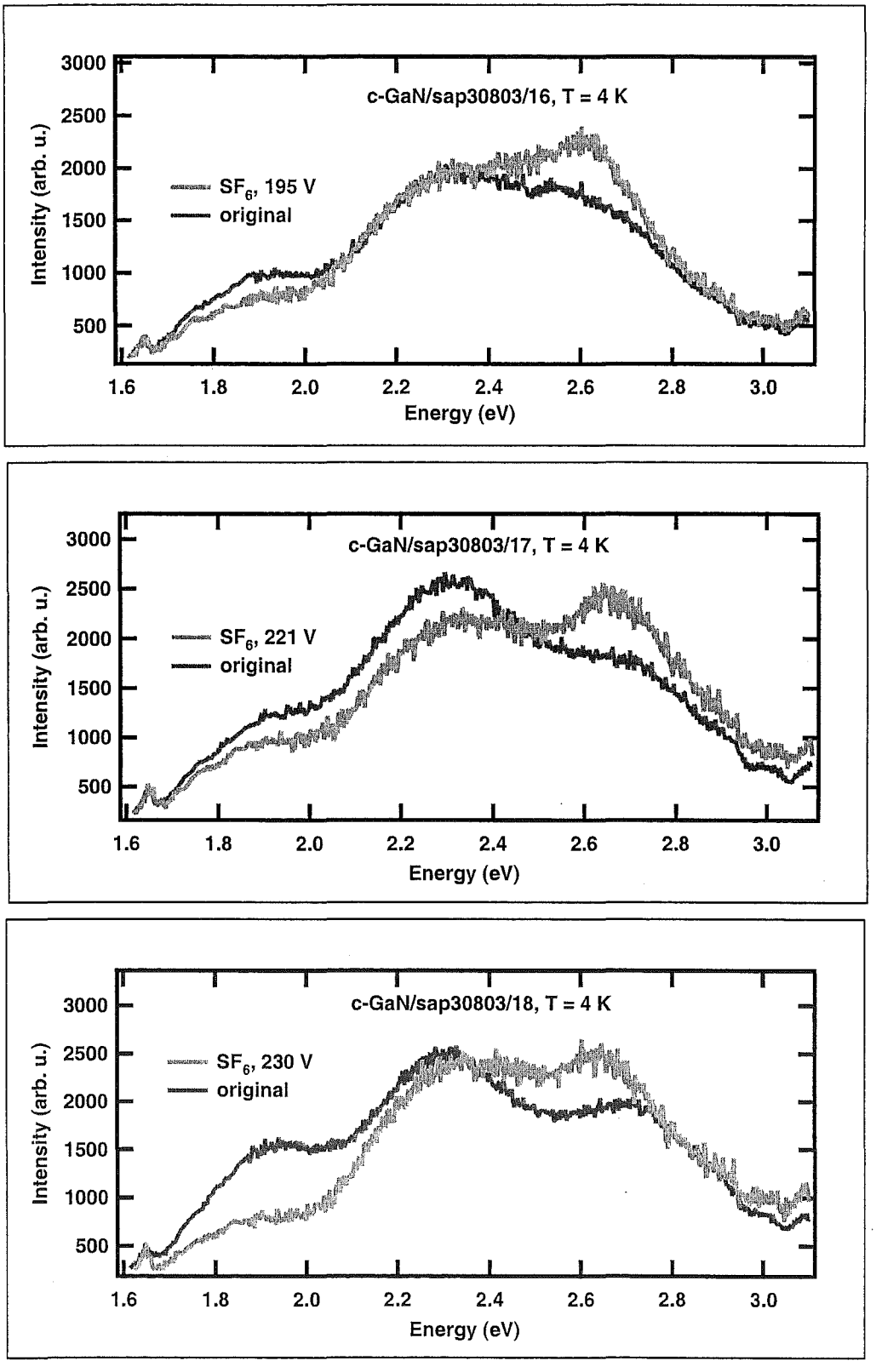

Figure 6.58: Yellow luminescence of unetched and etched c-GaN/sap/30803/ 16-18 by SF_6 gas, at T = 4 K.

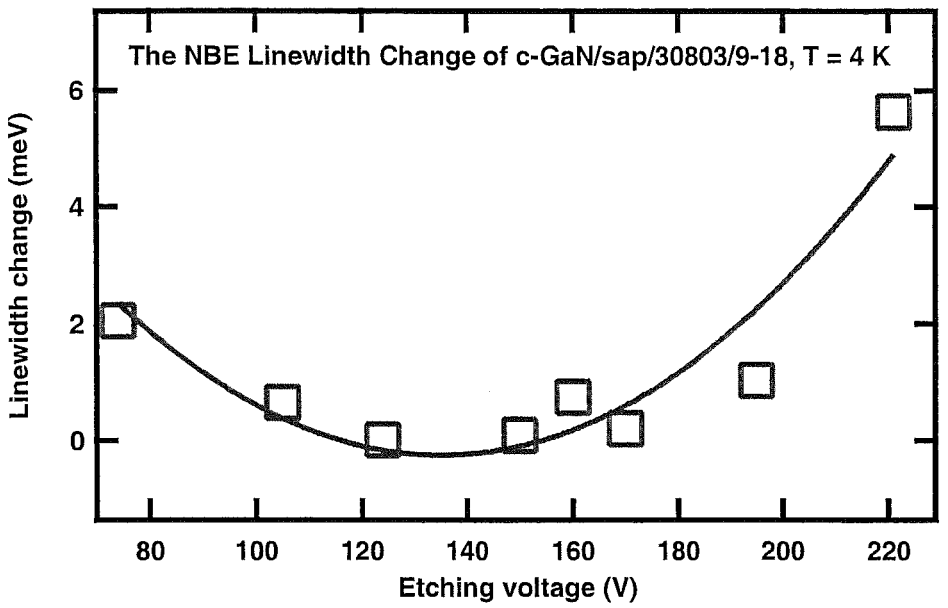

Figure 6.59: Near band edge PL relative linewidth change after etching of c-GaN/sap/30803/ 9-18 by SF_6 gas, at T = 4 K.

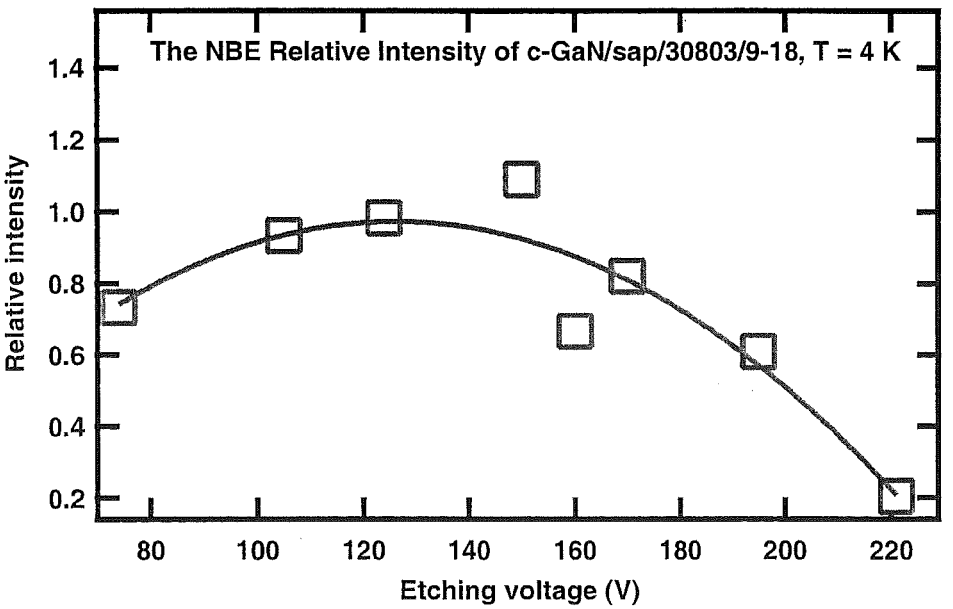

Figure 6.60: Near band edge PL intensity ratio etched/unetched of c-GaN/sap/30803/ 9-18 by SF_6 gas, at T = 4 K, as a function of etching voltage.

221 V.

The data from figures 6.59 and 6.60 can be combined as product of linewidth change and relative intensity of the NBE emission line. This product is plotted in figure 6.61 as a function of etching voltage. The product result is slightly varied from 0.02 to 0.15. At the etching voltage of 74 V the product result is 0.15, then decreases to a minimum value of 0.02 at the etching voltage of 150 V and increases back to 0.12 at the etching voltage of 221 V.

In this SF_6 gas etching series, the NBE peak relative intensity also correlates to its linewidth change in the way that the decreasing peak relative intensity is compensated by increasing its linewidth change and vice versa, thus the total PL does not greatly change.

Figure 6.62 shows YL1, YL2 and YL3 linewidth changes after etching as a function of the etching voltage. The YL1 linewidth after etching is narrower than before etching, and as the etching voltage increases, the YL1 linewidth change is narrowed. At the etching voltage of 74 V, the YL1 linewidth change is about -20 meV narrower than before etching, then narrowed down to -100 meV as the etching voltage increases to 230 V. A typical linewidth of YL1 or YL3 is about 150 meV to 200 meV and YL2 is about 250 meV to 300 meV. The analysis results of YL2 and YL3 linewidth change after etching is less conclusive, and quite scattered.

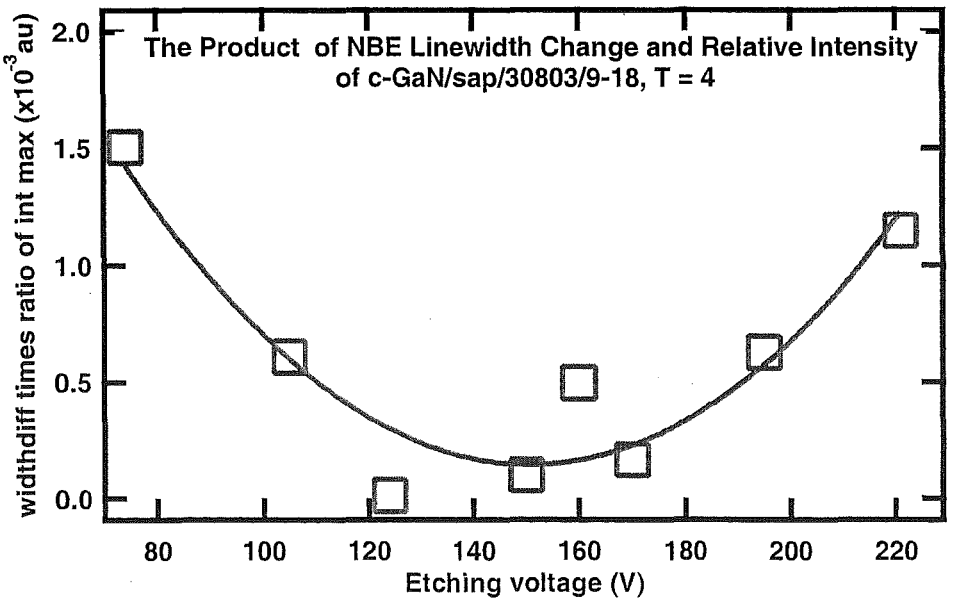

Figure 6.61: Product of the near band edge PL peak intensity ratio and the linewidth change of etched c-GaN/sap/30803/ 9-18 by SF_6 gas, at T = 4 K, as a function of etching voltage.

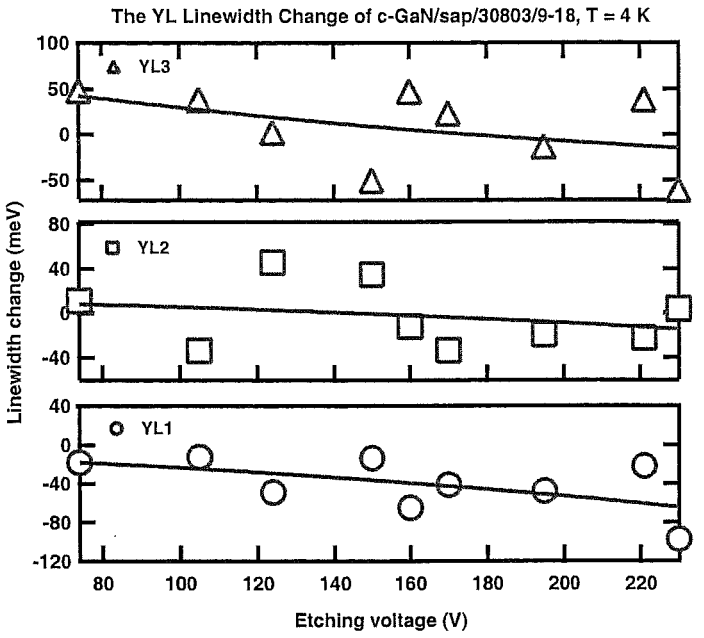

Figure 6.62: YL relative linewidth change after etching of c-GaN/sap/ 30803 / 9-18 by SF_6 gas, at T = 4 K, as a function of etching voltage.

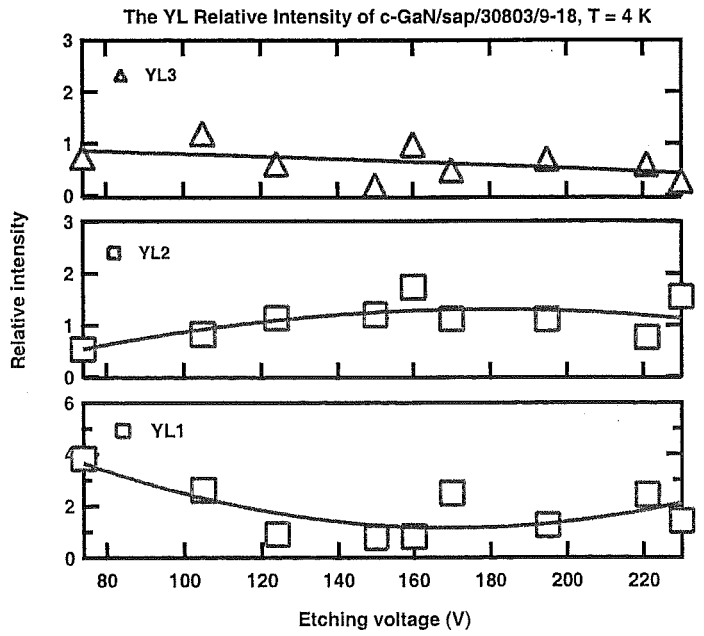

Figure 6.63: YL intensity ratio etched/unetched of c-GaN/sap/ 30803 / 9-18 by SF_6 gas, at T = 4 K, as a function of etching voltage.

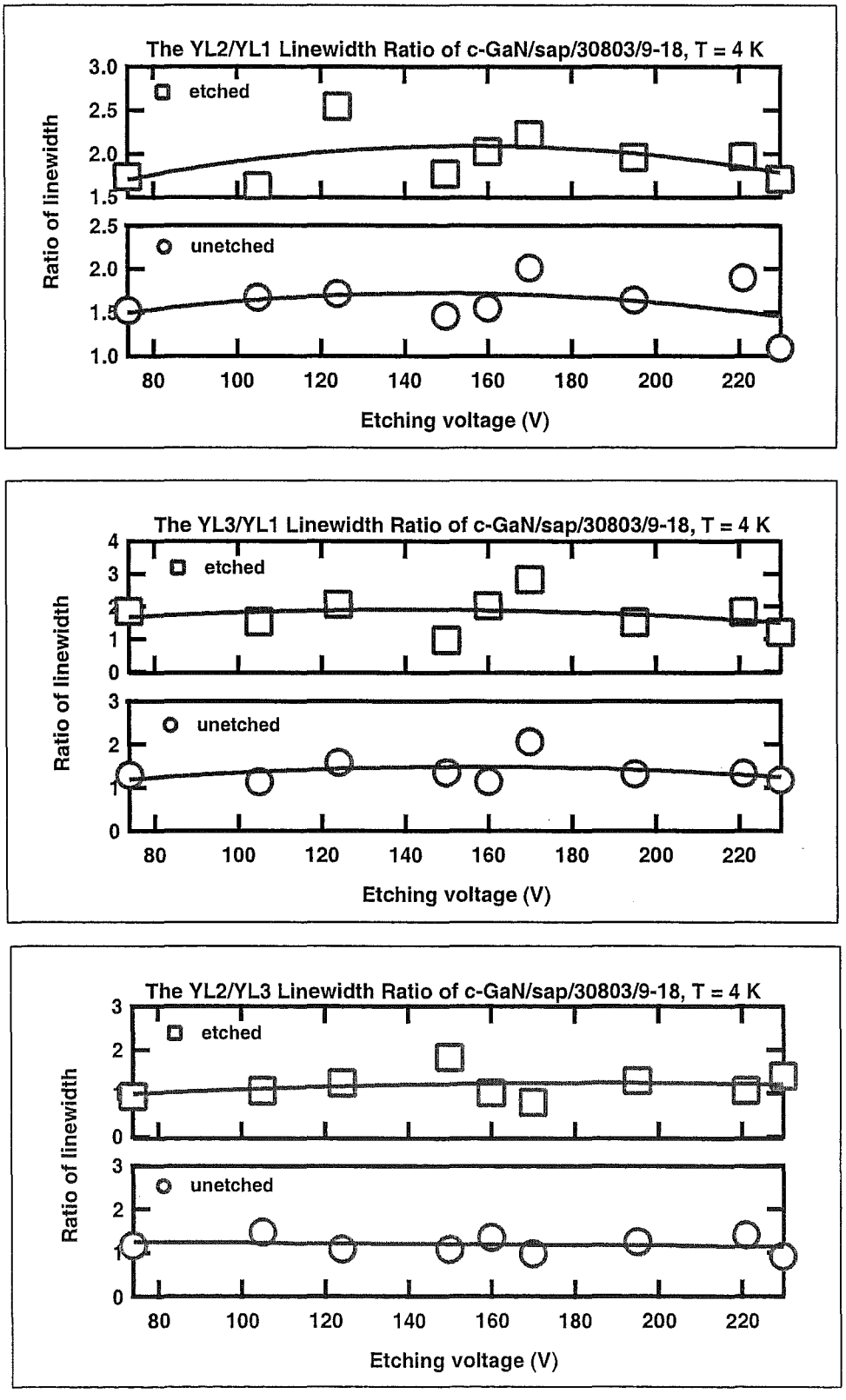

Figure 6.64: Relative linewidth change of YL2/YL1, YL3/YL1, and YL2/YL3 of unetched and etched c-GaN/sap/ 30803 / 9-18 by SF_6 gas, at T = 4 K, as a function of etching voltage.

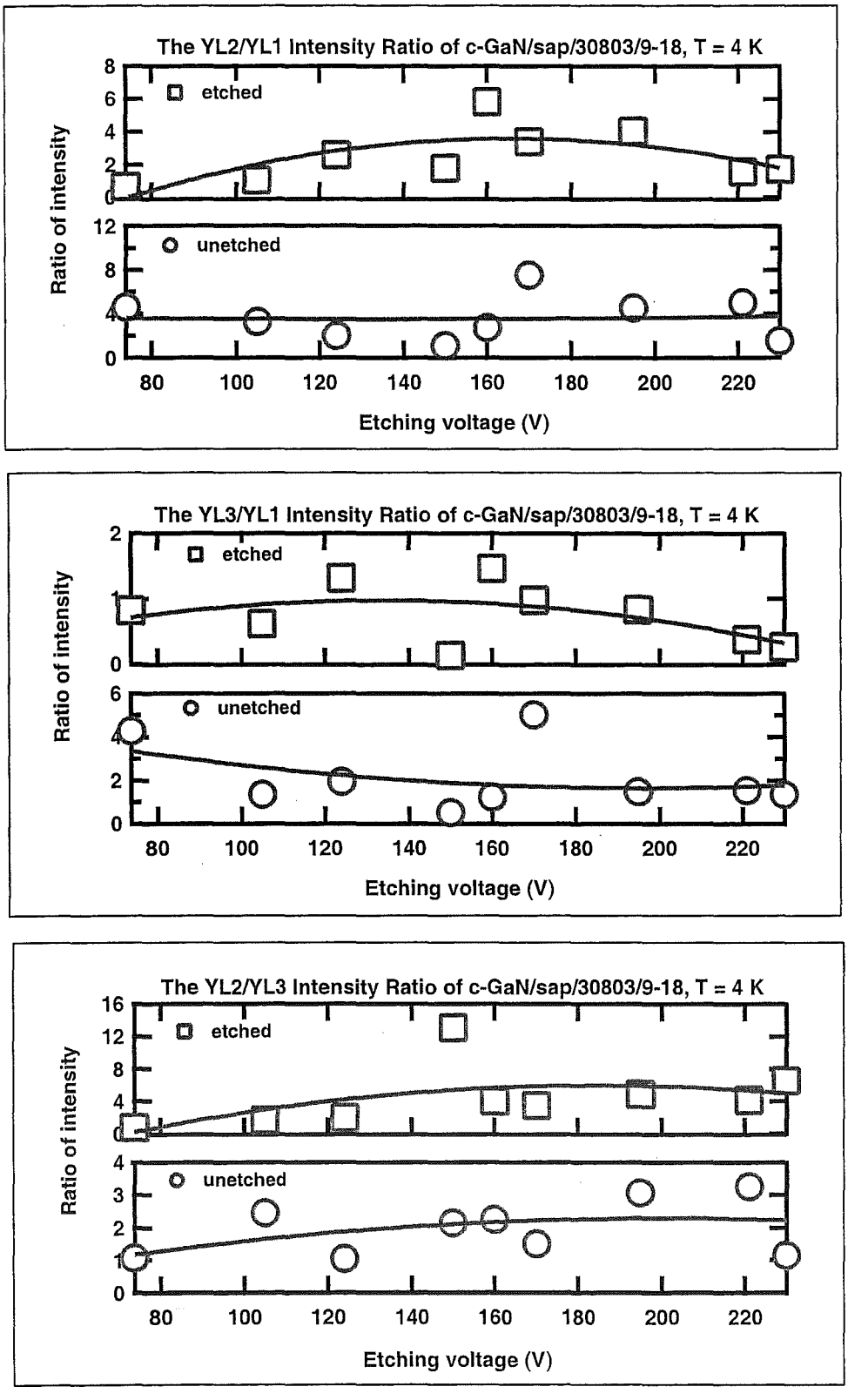

Figure 6.65: Relative peak intensities of YL2/YL1, YL3/YL1, and YL2/YL3 of unetched and etched c-GaN/sap/ 30803 / 9-18 by SF_6 gas, at T = 4 K, as a function of etching voltage.

Figure 6.63 shows the relative PL intensity of YL1, YL2, and YL3 after etching as a function of etching voltage. The data of the YL1 relative intensity after etching spreads from about 1 to about 4 times the intensity before etching. It only gives a general idea that after etching the YL1 intensity is higher than before etching.

The YL2 relative intensity after etching is about 1.2 times higher than before etching. As the etching voltage increases, the relative intensity of YL2 slightly increases. At the etching voltage of 74 V, the ratio of intensities after to before etching is about 0.8 then increases to about 1.5 at etching voltage 230 V.

The intensity of YL3 after etching is lower than before etching, and the relative intensity of YL3 after etching decreases as the etching voltage increases. At the etching voltage of 74 V the relative YL3 intensity after etching is about 0.8 times the intensity before etching, then decreases to about 0.3 times the intensity before etching at the etching voltage of 230 V.

Figure 6.64 shows the relative linewidth of YL2 to YL1, YL3 to YL1 and YL2 to YL3 before and after etching as a function of etching voltage.

YL2 has wider linewidth than YL1, before etching the relative linewidth of YL2 is 1.6 times wider than the relative linewidth of YL1, and after etching the relative linewidth of YL2 is 1.9 times wider than the relative linewidth of YL1. The relative linewidth change is weakly dependent on the etching voltage.

YL3 also has wider linewidth relatively to YL1. Before etching the relative linewidth of YL3 is 1.4 times wider than the relative linewidth of YL1, and after etching the relative linewidth of YL3 is about 1.7 times wider than the relative linewidth of YL1.

The linewidth of YL2 is slightly wider than of the YL3, the relative linewidth of YL2 is about 1.2 times wider than the relative linewidth of YL3 before etching. After etching at the voltage of 74 V, the linewidth of YL2 is as wide as the linewidth of YL3, then slowly increases, at the etching voltage of 150 V and 230 V the linewidth of YL2 is about 1.2 and 1.3 times wider than the linewidth of YL3.

Figure 6.65 shows the relative peak intensity of YL2 to YL1, YL3 to YL1 and YL2 to YL3 before and after etching as a function of etching voltage. The intensity of YL2 before and after etching are generally higher than the intensity of YL1. However, the data of the relative intensities of YL2/YL1 is scattered and quite inconclusive. In general, the relative intensity of YL2/YL1 after etching is lower than before etching, and slightly increases as the etching voltage increases.

Before etching, the intensity of YL3 is about 2 to 3 times higher than the intensity of YL1. But after etching, the intensity of YL3 becomes similar to the intensity of YL1, the ratio of intensities YL3/YL1 is about 1, and this ratio does not change as etching voltage increases.

Before etching, the intensity of YL2 is similar to the intensity of YL3. After

etching, the relative intensity of YL2 to YL3 increases as the etching voltage increases. At the etching voltage of 74 V the ratio of YL2/YL3 is about 1, then increases to about 5 at the etching voltage of 230 V.

AFM Pictures and Analysis

Figure 6.66 shows AFM images of c-GaN/sap/ 30803 / 9-18 after etching. The RMS roughness was measured for all samples after etching from AFM results and this data is plotted in figure 6.67 as a function of etching voltage.

In this SF_6 gas etching series, the RMS roughness of the sample's surface after etching is about 5.8 nm to 9.5 nm. The fitting result shows that the sample's surface is rougher as the etching voltage increases. At the etching voltage of 74 V, the RMS roughness is about 5.9 nm then increases to about 9 nm at the etching voltage of 230 V.

6.4.3 Discussion and Conclusion of SF_6 Gas Etching Series

About 94% of the SF_6 etched samples show wider PL linewidth of the NBE emission line after etching. The NBE line does not shift after SF_6 etching. As mentioned in the prior work of the University of Canterbury [17] and [12] that NBE line after etching is dominated by donor bound exciton (D^0X) and acceptor bound exciton (A^0X) related lines, it is interpreted that the wider linewidth after etching was the result of wider D^0X and/or A^0X related lines after etching.

The prior work on SF_6 gas etching shows an acceptor bound exciton (A^0X) peak at the lower energy side of the D^0X peak appear after SF_6 gas etching, when the exposure time is 2.5 minutes or longer [16],[17],[15]. However, in this result the new line that is associated with the acceptor bound exciton (A^0X) peak was not observed after SF_6 gas etching of about 2 minutes. It is probably because the 2 minutes exposure was too short to introduce A^0X and the D^0X peak is much stronger than A^0X on the samples used for this work.

In this work, about 87% of the results show that the PL intensity of the NBE line at 3.493 eV decreases after SF_6 gas etching. Generally, the PL intensity after SF_6 gas etching is lower compared to the case of Ar gas etching. Cheung *et al* [15] also observed similar result of SF_6 gas etching and interpreted this as follows. A loss of nitrogen on GaN surface is present after Ar and SF_6 gas etching. The XPS results show that after Ar gas etching, the ratio of raw Ga/N XPS line is 18.3, higher than 13.9, the ratio of raw Ga/N XPS line after SF_6 gas etching. Nitrogen vacancies on the GaN surface behave as native donors and contribute to the stronger donor peak observed in the NBE emission.

The relative NBE line PL intensity after etching also correlates to the linewidth change in the similar way to Ar etching, thus SF_6 gas etching processes also do not significantly increase the density of non radiative centres.

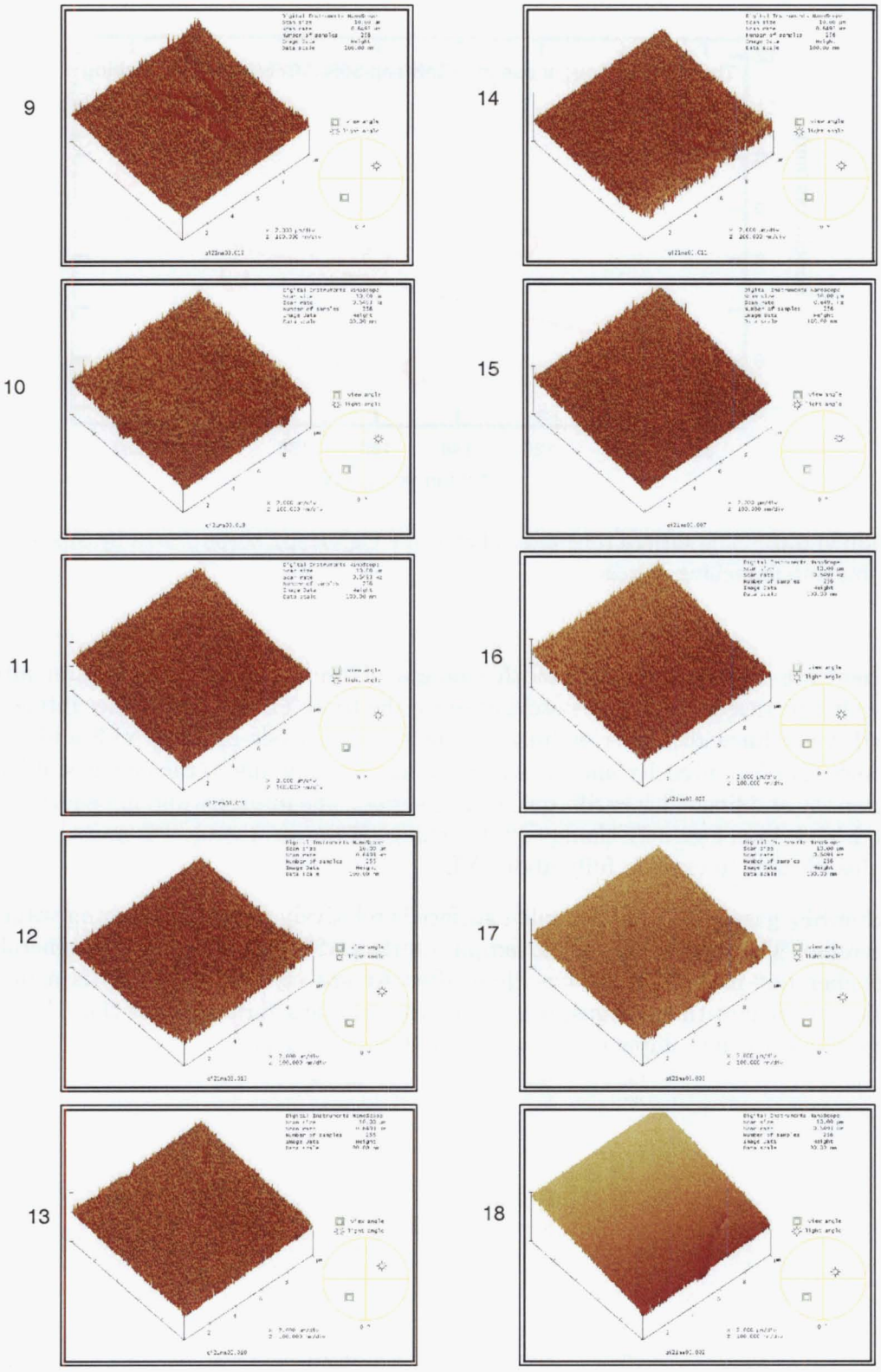

Figure 6.66: AFM images of the surface of etched c-GaN/sap/ 30803 / 9-18 by SF_6 gas.

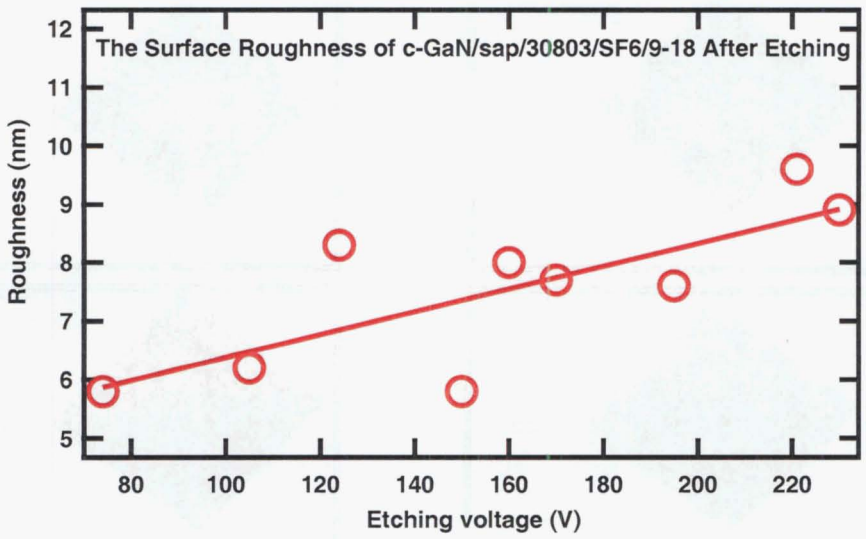

Figure 6.67: The surface roughness of etched c-GaN/sap/ 30803 / 9-18 by SF_6 gas as a function of etching voltage.

There are intensity and linewidth changes of the total of YL spectrum after etching processes, in SF_6 gas etching series the total YL also has higher intensity and wider linewidth after etching. Results and analysis of YL1, YL2 and YL3 shows that YL intensity and linewidth changes mainly due to the changes of YL2 intensity and linewidth in SF_6 gas etching series. The intensity and linewidth YL1 and YL3 do not greatly change after etching. However, merely PL measurement is insufficient to explain fully about YL.

After SF_6 gas etching, the sample's surface is relatively rougher as etching voltage increase. The morphology of the sample's surface after SF_6 gas etching is generally rougher but more homogenous than after Ar gas etching. SF_6 gas is a more efficient etchant than Ar gas, it can etch the sample's surface faster than Ar gas, and can etch the sample chemically as well as physically.

Chapter 7

Effects of Annealing on Optical Properties of GaN

7.1 Introduction

As grown GaN is typically n-type conductive and p-type doping levels are still limited. Amano *et al* [4] showed that p-type conductivity for GaN grown by metal organic chemical vapour deposition (MOCVD) and doped with Mg can be achieved by activating the Mg acceptors using low energy electron beam irradiation (LEEBI). Nakamura *et al* [54] demonstrated that the activation of Mg acceptors can also be achieved by thermal annealing, and that this process can be reversed by annealing in hydrogen ambient. It reveals that thermal annealing and annealing in hydrogen ambient have important effects in GaN.

In this study, we observe the effects of thermal annealing, annealing in hydrogen and nitrogen ambient on the optical properties of Ar-etched and SF_6-etched GaN samples. The analysis of the optical changes due to the annealing process have been determined from the PL results of peak relative intensity, peakshift and linewidth (FWHM) changes of the NBE emission line and the YL lines. The relative intensity was determined as the ratio of the intensity after and before annealing. The relative peakshift was determined as the shift of line position after annealing relative to the line position before annealing. The relative linewidth change was determined as the change in linewidth after annealing relative to the linewidth before annealing.

All samples for these annealing experiments are originally from c-GaN/ sap/ 30803/ AL31-38 for the Ar-etched samples, and c-GaN/ sap/ 30803/ 9-18 for the SF_6-etched samples. They are n-type, Si-doped GaN samples grown by molecular beam epitaxy (MBE).

7.2 Previous Works on Annealing of GaN

- Neugebauer *et al* [64] supports the potential use of hydrogen as a means of improving the doping in wide band gap semiconductors. The following are necessary conditions to use hydrogen passivation as a tool to enhance

doping:

- Hydrogen must be the dominant compensating defect (i.e., its formation energy must be lower than that of all native defects and comparable to the formation energy of the dopant impurity).
- The activation barriers to dissociate the hydrogen impurity complex and to remove or neutralize hydrogen must be lower than the activation energies for native-defect formation or the diffusion barrier of the impurity,
- The dissociated hydrogen atom must be highly diffusive.

These conditions are not particular for GaN but apply to any semiconductor.

- Eunsoon Oh *et al* [67] stated that some of the changes in the PL spectra of GaN upon annealing were associated with the properties of the surface layer, e.g: a new low temperature PL line associated with Donor Acceptor Pair (DAP) recombination appeared at around 3.40 eV upon annealing, but disappeared after etching off the surface layer. This indicates that the acceptors responsible for the DAP emission were created only near the surface.
  After the Rapid Thermal Annealing (RTA) process, the near band edge (NBE) emission was blueshifted and the relative intensity of yellow luminescence (YL) with respect to the NBE emission was increased which were also attributed to the influence of the surface layer.

- Li *et al* [38] investigated the RTA effect on the strain relaxation caused by the lattice and thermal expansion misfit between the GaN epilayer and the substrate. They showed that PL peak exhibited a blueshift in its energy position and a decrease in the full width at half maximum after annealing, indicating an improvement in the optical quality of the film. A green luminescence appeared after annealing and increased in intensity with increasing annealing time. This effect was attributed to hydrogen concentration variation in the GaN film, which was measured by nuclear reaction analysis (NRA). A high hydrogen concentration exist in as grown GaN, which can neutralize the deep level, and the hydrogen bonded complex dissociates during RTA. This leads to the appearance of a luminescence peak in the PL spectrum.

- Litwin *et al* [39] studied the annealing effects on two types of GaN samples: (i) lower resistivity samples ($\rho < 10^4\Omega$ cm at ambient temperature) with dominant E_A states or Mg-related state at about 0.15 eV and (ii) very high resistivity samples ($\rho > 10^6\Omega$ cm at ambient temperature) with dominant E_2 states or deeper states at about 0.95 eV, above the valence band. For the first type of samples, annealing at T < 500 °C leads to a decrease of their resistivity and is associated with an increase of the effective concentration

of the shallow Mg acceptors. Annealing of both types of samples at temperature between 600 °C and 750 °C leads to an increase of the deep state concentration. An increase of the sample resistivity and an appearance of a local vibrational mode of hydrogen at 3125 cm^{-1} were observed in the low-resistivity samples after annealing in hydrogen ambient. These effects can be removed by annealing in hydrogen free ambient.

- Annealing or RTA at temperatures as high as 700 °C-800 °C is usually applied to the Mg acceptor activation of the MOCVD grown GaN samples [54].

- Hydrogen is found to readily diffuse into the binary and ternary nitrides at temperatures in the range 85-250 °C. These are typical process temperatures for fabrication steps such as wet and dry etching, dielectric deposition, sintering of contacts, boiling in solvent and baking of resists. The hydrogen forms electrically neutral complexes with dopants, defects, and impurities in the epitaxial nitride films. Reactivation occurs at 450-550 °C, and the hydrogen is removed at temperatures $\geq$ 800 °C [69].

- Brandt *et al* [9] investigated the hydrogenation of p-type GaN. They stated that by introducing hydrogen into MBE-grown p-type GaN, the hole concentration can be substantially reduced, which suggests the formation of Mg-H complexes. Also they strongly stated that the electrical properties of n-type samples does not change up to 600 °C hydrogenation. A new PL line at 3.35 eV appears after hydrogenation in both p- and n-type samples. The PL indicates that hydrogen might have a donor level in GaN.

Prior work has been done mostly on Mg-doped GaN grown by MOCVD, where annealing in hydrogen ambient or thermal annealing and its effects on electronics properties of GaN samples were studied. There are only a few works on thermal annealing, hydrogen annealing and nitrogen annealing effects on optical properties of GaN [9, 28, 72].

7.3 Annealing in Vacuum and Hydrogen Ambient

7.3.1 Ar-etched Samples

Sample	AL32	AL34	AL38
Etching voltage (V)	328	360	526

Table 7.1: Ar-etched GaN samples of annealing in vacuum then hydrogen ambient.

Annealing at 700 °C in vacuum for eight hours then in hydrogen ambient for another eight hours have been done to three Ar-etched GaN samples. Those three samples with their etching voltages are listed in Table 7.1. In this series of

experiments, sample AL33 was kept as the original standard or reference sample. It was not etched or annealed. The standard sample was used to standarize and determine the relative intensity, peakshift and linewidth change between PL results of the samples taken at different time.

Figures 7.1 and 7.2 show the PL results of NBE emission line and YL line of samples AL32, AL34 and AL38 after annealing in vacuum for eight hours, then hydrogen ambient for another eight hours. All the PL measurements were taken at the temperature of 4 K.

Before annealing, the Ar-etched GaN samples show two NBE emission lines, which are peaking at 3.486 eV (BE1) and 3.493 eV (BE2), and two YL lines, which are peaking at about 2.53 eV (YL1) and 2.22 eV (YL2).

Analysis and Discussion of the PL Results

Figure 7.3 shows the relative intensity of the NBE peaks after annealing in vacuum as a function of etching voltage. Before annealing, the PL intensity of BE1 is about 2 or 2.5 times weaker than the intensity of BE2. After annealing, the intensity of BE1 is about 10 times weaker than the intensity of BE2.

Annealing lowered the PL intensity of BE1 down to about 4 to 10 times weaker than before annealing. The relative intensity of BE1 after annealing slightly increases as the etching voltage increases.

At the etching voltage of 328 V, the relative intensity of BE2 after annealing is 0.6 times of the intensity before annealing, then increases to about 0.8 times at the etching voltage of 360 V, and keep increasing to about 1.2 times at the etching voltage of 526 V.

Figure 7.4 shows the relative linewidth changes of BE1 and BE2 lines after annealing in vacuum as a function of etching voltage.

The linewidth of the BE1 line after annealing in vacuum is 7 to 10 meV narrower than before annealing, and a typical linewidth of BE1 line is about 20 meV. The BE1 linewidth is slightly wider at the etching voltage of 526 V than at the etching voltage of 328 V and 360 V.

After annealing in vacuum, the linewidth of the BE2 line is about 3 or 4 meV wider than before annealing. As the etching voltage increases from 328 V to 526 V, the linewidth change of the BE2 line after annealing increases from about 3 to 4 meV. A typical linewidth of Ar-etched GaN BE2 line is about 9 meV.

Figure 7.5 shows the changes of line position (peakshift) of the BE1 and BE2 peaks after annealing in vacuum as a function of etching voltage.

After annealing in vacuum the BE2 line position was not shifted largely. From the etching voltage of 328 V to 360 V, the BE2 peak position was constantly at 3.493 eV, and was not shifted after annealing. At the etching voltage of 526 V,

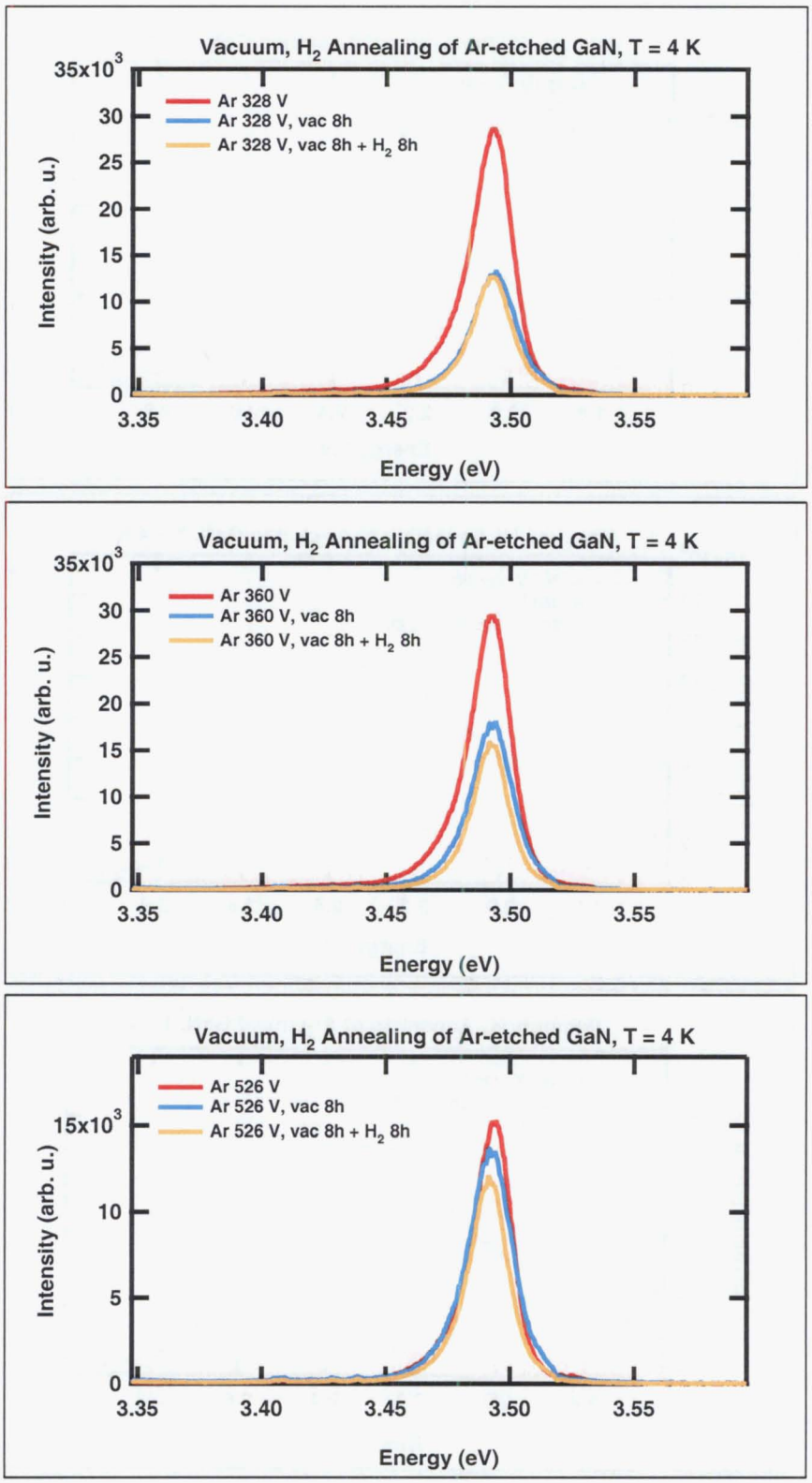

Figure 7.1: PL results of Ar-etched GaN NBE line before and after vacuum then hydrogen annealing.

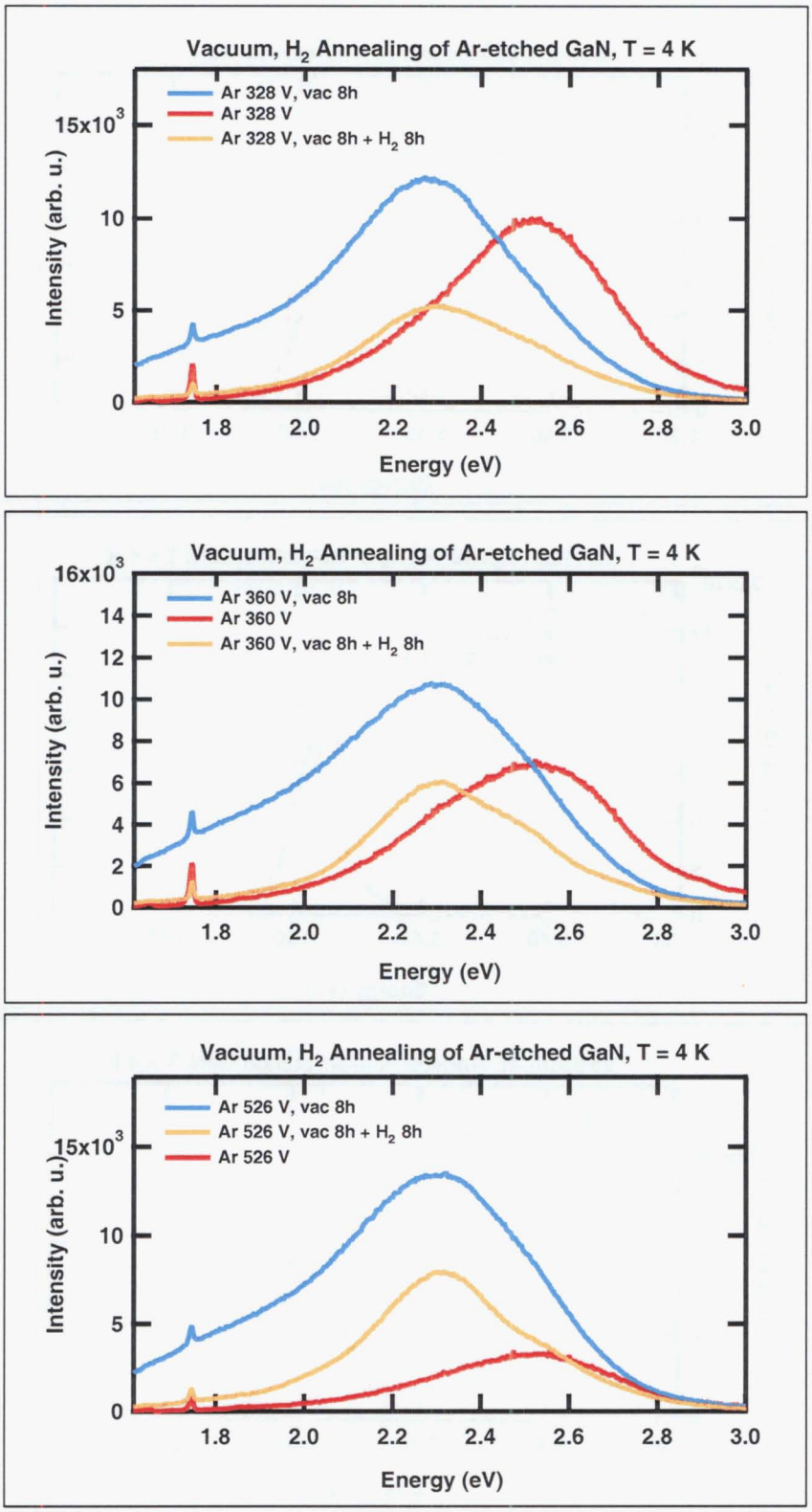

Figure 7.2: PL results of Ar-etched GaN YL line before and after vacuum then hydrogen annealing.

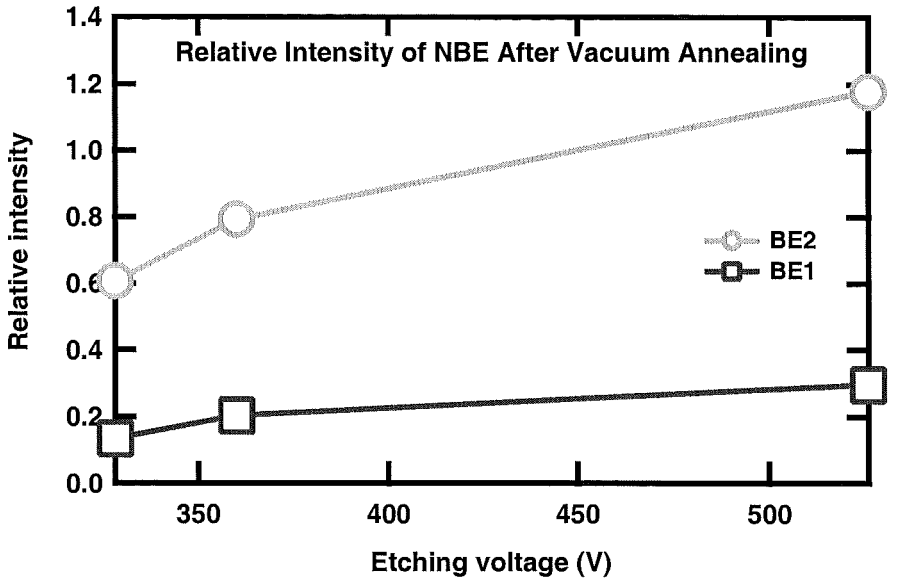

Figure 7.3: The relative intensity of Ar-etched GaN NBE (BE1 = 3.486 eV, BE2 = 3.493 eV) lines after annealing in vacuum as a function of etching voltage.

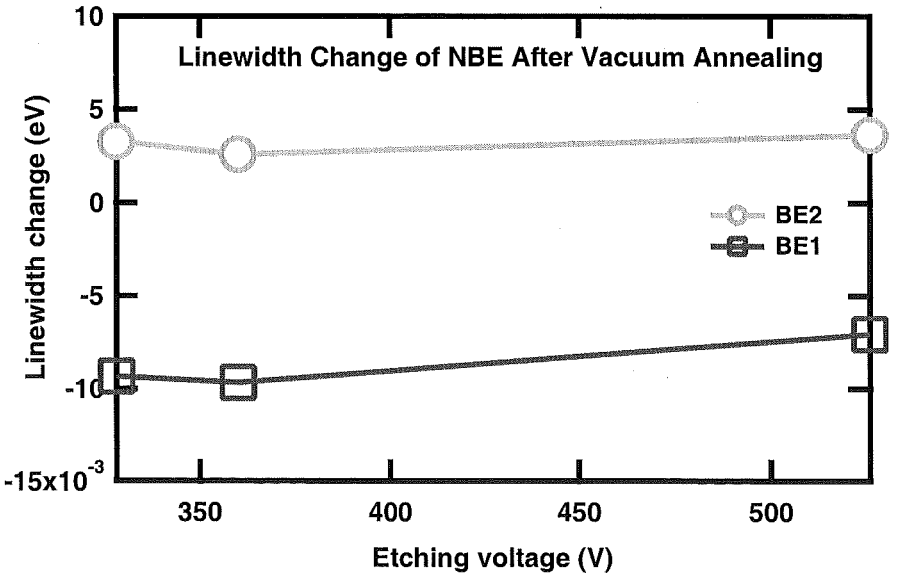

Figure 7.4: The linewidth change of Ar-etched GaN NBE (BE1 = 3.486 eV, BE2 = 3.493 eV) lines after annealing in vacuum as a function of etching voltage.

the BE2 peak position was redshifted about 2 meV after annealing, this value is comparable to the error. A typical error value of peakshift is about 1 meV.

The BE1 peak position was redshifted or shifted to the lower energy position after annealing. From the etching voltage of 328 V to 360 V, the BE1 peak position was redshifted about 14 meV after annealing. And as the etching voltage increases, the BE1 peak position after annealing experienced more redshift to about 17 meV at the etching voltage of 526 V.

The PL results of YL after annealing show that the YL1 line at 2.53 eV has disappeared, the YL2 line at 2.22 eV increases in its intensity and has a wider linewidth, the YL3 line at 1.81 eV appears after vacuum annealing.

Figure 7.6 shows the intensity ratio of the YL2 line after and before annealing in vacuum as a function of etching voltage. At the etching voltage of 328 V and 360 V the relative intensity of YL2 after annealing is about 7 and 5 times higher than before annealing. As the etching voltage increases from 360 V to 526 V, the relative intensity of YL2 after annealing increases steeply to about 24 times higher than the intensity before annealing.

Figure 7.7 shows the linewidth change of the YL2 line after annealing in vacuum as a function of etching voltage. The linewidth of the YL2 line after annealing is wider than before annealing. At the etching voltage of 328 V the YL2 line after annealing is 112 meV wider than before annealing. As the etching voltage increases, the linewidth change of the YL2 line after annealing decrease steeply

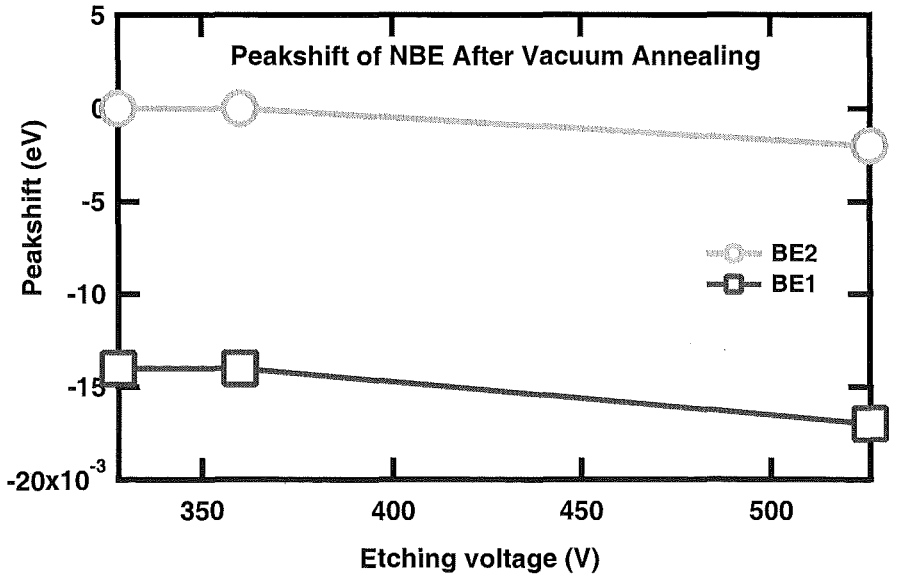

Figure 7.5: The peakshift of Ar-etched GaN NBE (BE1 = 3.486 eV, BE2 = 3.493 eV) lines after annealing in vacuum as a function of etching voltage.

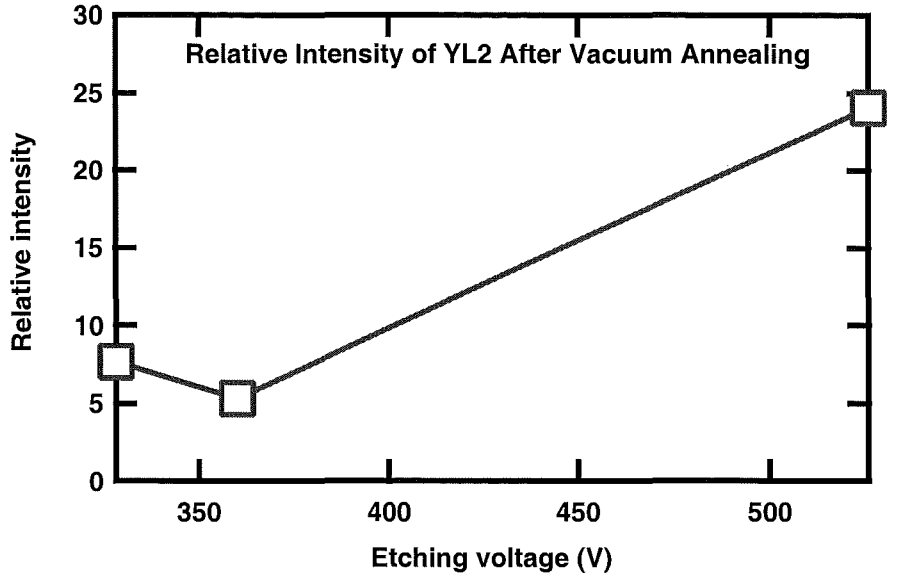

Figure 7.6: The relative intensity of Ar-etched GaN YL2 = 2.22 eV line after annealing in vacuum as a function of etching voltage.

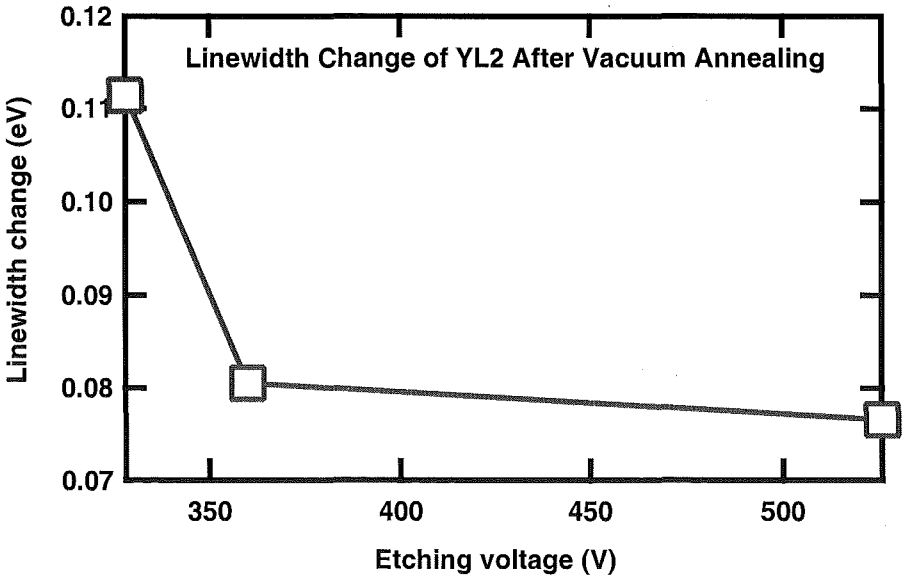

Figure 7.7: The linewidth change of Ar-etched GaN YL2 = 2.22 eV line after annealing in vacuum as a function of etching voltage.

to about 80 meV wider at the etching voltage of 360 V and 77 meV wider at the etching voltage of 526 V. A typical PL linewidth of the YL2 line is about 230 meV after Ar etching and 310 meV after vacuum annealing.

Figure 7.8 shows the YL2 line peakshift after annealing in vacuum as a function of etching voltage. The YL2 line experienced a blueshift after vacuum annealing. At the etching voltage of 328 V, 360 V and 526 V, the YL2 peak position was blueshifted about 100 meV, 50 meV and 110 meV, respectively. The YL2 line peakshift after vacuum annealing only weakly depends on the etching voltage.

Figure 7.9 shows the intensity ratio of the NBE lines after and before annealing in hydrogen ambient as a function of etching voltage. The PL intensity of BE2 is about 10 times higher than the intensity of BE1 after annealing in hydrogen ambient.

The intensity ratio of the BE1 and BE2 lines after annealing are slightly lower than before annealing and only weakly depend on the etching voltage. For the BE1 line, at the etching voltage of 328 V, 360 V and 526 V, the intensity after annealing is about 0.97, 0.90 and 0.95 times the intensity before annealing. For the BE2 line, the intensity after annealing is about 0.97, 0.88 and 0.87 times the intensity before annealing at the etching voltage of 328 V, 360 V and 526 V, respectively.

Figure 7.10 shows the linewidth changes of the BE1 and BE2 lines after annealing in hydrogen ambient as a function of etching voltage. Both BE1 and BE2 lines

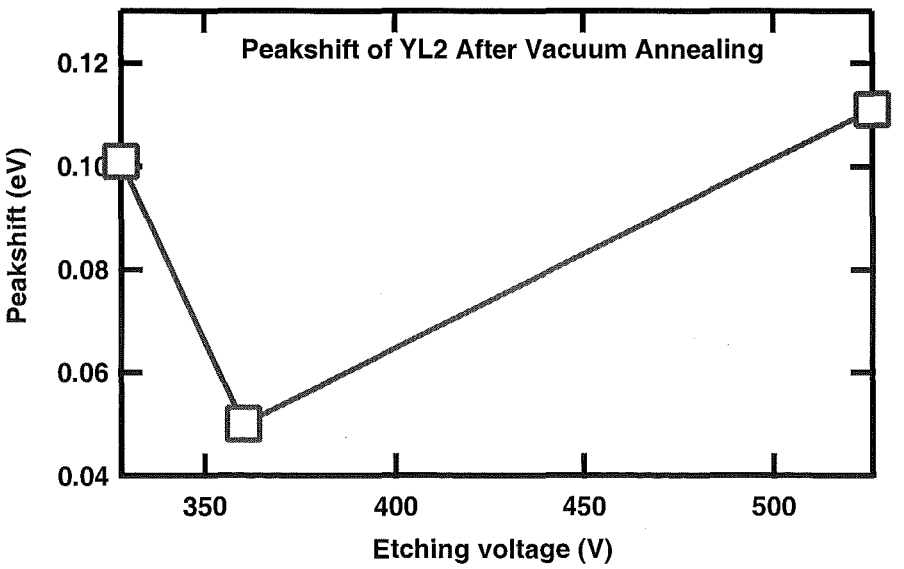

Figure 7.8: The peakshift of Ar-etched GaN YL2 = 2.22 eV line after annealing in vacuum as a function of etching voltage.

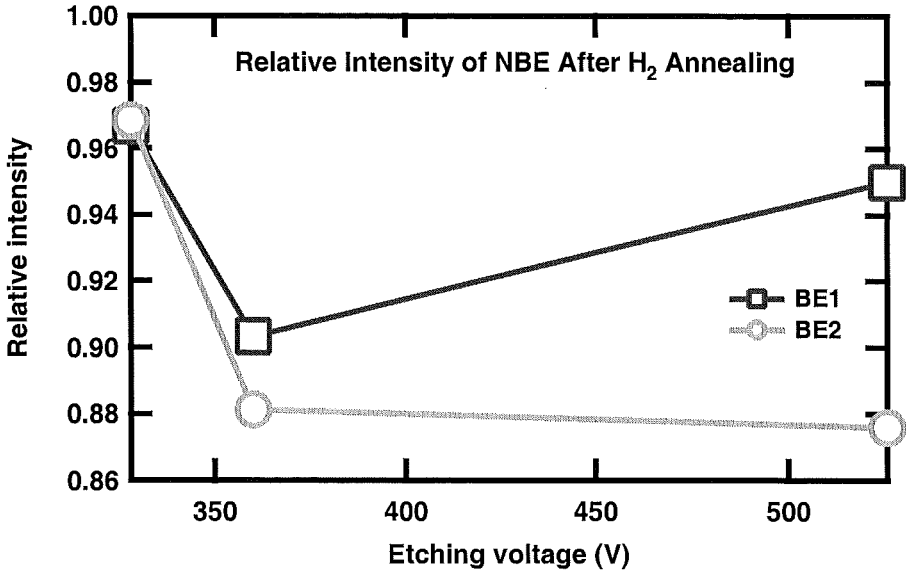

Figure 7.9: The relative intensity of Ar-etched GaN NBE (BE1 = 3.486 eV, BE2 = 3.493 eV) lines after annealing in hydrogen ambient as a function of etching voltage.

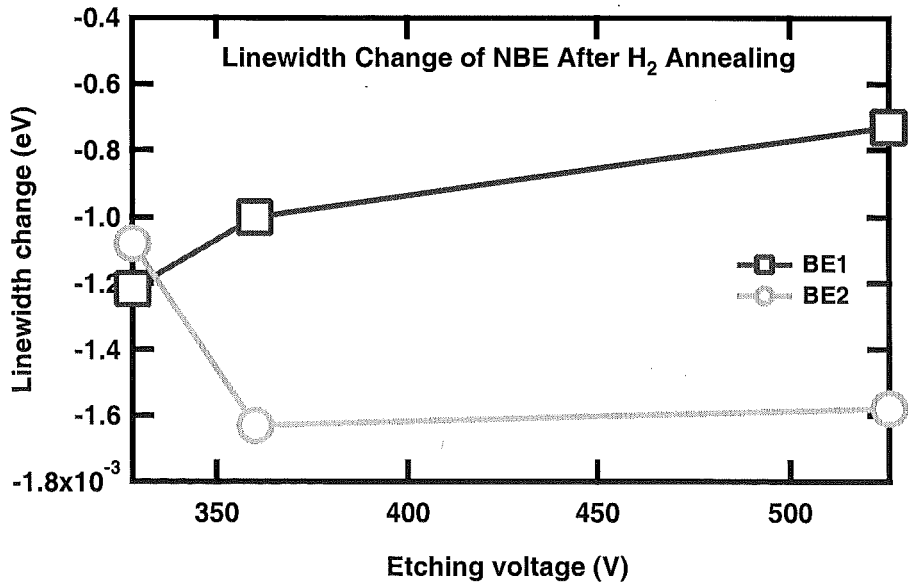

Figure 7.10: The linewidth change of Ar-etched GaN NBE (BE1 = 3.486 eV, BE2 = 3.493 eV) lines after annealing in hydrogen ambient as a function of etching voltage.

have a narrower linewidth after annealing, it is indicated by negative value of linewidth change.

The linewidth change of BE1 line after annealing at the etching voltage of 328 V is 1.2 meV narrower than before annealing, then as the etching voltage increases to 360 V and 526 V, the linewidth after annealing becomes wider, about 1.0 meV and 0.8 meV narrower than before annealing, respectively. In Ar-etched GaN, a typical linewidth of BE1 line is about 20 meV.

At the etching voltage of 328 V, the linewidth of BE2 line after annealing is 1.1 meV narrower than before annealing. The linewidth change of BE2 line decreases steeply to about 1.6 meV narrower than before annealing at the etching voltage of 360 V. At the higher etching voltage than 360 V, the linewidth change is almost constant at about 1.6 meV narrower than before annealing until the etching voltage of 526 V. In Ar-etched GaN, a typical linewidth of BE2 line is about 9 meV.

Figure 7.11 shows the peakshift or changes of line position of the NBE lines after annealing in hydrogen ambient as a function of etching voltage.

After annealing in hydrogen ambient the BE1 line experienced a blueshift. At the etching voltage of 328 V, the BE1 line was not shifted after annealing. As the etching voltage increases to 360 V, the BE1 line was shifted to about 2 meV, at a higher energy position than before annealing, then at the etching voltage higher than 360 V the BE1 line is blueshifted constantly about 2 meV until the etching

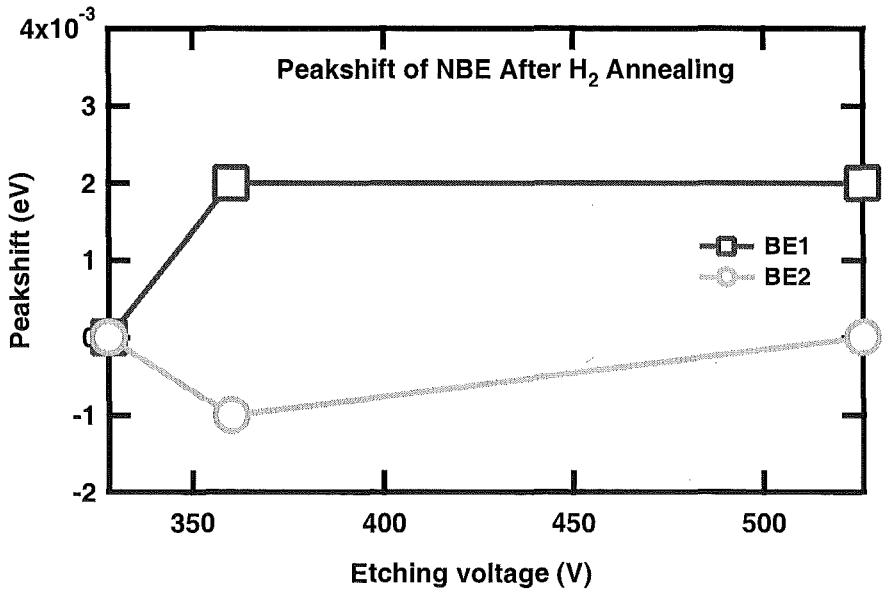

Figure 7.11: The peakshift of Ar-etched GaN NBE (BE1 = 3.486 eV, BE2 = 3.493 eV) lines after annealing in hydrogen ambient as a function of etching voltage.

voltage of 526 V.

The BE2 line did not experience peakshift at the etching voltage of 328 V and 526 V, and only 1 meV redshifted at the etching voltage of 360 meV. A typical error of peakshift is about 1 meV.

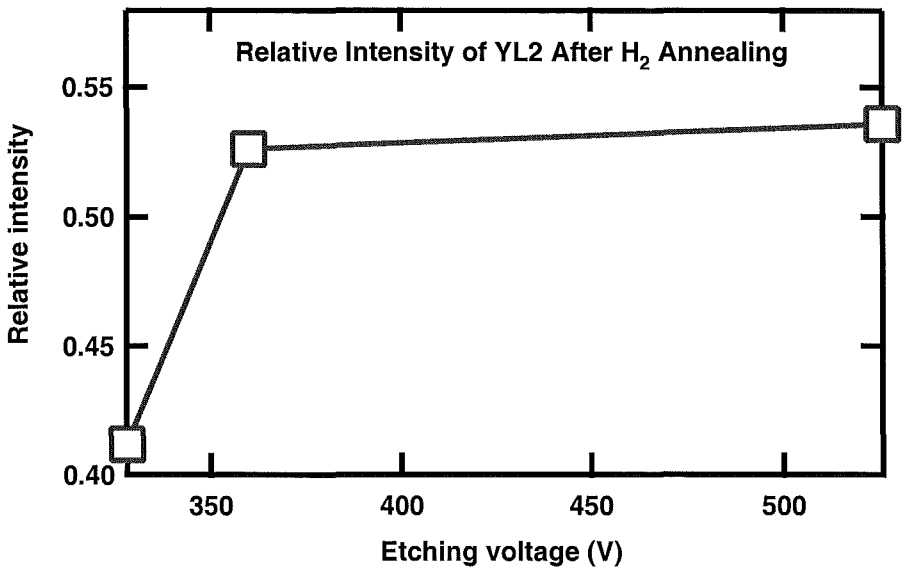

Figure 7.12: The relative intensity of Ar-etched GaN YL2 = 2.22 eV line after annealing in hydrogen ambient as a function of etching voltage.

After annealing in hydrogen ambient, the PL results of YL show that the YL1 line at 2.60 eV has reappeared, the YL2 line at 2.22 eV has lower intensity and wider linewidth than before hydrogen annealing, and the YL3 line at 1.81 eV has disappeared.

Figure 7.12 shows the relative intensity of the YL2 line after annealing in hydrogen ambient as a function of etching voltage. The relative intensity of YL2 line after annealing is lower than before annealing. At the etching voltage of 328 V, the intensity of YL2 line after annealing is about 0.41 times the intensity before annealing. As the etching voltage increases to 360 V, the relative intensity on the YL2 after annealing increases steeply to about 0.52 times the intensity before annealing. At the etching voltage higher than 360 V, the relative intensity of YL2 after annealing increases slightly to about 0.54 times the intensity before annealing at the etching voltage of 526 V.

Figure 7.13 shows the linewidth change of the YL2 line after annealing in hydrogen ambient as a function of etching voltage. Annealing in hydrogen ambient results in narrower linewidth of YL2 line, it is indicated by the negative value of linewidth change. At the etching voltage of 328 V, the YL2 linewidth after annealing

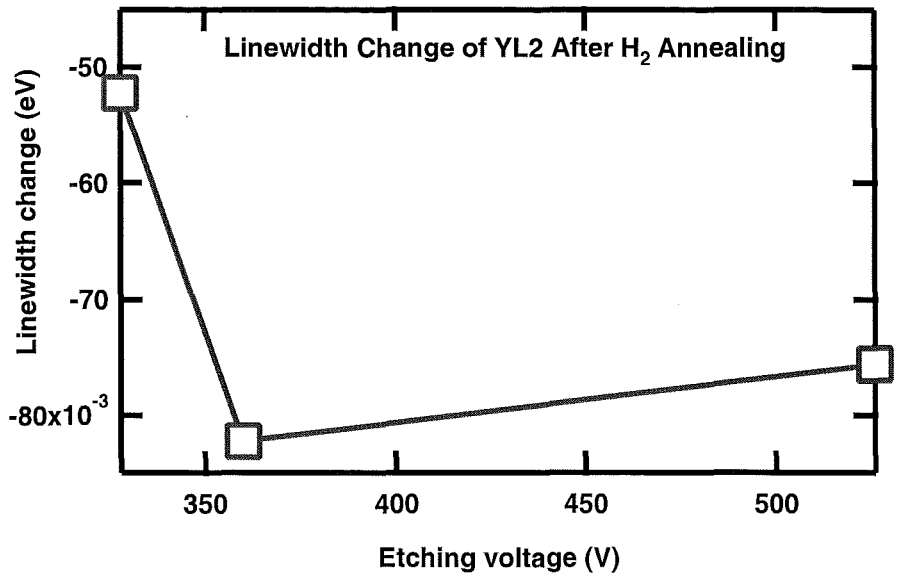

Figure 7.13: The linewidth change of Ar-etched GaN YL2 = 2.22 eV line after annealing in hydrogen ambient as a function of etching voltage.

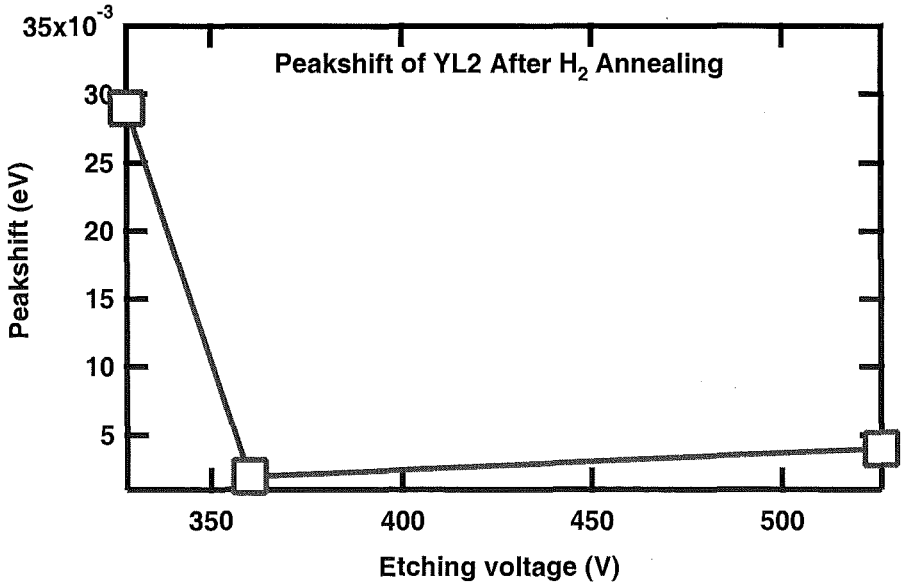

Figure 7.14: The peakshift of Ar-etched GaN YL2 = 2.22 eV line after annealing in hydrogen ambient as a function of etching voltage.

is about 52 meV narrower than before annealing. The linewidth of YL2 after annealing was narrowed, to about 82 meV narrower than before annealing, at the etching voltage of 360 V, then it was 6 meV widened, to about 76 meV narrower than before annealing, as the etching voltage increases to 526 V. The typical PL linewidth of YL2 line of Ar-etched GaN is about 230 meV

Figure 7.14 shows the peakshift of the YL2 peak after annealing in hydrogen ambient as a function of etching voltage. Annealing in hydrogen ambient results in blueshift of the YL2 line. At the etching voltage of 328 V, the YL2 line was about 29 meV blueshifted. As the etching voltage increases to 360 V, the blueshift of YL2 line after annealing decreases to about 2 meV, then at the etching voltage higher than 360 V, the YL2 line blueshift slightly increases to about 4 meV at the etching voltage of 526 V.

Conclusion of Ar-etched GaN Annealing in Vacuum and Hydrogen Ambient

Annealing in vacuum for 8 hours at the temperature of 700 °C then hydrogen ambient for another 8 hours at the same temperature has been done to three Ar-etched GaN samples. The PL results before annealing show two NBE emission lines at 3.486 eV (BE1) and 3.493 eV (BE2), two YL lines at 2.53 eV (YL1) and 2.22 eV (YL2) from these samples.

The intensity of BE1 line is lower than BE2 line. Before annealing, the intensity of the BE1 line is about 2 to 2.5 times lower than the BE2 line. After annealing in vacuum and hydrogen ambient, the intensity of the BE1 line is about 10 times lower than the BE2 line. A typical linewidth of the BE1 and BE2 lines are about 20 meV and 9 meV.

Vacuum annealing results in the disappearance of the YL1 line at 2.53 eV and the appearance of the YL3 line at 1.81 eV. After hydrogen annealing, the YL1 line appears back at 2.60 eV and the YL3 line at 1.81 eV disappears again. A typical linewidth of the YL2 line is about 310 meV after vacuum annealing and 230 meV after hydrogen annealing.

The results summary of the Ar-etched GaN vacuum and hydrogen annealing are showed in Table 7.2 and 7.3.

7.3.2 SF_6-etched Samples

Annealing at 700 °C in hydrogen ambient for eight hours has been done to four SF_6-etched GaN samples. The samples with their etching voltages are listed in Table 7.4. Sample 13 is an as-grown sample and was kept as the original standard sample. It was not etched or annealed.

Figures 7.15,7.16 and 7.17,7.18 show the PL results of the NBE emission and YL lines of samples 9, 11, 15, 17 after annealing in hydrogen ambient, respectively.

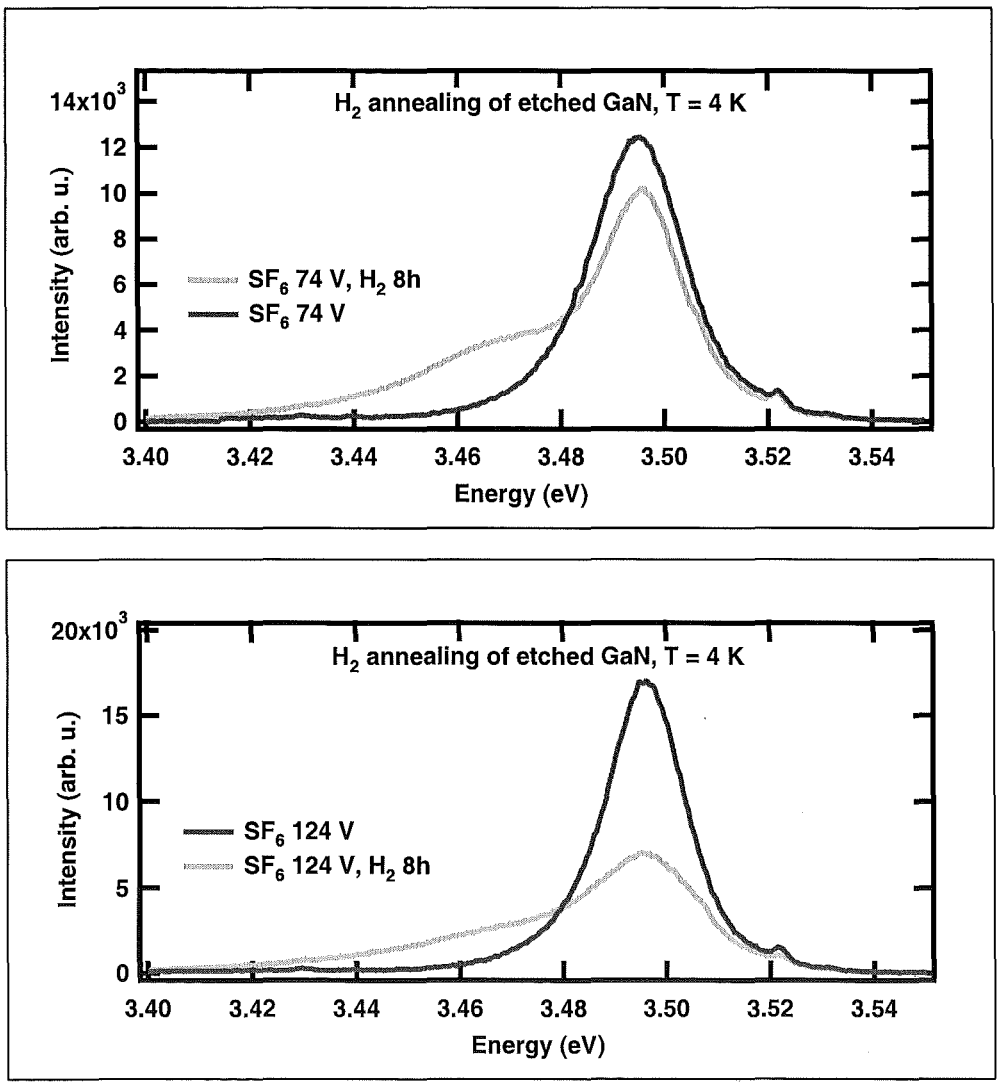

Figure 7.15: PL results of SF_6-etched GaN near band edge line before and after annealing in hydrogen ambient.

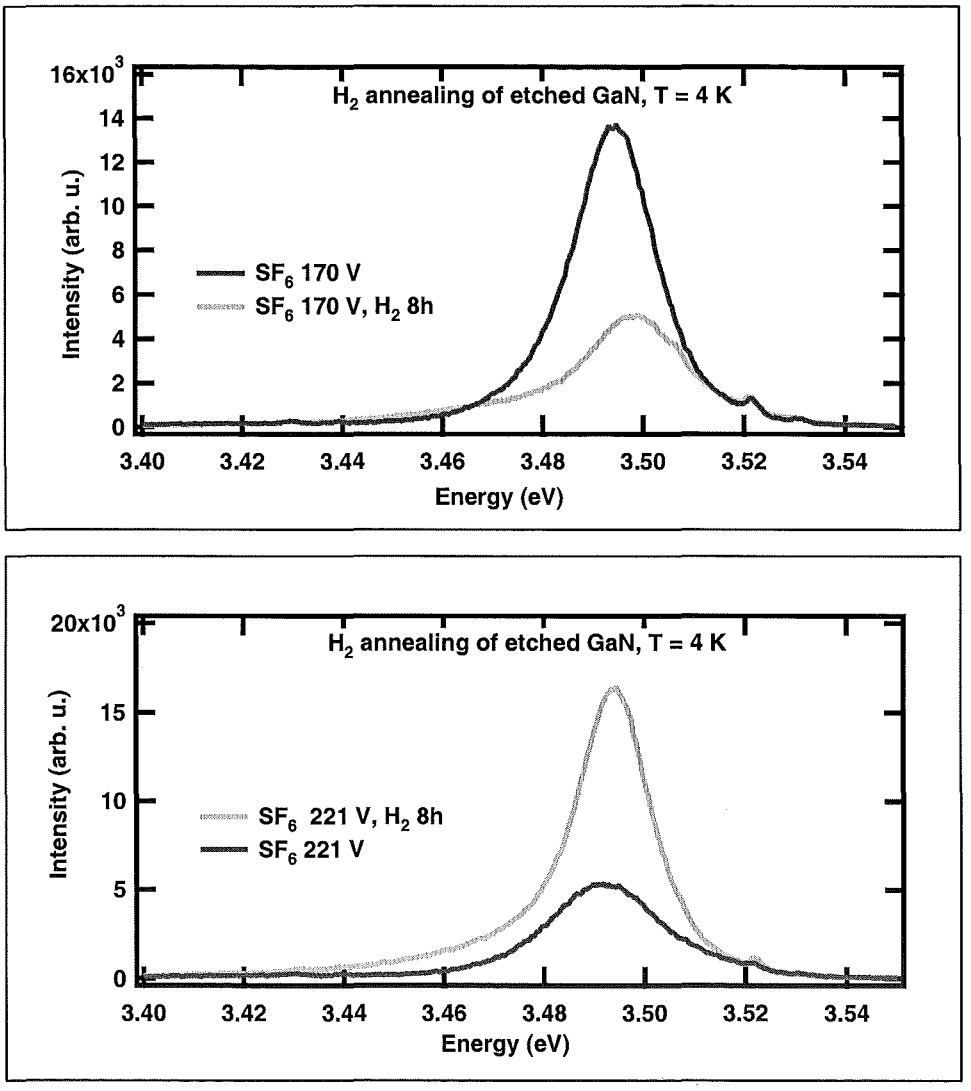

Figure 7.16: PL results of SF_6-etched GaN near band edge line before and after annealing in hydrogen ambient.

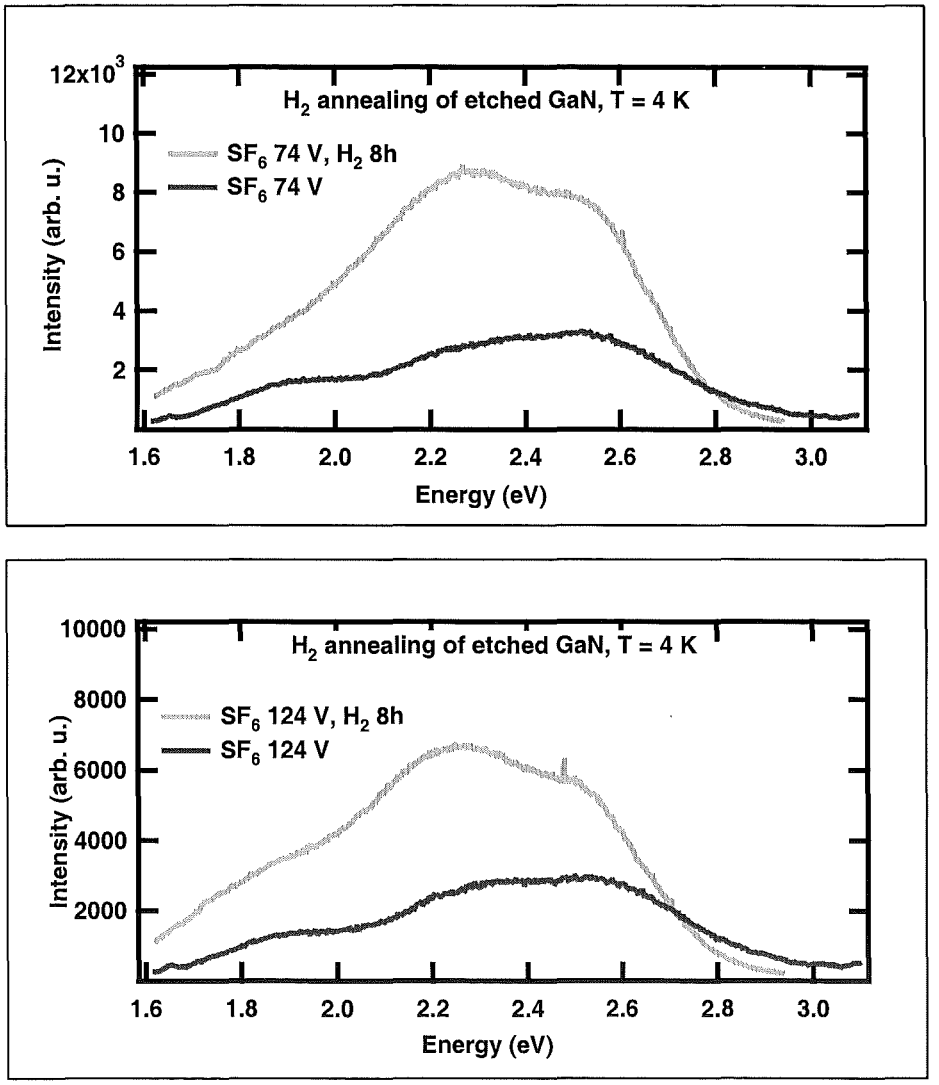

Figure 7.17: PL results of SF_6-etched GaN YL line before and after annealing in hydrogen ambient.

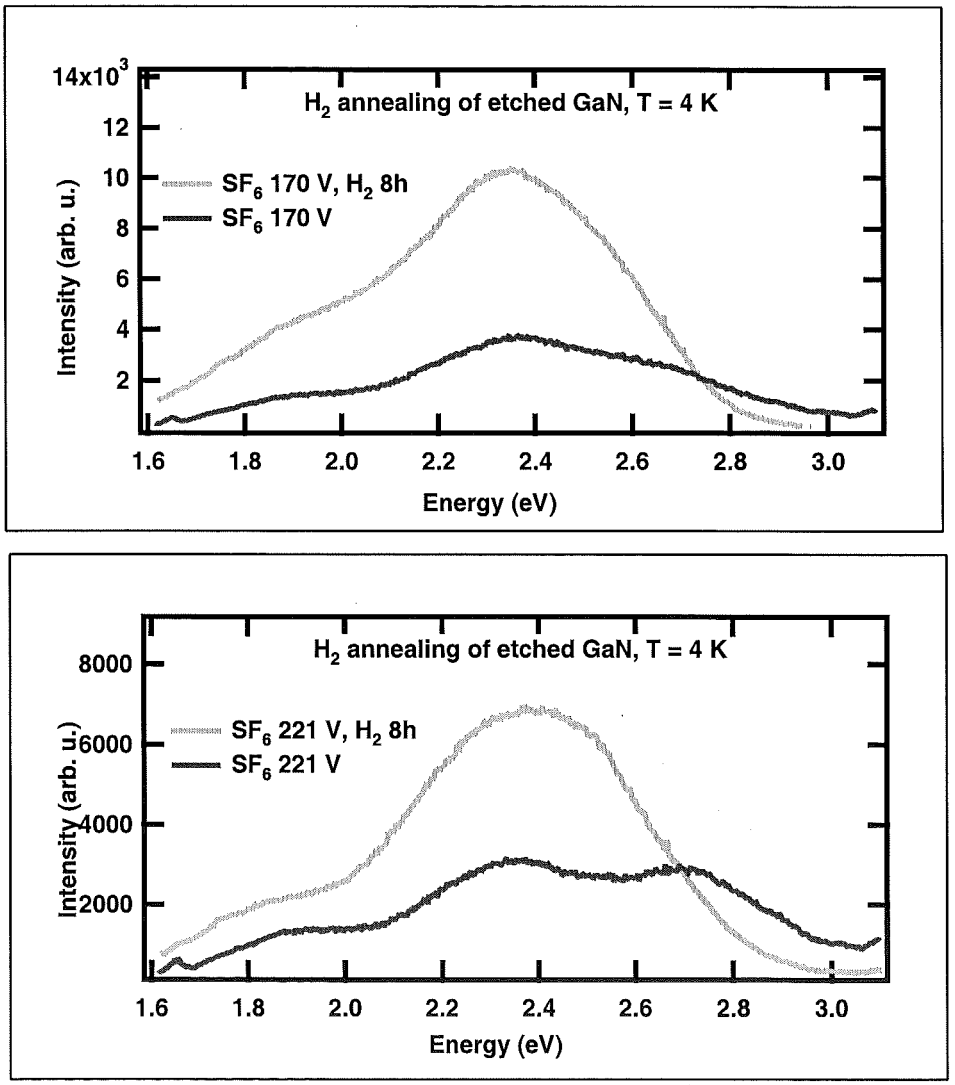

Figure 7.18: PL results of SF_6-etched GaN YL line before and after annealing in hydrogen ambient.

BE1 line	**After vacuum annealing**
Intensity	4 to 10 times lower than before annealing slightly increases as the etching voltage increase
Peakshift	14 to 17 meV redshifted increasing the etching voltage increases the redshift
Linewidth	7 to 10 meV narrower than before annealing slightly wider as the etching voltage increases
BE2 line	**After vacuum annealing**
Intensity	0.6, 0.8 and 1.2 times of the intensity before annealing at the etching voltages of 328 V, 360 V and 526 V
Peakshift	does not shift largely
Linewidth	3 to 4 meV wider than before annealing slightly wider as the etching voltage increases
YL2 line	**After vacuum annealing**
Intensity	5 to 7 times higher than before annealing increases as the etching voltage increase
Peakshift	50 to 100 meV blueshifted weakly depends on the etching voltage
Linewidth	112 meV wider than before annealing narrower as the etching voltage increases

Table 7.2: The result summary of Ar-etched GaN samples annealing in vacuum.

The PL measurements were taken at temperature 4 K.

The PL results, see figures 7.15 and 7.16, show that NBE emission line consists of two lines at 3.473 eV(BE1) and 3.495 eV (BE2). The prior work of the University of Canterbury show a similar PL results of the NBE emission line after SF_6 etching without annealing, and it was determined that the lower energy line is an acceptor related emission line (A^0X) and the higher energy line is a donor related emission line (D^0X) [15, 16, 17, 12, 11].

The YL line of the SF_6-etched GaN has three emission lines at 2.60 eV (YL1), 2.24 eV (YL2), and 1.91 eV (YL3).

Analysis and Discussion of the PL Results

Figure 7.19 shows the relative intensity of the $A^0X = 3.473$ eV and $D^0X = 3.495$ eV lines after annealing in hydrogen ambient as a function of etching voltage.

Annealing in hydrogen ambient results in a relatively much stronger A^0X line. On average, the A^0X line becomes 2 times higher than the intensity before annealing, except for the intensity from the first sample, etched at 74 V, where A^0X is about 4.8 times higher than the intensity before annealing.

Three results out of four show the relative intensity of the D^0X line is about 50%

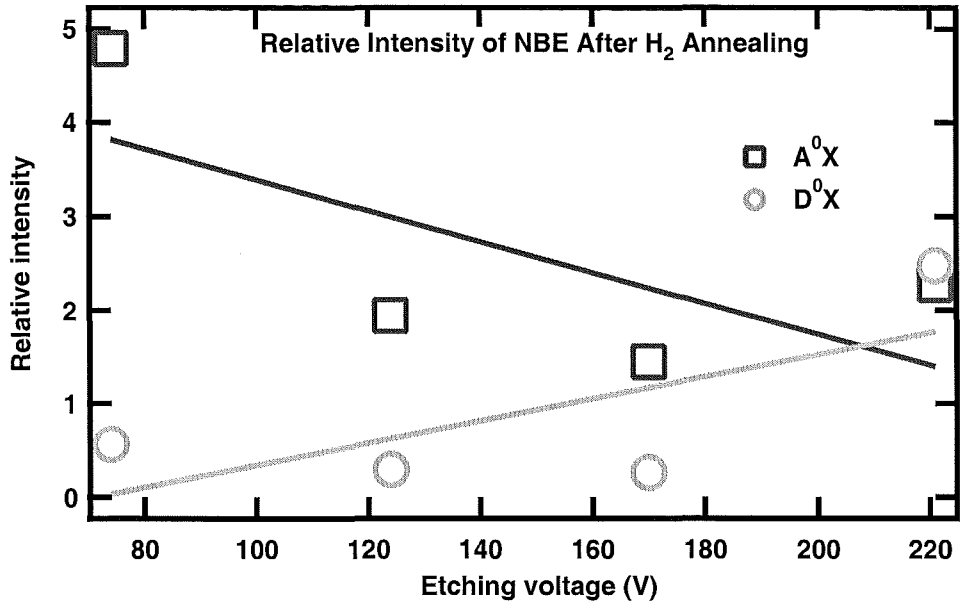

Figure 7.19: The relative intensity of SF_6-etched GaN $D^0X = 3.495$ eV and $A^0X = 3.473$ eV lines after annealing in hydrogen ambient as a function of etching voltage.

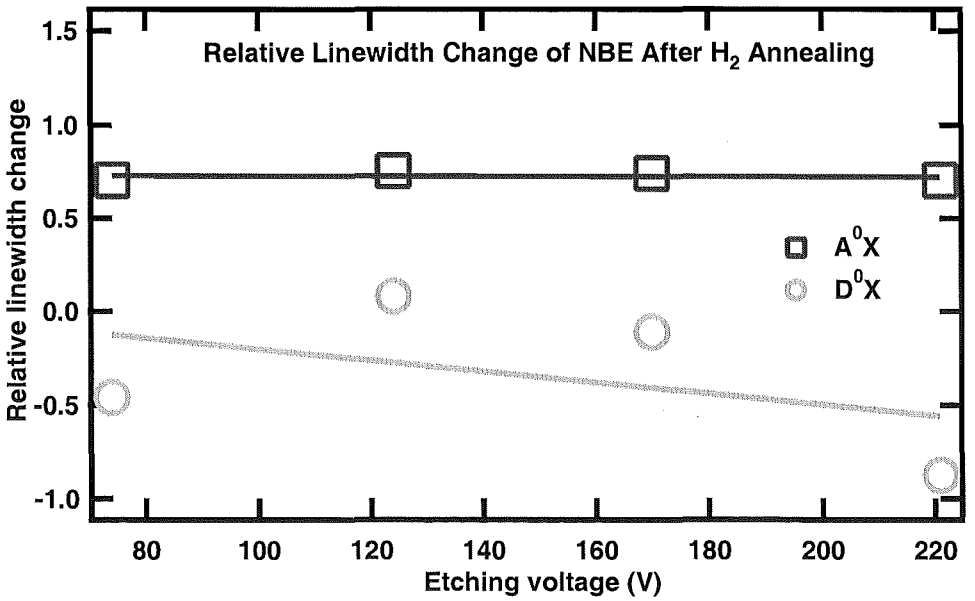

Figure 7.20: The relative linewidth change of SF_6-etched GaN $D^0X = 3.495$ eV and $A^0X = 3.473$ eV lines after annealing in hydrogen ambient as a function of etching voltage.

BE1 line	**After H_2 annealing**
Intensity	0.9 to 0.97 times of the intensity before annealing weakly depends on the etching voltage
Peakshift	0 to 2 meV blueshifted typical peakshift error is 1 meV
Linewidth	0.8 to 1.2 meV narrower than before annealing wider linewidth at higher etching voltage
BE2 line	**After H_2 annealing**
Intensity	0.87 to 0.97 times of the intensity before annealing weakly depends on the etching voltage
Peakshift	0 to 1 meV redshifted typical peakshift error is 1 meV
Linewidth	1.1 to 1.6 meV narrower than before annealing wider linewidth at higher etching voltage
YL2 line	**After H_2 annealing**
Intensity	0.41 to 0.54 times of the intensity before annealing slightly increases as the etching voltage increases
Peakshift	29 meV blueshifted at 328 V 2 to 4 meV blueshifted at 360 V and 526 V
Linewidth	52 to 76 meV narrower than before annealing weakly depends on the etching voltage

Table 7.3: The result summary of Ar-etched GaN samples annealing in hydrogen ambient.

Sample	**9**	**11**	**15**	**17**
Etching voltage (V)	74	124	170	221

Table 7.4: SF_6-etched GaN samples of annealing in hydrogen ambient.

to 70% lower after annealing in hydrogen ambient. Except for the last point, at 221 V etching voltage, the intensity after annealing is about 2.5 times higher than the intensity before annealing.

The relative intensity changes of A^0X line does not correlate to the relative intensity changes of D^0X line after annealing. The relative intensity after annealing of both lines only weakly depend on the etching voltage.

Figure 7.20 shows the relative linewidth changes of A^0X and D^0X lines after annealing in hydrogen ambient as a function of etching voltage.

The linewidth of the A^0X line is about 70% wider after annealing in hydrogen ambient. The relative linewidth changes of A^0X line is constant and does not depend on the etching voltage.

Three results out of four show that the linewidth of D^0X peak after annealing in

hydrogen ambient is about 20% to 70% narrower than before annealing, denoted by negative values of the linewidth changes. And the relative linewidth changes of D^0X line only weakly depend on the etching voltage.

Figure 7.21 shows the relative changes of line position (peakshift) of A^0X and D^0X lines after annealing in hydrogen ambient as a function of etching voltage. For both A^0X and D^0X peaks the position of the peak is slightly blueshifted after annealing in hydrogen ambient.

The relative peakshift of A^0X line is about 0.25% bluer than of the position before annealing at etching voltage 74 V, then increases to 0.8% bluer as the etching voltage increases to 221 V.

The relative peakshift of D^0X line is about 0.12% bluer or less after annealing, this value is comparable to the uncertainty of the line position. The relative line position of D^0X only weakly depend on the etching voltage, showing only a slight increase as the etching voltage increases.

The analysis of YL have been determined from 2.60 eV (YL1), 2.24 eV (YL2), and 1.91 eV (YL3) lines.

Figure 7.22 shows the relative intensity of the YL peaks after annealing in hydrogen ambient as a function of etching voltage. For SF_6-etched samples, almost all the relative intensity of the YL peaks are higher after annealing in hydrogen ambient, it results in the higher total YL relative intensity after annealing.

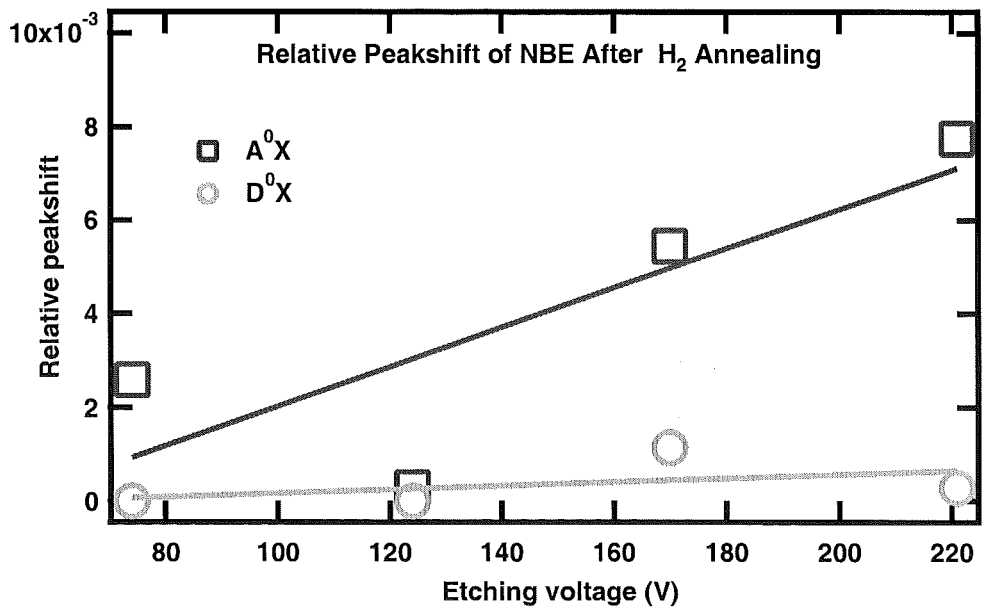

Figure 7.21: The reltive peakshift of SF_6-etched GaN D^0X = 3.495 eV and A^0X = 3.473 eV lines after annealing in hydrogen ambient as a function of etching voltage.

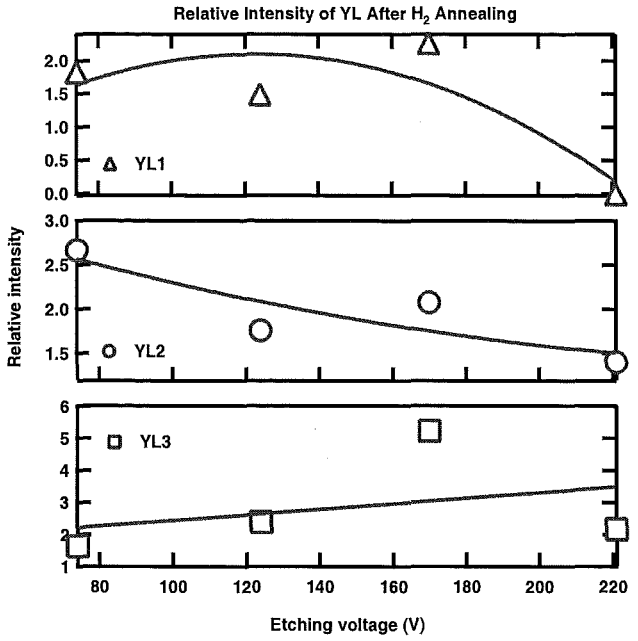

Figure 7.22: The relative intensity of SF_6-etched GaN YL (YL1 = 2.60 eV, YL2 = 2.24 eV, YL3 = 1.91 eV) lines after annealing in hydrogen ambient as a function of etching voltage.

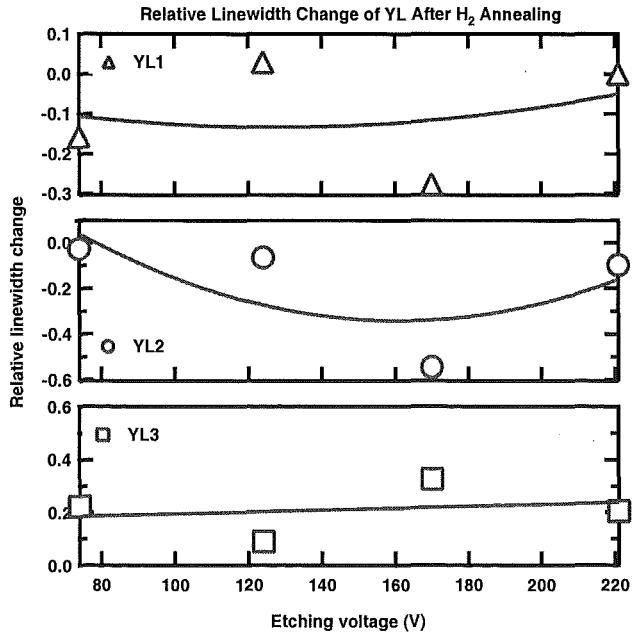

Figure 7.23: The relative linewidth change of SF_6-etched GaN YL (YL1 = 2.60 eV, YL2 = 2.24 eV, YL3 = 1.91 eV) lines after annealing in hydrogen ambient as a function of etching voltage.

The relative intensity of YL1 peak after annealing is about 1.5 times to 2.3 times of the intensity before annealing, except for sample 17, which was etched at 221 V etching voltage, it does not show the YL1 peak. The relative intensity of YL2 peak after annealing is about 2.7 times of the intensity before annealing at the etching voltage 74 V, then decreases to about 1.4 times as the etching voltage increases to 221 V.

The relative intensity of YL3 peak after annealing is about 1.8 times to 2.4 times of the intensity before annealing, except the third sample which was etched at 170 V, its relative intensity after etching is about 5.3 times of the intensity before etching.

The relative intensity of all the YL peaks after hydrogen annealing only weakly depend on the etching voltage.

Figure 7.23 shows the relative linewidth change of the YL peaks after annealing in hydrogen ambient as a function of etching voltage.

The relative linewidth change of the YL3 line after annealing is about 10% to 30% wider than before annealing. The linewidth of the YL2 line after annealing is 2% to 10% narrower than before annealing, except for sample 15 which was etched at 170 V, the linewidth of the YL2 peak after annealing is 55% narrower than before annealing. The linewidth of YL1 line after annealing is 28% narrower to 3% wider than before annealing. All the relative linewidth change of YL1, Yl2

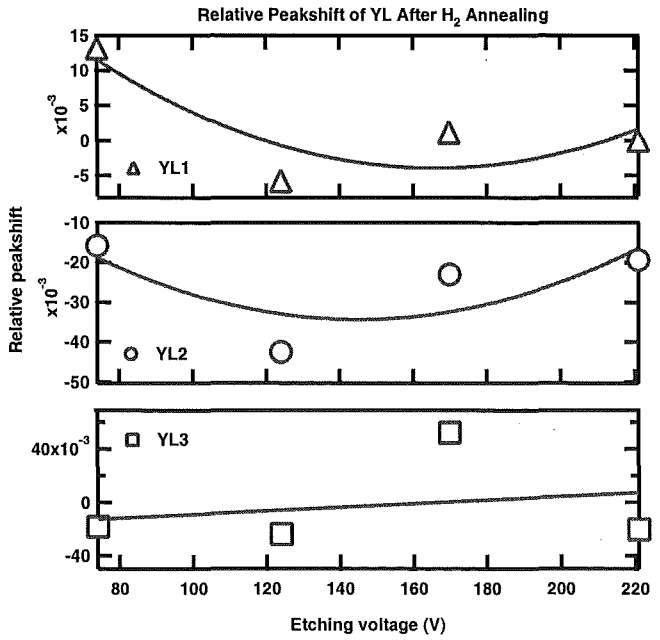

Figure 7.24: The relative peakshift of SF_6-etched GaN YL (YL1 = 2.60 eV, YL2 = 2.24 eV, YL3 = 1.91 eV) lines after annealing in hydrogen ambient as a function of etching voltage.

and YL3 only weakly depend on the etching voltage.

Figure 7.24 shows the relative peak position change or peakshift of the YL lines after annealing in hydrogen ambient as a function of etching voltage.

About 80% of the PL analysis results show that the YL peaks position were redshifted after annealing in hydrogen ambient. However, all the YL peaks position were not largely redshifted. The relative peakshift of YL peaks after annealing is about 0% or unshifted to 4% redshifted of the peak position before annealing. Except the YL3 peak position of sample 17, etched at 221 V, it is blueshifted about 5% of the peak position before annealing. The relative peak position changes after annealing in hydrogen ambient of YL1, YL2 and YL3 only weakly depend on the etching voltage.

Conclusion of SF_6-etched GaN Annealing in Hydrogen Ambient

Four SF_6-etched GaN samples have been annealed in hydrogen ambient for 8 hours at the temperature of 700 °C.

The SF_6-etched GaN PL results show that NBE emission line consists of two lines at 3.473 eV(BE1) and 3.495 eV (BE2). From the prior work of the University of Canterbury, it was known that the BE1 line is an acceptor related line or A^0X and the BE2 line is a donor related line or D^0X [11, 12, 15, 16, 17]. The intensity of the A^0X line is about 10 times lower than the D^0X line before annealing and 2 to 3.5 times lower than the D^0X line after annealing. A typical PL linewidth of A^0X and D^0X lines are 10 meV and 12 meV before annealing, 33 meV and 11 meV after hydrogen annealing.

The PL results of SF_6-etched samples show YL lines at about 2.60 eV (YL1), 2.24 eV (YL2), and 1.91 eV (YL3). Before annealing the YL1 line at about 2.60 eV has the highest intensity and the YL3 line has the lowest intensity. Annealing in hydrogen results in increasing all the YL lines intensity. After annealing, the YL2 line becomes the strongest and the YL3 line becomes the lowest in intensity among those lines. A typical PL linewidth of YL1, YL2 and YL3 before annealing are about 260 meV, 200 meV and 160 meV, respectively.

The intensity of the A^0X line after annealing is 2 times higher than before annealing at the etching voltages 124 V, 170 V ,221 V, and 4.8 times higher than before annealing at the etching voltage of 74 V. After annealing the A^0X line has 70% wider linewidth than before annealing, and does not depend on the etching voltage. The A^0X line experienced a slight blueshift, about 0.25%, after annealing.

Hydrogen annealing results in 50% to 70% lower intensity of the D^0X line than before annealing, except for the point at the etching voltage of 221 V, it is 2.5 times higher intensity than before annealing. The D^0X linewidth after annealing becomes 20% to 70% narrower than before annealing, and weakly depends on the

etching voltage. A small blueshift, about 0.12%, of the D^0X line was observed after annealing in hydrogen.

The intensity of YL1, YL2 and YL3 lines after annealing are 1.4 to 2.7 times higher than before annealing. Only a small peakshift, 0% to 5%, of YL1, YL2 and YL3 lines were observed after hydrogen annealing. The linewidth of the YL1 and YL2 lines after annealing are 2% to 28% narrower than before annealing. In contrast, the linewidth of the YL3 line after annealing is 10% to 30% wider than before annealing. The changes in intensity, linewidth and peak position of YL lines after annealing only weakly depend on the etching voltage.

7.4 Annealing in Nitrogen Ambient

7.4.1 Ar-etched Samples

Sample	AL31	AL35	AL37
Etching voltage (V)	260	380	480

Table 7.5: Ar-etched GaN samples of annealing in nitrogen ambient.

Annealing at 700 °C in nitrogen ambient for eight hours has been done to three Ar-etched GaN samples. Those three samples with their etching voltages are listed in Table (7.5).

Figures 7.25 and 7.26 show the PL results of the NBE emission and YL of samples AL31, AL35 and AL37 after annealing in nitrogen ambient. The PL measurements were taken at the temperature of 4 K.

Before annealing in nitrogen ambient, the NBE emission line consists of two lines, peaking at 3.486 eV (BE1) and 3.493 eV (BE2), and there are two YL lines, peaking at 2.53 eV (YL1) and 2.22 eV (YL2).

The PL results of Ar-etched GaN show that the BE1 line at 3.486 eV has disappeared, and the BE2 line appears with lower intensity but wider linewidth after annealing in nitrogen ambient. There is no YL3 line at 1.8 eV appearing from the Ar-etched samples after nitrogen annealing as it is after vacuum annealing. Generally, the YL1 at 2.53 eV and YL2 at 2.22 eV lines appear with higher intensity after annealing.

Analysis and Discussion of the PL Results

Figure 7.27 shows the relative intensity of the NBE (BE2 = 3.493 eV) line after annealing in nitrogen ambient as a function of etching voltage. The annealing in nitrogen ambient results in a lower relative intensity of BE2 line after annealing than before annealing. As the etching voltage increases from 260 V to 380 V then

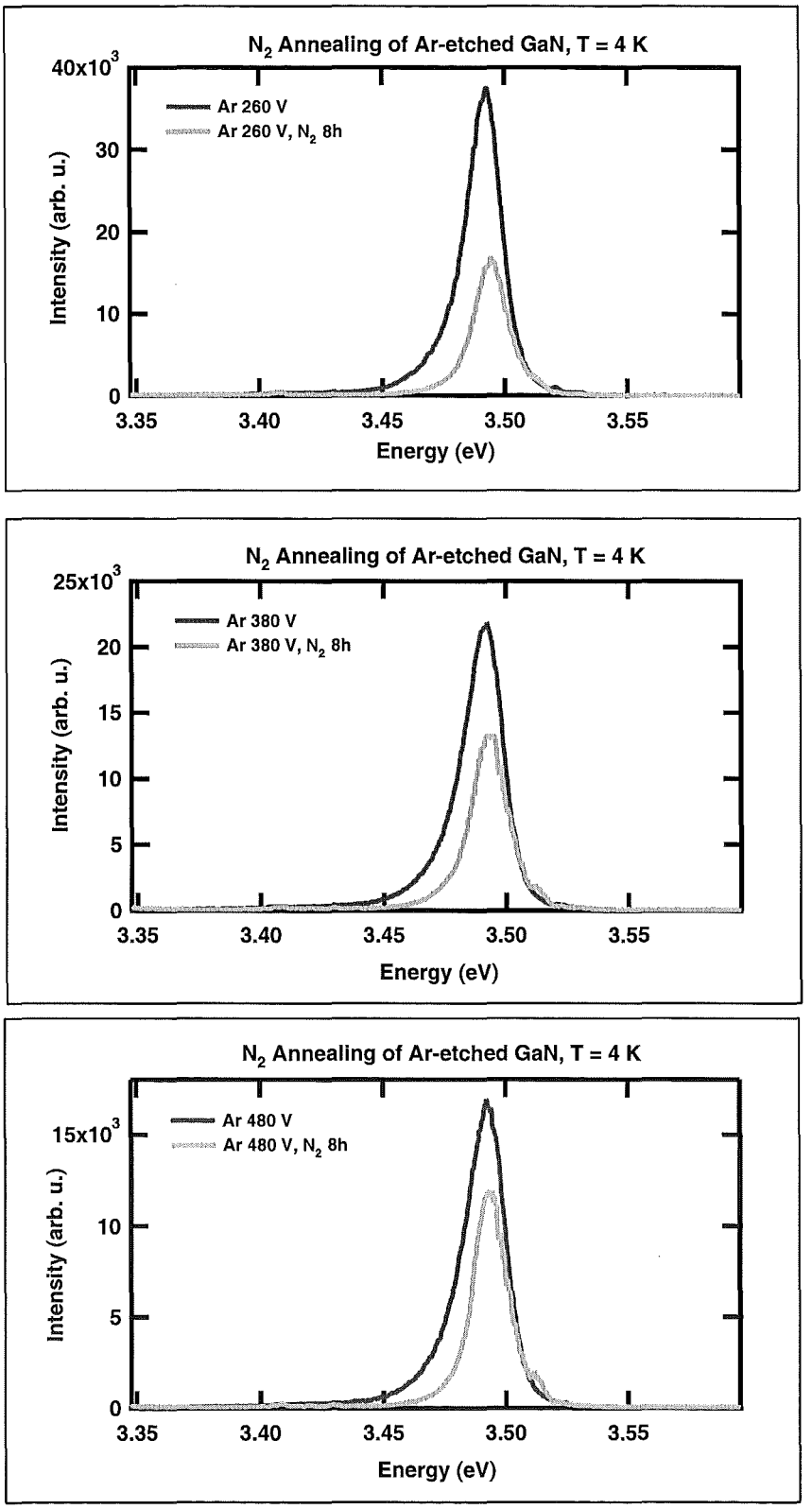

Figure 7.25: PL results of Ar-etched GaN NBE line before and after annealing in nitrogen ambient.

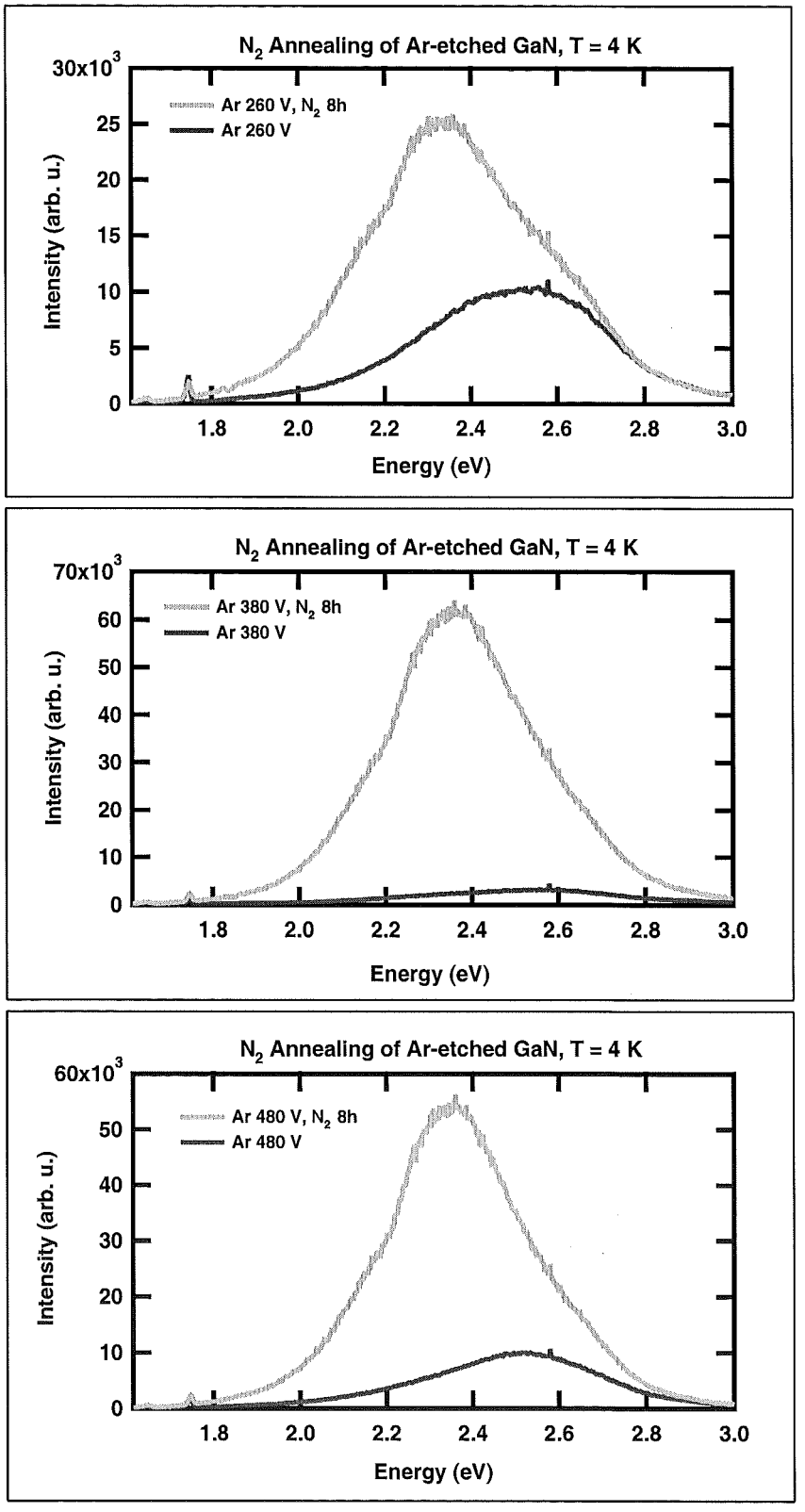

Figure 7.26: PL results of Ar-etched GaN YL lines before and after annealing in nitrogen ambient.

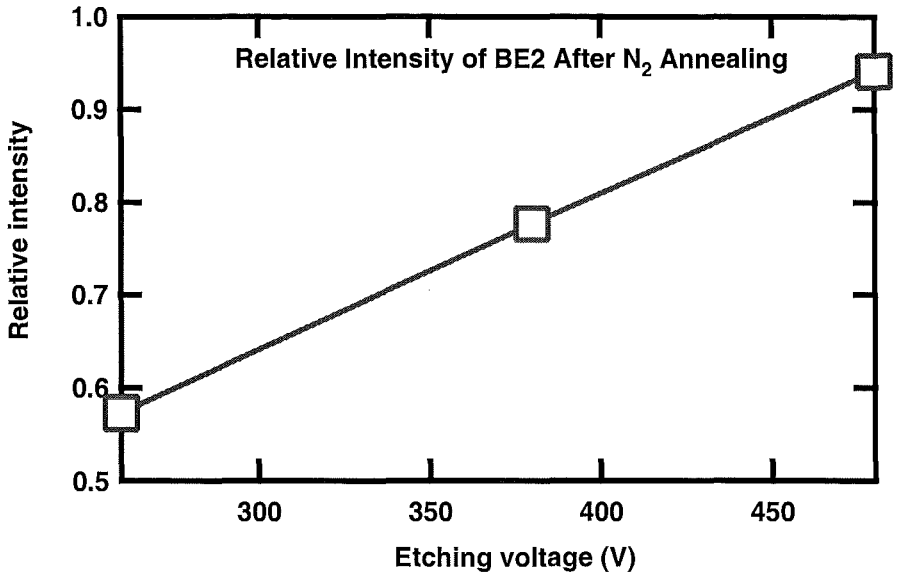

Figure 7.27: The relative intensity of Ar-etched GaN NBE (BE2 = 3.493 eV) line after annealing in nitrogen ambient as a function of etching voltage.

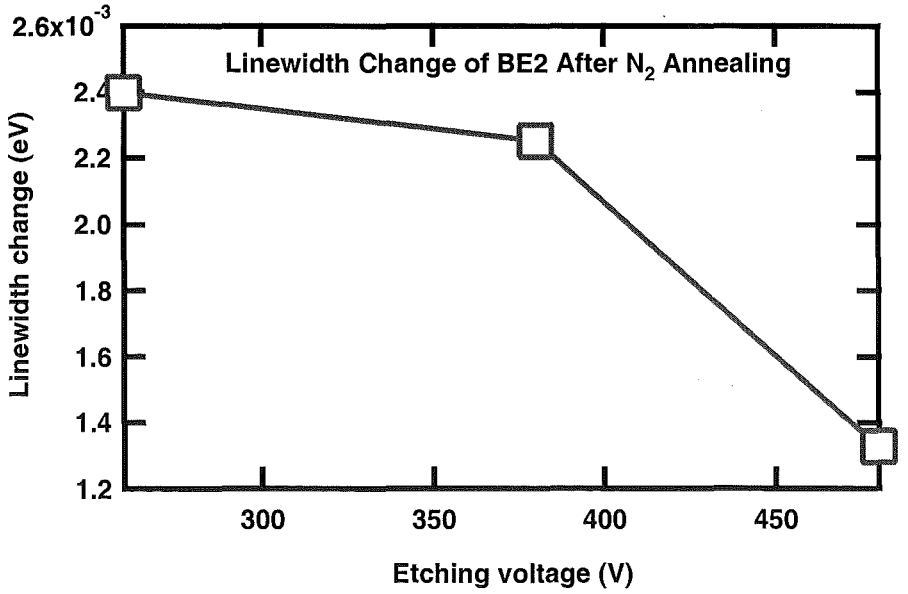

Figure 7.28: The linewidth change of Ar-etched GaN NBE (BE2 = 3.493 eV) line after annealing in nitrogen ambient as a function of etching voltage.

480 V, the relative intensity of BE2 after annealing also increases sharply from 0.57 to 0.78 then 0.95 times of the intensity before annealing, respectively.

Figure 7.28 shows the linewidth changes of the NBE line after annealing in nitrogen ambient as a function of etching voltage. The linewidth of BE2 line after annealing is wider than before annealing. At the etching voltage of 260 V, the linewidth of BE2 line after annealing is 2.4 meV wider than before annealing. As the etching voltage increases to 380 V and 480 V, the linewidth of BE2 line is narrowed to 2.3 meV and 1.3 meV wider than before annealing. A typical PL linewidth of Ar-etched GaN BE2 line is about 9 meV.

Figure 7.29 shows the peakshift of the NBE lines after annealing in nitrogen ambient as a function of etching voltage. The BE2 line experienced blueshift after nitrogen annealing. The blueshift of the BE2 line after annealing is 2 meV at the etching voltage of 260 V, then decreases to 1 meV as the etching voltage increases to 380 V, then 480 V.

Figure 7.30 shows the relative intensity of the YL1 = 2.53 eV and YL2 = 2.22 eV lines after annealing in nitrogen ambient as a function of etching voltage.

At the etching voltages of 260 V and 380 V, the intensity of the YL1 line after annealing is about 2.5 times of the intensity before annealing, then decreases steeply to about 0.5 times of the intensity before annealing as the etching voltage increases to 480 V.

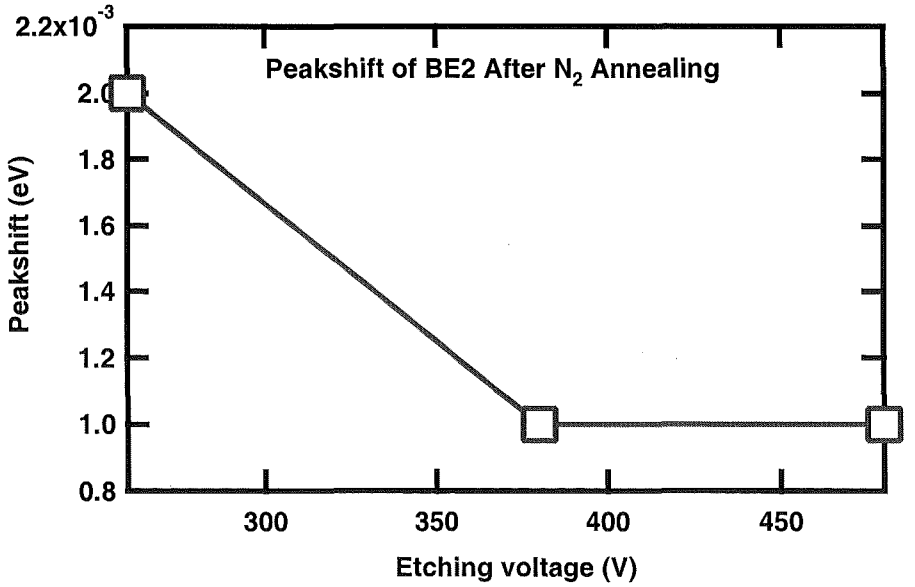

Figure 7.29: The peakshift of Ar-etched GaN NBE (BE2 = 3.493 eV) line after annealing in nitrogen ambient as a function of etching voltage.

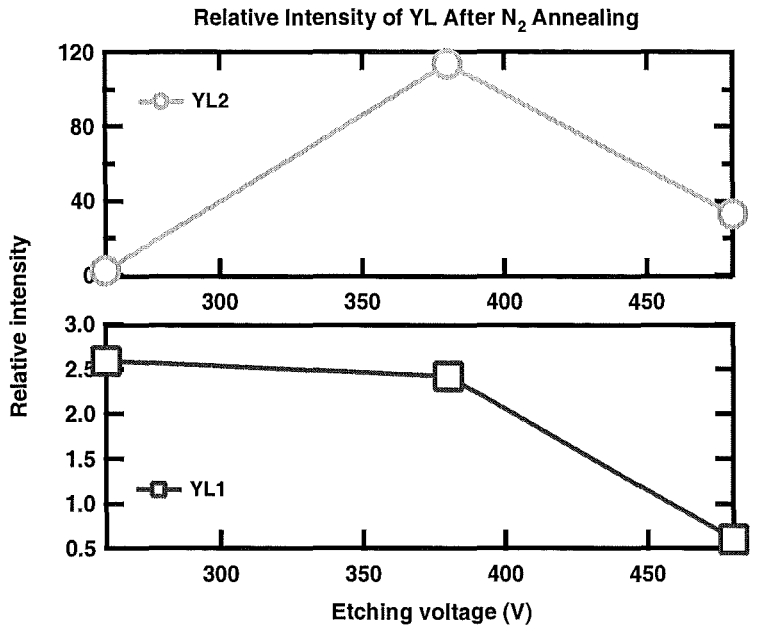

Figure 7.30: The relative intensity of Ar-etched GaN YL (YL1 = 2.53 eV, YL2 = 2.22 eV) lines after annealing in nitrogen ambient as a function of etching voltage.

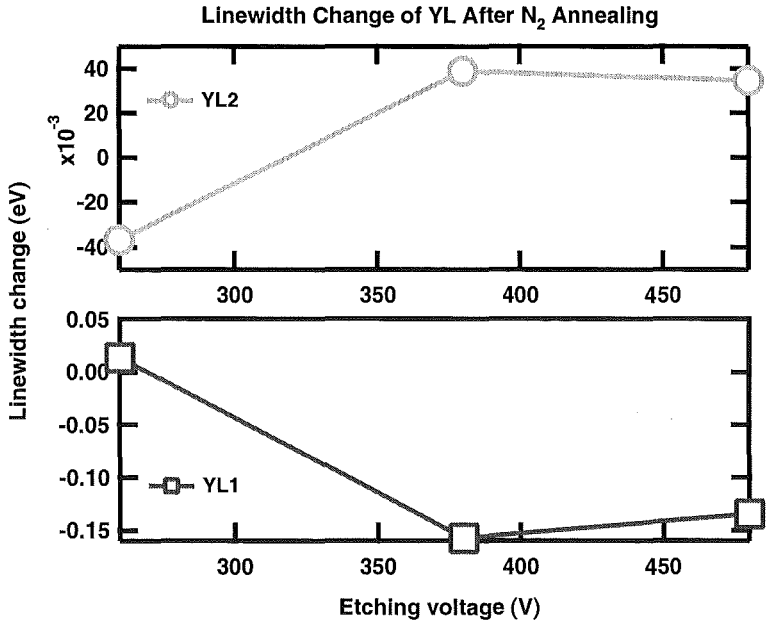

Figure 7.31: The linewidth change of Ar-etched GaN YL (YL1 = 2.53 eV, YL2 = 2.22 eV) lines after annealing in nitrogen ambient as a function of etching voltage.

The intensity of the YL2 line after annealing is much higher than before annealing, especially at the etching voltage of 380 V, it is 110 times higher than before annealing. At the etching voltage of 260 V and 480 V, the intensity of YL2 line after annealing are about 4 and 35 times higher than before annealing.

Figure 7.31 shows the linewidth change of the YL1 and YL2 lines after annealing in nitrogen ambient as a function of etching voltage. Typically, the YL1 and YL2 PL linewidth of these Ar-etched GaN samples before annealing are about 120 to 290 meV and 190 to 290 meV.

At the etching voltage of 260 V, the linewidth of YL1 line after annealing is about 20 meV wider than before annealing. At the etching voltage of 380 V and 480 V, the linewidth of YL1 line after annealing are 150 meV and 140 meV narrower than before annealing.

The linewidth of YL2 line after annealing is 38 meV narrower than before annealing at the etching voltage 260 V. As the etching voltage increases to 380 V and 480 V, the linewidth change of YL2 line also increases to about 40 meV and 37 meV wider than before annealing.

Figure 7.32 shows the peakshift of the YL1 and YL2 lines after annealing in nitrogen ambient as a function of etching voltage.

The YL1 line experienced blueshift after annealing in nitrogen ambient, and the amount of the blueshift increases as the etching voltage increases. At the etching

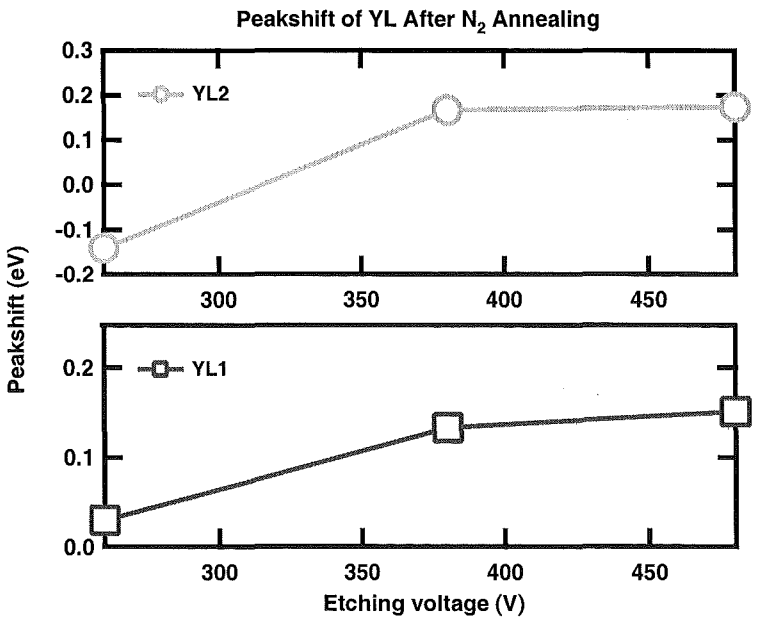

Figure 7.32: The peakshift of Ar-etched GaN YL (YL1 = 2.53 eV, YL2 = 2.22 eV) lines after annealing in nitrogen ambient as a function of etching voltage.

voltage of 260 V, the amount of the blueshift is about 30 meV, then increases to 130 meV then 150 meV as the etching voltage increases to 380 V then 480 V.

At the etching voltage of 260 V, the YL2 line was redshifted about 150 meV after annealing in nitrogen ambient. At the etching voltages of 380 V and 480 V, the YL2 line was blueshifted about 180 meV.

7.4.2 SF_6-etched Samples

Sample	10	12	14	16	18
Etching voltage (V)	105	150	160	195	230

Table 7.6: SF_6-etched GaN samples of annealing in nitrogen ambient.

Annealing at 700 °C in nitrogen ambient for eight hours have been done to five SF_6-etched GaN samples. The samples with their etching voltages are listed in Table 7.6.

Figures 7.33,7.34 and 7.35,7.36 show the PL results of the NBE emission and the YL of SF_6-etched GaN samples 10, 12, 14, 16 and 18 after annealing in nitrogen ambient. The PL measurements were taken at temperature 4 K. Appearing are the NBE line at 3.493 eV and the YL lines at 2.63 eV (YL1), 2.31 eV (YL2) and 1.88 eV (YL3).

Analysis and Discussion of the PL Results

The PL result of the NBE emission line before annealing of sample 16 (etched at 195 V) is somehow unreliable. It is probably because the PL was measured in a damaged surface of the sample. Unfortunately, it was found when the sample had been annealed, and the PL measurement could not be repeated.

Figure 7.37 shows the relative intensity of the NBE = 3.493 eV line after annealing in nitrogen ambient as a function of etching voltage.

Three out of four reliable results show the relative intensity of the NBE line are higher after annealing in nitrogen ambient. At the etching voltage 105 V, the relative intensity of the NBE line after annealing is about 0.8 times the intensity before annealing then increases to about 1.25 times the intensity before annealing at the etching voltage 150 and 160 V, and keep increasing to 1.8 times the intensity before annealing at the etching voltage 230 V.

Figure 7.38 shows the relative linewidth changes of the NBE line after annealing in nitrogen ambient as a function of etching voltage.

The linewidth of the NBE line of SF_6-etched sample after annealing in nitrogen ambient becomes narrower than before annealing, are indicated by the negative

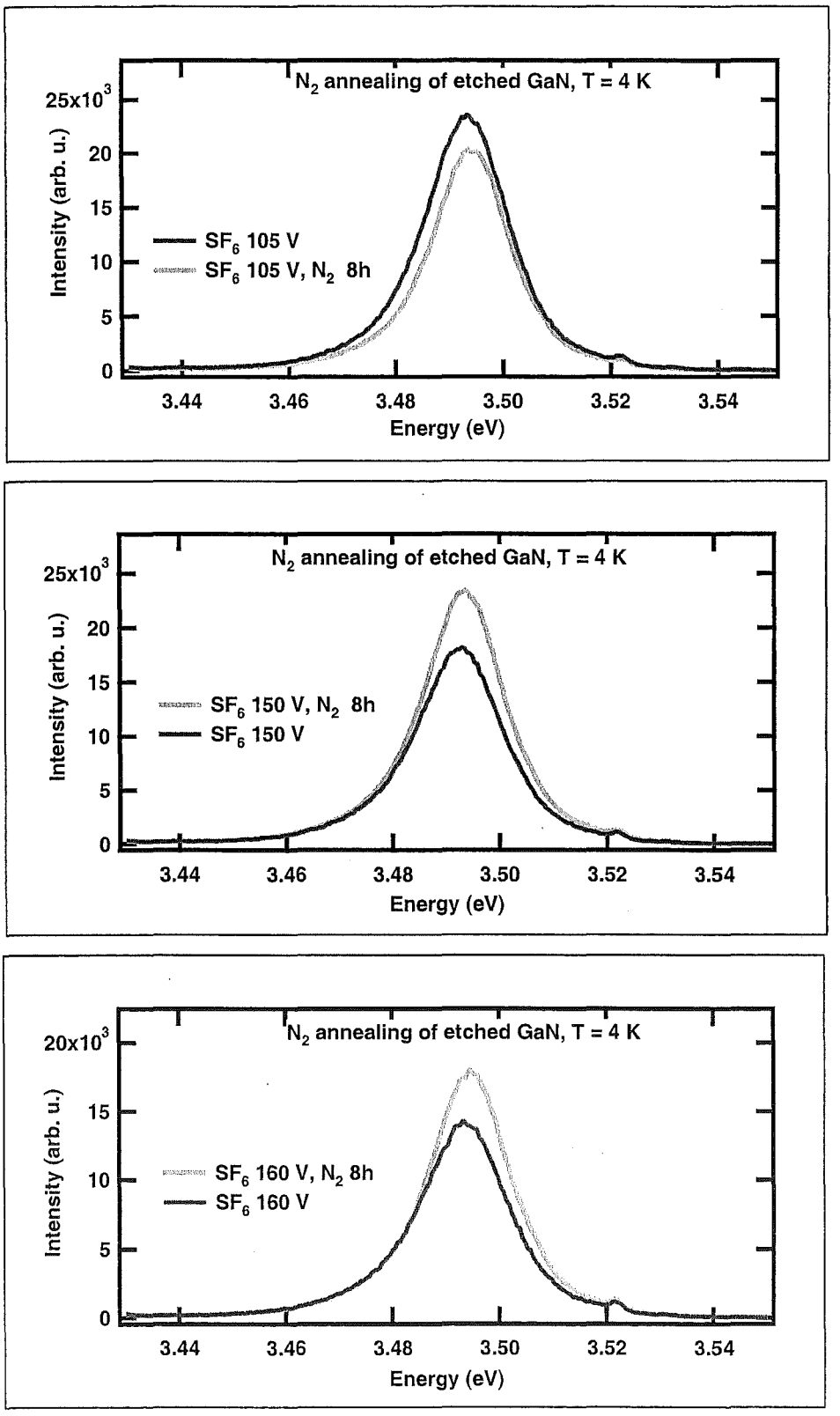

Figure 7.33: PL results of SF_6-etched GaN NBE line before and after annealing in nitrogen ambient.

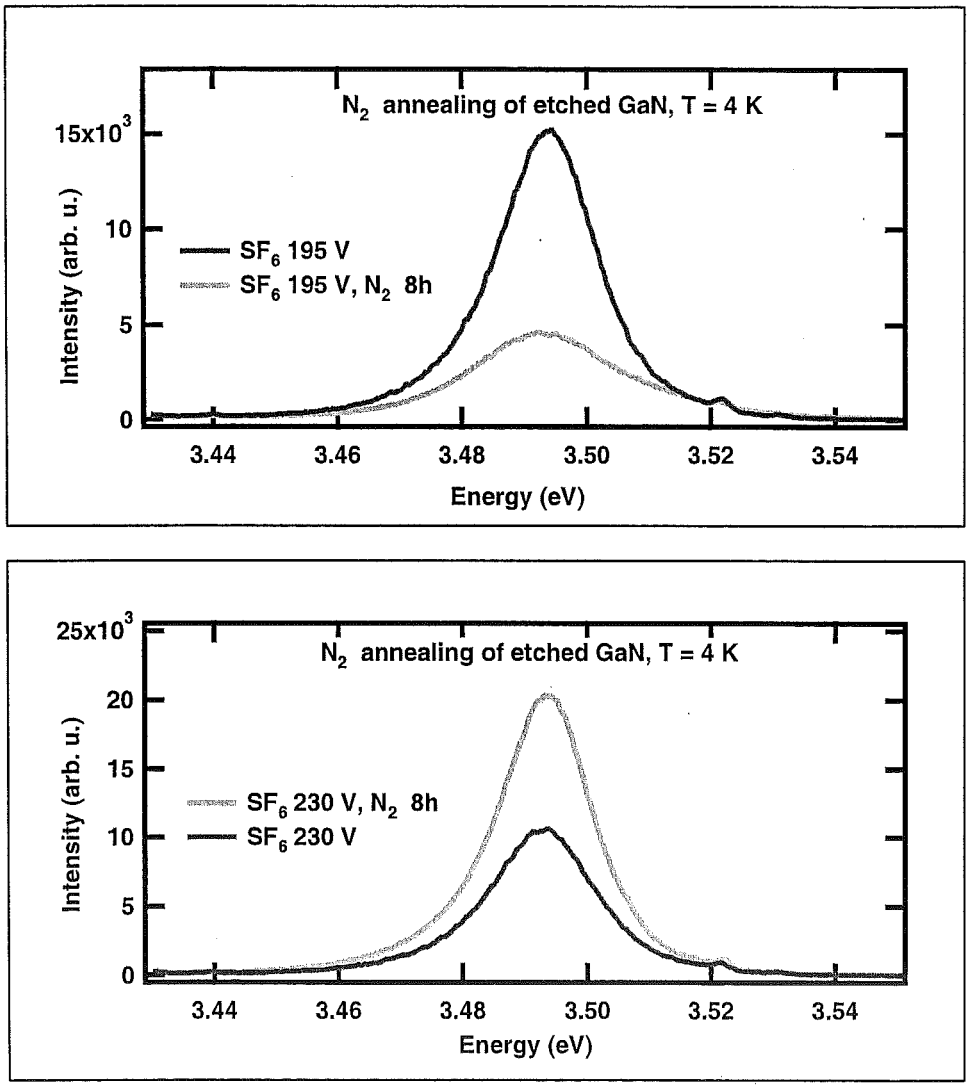

Figure 7.34: PL results of SF_6-etched GaN NBE line before and after annealing in nitrogen ambient.

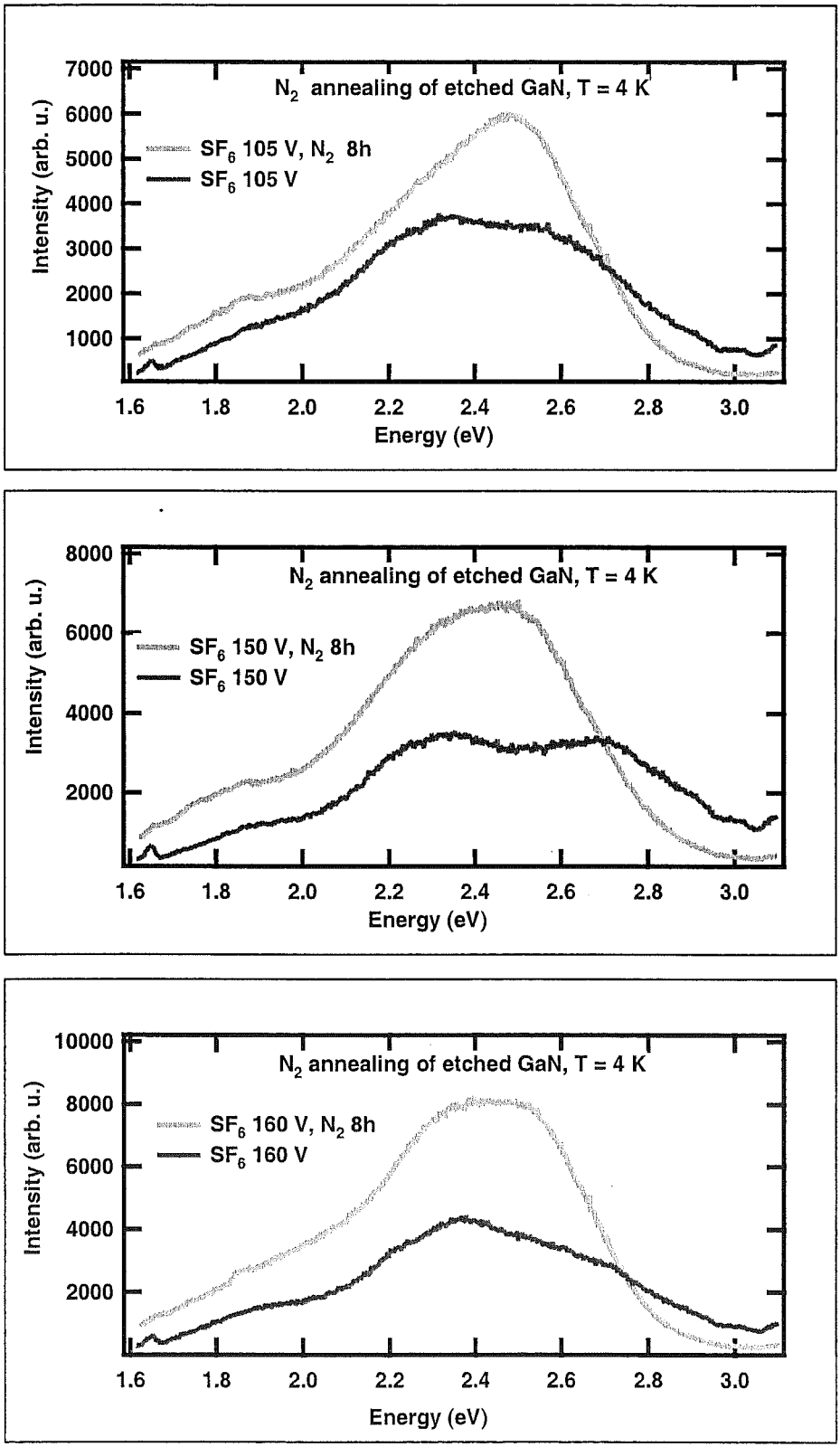

Figure 7.35: PL results of SF_6-etched GaN YL line before and after annealing in nitrogen ambient.

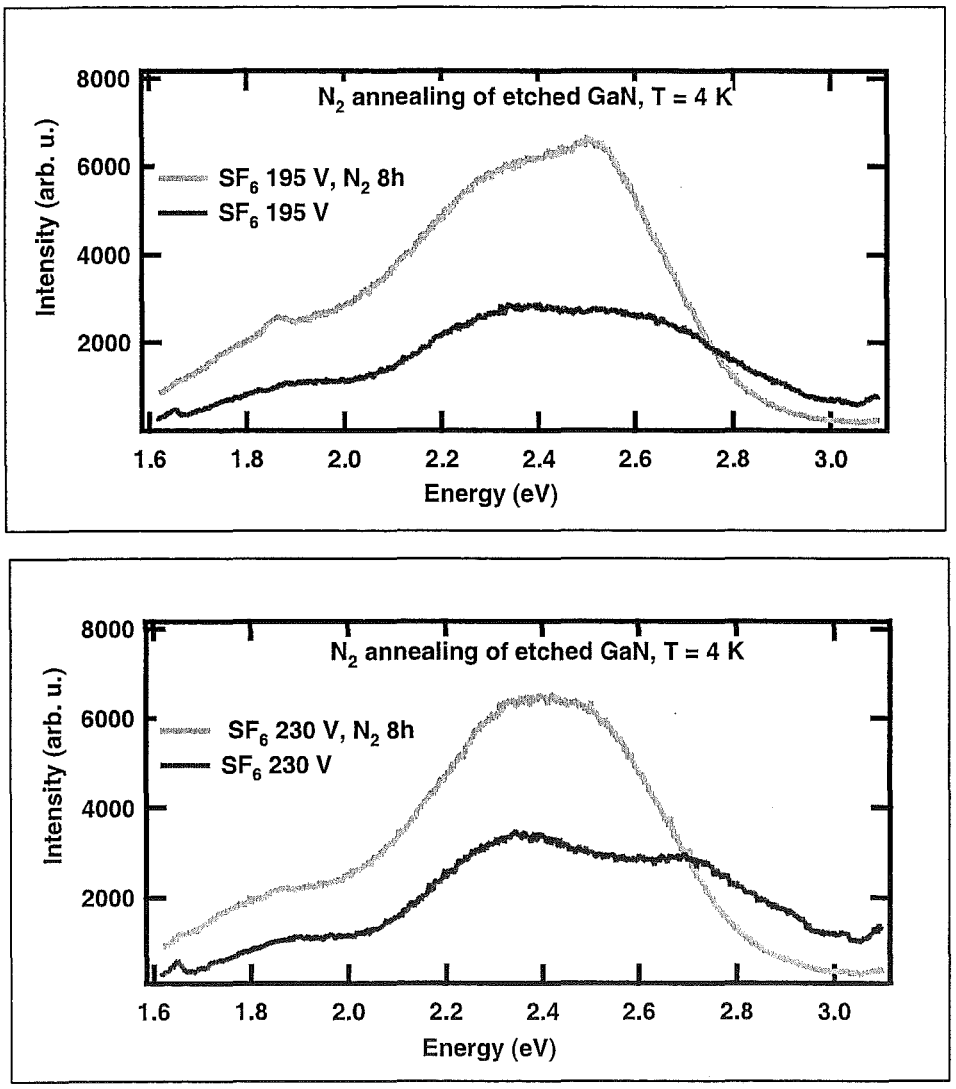

Figure 7.36: PL results of SF_6-etched GaN YL line before and after annealing in nitrogen ambient.

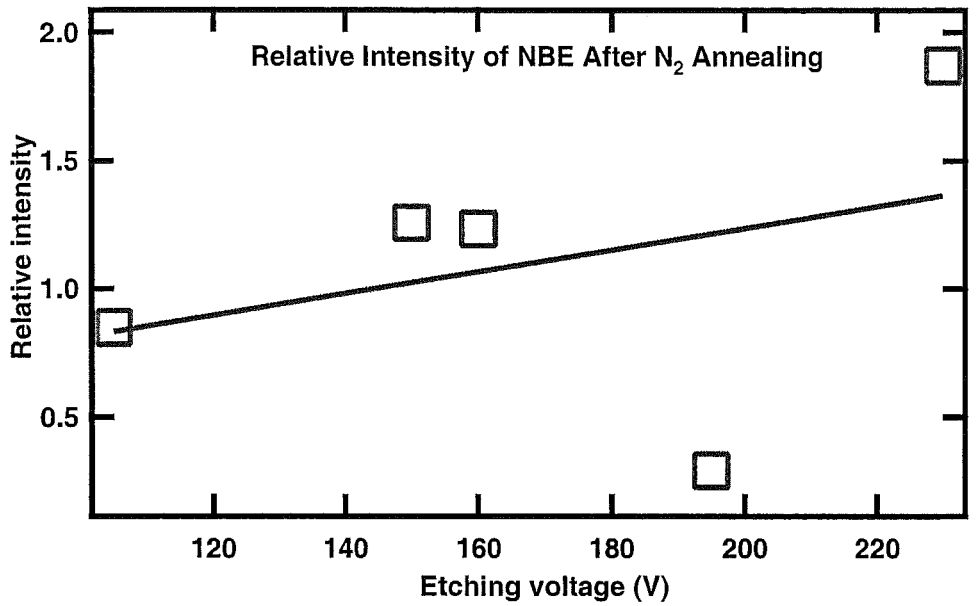

Figure 7.37: The relative intensity of SF_6-etched GaN NBE = 3.493 eV line after annealing in nitrogen ambient as a function of etching voltage.

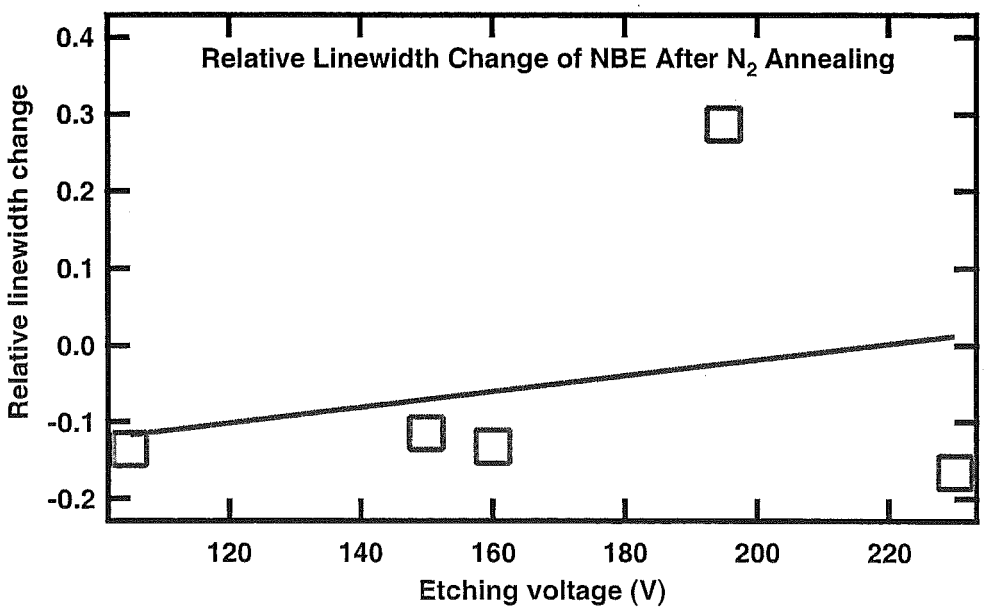

Figure 7.38: The relative linewidth change of SF_6-etched GaN NBE = 3.493 eV line after annealing in nitrogen ambient as a function of etching voltage.

values of the relative linewidth changes. The relative linewidth changes of this line after etching is almost constant at about 13% narrower than the linewidth before annealing, only weakly depend on the etching voltage, showing only a slight decrease as the etching voltage increases.

Figure 7.39 shows the relative change of line position (peakshift) of the NBE line after annealing in nitrogen ambient as a function of etching voltage.

Annealing in nitrogen ambient result in a really small peakshift to the NBE line of SF_6-etched samples, the figure shows there is only less than 0.014% relative changes of line position after annealing, this value is comparable to the uncertainty or error.

The analysis of YL lines have been done on the three YL lines at 2.63 eV (YL1), 2.31 eV (YL2) and 1.88 eV (YL3).

Figure 7.40 shows the relative intensity of the YL peaks of SF_6-etched samples after annealing in nitrogen ambient as a function of etching voltage. Annealing in nitrogen ambient of SF_6-etched samples results in higher intensity of YL lines after annealing.

Relative intensity of YL1 lines after annealing only weakly depend on the etching voltage, the results are within 1.2 to 2.2 times higher than the intensity before annealing.

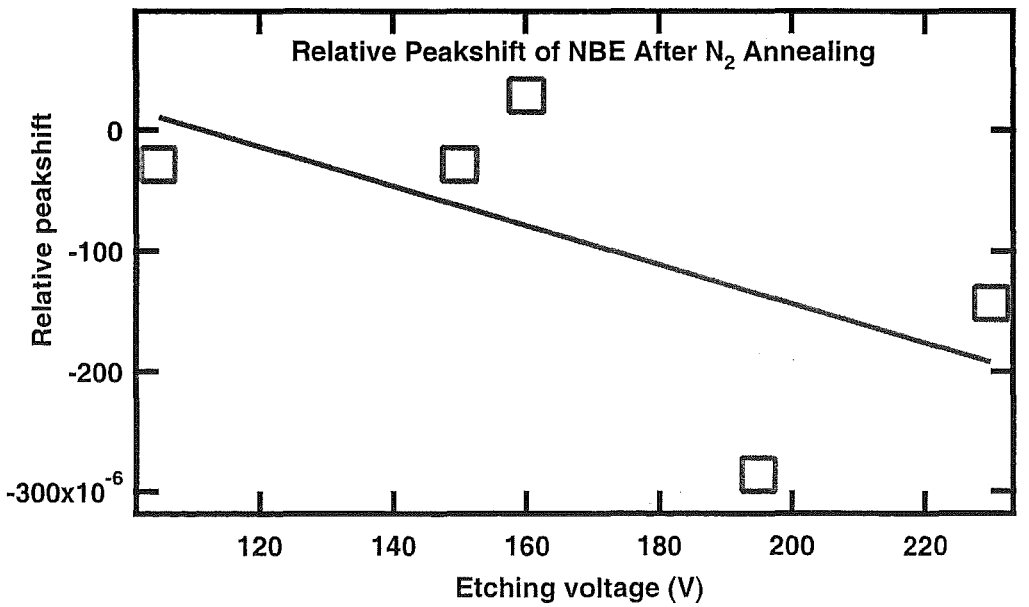

Figure 7.39: The relative peakshift of SF_6-etched GaN NBE = 3.493 eV line after annealing in nitrogen ambient as a function of etching voltage.

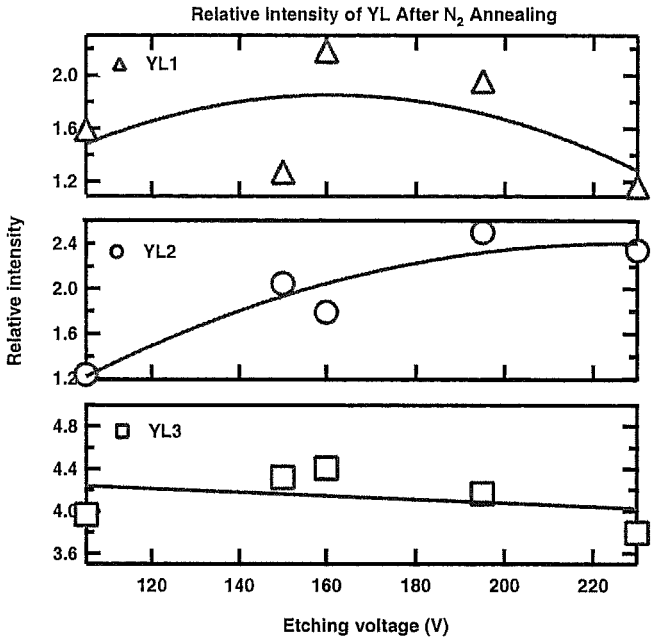

Figure 7.40: The relative intensity of SF_6-etched GaN YL (YL1 = 2.63 eV, YL2 = 2.31 eV, YL3 = 1.88 eV) lines after annealing in nitrogen ambient as a function of etching voltage.

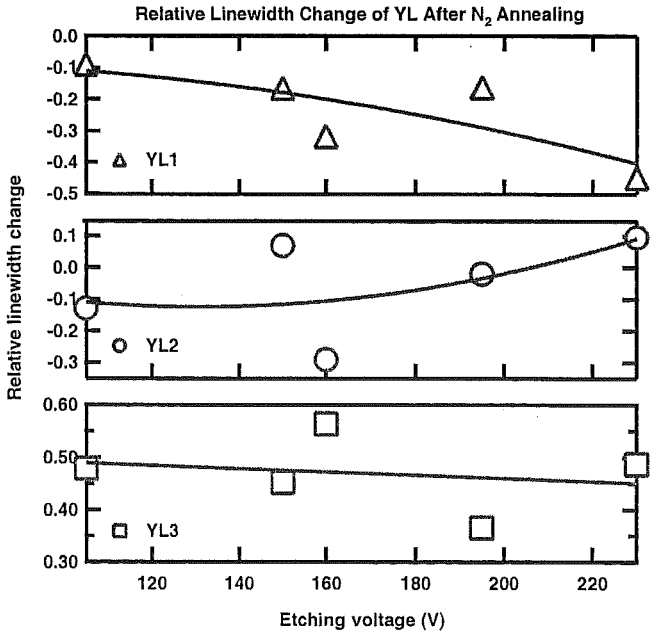

Figure 7.41: The relative linewidth change of SF_6-etched GaN YL (YL1 = 2.63 eV, YL2 = 2.31 eV, YL3 = 1.88 eV) lines after annealing in nitrogen ambient as a function of etching voltage.

The relative intensity of the YL2 line after annealing is about 1.2 times of the intensity before annealing at etching voltage 105 V, then increases to about 2.3 times of the intensity before annealing at etching voltage 230 V.

The relative intensity of the YL3 line after annealing in nitrogen ambient is about 4 times to 4.4 times of the intensity before annealing at etching voltage 105 V to 160 V, then slightly decreases to 3.8 times of the intensity before annealing as the etching voltage increases to 230 V. The relative increase of YL3 line is dominant compare to YL1 and YL2.

Figure 7.41 shows the relative linewidth change of the YL peaks of SF_6-etched samples after annealing in nitrogen ambient as a function of etching voltage.

The relative linewidth change of YL1 line after annealing is about 10% narrower than the linewidth before annealing at etching voltage 105 V, then decreases to about 45% narrower than the linewidth before annealing as the etching voltage increases to 230 V.

There is about 13% changes, wider or narrower, of the YL2 linewidth after annealing in nitrogen ambient. At the lower etching voltage the linewidth is relatively narrower than the linewidth before annealing and at the higher etching voltage the linewidth is relatively wider than the linewidth before annealing.

The relative linewidth change of YL3 line after annealing is about 50% wider

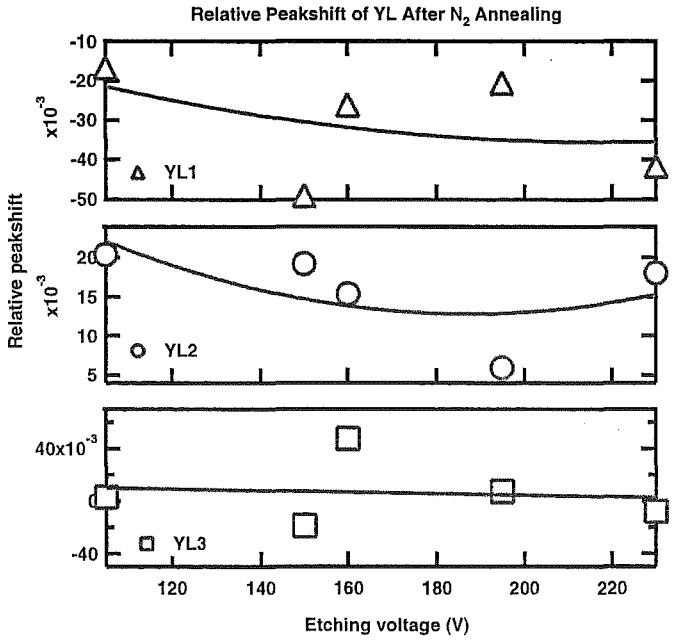

Figure 7.42: The relative peakshift of SF_6-etched GaN YL (YL1 = 2.63 eV, YL2 = 2.31 eV, YL3 = 1.88 eV) lines after annealing in nitrogen ambient as a function of etching voltage.

than the linewidth before annealing, and it does not greatly change to the etching voltage.

Figure 7.42 shows the relative peak position or peakshift of the YL peaks of SF_6-etched samples after annealing in nitrogen ambient as a function of etching voltage.

There is only a really small peakshift of the YL1, YL2, YL3 lines after annealing in nitrogen ambient of SF_6-etched samples. The analysis of PL results show there is only less than $\pm$ 0.005 % relative peakshift after annealing, this value is comparable to the uncertainty.

7.4.3 Conclusion of Ar- and SF_6-etched GaN Annealing in Nitrogen Ambient

Annealing in nitrogen ambient for 8 hours at the temperature of 700 °C has been done to three samples of Ar-etched GaN, and five samples of SF_6-etched GaN.

The Ar-etched GaN samples show two NBE lines at 3.486 eV (BE1) and 3.493 eV (BE2), and two YL lines at 2.53 eV (YL1), 2.22 eV (YL2). No YL3 line was observed from these samples. Before annealing, BE2 has 2.3 times higher intensity than BE1. No BE1 line was observed after annealing in nitrogen ambient. The intensity of the YL1 line is 5 to 6 times higher than the YL2 line before annealing. In contrast, after annealing the intensity of the YL2 line is 5 to 9 times higher than the YL1.

There was one NBE line at 3.493 (BE2) and three YL lines at 2.63 eV (YL1), 2.31 eV (YL2) and 1.88 eV (YL3) observed from the SF_6-etched GaN samples. No BE1 line at 3.486 eV was observed from these samples before or after annealing. The intensity of the YL1 and YL2 lines are similar and the YL3 line has the weakest intensity among those lines, before and after annealing. Annealing results in much stronger intensity of the three YL lines.

Ar-etched GaN has typical linewidth about 20 meV, 9 meV of the BE1, BE2 lines, and 150 to 290 meV, 200 to 290 meV of the YL1 and YL2 lines. Typical linewidth of BE2, YL1, YL2 and YL3 lines of SF_6-etched GaN are 9 meV, 250 meV, 200 to 260 meV, and 70 to 150 meV, respectively.

The changes of the intensity, linewidth and peak position of YL lines weakly depend on the the etching voltage.

A summary of the Ar- and SF_6-etched GaN annealing in nitrogen results are shown in Table 7.7 and 7.8.

BE1 line	**Ar-etched GaN after N_2 annealing**
	No BE1 line was observed after annealing
BE2 line	**Ar-etched GaN after N_2 annealing**
Intensity	0.57, 0.78 and 0.95 times of the intensity before annealing at the etching voltages of 260 V, 380 V and 480 V
Peakshift	1 to 2 meV blueshifted, a typical error is 1 meV
Linewidth	1.3 to 2.4 meV wider than before annealing
YL1 line	**Ar-etched GaN after N_2 annealing**
Intensity	2.5 times higher than before annealing at 260 V and 380 V 0.5 times lower than before annealing at 480 V
Peakshift	30 meV, 130 meV and 150 meV blueshifted at the etching voltages of 260 V, 380 V and 480 V
Linewidth	20 meV wider, 150 meV and 140 meV narrower than before annealing at the etching voltages of 260 V, 380 V and 480 V
YL2 line	**Ar-etched GaN after N_2 annealing**
Intensity	4, 110 and 35 times higher than before annealing at the etching voltages of 260 V, 380 V and 480 V
Peakshift	150 meV redshifted at the etching voltage of 260 V 180 meV blueshifted at the etching voltages of 380 V and 480 V
Linewidth	38 meV narrower at the etching voltage of 260 V and 40 meV 37 meV wider at the etching voltages of 380 V and 480 V meV
YL3 line	**Ar-etched GaN after N_2 annealing**
	No YL3 line was observed before or after annealing

Table 7.7: Summary of Ar-etched GaN samples annealing in nitrogen ambient results.

7.5 Discussion and Conclusion

Three samples of Ar-etched GaN were annealed in vacuum, and the summary of the results was shown in Table 7.2. Hydrogen annealing has been done to three Ar-etched and four SF_6-etched GaN samples, the results summary of these annealing processes was shown in Table 7.3 and Subsection 7.3.2 on page 162. Annealing in nitrogen ambient has been done to three Ar-etched and five SF_6-etched GaN samples, the results summary was shown in Table 7.7 and 7.8. In this project, it was determined that 700^0C is the suitable temperature to anneal GaN, and it is in agreement with the prior works [54, 69].

The prior work of The University of Canterbury [72] showed SF_6 plasma etching results in the appearance of the A^0X line at 3.439 eV, the A^0X line is split about 6 meV from the D^0X line at 3.445 eV. Brandt *et al* [9] observed a new PL line at 3.35 eV appears in both p- and n-type GaN samples after hydrogenation .

Two NBE lines at 3.485 eV (BE1) and 3.493 eV (BE2) were observed from the Ar-etched GaN samples before annealing. After annealing in vacuum and hydrogen, the BE1 line was shifted to 3.473 eV and with lower intensity and wider linewidth

than before annealing. Annealing in nitrogen results in disapperance of the BE1 line of these samples.

There were also two NBE lines observed from the SF_6-etched GaN samples 9, 11, 15 and 17, but not from the samples 10, 12, 14, 16 and 18.

If the BE1 line is associated with the A^0X line from the prior work of The University of Canterbury or the new PL line from the work of Brandt *et al*, it can be interpreted that the line is not merely a result of SF_6 plasma etching nor hydrogenation. However, the GaN samples that were etched by SF_6 plasma then annealed in hydrogen ambient give the most dominant BE1 line than other samples BE1 line. In conclusion, SF_6 plasma etching then annealing in hydrogen ambient process is able to enhance the acceptor level and defect level.

The results of annealing in nitrogen ambient of Ar-etched GaN sample show that the BE1 line at 3.484 eV disappeared after annealing, but not after hydrogen and vacuum annealing. It is interpreted that the BE1 line is nitrogen vacancy defect related state. Further investigation such as Rutherford Back Scattering (RBS) experiment is needed to confirm this conclusion. RBS experiment done to the samples before and after annealing can show information about Ga:N ratio.

In the result summary it is shown the relative intensity of the BE2 line is lower after annealing in vacuum, hydrogen or nitrogen ambient. In most cases, the relative linewidth of the BE2 line is narrower after annealing. These results are in agreement with the results of Eunsoon *et al* [67] and Li *et al* [38] when the BE2 line is associated with the D^0X. But in contrast to their works, which show a blueshift after annealing, there is only a small and comparable to the uncertainty peakshift after annealing observed from this work. It is probably because of the samples used in this work originally have less strain than their samples.

There are two or three YL lines that were observed from the samples before and after annealing. In general, the YL lines relative intensity after annealing are stronger than before annealing in vacuum, hydrogen and nitrogen ambient, and only weakly depend on the etching voltage. An increase of YL relative intensity after annealing was also mentioned by Eunsoon *et al* [67]. This might be due to the defect level creation and enhancement by annealing process.

No strong correlation appears between the annealing processes and the etching voltage effects on the optical properties of GaN.

BE1 line	**SF_6-etched GaN after N_2 annealing**
	No BE1 line was observed before or after annealing
BE2 line	**SF_6-etched GaN after N_2 annealing**
Intensity	0.8 to 1.8 times of the intensity before annealing in the etching voltage from 105 V to 230 V
Peakshift	does not shift largely
Linewidth	13% narrower than before annealing
YL1 line	**SF_6-etched GaN after N_2 annealing**
Intensity	1.2 to 2.2 times higher than before annealing
Peakshift	almost no peakshift
Linewidth	10% to 40% narrower than before annealing
YL2 line	**SF_6-etched GaN after N_2 annealing**
Intensity	1.2 to 2.3 times higher than before annealing
Peakshift	almost no peakshift
Linewidth	13% wider or narrower than before annealing
YL3 line	**SF_6-etched GaN after N_2 annealing**
Intensity	3.8 to 4.4 times higher than before annealing
Peakshift	almost no peakshift
Linewidth	50% wider than before annealing

Table 7.8: The result summary of SF_6-etched GaN samples annealing in nitrogen ambient.

Chapter 8

Conclusions and Recommended Further Work

In this project, PL technique was successfully used to study the optical properties of GaN. There are three main subjects that have been done. The first main subject is the cooperative work with the Victoria University, Wellington and the Electrical Engineering department of the University of Canterbury, Christchurch to investigate the PL of their ion deposition grown a-GaN and MBE grown poly-GaN samples. The second subject is the study of the influence of ion energy on RIE induced optical damage of GaN. And the third subject is a study of the annealing process in vacuum, hydrogen and nitrogen ambient effect on the optical properties of GaN.

Six samples of ion deposited a-GaN from the Victoria University of Wellington have been investigated. The PL results of these a-GaN samples do not show a NBE emission line in the UV region, but show a broad YL line from 1.8 eV to 3.0 eV, peaking at about 2.5 eV, at our level of sensitivity. The YL line of these samples is much wider and has stronger PL intensity than the typical YL line of c-GaN, see appendix B on page 193 for a comparison to a typical PL result of c-GaN.

Seventeen samples of MBE grown poly-GaN and c-GaN made by the Electrical Engineering Department of the University of Canterbury have also been investigated.

The PL results of ten MBE poly-GaN samples on quartz substrate grown at the temperature of mostly 500 °C show a broad NBE emission line in the UV region, a broad and strong YL line in the visible region. These poly-GaN samples are considered as promising samples, especially samples 26-02GN/ Q-10, 27-02GN/ Q-12, and 32-02GN/ Q-15. However, their NBE line is much broader than the NBE line of a good quality GaN sample and the YL line is too dominant, having a much stronger intensity than the NBE line.

Seven MBE grown c-GaN samples, two samples grown on gallium arsenide and five samples grown on sapphire substrate, were investigated. The growth temperature of these c-GaN samples was about 500 °C to 800 °C. The c-GaN samples grown on gallium arsenide or sapphire substrate show a near band edge (NBE)

emission and a blue (BL) or yellow emission (YL) lines, except for the sample 37-02GaN/ Sa-03 which only has a weak and broad YL line. The NBE line of these c-GaN samples have stronger intensity than the poly-GaN samples grown on quartz substrate. However, most of the NBE line of these c-GaN samples are weak and broad compared to a good quality GaN sample, and the YL line is too dominant, showing a much stronger intensity than the NBE line.

The most promising MBE grown c-GaN sample is 70-02GaN/ Sa-12 on sapphire substrate. It shows a strong and narrow (about 5 nm in linewidth) NBE line, and the NBE line intensity is comparable to the intensity of the YL line. The NBE line peak position of this sample is shifted to the higher wavelength or lower energy as temperature increases, this behaviour is similar to a good quality c-GaN sample, see appendix B on page 193 for a comparison to a typical PL result of a good quality c-GaN.

A significant problem found from GaN samples is that the variation of optical properties of different samples taken from different parts of the same wafer can hide any changes in optical properties due to etching or annealing. To minimize the problem, a complete characterisation of each individual sample before etching or annealing was done to accurately determine the effect of etching or annealing on a particular sample.

Three series of Ar plasma and two series of SF_6 plasma RIE induced damage on the optical properties of GaN have been studied. The analysis of the optical changes due to RIE have been determined from the PL peak relative intensity, linewidth (FWHM), and peak position of the NBE emission and the YL lines.

In most cases, Ar and SF_6 plasma etching results in a wider NBE PL linewidth than before etching and no NBE line peakshift after etching. The wider NBE linewidth after Ar etching can be interpreted as a result of a wider D^0X and/or A^0X related lines. However, Ar and SF_6 plasma etching does not necessarily result in a new or much stronger A^0X line. About 87% of the results show that D^0X (3.493 eV) PL intensity decreases after SF_6 plasma etching. Generally, the PL intensity of the NBE line after SF_6 gas etching is lower compared to the case of Ar gas etching.

After Ar and SF_6 plasma etching, the NBE line PL intensity correlates with the PL linewidth change, showing the total PL slightly decreases as the etching voltage increases. It means that Ar and SF_6 plasma etching processes do not significantly increase the density of non radiative centres, even though the etching voltage was increased.

The PL results show that Ar and SF_6 plasma etching increases the total YL linewidth and intensity. The increased in linewidth and intensity of the total YL after etching is dominated by the increased in linewidth and intensity of the YL2 line at 2.375 eV.

A narrow linewidth or low intensity of one YL line will be compensated with a wide linewidth or high intensity of another (in the case of two YL lines) or the

other two YL lines (in the case of three YL lines), and vice versa. The increase in linewidth and intensity of YL after etching, also the correlation between YL1 and YL2 were also reported from the prior work of the University of Canterbury [11, 12, 13, 16, 71].

YL is originated from defects and these defects are metastable states [11, 16]. It implies that Ar and SF_6 plasma etching enhances or creates metastable states.

Ar etching results in smoother surface as etching voltage increases, it is shown by the AFM sample surface images. After SF_6 gas etching, the sample's surface is relatively rougher as etching voltage increase. The morphology of the sample's surface after SF_6 gas etching is generally rougher but more homogenous than after Ar gas etching. SF_6 gas is a more efficient etchant than Ar gas. SF_6 gas etches the sample's surface faster than Ar gas, and it can etch the sample chemically as well as physically.

Annealing study has been done on three Ar-etched GaN, annealed in vacuum then hydrogen ambient; four SF_6-etched GaN, annealed in hydrogen ambient; and five SF_6-etched GaN, annealed in nitrogen ambient. The temperature of 700 °C was determined as the most suitable temperature to anneal GaN in this project, and it is in agreement with the prior work of Nakamura *et el* [54] and Pearton *et al* [69]. All the samples were annealed for eight hours.

For the Ar-etched GaN, annealing in vacuum and hydrogen ambient resulted in a peakshift of the BE1 line to 3.473 eV, lower intensity and wider linewidth than before annealing. Annealing in nitrogen results in disapperance of the BE1 line of Ar-etched samples. These results were interpreted that the BE1 line is nitrogen vacancy defect related state. For further investigation Rutherford Back Scattering (RBS) experiment is suggested to be done to these samples before and after annealing to give information on Ga:N ratio.

The annealing results show that the BE1 or A^0X line is not merely a result of SF_6 plasma etching nor hydrogenation. However, SF_6 plasma etching then annealing in hydrogen ambient process is able to enhance the acceptor and defect related states.

In most cases, the relative intensity of the BE2 line after annealing in vacuum, hydrogen or nitrogen ambient is lower than before annealing. And the relative linewidth of the BE2 line after annealing is narrower than before annealing.

In general, the YL line intensities after annealing are stronger than before annealing in vacuum, hydrogen and nitrogen ambient. This might be due to the defect level creation and enhancement by annealing process.

No strong correlation appears between the annealing processes and the etching voltage effects on the optical properties of GaN.

However, PL technique is not sufficient to fully explain the properties of GaN, especially YL lines. Further investigation using different techniques such as

Raman Scattering, photoconductivity, and RBS can give more information and understanding on GaN properties. A PL temperature dependence study will also give more understanding of the optical changes of GaN due to RIE and annealing processes.

To include a system response calibration, which gives more accurate result, in the analysis is strongly suggested for the future work. The system response calibration was briefly done in this project and was not included in the analysis, see appendix A, on page 187.

Appendix A

Standard Experiment and Instrument Calibration

There are several combinations for the set up of spectrometer, detector and focusing lens that can be used for photoluminescence (PL) experiment, however, only the best set up will give optimum measurement results. A standard experiment has been done in this project to understand and decide the best combination to use and calibrate the measured spectra with the system response to get real spectra of samples.

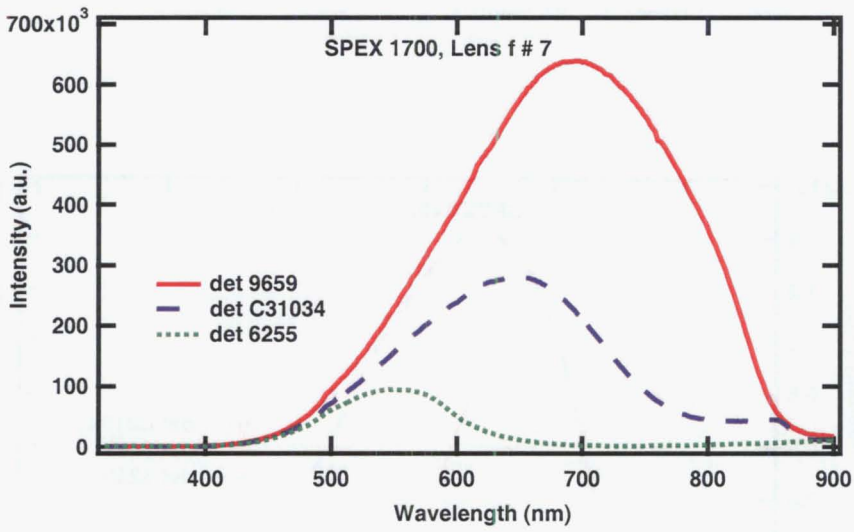

Figure A.1: Results of white light measurement using SPEX 1700, lens with f# 7, and detectors 9659, C31034, 6255.

Nine different set up of spectrometer, detector and focusing lens were tried and used to measure 12 volt DC white light.

The first three settings are SPEX 1700 and f# 7 focusing lens combined with each of three different detectors, those are: detector 9659, C31034, and 6255, the results are shown in figure A.1. It is apparent that the SPEX 1700 when combined

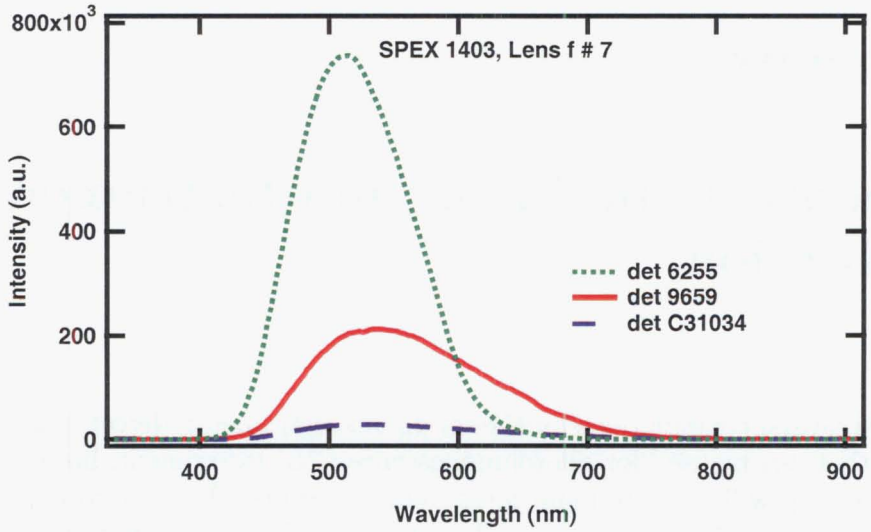

Figure A.2: Results of white light measurement using SPEX 1403, lens with f# 7, and detectors 9659, C31034, 6255.

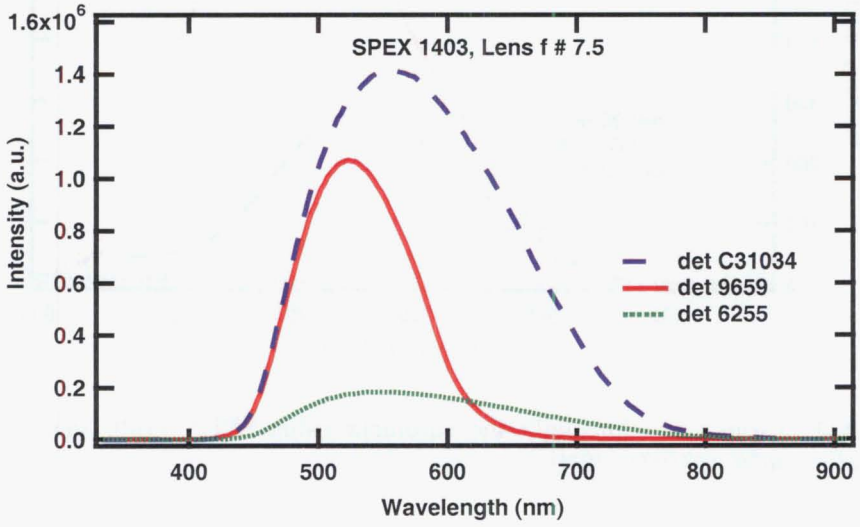

Figure A.3: Results of white light measurement using SPEX 1403, lens with f# 7.5, and detectors 9659, C31034, 6255.

with detector 9659 and f# 7 focusing lens gives the strongest intensity compared to the combinations of SPEX 1700, f# 7 focusing lens, detector C31034 or detector 6255. The combination is best for measuring PL spectrum at the visible light region from 400 nm to 900 nm, with best sensitivity at around 700nm. The detectors C31034 and 6255 are more sensitive at lower wavelength. The best sensitivity for detector C31034 and detector 6255 is at around 650 nm and 550 nm. Detectors C31034 and 6255 are only fairly good when combined with SPEX 1700 and f# 7 focusing lens.

The second setting is SPEX 1403 and f# 7 focusing lens combined with each of those three different detectors. The results are shown in figure A.2. SPEX 1403 is good to be combined with the f# 7 focusing lens and detector 6255 for measuring spectrum in the region from 400 nm to about 680 nm and the best sensitivity is at around 520 nm. The combination of SPEX 1403 with f# 7 focusing lens and detector 9659 is fairly good for measuring spectrum from 430 nm to 730 nm, and its best sensitivity is at around 550 nm. When SPEX 1403 is combined with detector C31034, it is better to avoid using f# 7 focusing lens, it is only weakly sensitive from 430 nm to 730 nm.

The results of the third setting is shown in figure A.3. The instrument setting uses SPEX 1403, detector C31034 and f# 7.5 focusing lens.

A measured spectrum is a convolution of the sample and the system response spectrum. To correct the spectrum, it is important to know the system response, and this can be obtained by measuring a standard light source.

In this project, a source of 12 DC volt white light was used that is known as a black body radiator. The system response spectrum was obtained by dividing the measured spectrum of the white light by the black body spectrum of the white light.

The source of 12 DC volt white light was thought as a black body radiator at T = 6500 K, in the analysis and calculation of the system response spectrum. However, it was found inconsistent later on, and there was no way to find the correct temperature out from an experiment.

Figure A.4 shows a measured white light spectrum using SPEX 1700, detector 9659 and f# 7 focusing lens, the black body spectrum at T = 6500 K, and the system response spectrum. The system response result shows that this set up is good at measuring spectra from 400 nm to 900 nm with best sensitivity at around 680 nm.

Figure A.5 shows the system response of instrument set up using SPEX 1403, detector 6255 and f# 7 focusing lens. This set up is good at measuring spectra from 400 nm to 650 nm with best sensitivity at around 520 nm.

Figure A.6 shows the system response of instrument set up using SPEX 1403, detector C31034 and f# 7.5 focusing lens. This is the best set up available in the lab for measuring GaN samples, which has emission lines at about 355 nm (band

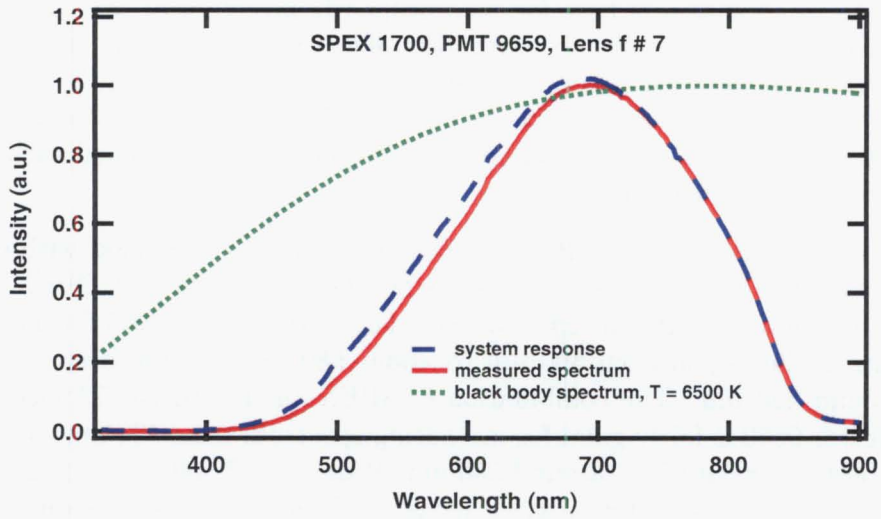

Figure A.4: Detector sensitivity or system response of using SPEX 1700, detector 9659 and f# 7 focusing lens, measured white light spectrum and calculated black body spectrum at T = 6500 K.

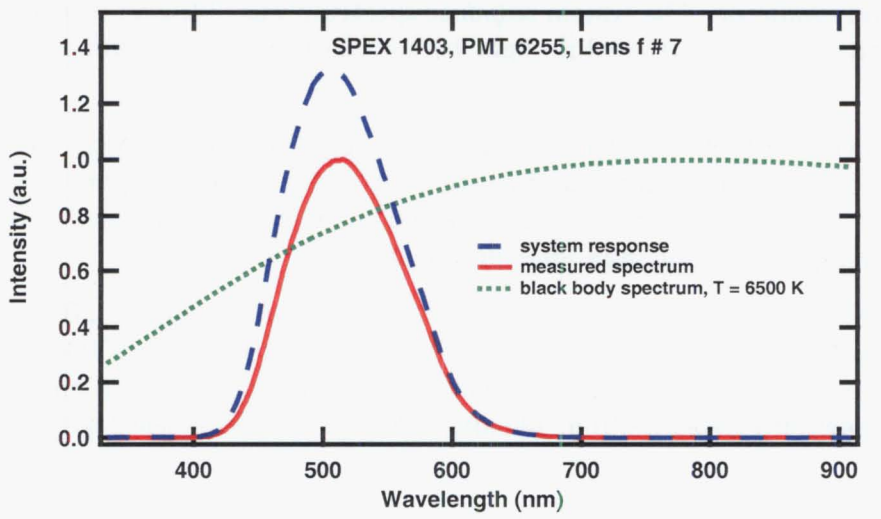

Figure A.5: Detector sensitivity or system response of using SPEX 1403, detector 6255 and f# 7 focusing lens, measured white light spectrum and calculated black body spectrum at T = 6500 K.

edge emission line), 375 nm (donor acceptor emission line) and from 450 nm to 600 nm (three yellow luminescence peaks).

This detector sensitivity spectrum can be used to correct all measured spectra by the system response to obtain the real spectra originating from the samples.

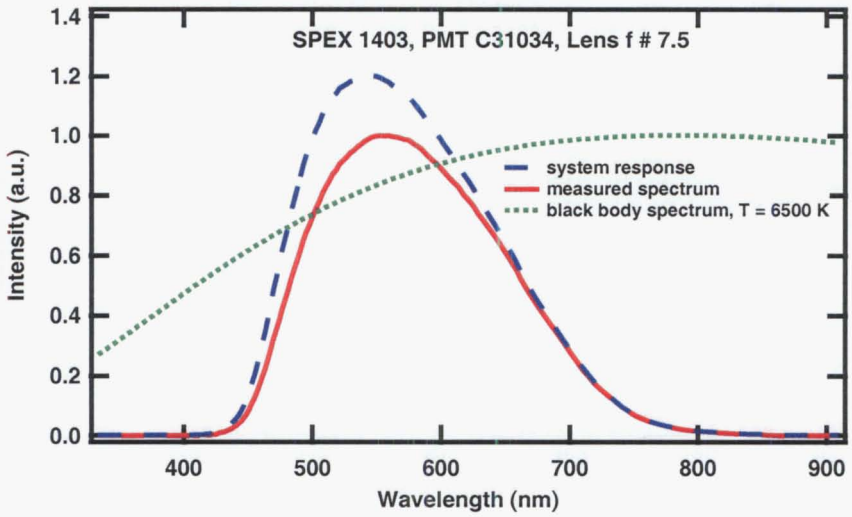

Figure A.6: System response of using SPEX 1403, detector C31034 and f# 7.5 focusing lens, measured white light spectrum and calculated black body spectrum at T = 6500 K.

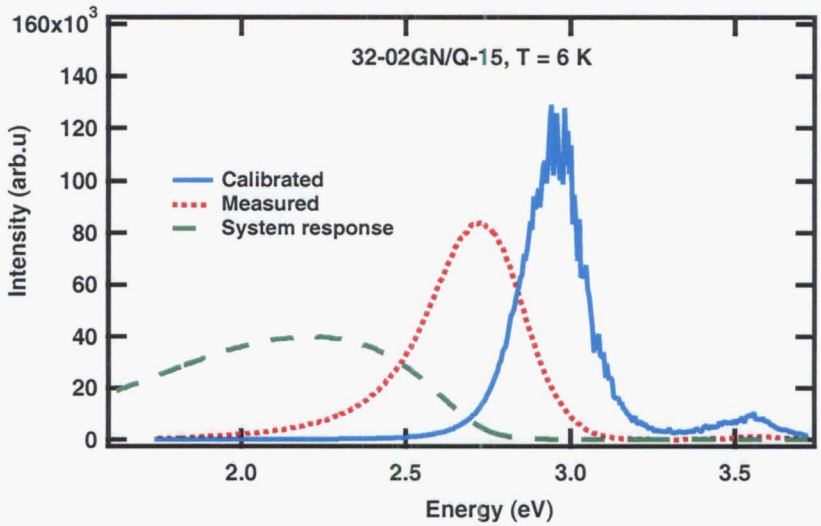

Figure A.7: PL result of poly-GaN sample 32-02/GN-Q15 at the temperature of 6 K

Figure A.7 shows the PL result of poly-GaN sample 32-02/GN-Q15 on quartz substrate at the temperature 6 K. The calibrated PL peak was shifted about 240 meV to 2.961 eV from the measured PL peak at 2.723 eV. Further investigation is suggested to confirm all the system response of the instrument settings.

Appendix B

A Typical PL and Temperature Dependence of Crystalline GaN

A typical PL result and the temperature dependence of an as-grown crystalline GaN (c-GaN) was measured from sample c-GaN/sap/30803/10. This sample is a 0.3 μm thick c-GaN film MBE grown on sapphire substrate (0001) with a thin AlN nucleation layer, silicon doped at 5×10^{17} cm^{-3}.

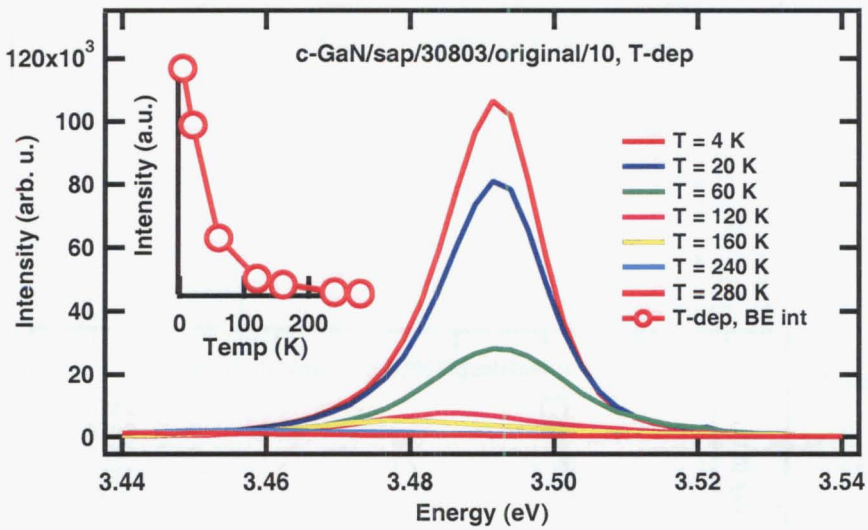

Figure B.1:

Figure B.1 shows the NBE emission line in the UV region at different temperatures. As the temperature increases from 4 K to 120 K, the peak intensity of the NBE line decreases sharply, then keeps decreasing gradually at the temperature of 120 K to 280 K. Increasing the temperature results in the redshift of the NBE line peak position, from 3.491 eV at the temperature 4 K to 3.435 eV at the temperature of 280 K. The linewidth of the NBE line is widened as the temperature increases, typically about 10 meV at the temperature of 4 K and 20 meV at the temperature of 160 K.

Figure B.2 shows the YL emission lines, peaking at 2.57 eV (YL1), 2.25 eV (YL2) and 1.89 eV (YL3), at different temperatures. The linewidth of these YL lines at the temperature lower than 120 K are 300 meV (YL1), 200 meV (YL2) and 170 meV (YL1). At the temperature higher than 120 K, the YL1 is narrowed to about 200 meV, the YL2 is widened to about 320 meV and YL3 has disappeared. In contrast with the intensity of NBE line, increasing temperature results in an increase in the intensity of YL lines.

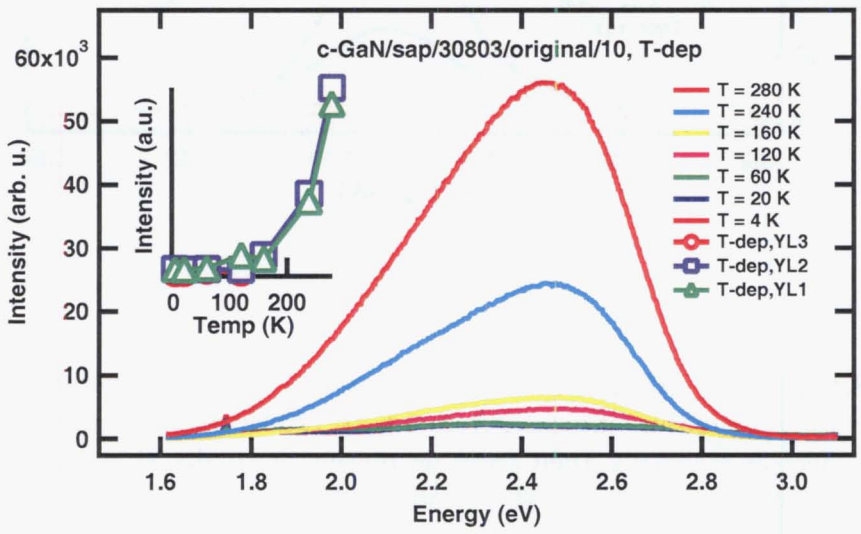

Figure B.2:

Appendix C

Multipeak Fitting

The fitting of the PL results has been done using multipeak fitting with a gaussian distribution. The typical chi square of the fitting results are from 2×10^6 to 5×10^6 for NBE line and 1×10^7 to 3×10^7 for YL line.

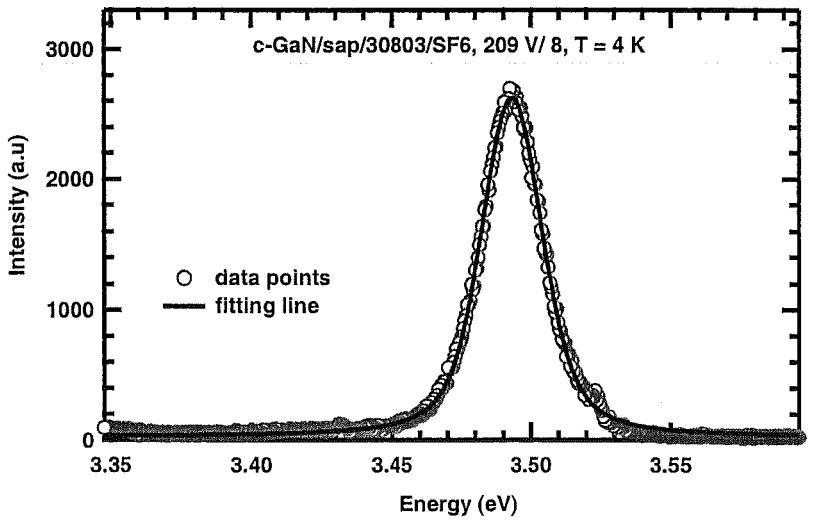

Figure C.1: The fitting result of the PL NBE emission of SF_6-etched c-GaN/sap/30803/8 sample.

Figure C.1 shows the fitting result of PL spectrum from SF_6-etched c-GaN/sap/30803/8 sample. Apparent is the NBE line, peaking at 3.493 eV $\pm$ 2 meV and linewidth (FWHM) 17 meV $\pm$ 3 meV.

Figure C.2 shows the multipeak fitting result of PL spectrum from SF_6-etched c-GaN/sap/30803/9 sample. Apparent is the NBE line, peaking at 3.479 eV $\pm$ 2 meV (BE1) and 3.496 eV $\pm$ 2 meV (BE2). The linewidth (FWHM) 33 meV $\pm$ 4 meV (BE1) and 10 meV $\pm$ 3 meV (BE2).

The so-called YL line in this project commonly consists of three or two lines. Figure C.3 shows multipeak fitting result of the YL line of SF_6-etched c-GaN/sap/30803/8.

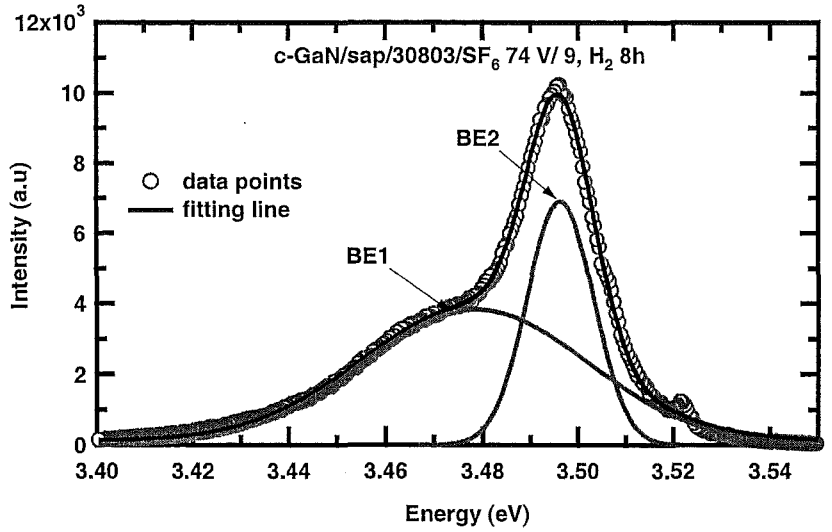

Figure C.2: The fitting result of the PL NBE emission of SF_6-etched c-GaN/sap/30803/9 sample.

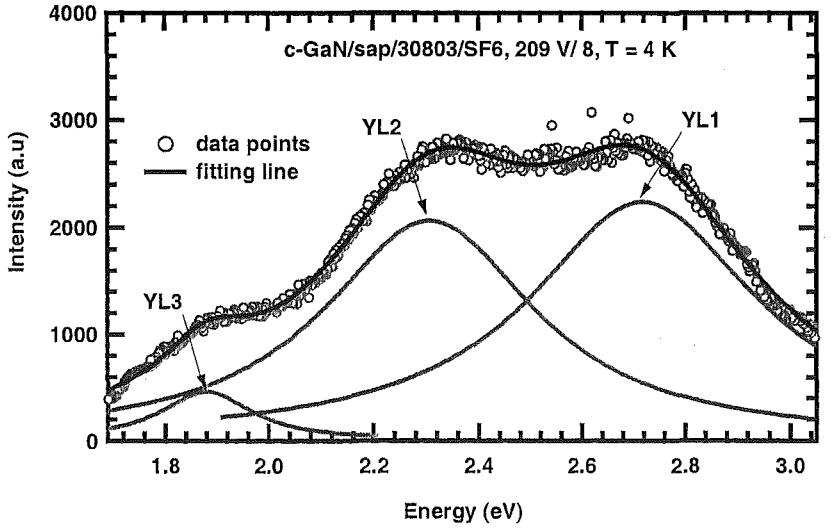

Figure C.3: The fitting result of the PL YL line of SF_6-etched c-GaN/sap/30803/8 sample.

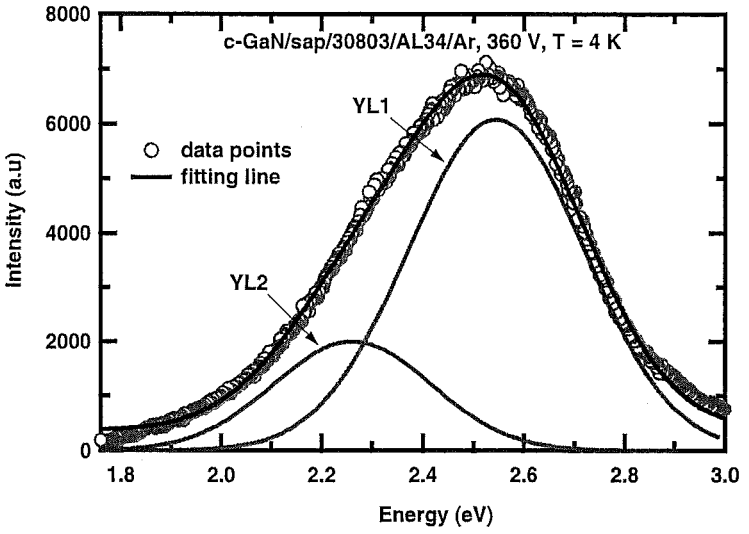

Figure C.4: The fitting result of the PL YL line of Ar-etched c-GaN/sap/30803/AL34 sample.

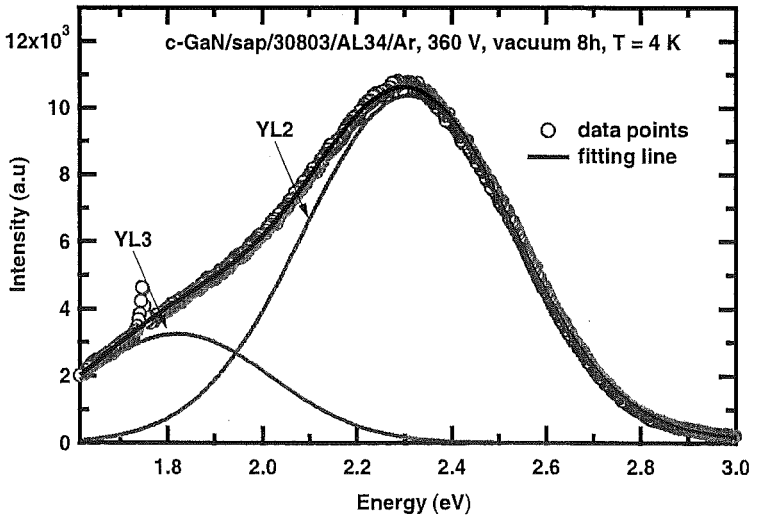

Figure C.5: The fitting result of the PL YL line of Ar-etched c-GaN/sap/30803/AL34 sample.

The YL line of this sample consists of three lines YL1, YL2, and YL3. The peak position of those lines are at 2.72 eV ± 10 meV (YL1), 2.31 eV ± 10 meV (YL2) and 1.88 eV ± 10 meV (YL3). The linewidth (FWHM) of the YL1, YL2 and YL3 are 270 meV ± 10 meV, 250 meV ± 10 meV and 110 meV ± 10 meV, respectively.

Figure C.4 shows multipeak fitting result of Ar-etched c-GaN/sap/30803/AL34 YL line. This sample has two YL lines, those are YL1 and YL2. The YL1 and YL2 peak position are at 2.55 eV ± 10 meV and 2.26 eV ± 10 meV with linewidth (FWHM) 250 meV ± 10 meV and 220 meV ± 10 meV, respectively.

Figure C.5 shows multipeak fitting result of Ar-etched then H-annealed c-GaN/sap/30803/AL34 YL line. This sample has also two YL lines, those are YL2 and YL3. The YL2 and YL3 peak position are at 2.31 eV ± 10 meV and 1.82 eV ± 10 meV with linewidth (FWHM) 310 meV ± 10 meV and 280 meV ± 10 meV, respectively.

Appendix D

Publications

- V.A. Christie, S.I. Liem, R. Reeves, V.J. Kennedy, A. Markwitz and S.M. Durbin, *Characterisation of polycrystalline gallium nitride grown by plasma-assisted evaporation*, Current Applied Physics (to appear, January 2004).
- V.A. Christie, S.I. Liem, R. Reeves, V.J. Kennedy, A. Markwitz and S.M. Durbin, *Characterisation of polycrystalline gallium nitride grown by plasma-assisted evaporation*, AMN-1 The MacDiarmid Institute for Advanced Materials and Nanotechnology, 9-13 February 2003, Wellington, New Zealand.
- Suk Ing Liem, Roger J. Reeves, *Influence of ion energy on the reactive ion etching induced optical damage of gallium nitride*, AMN-1 The MacDiarmid Institute for Advanced Materials and Nanotechnology, 9-13 February 2003, Wellington, New Zealand.
- S.M. Durbin, V.A. Christie, S.I. Liem, R. Reeves, V.J. Kennedy, A. Markwitz, *Characterisation of low-temperature gallium nitride*, 2003 March Meeting of the American Physical Society, (Austin, TX, USA, March 3-7 2003).
- Suk Ing Liem, Roger J. Reeves, *Influence of ion energy on the reactive ion etching induced optical damage of gallium nitride*, MRS Symp. Proc. Vol 764, C3.46, page 221-226, 2003.
- Suk Ing Liem, Roger J. Reeves, *Influence of ion energy of the reactive ion etching and annealing on optical properties of gallium nitride*, DPC-14, Dynamical Processes in Excited States of Solids, 3-8 August 2003, Christchurch, New Zealand.
- A Koo, U D Lanke, B J Ruck, S Brown, R Reeves, I Liem, A Bittar and H J Trodahl, *Conductivity, photoconductivity and optical properties of amorphous GaN films*, MRS Symp. Proc. Vol. 693, I10.10.1, 2002.

Bibliography

[1] I. Akasaki and H. Amano. *J. Cryst. Growth*, 163:86, 1996.

[2] I. Akasaki, S. Sota, H. Sakai, T. Tanaka, M. Koike, and H. Amano. *Electron Lett.*, 32:1105, 1996.

[3] H. Amano, I. Akasaki, K. Hiramatsu, N. Koide, and N. Sawaki. *Thin Solid Films*, 163:1156, 1988.

[4] H. Amano, M. Kito, K. Hiramatsu, and I. Akasaki. P-type conduction in Mg-doped GaN treated with low-energy electron beam irradiation (LEEBI). *Jpn. Journal of Applied Physics*, 28(12):L2112–L2114, December 1989.

[5] H. Amano, N. Sawaki, I. Akasaki, and Y. Toyoda. Metal organic vapor phase epitaxial growth of a high quality GaN film using an AlN buffer layer. *Appl. Phys. Lett.*, 48:353, 1986.

[6] J.M. Baranowski and S. Porowski. In *Proc. 23rd International Conference on Physics of Semiconductors*, page 497. World Scientific, 1996.

[7] A. Bittar, H.J. Trodahl, N.T. Kemp, and A. Markwitz. Ion-assisted deposition of amorphous GaN: Raman and optical properties. *Appl. Phys. Lett.*, 78(5):619–621, January 2001.

[8] P. Boguslawski, E.L. Briggs, and J. Bernholc. Native defects in gallium nitride. *Phys Rev. B*, 51:17255, 1995.

[9] M.S. Brandt, N.M. Johnson, R.J. Molnar, R. Singh, and T.D. Moustakas. Hydrogenation of p-type gallium nitride. *Appl. Phys. Lett.*, 64(17):2265, April 1994.

[10] I. Brodie and J.J. Muray. *The Physics of Microfabrication.* Plenum Press, New York, 1982.

[11] S.A. Brown, R.J. Reeves, C. Haase, R. Cheung, C. Kirchner, and M. Kamp. Reactive-ion-etched gallium nitride: metastable defects and yellow luminescence. *Appl. Phys. Lett.*, 75(21), November 1999.

[12] S.A. Brown, R.J. Reeves, C. Haase, R. Cheung, C. Kirchner, and M. Kamp. Long-period time-dependent luminescence in reactive ion-etched GaN. *Physica*, E7:958–962, 2000.

[13] S.A. Brown, R.J. Reeves, B. Rong, R. Cheung, M. Seyboth, C. Kirchner, and M. Kamp. Argon plasma etching of gallium nitride: spectroscopic surprise. *Nanotechnology*, 11:1–7, 2000.

[14] G.D. Chen, M. Smith, J.Y. Lin, H.X. Jiang, S.H. Wei, M.A. Khan, and C.J. Sun. Fundamental optical transitions InGaN. *Appl. Phys. Lett.*, 68(20):2784–2786, 1996.

[15] R. Cheung, R.J. Reeves, S.A. Brown, E.J.M. Fakkeldij, E. van der Drift, and M. Kamp. High resolution reactive ion etching of GaN and etch-induced effects. *J. Vac. Sci. Technol.*, B17(6), Nov/Dec 1999.

[16] R. Cheung, R.J. Reeves, S.A. Brown, E. van der Drift, and M. Kamp. Effects of dry processing on the optical properties of GaN. *Journal of Applied Physics*, 88(12), December 2000.

[17] R. Cheung, S. Withanage, R.J. Reeves, S.A. Brown, I. Ben-Yaacov, C. Kirchner, and M. Kamp. Reactive ion etch-induced effects on the near-band-edge luminescence in GaN. *Appl. Phys. Lett.*, 74(21), May 1999.

[18] V. Comello. ICP etchers start to challenge ECR. *R and D Magazine*, pages 79–80, 1993.

[19] R.F. Davis. *Physica*, B 185:1, 1993.

[20] R.F. Davis, M.J. Paisley, Z. Sitar, D.J. Kesler, K.S. Ailey, and C. Wang. *Microelectron J.*, 251, 1994.

[21] V.Yu. Davydov, A.A. Klochikhin, V.V. Emtsev, D.A. Kurdyukov, S.V. Ivanov, V.A. Vekshin, F. Bechstedt, J. Furthmuller, J. Aderhold, J. Graul, A.V. Mudryi, H. Harima, A. Hashimoto, A. Yamamoto, and E.E. Haller. Band gap of hexagonal InN and InGaN alloys. *Phys. Stat. Sol. (b)*, 234:787–795, 2002.

[22] R. Dingle and M. Ilegems. Donor-acceptor pair recombination in GaN. volume 9, page 175, February 1971.

[23] R. Dingle, D.D. Sell, S.E. Stokowski, and M. Ilegems. *Phys. Rev. B*, 4(4):1211–1218, 1971.

[24] J.H. Edgar. *Properties of group III nitrides.* Emis Data Reviews series 11. Inspec, 1994.

[25] A. Einstein. *Physik Z*, chapter 18, page 121. 1917.

[26] Elliott. Intensity of optical absorption by excitons. *Phys. Rev.*, 108:1384, 1957.

[27] B. Gil, O. Briot, and R.L. Aulombard. Valence-band physics and the optical properties of GaN epilayers grown onto sapphire with wurtzite symmetry. *Phys. Rev. B*, 52:17028–17031, 1995.

[28] W. Gotz, N.M. Johnson, D.P. Bour, M.D. McCluskey, and E.E. Haller. Local vibrational modes of the Mg-H acceptor complex in GaN. *Appl. Phys. Lett.*, 69(24):3725, December 1996.

[29] R. Gunshore, A. Nurmikko, and M. Kobayashi. *Physics World*, 47, March 1992.

[30] T. Hariu, T. Usuba, H. Adachi, and Y. Shibata. *Appl. Phys. Lett.*, 32:252, 1978.

[31] J.R. Haynes. Isotopic composition of primodial xenon. *Phys. Rev. Lett.*, 4:351, 1960.

[32] D.M. Hofmann, D. Kovalev, G. Steude, B.K. Meyer, A. Hoffmann, L. Eckey, R. Heitz, T. Detchprom, H. Amano, and I. Akasaki. Properties of the yellow luminescence in undoped GaN epitaxial layers. *Phys. Rev. B*, 52:16702, 1995.

[33] M. Ilegems. *J. Cryst. Growth*, 13/14:360, 1972.

[34] D.W. Jenkins and J.D. Dow. Electronic structures and doping of InN, $In_xGa_{1-X}N$ and $In_XAl_{1-X}N$. *Phys. Rev. B*, 39:3317, 1989.

[35] M.A.L. Johnson, Z. Yu, C. Boney, W.C. Hughes, J.W. Cook Jr., J.F. Schetzina, H. Zao, B.J. Skromme, and J.A. Edmond. MBE growth of III-V nitride films and quantum-well structures using multiple rf plasma source. volume 449, 1997.

[36] C. Kittel. *Elementary Statistical Physics*, page 175. Wiley, New York, 1958.

[37] K.P. Korona, A. Wysmolek, K. Pakula, R. Stepniewski, J.M. Baranowski, I. Grzegory, B. Lucznik, M. Wroblewski, and S. Porowsky. Exciton region reflectance of homoepitaxial GaN layers. *Appl. Phys. Lett*, 69:788, 1996.

[38] X.B. Li, D.Z. Sun, J.P. Zhang, M.Y. Kong, and S.F. Yoon. Influence of rapid thermal annealing on the optical properties of gallium nitride grown by gas-source molecular beam epitaxy. *Appl. Phys. Lett.*, 72(8), February 1998.

[39] E. Litwin-Staszewska, T. Suski, R. Piotrzkowski, I. Grzegory, M. Bockowski, J.L. Robert, L. Konczewicz, D. Wasik, E. Kaminska, D. Cote, and B. Clerjaud. Temperature dependence of electrical properties of gallium-nitride bulk single crystal doped with Mg and their evolution with annealing. *Journal of Applied Physics*, 89(12):7960, June 2001.

[40] Marc Madou. *Fundamentals of Microfabrication.* CRC Press LLC, 1997.

[41] H.M. Manasevit, F.M. Erdman, and W.I. Simpson. *J. Electrochem. Soc*, 118:1855, 1971.

[42] C. Merz, M. Kunzer, U. Kaufmann, H. Amano, and I. Akasaki. Free and bound excitons in thin wurtzite GaN layers on sapphire. *Semiconductor Sci. Technol*, 11:712, 1996.

[43] R.A. Metzger. *Compound Semiconductor*, 1:26, 1995.

[44] B.K. Meyer. Free and bound excitons in GaN epitaxial films. volume 449. MRS Proc., 1997.

[45] S.N. Mohammad, Z. Fan, A.E. Botcharev, W. Kim, O. Aktas, A. Salvador, and H. Morkoc. *Electron Lett.*, 32:598, 1996.

[46] S.N. Mohammad and H. Morkoc. *Progress in Quantum Electronics.* Elsevier, London, 1995.

[47] S.N. Mohammad and H. Morkoc. volume 20, pages 361–525. Progr. Quant. Electron, 1996.

[48] B. Monemar. *Phys. Rev. B*, 10(2):676–681, 1974.

[49] B. Monemar. *Optical Properties of GaN, In Semiconductors and Semimetals*, chapter 30, page 305. Academic San Diego, 1997.

[50] B. Monemar, J.P. Bergman, and I.A. Buyanova. *Optical characterisation of GaN and related material: in GaN and related material.* Gordon and Breach Amsterdam, 1997.

[51] H. Morkoc. *Nitride Semiconductors and Devices.* Springer-Verlag, Germany, 1999.

[52] H. Morkoc, S. Strite, G.B. Gao, M.E. Lin, B. Sverdlov, and M. Burns. Large bandgap SiC, III-V nitride and II-VI ZnSe based semiconductor device technologies. *J. Appl. Phys.*, 76:1363, 1994.

[53] S. Nakamura and G. Fasol. *The Blue Laser Diode GaN Based Light Emitters and Lasers.* Springer, 1997.

[54] S. Nakamura, N. Iwasa, M. Senoh, and T. Mukai. Hole compensation mechanism of p-type GaN films. *Jpn. J. Appl. Phys.*, 31(5A):1258–1266, May 1992. Part 1.

[55] S. Nakamura, M. Senoh, N. Iwasa, and S. Nahagama. *Japan J. Appl. Phys.*, 34:L797, 1995.

[56] S. Nakamura, M. Senoh, N. Iwasa, and S. Nahagama. High power InGaN single quantum-well-structure blue and violet light emitting diodes. *Appl. Phys. Lett.*, 67:1868, 1995.

[57] S. Nakamura, M. Senoh, N. Iwasa, S. Nahagama, T. Yamada, and T. Mukai. *Japan J. Appl. Phys.*, 34:L1332, 1995.

[58] S. Nakamura, M. Senoh, S. Nahagama, N. Iwasa, T. Yamada, T. Matsushita, H. Kiyoku, and Y. Sugimoto. *Japan J. Appl. Phys.*, 35:L74, 1996.

[59] S. Nakamura, M. Senoh, S. Nahagama, N. Iwasa, T. Yamada, T. Matsushita, H. Kiyoku, and Y. Sugimoto. *Japan J. Appl. Phys.*, 35:L217, 1996.

[60] S. Nakamura, M. Senoh, S. Nahagama, N. Iwasa, T. Yamada, T. Matsushita, H. Kiyoku, and Y. Sugimoto. Characteristics of InGaN multi-quantum-well structure laser diode. *Appl. Phys. Lett.*, 68:3269, 1996.

[61] S. Nakamura, M. Senoh, S. Nahagama, N. Iwasa, T. Yamada, T. Matsushita, H. Kiyoku, and Y. Sugimoto. InGaN multi-quantum-well structure laser diodes grown on $MgAl_2O_4$ substrate. *Appl. Phys. Lett.*, 68:2105, 1996.

[62] S. Nakamura, M. Senoh, S. Nahagama, N. Iwasa, T. Yamada, T. Matsushita, Y. Sugimoto, and H. Kiyoku. Optical gain and carrier lifetime of InGaN multi-quantum-well structure laser diodes. *Appl. Phys. Lett.*, 69:1568, 1996.

[63] J. Neugebauer and C.G. Van de Walle. Hydrogen in GaN: Novel aspects of a common impurity. *Phys. Rev. Lett.*, 75 68:4452 1829, 1995 1996.

[64] J. Neugebauer and Chris G. Van de Walle. Role of hydrogen in doping of GaN. *Appl. Phys. Lett.*, 68(13):1829, March 1996.

[65] D.A. Neumayer and J.G. Ekerdt. *Chem. Mater*, 8:9, 1996.

[66] S. Nonomura, S. Kobayashi, T. Gotoh, S. Hirata, T. Ohmori, T. Itoh, S. Nitta, and K. Marigaki. *J. Cryst. Solids*, 200:174, 1996.

[67] Eunsoon Oh, Bongjin Kim, Hyeongsoo Park, and Yongjo Park. Effect of surface layer on optical properties of GaN and $In_xGa_{1-x}N$ upon thermal annealing. *Appl. Phys. Lett.*, 69(9), August 1996.

[68] S.J. Pearton, R.J. Shul, and F. Ren. *MRS Internet J. Nitride Semicond. Res.*, 5(11), 2000.

[69] S.J. Pearton, R.J. Shul, R.G. Wilson, F. Ren, J.M. Zavada, C.R. Abernathy, C.B. Vartuli, J.W. Lee, J.R. Mileham, and J.D. MacKenzie. The incorporation of hydrogen into III-V nitrides during processing. *Journal of Electronic Materials*, 25(5):845, January 1996.

[70] F.A. Ponce and D.P. Bour. *Nature*, 386:351, 1997.

[71] R.J. Reeves, S.A. Brown, C.S. Haase, B. Rong, R. Cheung, C. Kirchner, and M. Kamp. Origin of the yellow luminescence in gallium nitride: importance of metastability and blue luminescence. In *Proceeding International Conference of Physics Semiconductor*, pages 1535–1536, 2000.

[72] R.J. Reeves, O. Dickie, B. Rong, R. Cheung, and S.A. Brown. Photoluminescence and photoconductivity studies of reactive-ion-etched GaN on SiC substrates. In *Proceeding International Workshop on Nitride Semiconductor (IPAP) CSI*, pages 774–777, 2000.

[73] S.Y. Ren, J.D. Dow, and J. Shen. Deep impurity levels in semiconductor superlattices. *Phys. Rev. B*, 38:10677, 1988.

[74] D.C. Reynold, D.C. Look, W. Kim, O. Aktas, A. Salvador, H. Morkoc, and D.N. Talwar. Ground and excited state exciton spectra from GaN grown by molecular-beam epitaxy. *Appl. Phys. Lett.*, 80:594, 1996.

[75] D.C. Reynolds, D.C. Look, B. Jogai, and H. Morkoc. Similarities in the bandedge and deep-centre photoluminescence mechanisms of ZnO and GaN. *Solid State Commun.*, 101:643–725, March 1997.

[76] D.C. Reynolds, D.C. Look, R. Jogai, V.M. Phanse, and R.P. Vaudo. *Solid State Commun*, 103:533, 1997.

[77] W. Shan, R.J. Hauenstein, A.J. Fischer, J.J. Song, W.G. Perry, M.D. Bremser, R.F. Davis, and B. Goldenberg. Strain effects on excitonic transitions in GaN: deformation potentials. *Phys. Rev. B*, 54:13460, 1996.

[78] H.P. Singer. ECR: Is the magic gone? *Semicond. Int.*, pages 46–48, July 1991.

[79] P. Singer. Trends in plasma sources: The search continues. *Semicond. Int.*, pages 52–56, July 1992.

[80] M. Smith, G.D. Chen, J.I. Li, J.Y. Lin, H. Jiang, A. Salvador, B.N. Sverdlov, A. Botchkarev, and H. Morkoc. Excitonic recombination in GaN grown by molecular beam epitaxy. *Appl. Phys. Lett.*, 67:3387, 1995.

[81] A.R. Stonas, N.C. MacDonald, K. Turner, S.P. DenBaars, and E.L. Hu. *The 45^{th} International Conference on Electron, Ion and Photon Beam Technology and Nanofabrication (EIPBN)*, June 2001.

[82] S. Strite and H. Morkoc. *J. Sci. Technol*, B 10:1237, 1992.

[83] P. Stumm and D.A. Drabold. Can amorphous GaN serve as a useful electronic material? *Phys. Rev. Lett.*, 79(4):677–680, July 1997.

[84] T.L. Tansley and R.J. Eagen. Point-defect energies in the nitrides of aluminum gallium and indium. *Phys. Rev. B*, 45:10942, 1992.

[85] T.L. Tansley and C.P. Foley. Optical band gap of indium nitride. *J. Appl. Phys*, 59:3241, 1986.

[86] Texas Engineering Extension Service (TEEX). *Wet/Dry Etch Overview.* The Texas AM University System, 2000.

[87] Y.P. Varshni. *Physica*, 34:149, 1967.

[88] S. Wang. *Fundamentals of Semiconductor Theory and Device Physics.* Prentice Hall, Englewood Cliffs NJ, 1989.

[89] S. Wolf and R.N. Tauber. *Silicon Processing for the VLSI Era.* Lattice Press, Sunset Beach, 1987.

[90] Z. Yang, L.K. Li, and W.I. Wang. GaN grown by MBE at high growth rates using amonia as the nitrogen source. *Appl. Phys. Lett.*, 67:1686, 1995.

[91] S. Yoshida, S. Misawa, Y. Fujii, S. Takada, H. Hayakawa, S. Gonda, and A. Itoh. *J. Vac. Sci. Technol.*, 16:990, 1979.

[92] S. Yoshida, S. Misawa, and S. Gonda. Porperties of $Al_xGa_{1-x}N$ films prepared by reactive molecular beam epitaxy. *J. Appl. Phys.*, 53:6844, 1982.

[93] S. Yoshida, S. Misawa, and S. Gonda. *J. Vac. Sci. Technol.*, B1:250, 1983.

[94] S. Yoshida, S. Misawa, and S. Gonda. Improvement on the electrical and luminescent properties of reactive molecular beam epitaxially grown GaN films. *Appl. Phys. Lett.*, 42:427, 1983.

[95] P.Y. Yu and M. Cardona. *Fundamentals of Semiconductors.* Springer, Heidelberg Berlin, 1995.